UNIVERSIDADE DE COIMBRA

EFFECT OF BIOPOLYMER-BASED NANOPARTICLES ON ENHANCING INSULIN PERMEATION THROUGH INTESTINAL EPITHELIUM

MARLENE ALMEIDA LOPES MARQUES

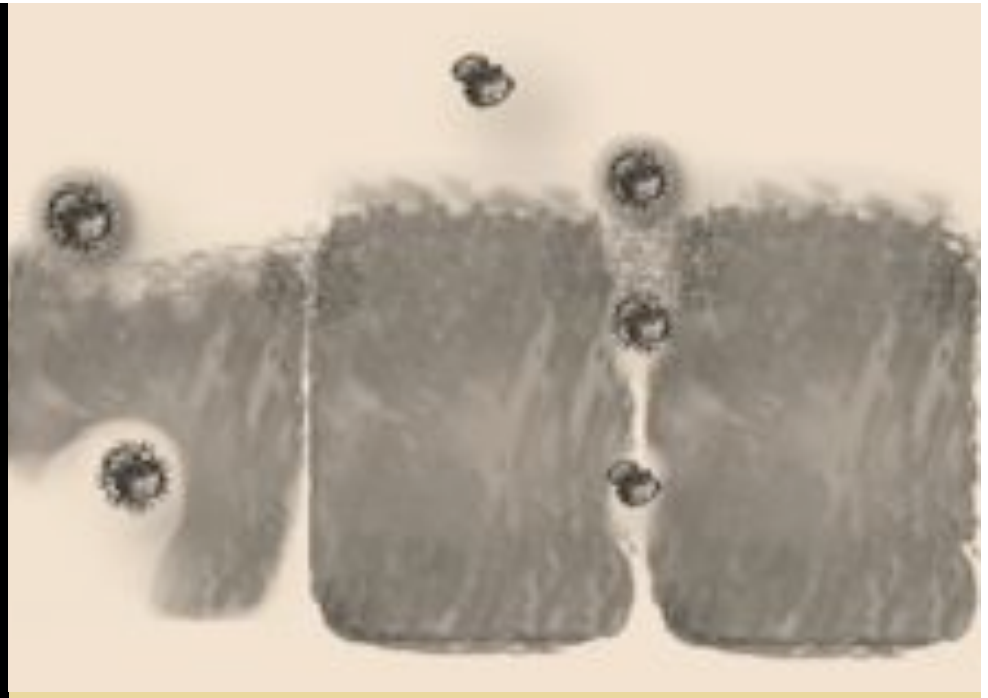

Marlene Almeida Lopes Marques

EFFECT OF BIOPOLYMER-BASED NANOPARTICLES ON ENHANCING INSULIN PERMEATION THROUGH INTESTINAL EPITHELIUM

Tese de Doutoramento em Ciências Farmacêuticas, ramo de Tecnologia Farmacêutica, orientada por Professor Doutor António Ribeiro, Professor Doutor Francisco Veiga e Professora Doutora Raquel Seiça e apresentada à Faculdade de Farmácia da Universidade de Coimbra

Agosto/2016

· U C ·

UNIVERSIDADE DE COIMBRA

Marlene Almeida Lopes Marques

EFFECT OF BIOPOLYMER–BASED NANOPARTICLES ON ENHANCING INSULIN PERMEATION THROUGH INTESTINAL EPITHELIUM

FACULTY OF PHARMACY

UNIVERSITY OF COIMBRA

2016

Marlene Almeida Lopes Marques

EFFECT OF BIOPOLYMER–BASED NANOPARTICLES ON ENHANCING INSULIN PERMEATION THROUGH INTESTINAL EPITHELIUM

FACULTY OF PHARMACY

UNIVERSITY OF COIMBRA

2016

DISSERTATION OF CANDIDATURE FOR
DOCTORAL DEGREE IN PHARMACEUTICAL TECHNOLOGY SUBMITTED TO
THE FACULTY OF PHARMACY OF THE UNIVERSITY OF COIMBRA

DISSERTAÇÃO DE CANDIDATURA AO
GRAU DE DOUTOR EM TECNOLOGIA FARMACÊUTICA APRESENTADA À
FACULDADE DE FARMÁCIA DA UNIVERSIDADE DE COIMBRA

The research work presented in this thesis was accomplished at the Laboratory of Pharmaceutical Technology of the Faculty of Pharmacy of the University of Coimbra, under the supervision of Professor António Ribeiro, Professor Francisco Veiga and Professor Raquel Seiça, and at the Division of Pharmaceutical Chemistry & Technology of the Faculty of Pharmacy of the University of Helsinki, under the supervision of Professor Hélder Santos. Granted by Portuguese Foundation for Science and Technology (SFRH/BD/79123/2011).

Os trabalhos experimentais apresentados na tese foram realizados no Laboratório de Tecnologia Farmacêutica da Faculdade de Farmácia da Universidade de Coimbra, sob a supervisão do Professor Doutor António Ribeiro, Professor Doutor Francisco Veiga e Professora Doutora Raquel Seiça, e na Divisão de Química & Tecnologia Farmacêutica da Faculdade de Farmácia da Universidade de Helsínquia, sob a supervisão do Professor Doutor Hélder Santos. Financiado pela Fundação para a Ciência e Tecnologia (SFRH/BD/79123/2011).

À minha querida avó Deolinda

AGRADECIMENTOS

Passaram anos desde o início do tão amedrontado doutoramento. Cresci, aprendi e mudei. A cada um dos que à sua maneira participaram no meu percurso, o meu mais sincero obrigada!

Ao Professor António Ribeiro, pela total disponibilidade prestada desde o primeiro ao último dia, pela confiança, pelo incentivo e pelas oportunidades que me facultou ao longo do projeto, por caminhar ao meu lado mesmo "nos becos sem saída". Porque só com um grande orientador se segue o melhor caminho, o meu profundo obrigada.

Ao Professor Francisco Veiga, queria expressar o meu apreço e agradecimento pelo acompanhamento, disponibilidade e apoio prestados.

À Professora Raquel Seiça, o meu reconhecimento pela ajuda e disponibilidade, pela simpatia e confiança e pelo enriquecimento que proporcionou ao projeto.

O meu agradecimento aos meus colegas de doutoramento da Faculdade de Farmácia da Universidade de Coimbra pela companhia, amizade e ajuda. Pelas tardes no Choupal e pelos programas inesperados. À Bárbara que trouxe do Brasil a força e determinação necessárias para o começo deste grande projeto, a amizade e experiência que me fizeram crescer e às quais sou imensamente grata. À Susana pelo apoio incondicional, conselhos, ajuda e sincera amizade. À Edna pela divertida companhia, bom humor e troca de boas conversas. À Marisa por caminhar a meu lado desde o primeiro dia e pela mútua partilha das vitórias e derrotas, o que as tornou ultrapassáveis. À Carla pela ajuda incansável e ensinamentos enriquecedores. Ao João, Joana Sousa e Joana Bicker pela amizade e apoio.

Ao Hélder Santos, a quem expresso o meu mais sincero obrigada pela amizade, permanente disponibilidade, apoio, dedicação e confiança. A sua visão e incentivo permitiram-me alcançar metas incríveis e não podia deixar de demonstrar o meu maior respeito, admiração e agradecimento. É alguém que guardo como uma referência.

Aos meus colegas da Faculdade de Farmácia da Universidade de Helsínquia com os quais tive oportunidade de fazer parte dum grande grupo de investigação científica do mais alto nível, expresso o meu profundo agradecimento. A sua união, conhecimento e experiência fizeram-me crescer como pessoa e como investigadora. À Alexandra, Mónica e Patrícia pela sua amizade, companheirismo e dedicação que tornaram a minha estadia numa experiência divertida e que guardo com imensas saudades. À Neha e ao Ali pela ajuda e pelos conhecimentos e experiência partilhados.

À Fundação para a Ciência e a Tecnologia , o meu agradecimento pela atribuição da Bolsa de Doutoramento que tornou viável a concretização deste projeto.

Aos meus amigos que tornam os meus dias mais alegres, que me fazem rir e me e me dão a mão sempre que preciso. A todas as Pranchettes, porque são as mais incríveis, porque sou uma lisonjeada por as ter conhecido, porque as adoro. À minha mestre da informática, Susana, que esteve sempre presente e disponível e às meninas de Mangualde que cresceram comigo. A todas elas, com orgulho e felicidade, o meu obrigada.

Àqueles a quem as palavras não bastam para tamanha gratidão. Aos meus pais, por me fazerem sentir a sua prioridade, pelos valores e educação que me transmitiram e me fizeram ser quem hoje sou e chegar aonde cheguei, estou infinitamente grata.

Ao Bruno, em quem encontrei tudo aquilo que desejava numa pessoa. Por me escutar, me apoiar e incentivar, me valorizar e me fazer sentir que era capaz. Porque sem ele, estes anos teriam sido sentidos como décadas. Porque com ele, a vida é simplesmente fácil.

Ao Filipe, que me acompanhou, literalmente, em todos os minutos da escrita da tese. Foi a minha maior inspiração, obrigada pequenino.

TABLE OF CONTENTS

CHAPTER 7. CONCLUSIONS AND FUTURE PERSPECTIVES

RESUMO

A via oral é considerada a via de administração mais adequada e fisiológica. Uma insulina oral capaz de induzir um efeito antihiperglicémico eficiente, quer para substituir ou complementar a terapia da diabetes, é o principal objetivo dos profissionais de saúde, governos e doentes diabéticos. A terapia oral está associada não apenas com o desejo de excluir agulhas da rotina diária do doente diabético, como também com a disposição fisiológica de insulina que iriam obter, resultando numa melhor homeostase da glucose. No entanto, a terapia oral é limitada por várias barreiras fisiológicas e apesar dos inúmeros esforços ao longo das últimas décadas para desenvolver sistemas de administração de insulina, ainda não existe nenhuma insulina oral comercialmente disponível. O desejo de administrar insulina por via oral de uma forma conveniente e eficaz levou à intensa investigação de novos sistemas de libertação.

Conhecer o efeito das nanopartículas ao nível da eficácia terapêutica da insulina após a administração oral é essencial para a concepção de um sistema de libertação adequado. Esta tese surgiu neste contexto, tendo como objectivo desenvolver um sistema de nanolibertação com características físicas adequadas para a administração oral de insulina, ao avaliar o seu comportamento em todo o trato gastrointestinal e, ao nível celular.

Em primeiro lugar, nanopartículas de alginato e sulfato de dextrano contendo insulina produzidas pelo método de emulsificação/gelificação interna foram desenvolvidas de forma a obter um nanosistema com base em biopolímeros com as propriedades físicas requeridas para a administração oral. O efeito do tamanho das gotículas da emulsão nas partículas finais foi avaliado cuidadosamente, enquanto a atividade da insulina foi monitorizada após cada passo do processo. Houve uma diminuição do tamanho das gotículas da emulsão quando a ultrasonicação foi utilizada durante a fase de emulsificação, efeito que foi ainda mais pronunciado quando um agente co−tensioactivo foi adicionado. As interações entre os biopolímeros e a insulina foram preditos através de estudos de modelagem molecular por meio de cálculos de mecânica quântica, o que permitiu a previsão do modelo de interação. Os estudos de libertação *in vitro* indicaram que a integridade das nanopartículas foi bem preservada em fluido gástrico artificial, e a estabilidade conformacional da insulina foi assegurada pelas técnicas de espectroscopia de dicroísmo circular e de infravermelho com transformada de Fourier (Capítulo 2). Os biopolímeros têm

um efeito importante sobre as propriedades das nanopartículas e podem ter influência sobre o seu comportamento biológico. Biopolímeros policatiónicos, tais como o quitosano, podem ser usados para reticular com nanopartículas com base em alginato polianiónico de forma a proporcionar−lhes a capacidade de melhorar a bioadesão e permeabilidade ao nível celular. Neste sentido, foi explorado um estudo racional envolvendo o revestimento das nanopartículas com quitosano de forma a melhorar os seus parâmetros físico−químicos (Capítulo 3).

Devido à elevada área de superfície das nanopartículas, os fatores que influenciam sua absorção gastrointestinal, mais precisamente o seu tamanho e fenómenos de agregação, foram estudados através de fluidos gastrointestinais artificiais. Os efeitos individuais do revestimento com quitosano, assim como do revestimento adicional de albumina, foram cuidadosamente avaliados. Foi realizada a aplicação da albumina como um revestimento mais externo para as nanopartículas revestidas com quitosano, uma vez que a albumina revelou atuar como um alvo sacrificial de forma a evitar a degradação de insulina, impedindo as proteases de alcançar a insulina que se encontra dentro das nanopartículas, e estabilizando as nanopartículas tanto no ambiente ácido como no ambiente intestinal. De seguida, o efeito das nanopartículas no aumento da permeação *in vitro* da insulina através da membrana intestinal foi também avaliado, utilizando modelos *in vitro* de co−culturas de células Caco−2, Caco−2/HT29−MTX, e Caco−2/HT29−MTX/Raji B (Capítulo 4). O duplo revestimento com quitosano e albumina foi concretizado com sucesso, usufruindo das suas propriedades de protecção, mucoadesão e melhor absorção. A aplicação da albumina proporcionou maior estabilidade ao nível do tamanho das nanopartículas em condições gastrointestinais, com menor agregação e mais uniformidade na distribuição de tamanhos, impedindo a libertação da maioria da insulina em pH gástrico e sustendo a libertação em pH intestinal, permitindo que a insulina possa ser libertada nos locais de absorção. Nas experiências celulares, as nanopartículas aumentaram significativamente a permeabilidade da insulina através dos modelos *in vitro*, um padrão que se apresentou em conformidade com o perfil de libertação de insulina.

De seguida, a capacidade deste nanosistema oral em melhorar a disponibilidade farmacológica da insulina em ambos os modelos animais de diabetes tipo 1 e tipo 2 foi pela primeira vez analisada (Capítulo 5). Houve um efeito antihiperglicémico significativo após a administração oral a ambos os modelos, embora o efeito antihiperglicémico tenha sido mais

prolongado no modelo de diabetes tipo 1. A biodistribuição das nanopartículas foi também avaliada, revelando uma maior interação das nanopartículas com as paredes do intestino delgado, o que pode ser justificado pelas propriedades mucoadesivas do quitosano.

Finalmente, nesta tese, a eficácia das nanopartículas ao nível da permeabilidade da insulina através das células epiteliais do intestino foi integralmente avaliada. Foi realizada uma avaliação sistemática dos mecanismos celulares e moleculares utilizados pelas nanopartículas para o transporte de insulina através do intestino (Capítulo 6). Até agora, se a absorção da insulina ocorria através de um ou mais mecanismos de transporte era ainda um facto desconhecido, uma vez que os estudos que elucidavam os mecanismos de absorção da insulina não usavam modelos celulares intestinais que representam simultaneamente os enterócitos, as células de goblet e as células M. A permeabilidade das nanopartículas contendo insulina diminuiu após redução da temperatura e após co−incubação com clorpromazina, sugerindo um transporte ativo da insulina por endocitose mediada por clatrina. Além disso, a inibição da permeabilidade com o pré−tratamento com clorato de sódio sugeriu que a interação entre o glicocálice e as nanopartículas foi crítica para a permeação de insulina.

ABSTRACT

The oral route is the most suitable and physiological delivery route. Oral insulin able to induce an efficient antihyperglycemic effect either to replace or complement diabetes therapy is the major goal of health providers, governments and diabetic patients. Oral therapy is associated not only with the desire to exclude needles from the daily routine of diabetic patient but also with the physiological provision of insulin they would get, resulting in a better glucose homeostasis. However, it is limited by various physiological barriers and despite the numerous efforts over the past few decades to develop insulin delivery systems, there is still no commercially available oral insulin. The desire to deliver insulin by the oral route in a conveniently and effectively way has led to the intense investigation of new delivery systems.

The understanding of the effect of nanoparticles (NP) on enhancing insulin therapeutic effect after oral delivery is crucial for the design of an adequate delivery system. This thesis emerged in this context and aims to develop a nanodelivery system with suitable physical characteristics for oral insulin administration, by evaluating its behavior across the gastrointestinal (GI) tract and at the cellular level.

First, insulin−loaded alginate/dextran sulfate−based NP (ADS−NP) produced by the emulsification/internal gelation technique were developed in order to achieve a biopolymer−based nanosystem with the required physical properties for oral delivery. The effect of the emulsion droplet size on the resultant particles was carefully evaluated, while probing the activity of insulin after each step of the process. There was a decrease in the emulsion droplet size when ultrasonication was used during emulsification, which was more pronounced when a cosurfactant was added. The interactions between the biopolymers and insulin were predicted using molecular modeling studies through quantum mechanics calculations that allowed for the prediction of the interaction model. The *in vitro* release studies indicated well−preserved integrity of the NP in simulated gastric fluid (SGF) and the conformational stability of insulin was ensured by circular dichroism (CD) spectroscopy and Fourier transform infrared (FTIR) spectroscopy technique (Chapter 2). Biopolymers have an important effect on the NP' properties and may have influence on their biological behavior. Polycationic biopolymers such as chitosan (CS) can be used to crosslink with polyanionic alginate−based NP to provide them the ability to improve bioadhesion and permeability at

the cellular level. In this sense, a rational study involving the CS coating of the NP to enhance their physicochemical parameters was explored (Chapter 3).

Giving the high surface area−to−volume ratio of NP, the factors influencing their GI uptake, more precisely their size and aggregation phenomena, were studied across simulated GI fluids. The individual effects of the CS coating, as well as the further coating of albumin (ALB), were carefully evaluated. The application of ALB as an outermost coat to the CS−coated NP was carried out, since ALB has revealed to act as a sacrificial target to avoid insulin degradation by preventing proteases from accessing insulin within the NP, and by stabilizing the NP either in the acidic or intestinal environment. Then, the effect of the NP on enhancing the insulin *in vitro* permeation through the intestinal membrane was also evaluated, using *in vitro* models of Caco−2, Caco−2/HT29−MTX and Caco−2/HT29−MTX/Raji B co−cultures (Chapter 4). The double coating with CS and ALB was successfully achieved, taking advantage of their protective, mucoadhesive and absorption−enhancing properties. The ALB application showed to provided better NP' size stability in GI conditions with less aggregation and more uniformity of size distribution, preventing the release of the majority of insulin in the gastric pH and sustaining the release in the intestinal pH to allow insulin to be released in the sites of absorption. In the cellular experiments, the NP were found to significantly increase the permeability of insulin across the *in vitro* models, a pattern that was in accordance with the insulin release profile.

Then, the ability of this nanosystem to improve the oral pharmacological availability (PA) of insulin in both the type 1 DM (T1D) and type 2 DM (T2D) animal models was for the first time carried out (Chapter 5). There was a significant antihyperglycemic effect after oral administration for both models, although the antihyperglycemic effect lasted longer in the model of T1DM. The biodistribution of the NP was also evaluated, revealing an augmented interaction of the NP with the small intestinal walls, which could be explained by the mucoadhesive properties of CS.

Finally, in this thesis, the effectiveness of the insulin−loaded NP on the insulin permeability across intestinal epithelial cells was thoroughly assessed. A systematic evaluation of the cellular and molecular mechanisms used by the NP to transport insulin across the intestine was performed (Chapter 6). So far, whether the insulin uptake occurred through one or more pathway was still unknown, since the studies elucidating the absorption mechanisms of insulin did not make use of cell−based intestinal models that

reproduce the enterocytes, and goblet and M cells simultaneously. The permeability of the insulin−loaded NP was reduced after the temperature was decreased and after co−incubation with chlorpromazine, suggesting an active insulin transport by clathrin−mediated endocytosis (CME). Moreover, the permeability inhibition with the pre−treatment with sodium chlorate suggested that the interaction between the glycocalix and the NP was critical for the insulin permeation.

LIST OF PUBLICATIONS

Lopes, M. A.; Abrahim, B. A.; Rodrigues, C. R.; Cabral, L. M.; Veiga, F.; Ribeiro, A. J. Alginate−based micro and nanoparticles coated with chitosan. Journal of Chitin and Chitosan Science 2013;1(3):1−4.

Lopes, M. A.; Abrahim, B. A.; Cabral, L. M.; Rodrigues, C. R.; Seiça, R. M. F.; Veiga, F. J.; Ribeiro, A. J. Intestinal absorption of insulin nanoparticles: Contribution of M cells. Nanomedicine: Nanotechnology, Biology and Medicine 2014;10(6):1139−1151.

Lopes, M. A.; Abrahim, B. A.; Seiça, R; Veiga, F.; Rodrigues, C. R.; Ribeiro, A. J. Intestinal uptake of insulin nanoparticles: Facts or myths? Current Pharmaceutical Biotechnology 2014;15:629−638.

Lopes, M. A.; Simões, S.; Veiga, F.; Seiça, R.; Ribeiro, A. Why most oral insulin formulations do not reach clinical trials. Therapeutic Delivery 2015;6(8):973−987.

Lopes, M. A.; Abrahim−Vieira, B.; Oliveira, C.; Fonte, P.; Souza, A. M. T.; Lira, T.; Sequeira, J. A. D.; Rodrigues, C. R.; Cabral, L. M.; Sarmento, B.; Seiça, R.; Veiga, F.; Ribeiro, A. J. Probing insulin bioactivity in oral nanoparticles produced by ultrasonication−assisted emulsification/internal gelation. International Journal of Nanomedicine 2015;10:5865−5880.

Lopes, M. A.; Derenne, A.; Pereira, C.:; Veiga, F.; Seiça, R.; Sarmento, B.; Ribeiro, A. J. Impact of *in vitro* gastrointestinal passage of biopolymer−based nanoparticles on insulin absorption. RSC Advances 2016;6:20155−20165.

Lopes, M. A.; Shrestha, N.; Correia, A.; Shahbazi, M.−A.; Sarmento, B.; Hirvonen, J.; Veiga, F.; Seiça, R.; Ribeiro, A. J.; Santos, H. A. Dual chitosan/albumin−coated alginate/dextrane sulfate nanoparticles for enhanced oral delivery of insulin. Jornal of Controlled Release 2016;28:29−41.

Lopes, M. A.; Aniceto, D.; Abrantes, M.; Simões, S.; Branco, F.; Vitória, I.; Botelho, M. F.; Seiça, R.; Veiga, F.; Ribeiro, A. *In Vivo* biodistribution of antihyperglycemic biopolymer−based nanoparticles for the treatment of type 1 and type 2 diabetes. (Submitted)

Other manuscripts not included in the thesis

Pupe, C. G.; Do Carmo, F. A.; De Sousa, V. P.; **Lopes, M. A.**; Abrahim−Vieira, B.; Ribeiro, A. J.; Veiga, F.; Rodrigues, C. R.; Padula, C.; Santi, P.; Cabral, L. M. Development of a doxazosin and finasteride transdermal system for combination therapy of benign prostatic hyperplasia. Journal of Pharmaceutical Science 2013;102(11):4057−4064.

Lopes, M. A.; Abrahim, B.; Veiga, F.; Seiça, R.; Cabral, L. M.; Ribeiro, A. J. Alginate−based micro− and nanoparticles: biocompatibility and biodegradability. In: Taylor & Francis Group. Encyclopedia of Biomedical Polymers and Polymeric Biomaterials: Taylor & Francis Group; 2014.

Silva, A. M.; Abrahim−Vieira, B.; do Carmo, F. A., do Amaral, L. H.; Silva, L. C.; Escudini, C. S.; **Lopes, M. A.**; Sousa, V. P.; Castro, H. C.; Veiga, F.; Rodrigues, C. R.; Ribeiro, A. J.; Cabral, L. M. Segregated delivery of rifampicin and isoniazid from fixed dose combination bilayer tablets for the treatment of tuberculosis. British Journal of Pharmaceutical Research, 2014;4(14):1781−1801.

Lopes, M. A.; Abrahim, B.; Veiga, F.; Seiça, R.; Cabral, L. M.; Arnaud, P.; Andrade, J. C.; Ribeiro, A. J. Preparation methods and applications behind alginate−based particles. Expert Opinion on Drug Delivery.

LIST OF ABBREVIATIONS

AAC	Area above the curve
ACN	Acetonitrile
ADS	Alginate/dextran sulfate
ALB	Albumin
ANOVA	Analysis of variance
BA	Bioavailability
(Asp−co−AspPBA)	b−poly(aspartic acid−co−aspartamidophenylboronic acid)
b−P(PBDEMAco−PyBDEMA)	Blockpoly([2−phenyl boronic esters−1,3−dioxane−5−ethyl] methylacrylate−co−[2−pyrenyl boronic
esters−1,3−dioxane−5−	ethyl] methylacrylate)
$CaCl_2$	Calcium chloride
CD	Circular dichroism
CME	Clathrin mediated endocytosis
C_{min}	Minimum glucose concentration in the blood
C_o	Concentration of insulin in n−octanol phase
CS	Chitosan
C_w	Concentration of insulin in water phase
DGAV	Direcção Geral de Alimentação e Veterinária
DLS	Dynamic light scattering
DMSO	Dimethyl sulfoxide
DSC	Differential scanning calorimetry
DTPA	Diethylene triamine pentaacetic acid
EDC	1−ethyl−3−(3−(dimethylamino)−propyl)−carbodiimide
EDTA	Ethylenediamine tetraacetic acid
EE	Encapsulation efficiency
FAE	Follicle associated epithelium
FBS	Fetal bovine serum
FE	Field environmental
FELASA	Federation of European Laboratory Animal Science Association

FITC	Fluorescein isothiocyanate
FTIR	Fourier transform infrared
GI	Gastrointestinal
GK	Goto−kakizaki
IGTT	Intraperitoneal glucose tolerance test
HBSS	Hank's balanced salt solution
HEM	Hydroxy ethyl methacrylate
HEPES	4−(2−hydroxyethyl)−1−piperazineethanesulfonic acid
HLB	Hydrophilic–lipophilic balance
HOMO	Highest occupied molecular orbital
HPLC	High−performance liquid chromatography
ITLC	Instant thin−layer chromatography
LC	Loading capacity
LD	Laser diffraction
LUMO	Lowest unoccupied molecular orbital
MAA	Methacrylic acid
MES	2−(*N*−morpholino)−ethanesulfonic acid
NaCac	Sodium cacodylate buffer
NEEA	Non−essential amino acids
NHS	*N*−hydroxysuccinimide
NP	Nanoparticles
NS	Not studied
PA	Pharmacological activity
P_{app}	Apparent permeability
PBS	Phosphate buffered saline
PCL	Poly(−ε−caprolactone)
PEG	Poly(ethylene glycol)
PdI	Polydispersity index
pI	Isoelectric point
PIDS	Polarization intensity differential scattering
PLGA	Poly(lactic−co−glycolic acid)

PNIPAM−b−P(Aspco−AspPBA)	Poly(N−isopropylacrylamide)−b−poly(aspartic acid−coaspartamidophenylboronic acid)
$P_{o/w}$	Water partition coefficients
PP	Peyer's patches
QA	Quaternary ammonium
RIA	Radioimmunoassay
S.c.	Subcutaneous
S.d.	Standard deviation
SEM	Scanning electron microscopy
SGF	Simulated gastric fluid
SIF	Simulated intestinal fluid
SLN	Solid lipid nanoparticles
SPC	Soybean phosphatidylcholine complex
STZ	Streptozotocin
T1D	Type 1 diabetes
T2D	Type 2 diabetes
TEER	Transepithelial electrical resistance
TFA	Trifluoroacetic acid
TJ	Tight junctions
TEM	Transmission electron microscopy
TMC	N−trimethyl chitosan
TMC−Cys	Trimethyl chitosan−cysteine
T_{min}	Time of minimum glycemia
TPP	Tripolyphosphate
W/O	Water−in−oil
WGA	Wheat germ agglutinin
$[\theta]_{MRW}$	Mean residue molar ellipticit
γ−PGA	Poly(γ−glutamic acid)
ζ−potential	Zeta potential
^{99m}Tc	Technetium−99m

LIST OF FIGURES

control ($^{*}p < 0.05$, $^{**}p < 0.01$, and $^{***}p < 0.001$). Error bars represent mean ± s.d. (n ≥ 3).

LIST OF TABLES

CHAPTER 1

GENERAL INTRODUCTION

1.1 INTESTINAL ABSORPTION OF INSULIN–LOADED NP: CONTRIBUTION OF M CELLS

1.1.1 Insulin – The pathway for oral administration

Diabetes is a chronic disease that has assumed epidemic dimensions around the world. Insulin administration is indispensable for the treatment of T1D patients and is required at a later stage in patients with T2D [1]. Currently, the most predictable and traditional method for administrating insulin is the parenteral route, specifically subcutaneous (s.c.) injections. However, nonparenteral routes of administration would minimize the health hazard created through repeated injection of insulin, surpass complications arising from the necessity for sterile techniques associated with parenteral formulations and could provide a more suitable way of controlling insulin release profile. Despite the limited success of these routes, the desirability of oral insulin encourages the continuation of the research [2]. The convenience of an oral pill would improve patient compliance to insulin therapy, and therefore, better metabolic control would be achieved as well as the reduction of diabetes–related complications and all of their consequences. However, the enhanced quality of life allowed by oral insulin is not the only characteristic that makes oral insulin the most desirable route.

The general therapeutic goal of insulin therapy is to reproduce, as accurately as possible, the physiological pattern of insulin secretion to control glycemia (which generally fluctuates between 4 and 8 mmol/L during the course of a day) [3], avoiding the complications arising from hyperglycemia [4]. Under normal physiological conditions, the liver receives a maximum of 75% of its blood from the digestive tract (portal veins), which contains 100% of the insulin produced by the pancreas. Subsequently, insulin is shed into the liver in response to elevated blood sugar. Thus, the liver metabolizes 50 to 75% of secreted insulin [5]. However, the liver only receives 25% of its blood supply from the heart via the hepatic artery, therefore only 25% of the s.c. insulin reaches the liver [6], which is its primary site of action [7]. Therefore, the oral route is the most convenient and physiologically relevant alternative, since after GI absorption, insulin may be taken up by the gut–associated lymphoid tissue. This causes it to undergo the first hepatic bypass, which provides better glucose homeostasis.

Overall, oral insulin is the optimal method of insulin delivery, as it is secure, makes

the hormone available in a way that compensates for the metabolic abnormalities of diabetes and is psychologically and socially acceptable [8].

After oral administration, insulin encounters several issues including proteolytic degradation and poor absorption through the intestinal mucosa. This is mainly due to its particularly high molecular weight, hydrophilicity and surface charge [9,10]. As with other peptides, insulin shows poor physical and chemical stability and a relatively short plasma half−time [11]. Therefore, strategies to enhance the oral BA of insulin have been developed, which include the use of absorption enhancers [10,12], enzyme inhibitors [13−16], chemical modifications [17,18], cell penetration peptides [19], vitamin B12 [20,21], conjugation of cyclodextrin [22], polymeric carriers [23,24], liposomes [25,26] and colon targeting where the enzymatic activity is relatively low [27,28].

The use of particulate systems is a promising strategy to improve the oral delivery of insulin. Insulin that is encapsulated in NP is less sensitive to enzymatic degradation [29] since its association with polymers facilitates better absorption through the GI tract compared to its native counterpart [30]. Consequently, the submicron size carrier favors the absorption of insulin through the intestinal membranes [29,31].

Several NP formulations have been disclosed to be able to protect insulin in the GI tract pH range and exposure to digestive enzymes [32−34]. Therefore, intestinal absorption of insulin−loaded NP is considered the main obstacle to be overcome. Thus, it is essential to better understand how insulin−loaded NP are trafficked through the intestinal epithelium by using translational *in vitro* or *in vivo* models whenever possible. Only a few orally administered NP are taken up across the intestinal epithelium and able to attain their pharmacological target [35,36]. Interactions between NP and biological barriers are extremely complex and several studies have been performed to elucidate the role of the intestinal cells in the transport of insulin−loaded NP. Some of these studies [37−39] have implicated M cells involvement in this process. However, many intestinal absorption studies have been performed using NP possessing peculiar physicochemical characteristics, in specific models and experimental conditions, which not allow the results to be accurately compared.

Intestinal absorption studies of insulin−loaded NP will be explored, followed by a critical analysis of the contribution of M cells in order to better understand the role of these specific cells. Redundancy was avoided, however, in some studies, i.e., experiments

assessing enterocytes and M cell uptake of insulin−loaded NP, the same formulation may appear in different sections.

1.1.2 Probing insulin−loaded NP pathways through the intestinal epithelium

The uptake of nanosystems through the GI tract is a well−known and accepted phenomenon on which excellent reviews have been published [3,40].

The study of the intestinal absorption pathways of insulin−loaded NP is mandatory since the administration of NP has led to antihyperglycemic effects. Different coexisting mechanisms allow insulin−loaded NP to be taken up by the intestinal epithelium, although uptake depends on the nature of the polymers and the coating material utilized. As a matter of fact, the properties of NP including size, charge and tendency to aggregate determine and define their uptake by intestinal cells. There is a tendency to increase the use of *in vitro* studies due to: the evolution of these same models, biological closure of the human intestinal epithelium and the possibility of simultaneously studying a large number of formulations.

The increasing usefulness of cell culture models that mimic the human intestinal epithelial barrier provides an ideal system for the rapid assessment of the intestinal permeability of drug candidates [41]. Further improvement of the permeability of candidate NP for oral delivery can be obtained if they are previously submitted to the GI tract environment. Therefore, the results will reveal a higher *in vitro*/*in vivo* correlation. Among the several human cell lines, Caco−2, HT29−MTX and Raji B cells have been considered for the screening of insulin−loaded NP as intestinal carriers, due to their ability to express morphologic features of mature enterocytes, goblet cells and M cells, respectively [42,43]. A schematic representation of the cell culture models that have been used to assess intestinal absorption of insulin−loaded NP can be seen in Figure 1.1.

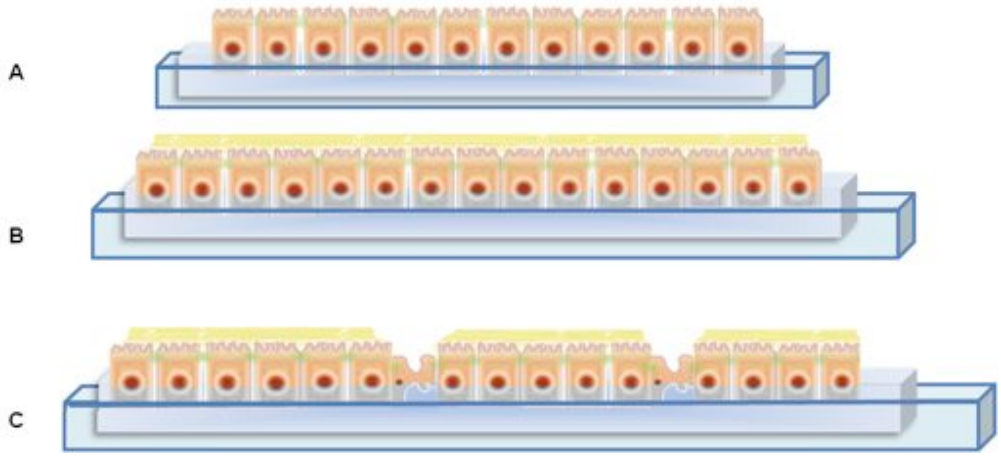

Figure 1.1. Schematic representation of the culture model systems utilized. (A) Human colonic epithelial cells (Caco−2) monolayer. (B) Co−culture of Caco−2/HT29−MTX mucus−producing goblet cells. (C) Triculture of Caco−2/HT29−MTX/Raji B cells.

Although Caco−2 cells monolayer (Figure 1.1A) is probably the most used *in vitro* model to assess NP crossing properties through enterocytes, these cells are not able to produce mucus. The co−culture of Caco−2 cells with mucus−secreting cells (Figure 1.1B) has disclosed the important role of HT29−MTX mucus producing goblet cells in insulin absorption [37,44,45]. An intimate contact of nanoencapsulated insulin to the intestinal mucosa has been described by the diffusion theory of mucoadhesion related to interpenetration and entanglement of NP polymer chains within the mucus layer [43]. Thus, the addition of mucus−producing cells to the monolayer provided a better simulation of the natural conditions, which contribute to insulin−loaded NP absorption [31].

The triple co−culture Caco−2/HT29−MTX/Raji B lymphocytes mimics in a more accurately way the small intestinal epithelial layer (Figure 1.1C), representing an *in vitro* model of the human follicle associated epithelium (FAE). Several studies revealed the ability of this triple co−culture model to transport NP [46−49]. The apparent permeability (P_{app}) coefficient values of nanoencapsulated insulin across the *in vitro* cellular model correlated well with the fractions of nanoencapsulated insulin that permeated the *ex vivo* model of the rat intestinal mucosa. Consequently, *in vitro* experimental models are available to effectively probe intestinal pathways that can be exploited for the transport of NP, particularly

insulin−loaded NP.

The microvilli present on the absorptive mucosal cells of the small intestine provide extended surface area for the absorption of NP after which they enter the bloodstream or lymphatic circulation [50]. After NP uptake by M cells, two main hypothesis can be considered [51], as can be seen in Figure 1.2 and 1.3. In the first, insulin is transported, free or encapsulated, to capillary vessels in the center of the villi and then carried to the portal circulation where it first reaches the liver. The insulin eventually results in first−pass metabolism by the hepatic enzymes before it reaches systemic circulation. In the case of insulin−loaded NP, when following this route, they are expected to behave similarly to the physiologic insulin. The other hypothesis consists of NP transport by the mesenteric lymph nodes in the center of the villi, which are situated next to the blood vessels, and then deliver to the systemic circulation by the thoracic duct. Here, insulin−loaded NP would act similarly to s.c. injected insulin [6]. Several studies in rodents [48,49] and pigs [48] have identified that the size of Pluronic® −stabilized polypropylene sulfide and expansile polymer NP must be between 25 and 100 nm in order to be transported by the lymphatic system. Other studies have characterized additional promigratory criteria using poly(lactic−co−glycolic acid) (PLGA) NP, with migration properties and lymphatic nodal retention directly related to the anionic charge since there is less particle aggregation and greater lymphatic uptake [52]. Similarly, rapid lymphatic migration of 50 nm of the above−mentioned expansile polymer NP was observed, which can be attributed to their smaller size and more negative ζ−potential when compared to nonmigratory 100 nm NP [48]. These studies confirm the impact of NP properties, including size, surface charge and aggregation, on their lymphatic migration. The influence of protein−loaded NP properties on the post−intestinal epithelium pathways remains unclear and the use of a lipoprotein assembly Caco−2 cells model may be useful in determining the effects of NP composition on the lymphatic transport of insulin [53].

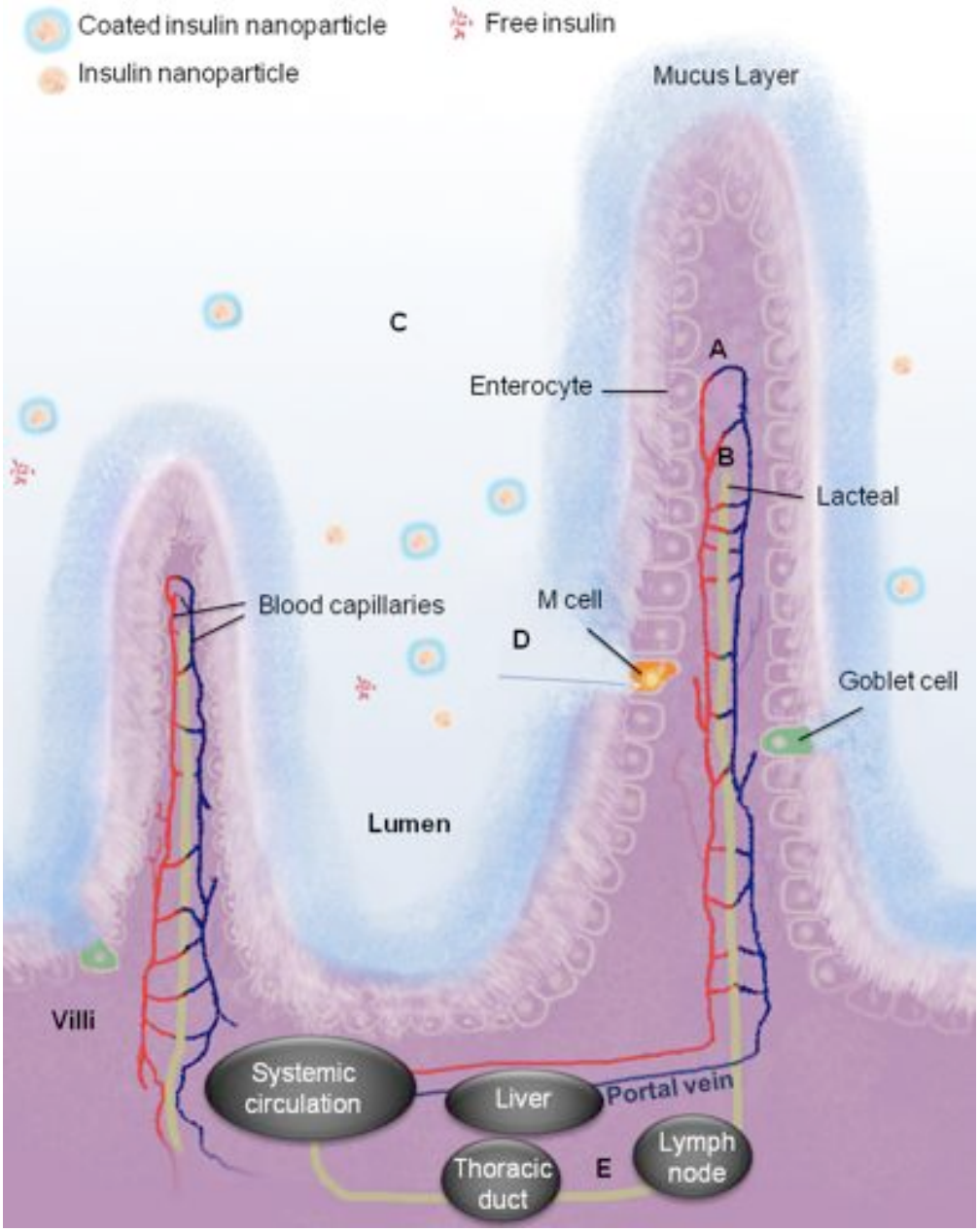

Figure 1.2. A diagrammatic representation (particles not drawn to scale) of some intestinal structures where the flow and transport of NP can occur. This can be in the direction of the (A) blood and (B) lymphatic flow. Following oral administration, insulin–loaded NP may (C) flow into the GI tract, (D) access and adhere to M cells of the Peyer's patches (PP) or enterocytes and (E) flow into the lymph vessels and entrap in the lymphatic pathway.

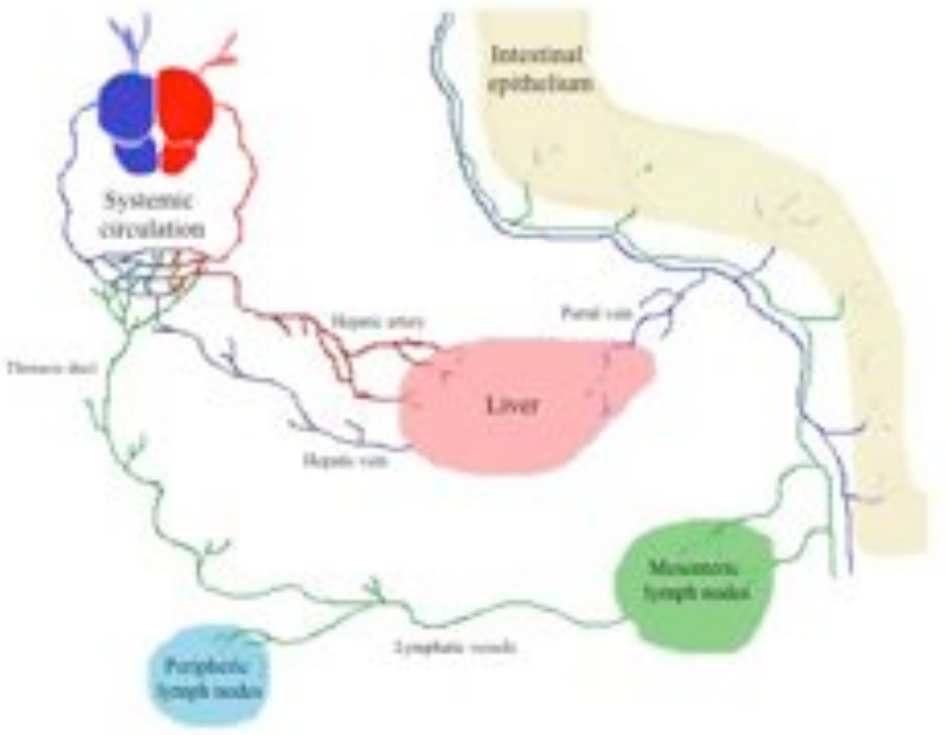

Figure 1.3. The possible pathways for insulin–loaded NP to reach the systemic circulation after intestinal uptake.

Once in the blood, NP might interact with erythrocytes, which can lead to increased particulate circulation times and thus marginally affect the circulation half–life of the erythrocytes themselves [54]. More research is needed to study the influence of NP on the flow of the systemic and lymphatic circulation. This is especially important to consider in the bifurcating and complex networks of the capillaries and in tissues. Because not all NP are spherical, it is a priority to understand their flow and deposition patterns as well as their aggregation potential. The shape of particles is an important consideration and can have an influence on the rate of cellular uptake, circulatory system and body distribution [55].

1.1.3 Pathways of insulin–loaded NP across the intestinal epithelium

The epithelium of the GI tract is composed of various cell types and the ease of permeation varies depending on the cell type. In the small intestine, the surface area is enlarged by folds, villi and microvilli (the brush border), which play an important role in the absorption of NP. The epithelium covering the villi is composed of approximately 85% absorptive cells and the additional 15% is a mixture of mucus–secreting globet, antimicrobial, peptide–secreting and endocrine cells. Interspersed between the villi are isolated lymphoid follicles or their aggregates, PP, which contain specialized M cells. M cells differ from columnar enterocytes since they have an underdeveloped microvillus and glycocalyx structures and contain apical microfolds, increased intracellular vacuolization and no mucus [56].

Figure 1.4 schematically illustrates intestinal structures and the different pathways that have been hypothesized to be involved in the transport of either free and/or NP–associated insulin. These pathways include: A) paracellular transport; B) transcytosis through enterocytes; C) receptor–mediated transcytosis; and finally, D) the transcellular pathway used by M cells in the PP.

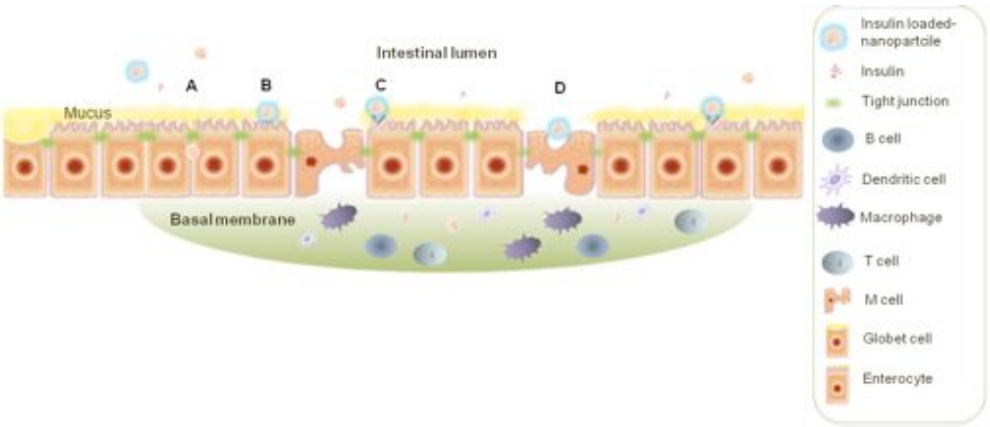

Figure 1.4. Schematic representation (particles not shown to scale) of the intestinal structures and the route of NP absorption across the intestinal epithelium: (A) paracellular transport; (B) transcytosis through enterocytes; (C) receptor–mediated transcytosis; and finally, (D) the transcellular pathway used by the M cells in the PP.

NP do not diffuse through the paracellular route, although NP' components, such as CS, can affect tight junctions (TJ) structure [3,57,58]. Rather, NP can be taken up by M cells, which demonstrate significantly higher transport activity than do enterocytes. According to the physicochemical properties of the NP and the nature of the target cells, two main absorption pathways may be utilized: either phagocytosis or the other endocytic pathways (i.e., clathrin− and caveolae−mediated endocytosis). The main assembly unit is clathrin, a cytosolic coat protein. CME occurs either via specific receptor–ligand interactions or via non−specific endocytosis [59]. Specific CME involves a concentration of high−affinity transmembrane receptors and their bound ligands within "coated pits" in the plasma membrane. Coated pits invaginate until the vesicle fission occurs, which requires the GTPase dynamin to form endocytic vesicles (100 to 120 nm). They are encapsulated by a polygonal clathrin coat and carry concentrated receptor–ligand complexes into the cell [3]. When CME involves non−specific charge or hydrophobic interactions with the cell membrane, it is considered to be a nonspecific adsorptive pinocytosis. In both cases, after the formation of vesicles, early endosomes are acidified by ATP−dependent proton pumps and the fusion occurs with late endosomes where the cargo will be degraded [59−61]. Both CME and phagocytosis are receptor−mediated uptake processes, and macropinacytosis is also an active, actin dependent process used for transferring large volumes of particles−containing fluid [62].

A systematic evaluation of the intestinal absorption studies for insulin−loaded NP, based on the characterized pathways, was performed. For some NP formulations, several reported pathways were based on previous works or disclosed properties of the NP' polymers rather than confirmed experimentally. For example, the absorption of insulin−loaded NP is often justified by the mucoadhesive properties of the NP' polymers without performing mucoadhesion studies of insulin−loaded NP, either intact or previously submitted to the GI tract. As a consequence, it may happen that the influence of parameters such as insulin loading, absorption enhancers and/or polymers interactions may have been neglected.

The reproducibility of the results is a main concern in the area of nanotechnology since many different characteristics of NP can affect the results. Thus, in order to keep focused on insulin−loaded NP intestinal absorption studies, whenever NP' properties such as size or charge, among others, were considered crucial for discussion of results, they were

discriminated.

1.1.3.1 Mucus layer

The major components of the mucus layer are glycoproteins (mucin), which act as a barrier to insulin−loaded NP absorption by stabilizing the unstirred water layer and the interactions between the diffusing NP and the components of the mucus gel layer [63−65]. The unstirred water layer separates the brush border membrane of the enterocytes from the bulk fluid phase of the small intestine lumen. Together with the intestinal mucus, the unstirred water layer forms an acidic microclimate adjacent to the brush border membrane, reducing the P_{app} of NP. NP in the bulk phase of the intestinal lumen must penetrate the unstirred water layer to closely contact with the cell membranes [66,67]. In addition to electrostatic interactions, mucoadhesion can arise from hydrophobic interactions, van der Waals interactions and polymer chain interpenetration [68].

Cationic polymers including CS and its derivatives, which coat NP with cationic groups or with mucin binding groups can form NP that maintain a prolonged contact time with the intestinal layer. This leads to a wide absorptive surface and subsequently enhanced absorption. Loaded NP, particularly with proteins such as insulin, are characterized by higher number of intermolecular interactions as compared to unloaded NP and the availability of less number of sites for mucoadhesion results in the reduction of the mucoadhesive properties. Still, several insulin−loaded NP have shown mucoadhesive properties as can be seen in Table 1.1.

Table 1.1. Composition of insulin−loaded NP formulations and impact of their mucoadhesivity on *in vitro* and *in vivo* intestinal absorption of insulin.

NP composition	Size (nm)	Study model	Outcome	Ref.
CS−coated alginate NP	750	*Ex vivo* Wistar rats	Retention of insulin on the mucosa due to NP' mucoadhesion and further	[69]

			insulin absorption appears to be demonstrated by the presence of FITC−insulin on the apical membrane of the intestine 3 h after administration.	
TMC−Cys NP	100−200	*In vitro* Mucin solution	TMC−Cys/insulin−loaded NP showed a 2.1–4.7−fold increase in the mucoadhesion compared to TMC/insulin−loaded NP, which might be partly attributed to disulfide formation between TMC−Cys and mucin.	[70]
TMC and PEGylated TMC NP	150−300	*In vitro* Mucin assay HT29−TX−E12 cells monolayer	Compared to TMC, insulin−loaded NP based on PEGylated TMC copolymers demonstrated no evidence of insulin uptake improvement due to complete release of insulin from NP after adhering to mucus.	[71]
Lauryl succinyl CS−based NP	315	*Ex vivo* Jejunum of rat intestine *In vitro* Caco−2 cells monolayer	Modified CS with both hydrophilic (succinyl) and hydrophobic (lauryl) moieties improved the release characteristics, mucoadhesivity as well as the absorption of insulin compared to the native CS−based particles.	[72]
ALB/CS−poloxamer 188−	300	*Ex vivo* Intestinal	The correlation of Caco−2/HT29 co−culture cells	[31]

coated ADS−NP		segments of Wistar rats *In vitro* Caco−2 cells monolayer and Caco−2/HT29 co−culture	with the animal−model intestinal membrane demonstrated that the mucus layer plays a significant role in determining the effectiveness of NP in delivering insulin.	
CS−coated SLN	450	*In vitro* Caco−2 cells monolayer and Caco−2/HT29 co−culture	The percentage of insulin transport for CS−coated SLN through the cells co−culture was higher than through Caco−2 monolayer, highlighting the enhancement of NP mucoadhesion properties due to CS.	[45]
CS/PLGA−based NP	135	*Ex vivo* Sprague−Dawley rats *In vivo* Sprague−Dawley rats	CS/PLGA−based NP exhibited stronger bioadhesive potency than PLGA–NP and much greater relative PA with regard to orally delivered insulin.	[73]

Abbreviations: FITC, fluorescein isothiocyanate; TMC−Cys, trimethyl chitosan−cysteine conjugate; TMC, N−trimethyl chitosan; PEG, poly(ethylene glycol); SLN, solid lipid nanoparticles.

Thiolated CS−based NP−bearing thiol groups [74] and TMC−Cys NP [70] with 100−200 nm have been described as mucoadhesion enhancers due to the formation of a disulfide bond between the cysteine−rich subdomains of the mucus layer and thiolated polymers.

The effect of a nanodelivery system was evaluated for the ability to enhance insulin

absorption through the intestinal epithelium. To accomplish this, different intestinal epithelial models were used including cell cultures and excised intestinal tissues [31,71−73]. The enhancement ratio of insulin transported by CS−coated SLN sizing 450 nm [75] and multilayered NP consisting of ALB/CS−poloxamer 188−coated ADS core sizing 300 nm [31] through Caco−2/HT29−MTX co−culture was approximately 3 and 3.7 times, respectively, than when transported through the Caco−2 cells monolayer. For the same co−culture system, it was found that the presence of mucus was propitious to the transport of insulin in TMC chloride NP (325 nm), which was further increased after CSKSSDYQC goblet cells targeting peptide modification [76]. These findings emphasize that the mucoadhesive properties of NP increase the concentration of insulin at the site of absorption and either its para− or transcellular absorption [75].

After injection of PEG−grafted SLN (commonly designated as pegylated SLN) sizing 190 nm into the Sprague–Dawley rat intestinal loop, they were found to permeate deeply into the villi [77]. The modification of the particle surface by the addition of PEG allowed poly(sebacic acid) NP (175 nm) to rapidly penetrate through the highly viscoelastic small intestinal mucus by facilitating its movement through the openings between mucin mesh fibers [78]. On the other hand, in the absence of PEG, poly(sebacic acid) NP would penetrate the mucus layer at a very low efficiency. Furthermore, these poly(sebacic acid) NP may be efficiently removed from mucosal surfaces as the mucus is cleared from the GI tract. This implies that PEGylated poly (sebacic acid) NP experience the low−viscosity environment of the interstitial fluid between the mucus mesh elements, which gives them the ability to rapidly penetrate secreted mucus [79].

The impact of mucin's role in the mucoadhesive properties of NP has been recently reviewed [32]. It seems clear and consensual that the role of mucin in NP transport is strongly dependent on NP composition [32,80] and an influence of the loaded protein cannot be excluded. When insulin is encapsulated with polymers capable of promote the mucoadhesion and prolong the contact time with the intestinal layer, wide absorptive surface and high concentration at the site of absorption are obtained.

Since NP immobilized by mucus can be cleared from the mucosal tissue, their size must be less than 500 nm [64] to avoid significant steric inhibition by the fiber mesh and adhesion to mucin fibers [79]. Concomitantly, NP should be mucoadhesive to prolong the retention time and contact with the intestinal mucosa [3]. Positive charged NP attract the

negatively charged mucin, however, as mentioned before, other type of interactions could occur between NP and the mucus layer.

1.1.3.2 Paracellular route

The paracellular route is limited due to restrictions in the permeation by TJ, which frequently block particles larger than 1 nm [81]. Additionally, the total area of the paracellular pathway, relative to the transcellular route, has been reported to range between 0.01% [82] and 0.1% [81]. The paracellular pathway can move insulin released from NP or incorporated on crumbled NP, by allowing its passage through junctional complexes [83]. To improve NP paracellular transport, the TJ must be reversibly opened using absorption enhancers including: cationic (polyethyleneimine, CS and its derivatives) and anionic (polyacrylic acid and its derivatives) polymers and calcium chelators (diethylene triamine pentaacetic acid [DTPA] and ethylene glycol tetraacetic acid [EDTA]) [40]. The opened TJ are less than 20 nm wide [84], therefore intercellular spaces remain limited in order to transport intact NP into the bloodstream. Those intact NP with a size of 150 nm, without disintegration, cannot permeate through the paracellular pathway in Caco−2 cells monolayer, even when their TJ are fully opened [25]. Therefore, it is difficult to expect that intact NP absorption can occur through the intestinal barrier along the paracellular route without unwanted secondary effects including irreversible opening of the TJ [3,40].

The colonic TJ are impermeable to molecules with radii larger than 8−9 Å. However, in the case of polypeptides with a high degree of conformational flexibility, as is the case of poly−D−glutamic acid, it is possible that even larger molecules are able to diffuse through the TJ. An absorption study of this model polypeptide across Caco−2 cells monolayer confirmed that the transport occurred through the paracellular pathway, since the EDTA treatment significantly increased its transport [85].

There are studies that report successful paracellular absorption of free or encapsulated insulin through the use of cationic polymers and also calcium chelation of NP, as can be seen in Table 1.2.

Table 1.2. Composition of insulin–loaded NP formulations and impact of their paracellular effect on *in vitro, ex vivo* and *in vivo* intestinal absorption of insulin.

NP composition	Size (nm)	Study model	Outcome	Ref.
CS–coated γ–PGA NP	250	*In vitro* Caco–2 cells monolayer	NP could transiently open the TJ between Caco–2 cells and thus increase the paracellular permeability.	[86]
CS/γ–PGA/TPP/ magnesium sulfate NP	220	*In vitro* Caco–2 cells monolayer	Insulin was more effectively transported with these NP than with TPP/magnesium sulfate–free NP; confocal visualization validated the enhanced absorption of insulin via the paracellular pathway.	[87]
Quaternized alkyl CS–based NP	200	*In vitro* Caco–2 cells monolayer	NP consisting of CS and its QA derivatives loaded with insulin were less effective in facilitating paracellular transport across Caco–2 cells monolayer than the corresponding free polymers.	[88]
Aspart–insulin loaded CS/γ–PGA NP	250	*In vitro* Caco–2 cells monolayer	NP could transiently and reversibly open the TJ between Caco–2 cells and allow the transport of aspart–insulin.	[89]
CS–based NP	NA	*In vitro* Caco–2 cells monolayer	The opening of the TJ by CS was transient and reversible, allowing the passage of soluble agents such as insulin.	[12]
CS/γ–PGA–DTPA NP	250	*Ex vivo* Segments of the small	NP may facilitate the paracellular absorption in the pH conditions from the proximal	[15]

	intestine	duodenum to the distal ileum along the intestinal tract.

Abbreviations: QA, quaternary ammonium; γ−PGA, poly(γ−glutamic acid); TPP, tripolyphosphate.

The mucoadhesive properties of NP facilitate their paracellular uptake, making somehow difficult to differentiate between both effects. The transepithelial electrical resistance (TEER) and the transport experiments demonstrated that multi−ion cross−linked NP (220 nm) composed of CS and γ−PGA blended with TPP and magnesium sulfate have the ability to significantly increase the paracellular flux of insulin. The visualization by confocal microscopy further validated that multi−ion cross−linkage could enhance NP absorption by this pathway [87]. While the addition of CS derivatives in free soluble forms can reversibly open TJ and thus increase insulin absorption, quaternized alkyl CS−based NP alone (200 nm) had only a minor effect on the TJ opening and on the paracellular transport of insulin across the Caco−2 cells monolayer. These data convincingly show that NP consisting of CS and its QA derivatives that are loaded with insulin are less effective in facilitating the paracellular transport across the Caco−2 cells monolayer than the corresponding free polymers. One possible explanation is due to the fact that CS derivatives in NP form have less positive surface charge and their interactions with TJ are limited [88].

Insulin-loaded NP coated with CS may transiently mediate TJ opening between the epithelial cells, while they become unstable and tend to degrade or break apart due to their sensitivity to pH. Insulin released from the fragmented NP, as can be seen in Figure 1.5, is then able to permeate the cells using the paracellular pathway until its release into the bloodstream, its ultimate destination [25,86]. Double−functional NP with tailored pH sensitivity and mucoadhesivity can be designed [89]. However, the properties of mucoadhesivity and pH sensitivity may not act synergistically, since in the stomach the positive charge of the mucoadhesive polymer may reduce NP stability [83], while in the intestine the pH−sensitive polymer would weaken the NP positive charge [90]. It was recently suggested that placing the double−functional NP into an enteric−coated capsule composed of Eudragit® S100 and L100−55, could promote the synergism and maintain the efficacy [83,91].

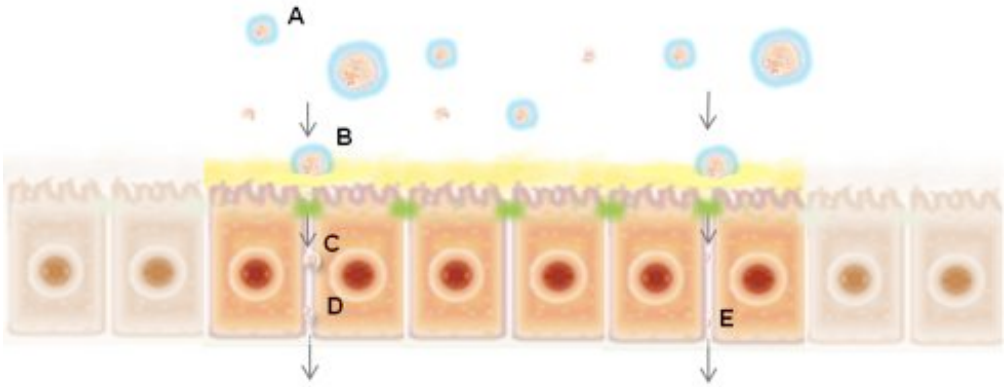

Figure 1.5. Schematic illustration (particles not shown to scale) shows the presumed mechanism of paracellular transport of insulin released from disintegrated CS−based NP. (A) pH−sensitive CS−based NP becoming (B) unstable and (C) broken apart, releasing (D) insulin. (E) Intact insulin−loaded NP can theoretically pass through opened TJ.

1.1.3.3 Transcellular route

The passage of insulin−loaded NP through the intestinal transcellular pathway may include passive, carrier−mediated (active or facilitated) and endocytic transport processes [92,93]. Theoretically, due to their size, insulin−loaded NP cannot permeate cells by passive diffusion, whereas the carrier−mediated route may occur when a NP' component interacts with key groups on the plasma membrane surface and binds reversibly to complexes. The bound molecule complex is then able to cross the plasma membrane to the inside of the cell. At this stage the bound molecule complex dissociates and passes to the basolateral side of the cell where the molecule forms a new complex with the bilayer and is then able to leave the cell [94].

Different types of endocytosis involve the formation of intracellular vesicles after invagination of the plasma membrane or ruffling which gives rise to larger vesicles [95]. Two main endocytosis mechanisms have been described for NP: phagocytosis, which is used to transport large particles; and pinocytosis, which is used to internalize fluid surrounding the cell. In regards to pinocytosis, all substances in the fluid phase area are simultaneously taken up [95].

Fluorescently labeled PLGA NP of 180 nm were incubated with the Caco−2 cells monolayer in order to study the uptake process and the intracellular fate of NP, assessed by flow cytometry and confocal laser scanning microscopy. The kinetics of absorption is time dependent and occurs by CME. Subsequently intracellular traffic leads to basolateral exocytosis of the NP [96]. Furthermore, NP endocytosis can be also mediated by adsorbing covalently conjugating ligands, including proteins or vitamins, to their surfaces. Then, insulin may be taken up by a receptor−mediated process as described by Bendayan *et al.* [97,98]. Shah and Shen [99] investigated the carrier−mediated transport of insulin across the Caco−2 cells monolayer. They observed that the transport of insulin−transferrin conjugate was mediated via the transferrin receptor and not through the insulin receptor. The study revealed that conjugated insulin transport across the Caco−2 cells monolayer was increased by 5− to 15−fold compared to free insulin.

Among several ligands available [100,101], some of them described in Table 1.3, we can find lectins [102], proteins that bind sugars reversibly and are involved in many cell recognition and adhesion processes [103]. Tomato lectin−conjugated NP resist the digestion process [104] and increase the bioadhesive and endocytic potential of latex particles [39,105]. Wheat germ agglutinin (WGA) specifically binds N−acetylglucosamine and sialic−acid [106] and has been described not only to bind to the surface of the Caco−2 cells monolayer and enterocytes, but also to be taken up by receptor mediated endocytosis. This process also involves the epidermal growth factor receptor that is expressed in considerable density on enterocytes [107]. Lectin insulin liposomes (190 nm) modified with a hydrophobic anchor, N−glut−PE, promoted the oral absorption of insulin due to the site−specific combination of the GI cell membrane [26] and vitamin B12−coated dextran NP (150−300 nm) improved the cellular uptake of absorptive enterocytes [108]. However, in both studies, the conclusions were based on PA rather than on experimental measurements of the intestinal absorption.

Despite the promising results with agents that increase specific receptor−mediated endocytosis, insufficient quantities of insulin−loaded particles are absorbed through the intestinal epithelium [40]. Ligand density on the particle surface is somehow difficult to reproduce and must be optimized to allow the cellular uptake in order to achieve optimal therapeutic efficacy.

Table 1.3. Composition of insulin−loaded NP formulations and impact of their transcellular contribution effect on *in vitro* and *in vivo* intestinal absorption of insulin.

NP composition	Size (nm)	Study model	Outcome	Ref.
Lectin−modified SLN	75	*In vivo* Sprague−Dawley rats	WGA−modified SLN enhanced the intestinal absorption of insulin sufficiently enough to drop the blood glucose level.	[102]
Vitamin B12−coated dextran NP	150−300	*In vivo* NOD/J mice	Insulin delivery was found to be predominantly vitamin B12 specific, as co−administration of excess of free vitamin B12 significantly reduced the hypoglycemic effects.	[108]
Quaternized alkyl CS−based NP	200	*In vitro* Caco−2 cells monolayer	The CS derivatives in NP form have less positive surface charge and their interactions with TJ are limited and hence insulin transport across the monolayer is more likely through the transcellular pathway.	[88]
QA moyeties−insulin nanocomplexes	120	*In vitro* Caco−2 cells monolayer	Insulin uptake was reduced by co−incubation with sodium azide, an active transport inhibitor.	[101]
PLGA NP	180	*In vitro* Caco−2 cells monolayer	CME of NP and intracellular traffic that leads to the basolateral exocytosis of NP was demonstrated.	[96]
Hyaluronic acid NP	180	*In vitro* Caco−2 cells	The efflux ratio of P_{app} (B to A) to P_{app} (A to B) less than 1	[100]

monolayer	demonstrated that hyaluronic acid NP−mediated the transport of insulin across the Caco−2 cells monolayer underwent active transport.

1.1.3.4 M cells

Among enterocytes in the villous epithelium, PP−independent M cells that share similar characteristics with the M cells originally found in the FAE were identified and termed villous M cells [109]. Due to their high transcytotic capacity and ability to transport NP [110], M cells offer a putative way for the oral delivery of nanoencapsulated peptides [111,112]. Villous M cells are recognized by Ulex europaeus agglutinin I lectin and M cell−specific NKM16−2−4 antibody, a marker of murine M cells, and represent an alternative internalization site, namely in the villi−containing portion of the intestine. The binding of orally administered NP to M cell lectins was studied in murine models and indicated that they are able to bind specifically to M cells and, to a lesser degree, enterocytes. However, the characterization of murine M cells by this lectin−binding pattern did not reflect the glycosylation patterns present on human M cells. Unfortunately, human M cells features, function, and differentiation from neighboring enterocytes are still not well understood [113].

Insulin−loaded NP may interact with M cells via both specific and non−specific receptor−mediated mechanisms. M cells are able to use CME [114,115], macropinocytosis [116] and phagocytosis [117] to uptake particles, as excellently reviewed elsewhere [3]. Nonspecific mechanisms allow insulin-loaded NP to interact selectively with M cells, as described for NP in general, and may depend on the surface charge and hydrophobicity of NP [118].

Several *in vitro*, *ex vivo* and *in vivo* studies showed partial or total intestinal absorption of insulin−loaded NP involving M cells (Table 1.4).

A pilot work demonstrated for the first time that insulin encapsulated in polyalkylcyanoacrylate NP with 285 nm remained biologically active after oral administration

in diabetic rats [119]. Those NP labeled with a tracer were administered in the lumen of an isolated rat ileal loop and were able to pass through the ileal mucosa via the paracellular pathway in the nonfollicular epithelium. The M cells and adjacent enterocytes in the PP were the predominant cells that took up the tracer [112]. The administration of the NP that were prepared using a blend of a biodegradable polyester poly(−ε−caprolactone) (PCL) [120,121] and a polycationic polymer (Eudragit® RS) (360 nm) increased the serum insulin levels and improved glycemia in response to a prolonged oral glucose challenge [38]. The mechanism of local absorption of insulin was examined using FITC−insulin. The FITC−insulin indicated that the NP strongly adhered to the intestinal mucosa. Insulin, either released and/or still inside the NP, appeared as isolated fluorescent particles or small clusters that were mainly concentrated in the PP. This agreed well with the hypothesis that lymphatic uptake occurred via M cells. After oral administration of alginate/CS−based NP (750 nm) containing FITC−insulin, fluorescence was observed on the surface of the M cells throughout the ileum. These data together with the longer antihyperglycemic response following oral administration of the insulin−loaded NP also suggested that they were taken up, at least partially, by the PP [69]. Similar conclusions were made by Yin *et al.* [70] following the detection of fluorescent particles or small clusters 15 min after oral administration of insulin−loaded TMC−Cys NP (100−200 nm). It was found that TMC−Cys NP induced increased the insulin transport through the rat intestine and promoted its internalization in the Caco−2 cells monolayer and augmented its uptake in the PP. The effect of these NP on facilitating the insulin transport was significantly higher than the corresponding soluble polymer. The transport of insulin−loaded TMC−Cys NP across the intestinal epithelium could be associated with lymphatic uptake of the PP via M cells among other pathways.

In order to better approach the absorption mechanisms of insulin−loaded ADS/CS/ALB NP (800 nm), FITC−insulin−loaded NP were tracked after injection into an *in situ* isolated intestinal loop and their uptake was monitored by spectrofluorometry and observation of intestinal mucosa cryosections [11]. The FITC−insulin concentration decreased as a function of time in the intestinal lumen and increased in parallel in the intestinal mucosa and mesenteric blood. This indicated that it passed from the intestinal lumen to the blood compartment. Insulin, either liberated from the NP in the intestinal lumen or still associated with the NP, could be taken up by the intestinal mucosa. This process mainly occurred at the tip of the villi where a physiological desquamation occurs in

the mature enterocytes. However, the PP were found to have the most intense labeling, which suggested that NP may be taken up by endocytosis of the M cell membrane. This labeling was more pronounced when compared to alternate strategies including PCL−Eudragit® RS insulin−loaded NP [38] or any type of alginate/CS−based NP [69]. The transport of insulin with the PP in the rat ileum also increased more than 2 times when it was delivered by TMC−Cys [70], ALB/CS−poloxamer 188−coated ADS core [31] and poly (acrylic acid−coacrylamide)/O−carboxymethyl CS−based porous NP [122]. In an attempt to assess the role of NP in the uptake of insulin and internalization by the small intestinal cells of Wistar rats, insulin and alginate were independently labeled with FITC and rhodamine B isothiocyanate, respectively. Following oral administration of the previously described insulin−loaded multilayered NP, the intestinal sections were observed, which revealed that the nanoencapsulated insulin permeated the intestinal mucosa by absorption into the enterocytes and uptake by the PP [123].

More recently, a Caco−2/HT29−MTX/Raji B lymphocytes triple coculture model was developed to obtain a simulated intestinal barrier [37]. This model with the mucus−producing properties and the M cells in the PP has been proposed to be a better system for assessing insulin absorption in a mechanistic manner. The small−scale size range is advantageous for assessing insulin absorption both in solution and associated with NP. It was found that the cocultured Caco−2/Raji B cells showed increased insulin permeability when compared to the Caco−2 cells monolayer. Still, no comparison between the permeability of insulin−loaded dextran sulfate/CS−based NP through the Caco−2/HT29−MTX and Caco−2/HT29−MTX/Raji B cells co−cultures could be performed to predict a more incisive role for the M cell−like Raji cells.

Among the possible strategies used for the oral delivery of insulin, SLN represent a promising approach. Besides their protective power against the GI tract, the carrier itself can be taken up, to a certain extent, by the epithelial cells or lymphoid tissues in the PP [124]. The concentration of insulin of WGA−modified SLN (< 100 nm) in the PP of jejunal or ileal tissues was higher than in the non−PP tissues, therefore we could conclude that most of the SLN were transported through the PP [125].

A size−dependent behavior of insulin liposomes containing sodium glycocholate suggested that the M cells uptake occurs for liposomes ranging in size between 150 and 400 nm. It was reported that phagocytic uptake by the M cells was the predominant mechanism

in the particle−facilitated absorption [126].

Additional studies that aim to evaluate the effect of the NP' components, such as the loaded therapeutic protein, on enhancing the insulin absorption through the PP rich in M cells are required. These studies should be expanded to mucoadhesive studies to better understand the role of the encapsulated protein either on mucoadhesion or uptake by M cells. Mostly conclusions are often based on previous results obtained with unloaded NP or standard behaved NP made of latex or polystyrenes, which are very far from the therapeutic active NP formulations.

Table 1.4. Results of intestinal permeability studies of insulin−loaded NP in the M cells−containing models.

NP Composition	**Size (nm)**	**Study model**	**Permeability quantification**	**Outcome**	**Ref.**
Polyalkylcyano−acrylate NP	285	*Ex vivo* Wistar rats	Iodine	NP were found in the intercellular spaces under the M cells where they were in close contact with the lymphoid cells.	[112]
Insulin−SPC nano−encapsulated in PLGA	200	*In vivo* Wistar rats	RIA*	Insulin–SPC NP showed a delay of insulin absorption in *in vivo* conditions; the posterior segment of the intestine (ileum) has been confirmed as the ideal site for the NP uptake, where abundant PP exist.	[111]
PCL/Eudragit® RS	360	*Ex vivo*	FITC	NP strongly adhered to	[38]

NP		Wistar rats		the intestinal mucosa and labeled insulin, either released and/or still inside NP, was mainly taken up by the PP.	
Alginate/CS−based NP	750	*Ex vivo* Wistar rats	FITC	Interaction of NP with the M cells of the PP suggested that NP gradient concentration on the FAE drove the absorption of the insulin.	[69]
ADS/CS/ALB NP	800	*Ex vivo* Wistar rats	FITC	NP strongly adhered to the villus apical enterocytes and markedly labeled the PP following their administration in an isolated intestinal loop.	[11]
Poly (acrylic acid−*co*−acrylamide)/*O*−carboxymethyl CS−based porous NP	NS	*Ex vivo* Sprague−Dawley rats	HPLC	The transport of insulin across the rat intestine and colon was enhanced around 2− to 3−fold after application of the (*O*−CMC)−based porous NP.	[122]
TMC−Cys NP	100−200	*Ex vivo* Sprague−Dawley rats *In vitro* Caco−2	HPLC	Compared to the insulin solution, TMC−Cys NP increased the insulin transport through the rat intestine by 3–12	[70]

		cells monolayer		folds, promoted the Caco−2 cells internalization by 8–13 folds, and augmented the uptake in the PP by 15–21 folds.	
ALB/CS−poloxamer 188−coated ADS NP	300	*Ex vivo* Wistar rats	FITC	Nanoencapsulated insulin permeated the intestinal mucosa by the internalization of NP in the enterocytes and uptake by the PP.	[31]
WGA−modified insulin SLN	<100	*In situ* Wistar rats	RIA*	The M cells containing−ileum contributed more to the absorption of insulin SLN.	[125]

Abbreviations: SPC, soybean phosphatidylcholine complex; RIA, radioimmunoassay; NS, not studied; HPLC, high−performance liquid chromatographic.

*Insulin quantification in plasma

1.2 INTESTINAL UPTAKE OF INSULIN–LOADED NP: FACTS OR MYTHS?

1.2.1 Insulin BA by means of NP

An extensive presystemic metabolism, inactivation in the acidic pH of the upper GI tract and poor penetration through the intestine membrane are responsible factors for the reduced BA of orally given peptide drugs. Accordingly, the improvement of the oral insulin BA is highly in demand. Different approaches have been explored, has already mentioned, although the obtained results are still lower than expected. There must be a balance

between NP characteristics to allow effective insulin delivery. Smaller particles are favorable to the diffusion and uptake, although they should be large enough to carry a favorable amount of insulin. The mucoadhesion prolongs the residence time of NP at the absorption sites, but can hinder the diffusion through the GI mucus layer [3]. Delivery systems capable of increase the residence time of insulin, that preserve its stability until it reaches the absorption site and enhance its permeability into the systemic circulation have been investigated and developed over the years, always with the ultimate goal of increasing the the insulin BA and PA. The hydrophilic, biocompatible and biodegradable properties of natural polymers, such as CS and alginate, make them a suitable choice to improve insulin oral BA. They improve the enzymatic resistance, preventing the insulin release at low pH. The bioadhesive properties of CS have proven to be essential in the development of bioadhesive insulin delivery systems in order to improve its BA by prolonging the residence time at the site of absorption. Therefore, the use of multifunctional polymers exhibiting permeation enhancing and mucoadhesive properties are considered a promising strategy. Depending on the polymer combinations, NP can be tailored to stabilize insulin, control the release kinetics, increase the oral BA and modulate the biological response [127,128]. The insulin−loaded NP BA and PA found for different formulations are represented in Table 1.5. In all cases, the oral BA and/or PA of insulin were found to be lower than its s.c. delivery. However, the oral insulin delivery action was sustained for a longer period of time and/or its biodistribution was modified. Compared to oral free insulin, the BA and PA of insulin−loaded NP were always higher, proving that nanoencapsulation protects insulin from the harsh environment of the GI tract and improves its absorption, leading it active to the final sites of action.

Table 1.5. The PA and/or BA of insulin−loaded NP.

Formulation (ref.)	**Size (nm)**	**Insulin dose (IU/kg)**	**PA (%)**	**BA (%)**	**Animal model**	**Animals' number (n)**	ζ−potential **(mV)**
PLGA−NP [73]	121.3 ± 13	15.0	7.6	NS	Sprague –Dawley	5	−1.7

CS−coated PLGA−NP [73]	134.4 ± 15	15.0	10.5		rats		+43.1
PLGA/Eudragit® RS/Hydroxypropyl methylcellulose phthalate NP [129]	285.6 ± 4.5	50	9.2	NS	Sprague –Dawley rats	3	+42.9
PCL and Eudragit® RS NP [38]	358 ± 12	50	NS	13	Wistar rats	8	+41.8
CS− and poly (γ−glutamic acid)−based NP coated with Eudragit® L100−55 capsule [83]	241.5 ± 13.8	30	NS	20	Wistar rats	5	+25.6
CS− and γ−PGA−based NP [15]	246.6 ± 4.8	30	NS	20	Wistar rats	5	+37.0
Alginate/CS−based nanoemulsion [130]	488	12.5 25 50	8.65 8.42 5.72	NS	GK rats	6	-55.6
CS−coated SLN [45]	470 ± 32	25	17.7	NS	Wistar rats	6	+34.2
CS/PEG/ALB−coated ADS NP [11]	812	25 50 100	42 21 10	NS	Wistar rats	8	+15.0
CS/PEG/ALB−coated ADS NP [123]	396	50	10.7	13	Wistar rats	6	−38.2
Dextran sulfate/CS NP [131]	527 ± 103	50 100	5.6 3.4	2.4 6 5.2 5	Wistar rats	6	−20.6
Alginate/CS NP [132]	551.67	10	43.6	NS	Albino	6	+25.70

	±45.5				rats		
CS NP [100]	123	10	10.2	NS	Wistar	8	NS
	± 40				rats		
	345		14.9				
	± 60						
	1061		7.3				
	± 200						
Self−emulsifying	264.7	2.5	15.2	NS	Beagle	3	NS
formulation [133]					dogs		
Vitamin B12−NP	160−	20	26.5	NS	Wistar	6	NS
conjugate [20]	250				rats		
CS NP[1] [134]	108	50	77.0	NS	Wistar	10	+30.0
	± 9				rats		
CS NP[2] [134]			2.57				

Abbreviations: GK, Goto−kakizaki.

[1]12 h fast/12 h fed, [2]free access to food for 24 h

1.2.1.1 Surface charge

It is still uncertain the role that the surface charge of NP plays in their non−specific transport by the enterocytes or M cells. In Table 1.5, it is difficult to found a relation between the NP charge and the insulin BA or PA, although positively charged NP showed the highest values of these parameters, whilst the lowest ones were obtained with negative NP. The slight negative surface charge associated with PLGA NP limit their ability to interact with the negatively charged plasmids and to the intracellular uptake. Therefore, CS−coated PLGA NP were prepared to enhance the insulin PA of the negatively charged PLGA NP. The PA of these two kinds of NP, PLGA NP and CS−coated PLGA NP, were 7.6 and 10.5%, respectively, at an insulin dose of 15 IU/Kg. CS−based NP are mucoadhesive due to the CS inherent cationic charges, which allow them to exhibit electrostatic attraction with the negatively

charged mucus (due to the presence of sialic−acid groups in the mucin). Furthermore, cationic NP increase the permeation by epithelial cells, which are equally negatively charged.

1.2.1.2 Size

The highest PA was obtained for 10 IU/Kg insulin−loaded alginate/CS NP (43.6%) and 25 IU/Kg insulin−loaded CS/PEG/ALB−coated ADS NP (42%), which to the best of our knowledge, were the maximum values reported until now. Amongst the other discriminated formulations displayed in Table 1.5, these NP presented the highest size (550 and 800 nm, respectively) as well as positive surface charges with the lowest absolute values. Theoretically, these NP would not be the most indicated to the oral delivery of insulin, since the reduction of the NP diameter leads to transcytosis increase [135]. Furthermore, low ζ−potential module values increase the repulsive interactions, leading to the formation of less stable NP with a less uniform size distribution [136]. It is admitted that the optimal size for NP to be taken up by the M cells would be below 1 μm [42], and more precisely below 200 nm [57,135]. The insulin BA can be improved by controlling the particle size along with prolonging the residence time of NP in the GI tract [137], although particles size is only one piece of the puzzle to achieve the desired PA. Han and coworkers studied the effect of CS−based NP size on the PA of oral delivery of insulin. Among particles of approximately 120, 350 and 1000 nm, the bigger particles had the lowest PA. Particles of 350 nm had more effect on reducing the glucose plasmatic levels than 120 nm, which raises doubts about the optimal particle size to improve the insulin PA.

1.2.1.3 Insulin dose

It is expected that the higher the BA obtained for oral insulin, the higher the PA. However, the results contradict this fact. For example, dextran sulfate/CS−based NP [131] with 50 IU/Kg of loaded insulin showed 2.46% of BA and 5.6% of PA, whereas a dose of 100 IU/Kg increased the BA to 5.25% but decreased the PA to 3.4%. Different formulations revealed an influence of insulin dose on its PA [11,130,131]. All cases appear to have consistent results with higher doses of insulin leading to smaller values of PA.

1.2.1.4 Food effect

The absorption of oral delivered insulin was affected by food ingestion, which decreased its PA [134]. Insulin loaded CS−based NP had a PA of 7% for 12 h fast/12 h fed state rats compared to a PA of 2.57% obtained for rats persisted in free access to food. If all the studies concerning the PA of oral insulin delivery are influenced in a similar manner as the described study, the results obtained so far are overestimated, since few evaluated the effect of food intake. One must keep in mind that the liver receives a maximum of 75% of its blood from the digestive tract (portal veins). After, the liver metabolizes 50 to 75% of the secreted insulin [5]. Therefore, the insulin levels in the peripheral blood after orally delivery of insulin do not reflect the pharmacokinetic properties as s.c. insulin administration. Instead of provide the relative BA of an oral insulin formulation, the relative biopotency is the value that should be stated when studying oral insulin delivery, which demands performance of adequately designed glucose clamp studies [138]. It appears that oral insulin has low relative biopotency, which is even more reduced after a meal. Low biopotency of oral insulin requires higher amounts of insulin comparatively with s.c. insulin and, therefore, higher costs, a fact that tends to be avoided by the pharmaceutical industry [138].

1.3 WHY MOST ORAL INSULIN FORMULATIONS DO NOT REACH CLINICAL TRIALS

1.3.1 Oral insulin: From the beginning

After the development of insulin in 1921, scientists and clinicians began the study of almost all of the alternative routes of insulin administration with the oral route as the most exciting option. Since the first and unsuccessful attempts of oral insulin made by Joslin in 1922, various ways for incorporating insulin in various substances and in various forms were developed to overcome the barriers that insulin undergoes in the GI tract [139]. The history and development of insulin since the early 1990s to the present are displayed in Figure 1.6. After the first scientific publication about oral insulin 92 years ago [140], there is still no oral insulin on the market. In fact, more than 50 years passed until the first study on an oral insulin formulation had been published [141]. Clinical trials are ongoing since 2000, and in 2014, a company received for the first time Phase III approval from the US FDA [142].

Unfortunately, the failure of oral insulin persists. Few insulin formulations designed for oral administration reach clinical trials. This review analyses the current status of oral insulin and focuses on the main reasons for failure of the formulations for oral administration of insulin.

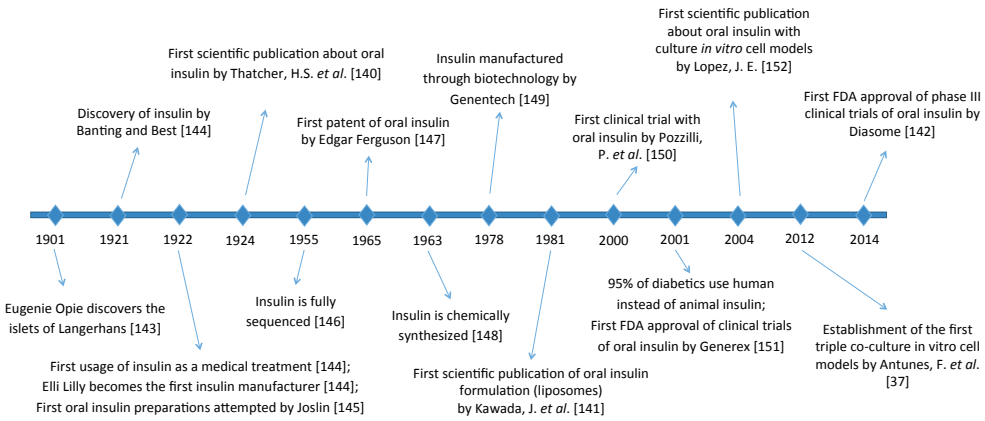

Figure 1.6. Timeline of the oral insulin history and development to the present day. The search engine Web of Science™ was used to search for scientific publications.

1.3.2 Obstacles for oral insulin: Industrial perspective

The main obstacles faced by oral insulin are the barriers across the GI tract (enzymatic, chemical and physical) until it reaches its final destination, the scaling up of the technology from the laboratory scale to pilot batches to the industrial scale and the cost/benefit ratio implied in its manufacturing. During the last three decades, great advances in protecting insulin in the GI tract were achieved, but the intestinal epithelium permeability is still the main obstacle to overcome. The rapid secretion and shedding of the GI tract mucus can significantly limit the effectiveness of insulin delivery systems [32]. Nevertheless, two parameters are of major concern: the scale−up potential of the production methodology and the amount of insulin required for therapeutic effects.

1.3.2.1 Scale–up

There are several techniques attempting to successfully achieve an oral insulin formulation, although most remain at the laboratory research level. Scaling the production process from the laboratory to the industrial level depends on the factors involved in the techniques, such as temperature, biodegradability and biocompatibility of excipients, use of organic solvents, energetic yield, simplicity, etc. A crucial inconvenience of most NP is the poor potential and reproducibility of particle production, which prevents the commercial/ clinical use of NP [153].

After the laboratory stage and before industrial–scale production, a pilot–scale stage should be performed. The pilot–size production intends to mimic the industrial production and should therefore integrate all the parameters that need to be optimized before reaching the industrial production [154]. The design and development of the scale–up are considered arduous because there is no framed algorithm to help the formulators to predict the large–scale performance of a product based on its small–scale behavior [155]. Furthermore, the process involves several formulation parameters to be modulated all simultaneously. There are few publications reporting the preparation of large amounts of NP for drug delivery applications [156–158], and according to the authors' knowledge, no studies have contemplated insulin formulations.

To fulfill challenges found during up–scaling studies, four basic parameters should be cogitated, beginning at the formulation development stage: process characterization, choice of equipment, development of robust formulation and stability studies [159]. The pathway to the market is extensive and includes the optimization of the therapeutic need, market demand, research and development, production steps, scale–up feasibilities, clinical trials and regulatory issues.

1.3.2.2 Cost–benefit ratio

The major concern about oral insulin lies in the potential reduction of its cost–benefit ratio. Earlier treatment and slower progression of the disease could potentially reduce the costs associated with diabetes–related complications. Oral insulin delivery is

expected to either replace or complement diabetes therapy. Cost reduction would be of great interest to health providers, payers and governments because the diabetic population keeps growing. The removal of the social stigma of insulin needles can guarantee the willingness of diabetic patients to purchase the product. This factor is not the only advantage provided by an oral insulin formulation, as detailed previously. Problems associated with oral insulin delivery systems include poor LC of insulin into the capsules [160]. The development of such delivery systems capable of improving the insulin LC and assuring full insulin biological activity would reduce the associated costs. Therefore, important obstacles in the engineering of micro− and nanosystems and in the achievement of high−efficiency persist, which should be evaluated to further acquire low−cost oral insulin delivery. This goal will depend on the ability to manufacture insulin in sufficient quantities for oral delivery and in an efficient cost−conscious pharmaceutical marketplace [161]. However, even if sufficient quantities of insulin are traduced in efficient costs, another concern arises if elevated doses of insulin are needed to achieve a therapeutic response, leading to the theoretical possibility of an insulin overdose [162].

Large−scale production of human insulin was achieved in 1982, when the first commercially available recombinant therapeutic protein was approved. It was due to engineering *Escherichia coli* to express human insulin by using recombinant DNA technology. The resulting insulin was abundant, inexpensive, of low immunogenicity and free from other animal pancreatic substances [163]. Since then, the cost of insulin production has remained relatively affordable. The actual reason for the increase in insulin prices is partly due to better options for insulin therapy. However, patents are expiring for several popular insulin formulas and, with competition, there is an expectation that the costs of insulin will decrease.

1.3.3 Nanosystems: 'a means to an end'

There is a need to develop an adequate oral delivery system that not only protects insulin from enzymatic degradation but also aids in enhancing its absorption without altering its biological activity. Accordingly, each form of drug delivery system contains functional excipients that protect insulin from aggregation and enzymatic breakdown, enhance the

retention time of insulin in the intestinal tract for greater absorption and facilitate the transport of insulin through the epithelium via paracellular and/or transcellular pathways [127,164,165]. The physical and chemical states of drug delivery systems can be modified by mechanical processes and/or the addition of alternative processing materials of specific characteristics, thereby elevating their recognition by the intended biological epithelium and final target [164,166]. A summary of the types of functional excipients and forms of insulin and drug delivery systems is shown in Figure 1.7.

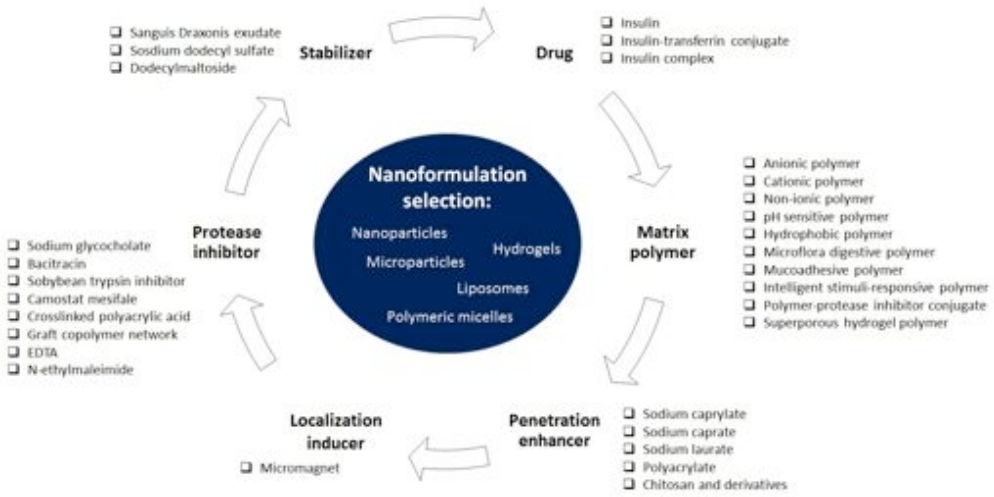

Figure 1.7. Some forms of insulin, functional excipients and drug delivery systems used in the design of oral insulin dosage forms.

Promising carrier systems for insulin delivery can be categorized into the following: polymeric NP, microparticles, hydrogels, polymeric micelles, liposomes and SLN. There are two types of polymeric NP: the matrix particles called 'nanospheres' [127] and the reservoir−type named 'nanocapsules' [167]. Liposomes are vesicles developed by the self−assembly of phospholipids in an aqueous environment [168]. SLN are colloidal carriers made of solid lipids (lipids with a melting point higher than room and body temperatures), such as triglycerides, complex monoglyceride combinations or waxes, dispersed in water or in aqueous solution containing a surfactant [168]. The most important features of various

nanosystems are illustrated in Table 1.6.

Table 1.6. Nanosystems approaches for developing oral insulin delivery.

Nanosystems (Ref.)	Principle	Outcomes	Limitations	Examples
NP [169−172]	Nanospheres/ nanocapsules developed to control the release of the entrapped insulin. Size range: 10−1000 nm	Hydrophobic/ hydrophilic polymeric materials can be used to modulate the properties of NP.	Denaturation can occur during encapsulation in synthetic polymers due to exposure to harsh conditions; Possible cytotoxicity of polymers after internalization into cells.	Nanospheres; Nanocapsules; pH sensitive NP; Bioadhesive NP.
Microparticle [173,174]	Solid polymeric matrix. Size range: 1−1000 µm	Insulin may be either adsorbed at the surface of the polymer or encapsulated.	Particle size may remain large and be critical to be absorbed by the intestinal tract.	pH sensitive microparticles
Hydrogels [175,176]	Three−dimensional polymer matrices with the ability to absorb large amounts of water and biological	Polymeric hydrogels that protect insulin from enzymatic degradation and deliver it effectively in the intestine.	Swelling and de−swelling mechanisms under pH conditions of the body can promote a faster and unwanted release of insulin.	Glucose responsive hydrogel matrix

	fluids.			
Polymeric micelles [177–179]	Nanocarriers generated by self–assembly of amphiphilic polymers in water above the critical micellar concentration. Size range: 10–100 nm	Due to their nanoscopic size, they have the ability to solubilize hydrophobic drugs in large amounts and achieve site–specific delivery.	Disaggregation of micelles upon dilution in physiological fluids.	Reverse polymeric micelles; Mixed polymeric micelles.
Liposomes [26,180,181]	Vesicles formed by one or multiple lipid bilayers made of a mixture of phospholipids. Size range: 20 nm to 10 µm	Good permeation properties because their bilayer structure is similar to that of the cell membrane.	Poor EE and stability in biological fluids.	Niosomes; Archaeosomes
SLN [75,102,182]	Produced with one single solid lipid and surfactants, with perfect crystalline lattice. Size range: 50–1000 nm	Tolerability/ Biodegradability; Possess physiological lipids that minimize the risk of acute and chronic toxicity.	Poor EE of insulin into the lipid core. The high temperatures required to melt the lipid may affect the stability of insulin. Slow degradation.	Lipid drug conjugates

Abbreviations: EE, encapsulation efficiency.

1.3.3.1 Micro- and NP

Micro- and NP have been extensively researched for oral insulin delivery. NP are polymeric, submicron colloidal systems that can be used to encapsulate and deliver drug moieties into the systemic circulation. Various NP types have been investigated for oral insulin delivery, and many publications have already been published [161,165,166,171,172]. NP protect insulin against degradation and facilitate the uptake of insulin through paracellular or transcellular pathways. Microparticles have also been shown to be capable of protecting encapsulated insulin from degradation, but the enteral absorption and transport have been shown to be favored by making particles with smaller sizes [183]. Several properties have been considered important for the uptake of NP, including size, surface charge and hydrophobicity [64,184]. Depending on the method of preparation, nanospheres or nanocapsules can be obtained. Nanospheres are matrix systems that contain the drug dispersed throughout a polymer matrix, whereas the vesicular structures called nanocapsules are made of a fluid drug-loaded core surrounded by a singular polymeric wall [185].

The mechanism of absorption of NP in the GI tract depends on the physicochemical properties of the constituent polymer and surface properties. NP with different functionalities can be tailor-made by careful selection of polymers that possess target properties. For example, NP with prolonged activity and long-circulating half-lives can be created by coating them with PEG, which provides a hydrophilic coating that repels plasma proteins and prevents degradation [186]. This effect has also been achieved by the addition of poloxamer 188 to insulin-loaded CS/TPP NP, which elicited a prolonged antihyperglycemic effect in diabetic rats after oral administration due to delayed clearance [170].

CS has been shown to improve the paracellular transport of insulin by mediating the reversible opening of TJ between cells. Insulin-loaded CS-based NP given orally to diabetic rats normalized the glucose levels for several hours [131,187]. pH-sensitive NP containing methacrylic acid (MAA) grafted with PEG have been shown to curtail the release of insulin in the stomach, facilitating its release at near neutral pH [188]. These particles exhibited antihyperglycemic effects that lasted for ~ 6 h in diabetic rats.

Insulin-loaded NP bearing receptor-recognizable ligands, such as Vitamin B12, on

their surfaces have also been used to facilitate the internalization of insulin by receptor−mediated endocytosis [108]. A significant advantage of NP in the delivery of oral insulin is that NP tend to concentrate mostly in the liver irrespective of their composition [189,190]. The uptake of insulin−loaded NP by the liver enhances glycemic control by suppressing hepatic glucose production, similarly to physiological insulin. Insulin−loaded pH−sensitive microspheres composed of poly(MAA) and PEG have been shown to be well absorbed in the ileum and have elicited a marked antihyperglycemic effect in healthy rats [173]. These microspheres exhibited good mucoadhesive properties due to the presence of PEG moiety and pH modulated insulin release by pH−dependent swelling of interpolymer complexes formed between protonated components of microspheres [173]. Microspheres have also demonstrated marked inhibition of tryptic activity, which may be ascribed to the ability of the matrix polymer to bind to calcium ions required for the initiation of the enzymatic activity. Another novel formulation of insulin microspheres consists of charge−interaction complexes containing negatively charged insulin−loaded PLGA microparticles coupled with positively charged micromagnets [174]. These charge−interaction complexes were localized at the intestinal region through the application of an external magnetic field to the subjects ingesting the formulation. The complex was given to mice fitted with a magnetic belt, and the amount of insulin retained in the intestinal tract was compared with that retained in the control group (in the absence of an external magnetic field). Mice in which a magnetic field was applied after administration retained 32.5% of insulin in the small intestine, whereas the control group only retained 5.4% [174]. Additional formulations of microspheres useful in enhancing oral insulin delivery include mucoadhesive CS−based microspheres and microspheres enclosing absorption enhancers and protease inhibitors [191].

Problems associated with the use of micro− and NP in oral insulin delivery include the risk of disruption of the delicate insulin structure during the intense processing conditions required for their production [192].

1.3.3.2 Hydrogels

Hydrogels are tridimensional networks composed of natural or synthetic hydrophilic

polymers. Due to the presence of physical and/or chemical cross−linking agents, polymeric materials are insoluble in water, which allows the retention of a large amount of fluids, combining structural integrity and elasticity to the system [193,194]. There are good overviews on the use of hydrogels for oral insulin drug delivery [195,196]. Hydrogels are able to prevent insulin release in the stomach (acidic pH). As the pH increases toward the small intestine, insulin is released from the hydrogel due to the interaction with the intestinal fluid [195,196]. An example of temperature and pH−sensitive hydrogels is the cross−linked poly(N−isopropylacrylamide (PNIPAM)−MAA−hydroxy ethyl methacrylate (HEM) hydrogel with an insulin EE of ∼54% [175]. These pH−sensitive hydrogels released only 20% of insulin at pH 2, indicating pH responsive behavior due to the MAA and HEM monomers in the smart polymer. This pH−responsiveness led to a higher insulin release (80%) at higher pH (7.4), similar to the intestinal pH. Another study involving MAA and PEG pH−responsive microparticles suggested that this system is a promising carrier for insulin enhanced transport and absorption [197]. Studies with two different intestinal epithelial models, Caco−2 and Caco−2/HT29−MTX monolayer cultures, demonstrated an increase in the insulin permeability of 5− and 9−fold, respectively [197].

Additional oral insulin delivery systems based on cyclodextrin complexed insulin encapsulated poly(MAA) hydrogel have been investigated [198]. Cyclodextrins are cyclic oligosaccharides capable of forming noncovalent inclusion complexes with a variety of drugs [199−201], including proteins [22,202]. Combining cyclodextrin complexed systems with hydrogels was described as an interesting strategy in improving drug delivery by the oral route [198]. The methyl–β–cyclodextrin was effective in increasing the insulin permeability across the Caco−2 cells, and that effect was higher if methyl−β−cyclodextrin was combined with hydrogels made of poly(MAA) acid [22]. Methyl–β–cyclodextrin complexed insulin encapsulated in the poly(MAA)−PEG−CS hydrogel microparticles led to a better pharmacological response in diabetic animals compared with microparticles containing original insulin [22,198].

Hydrogels are widely studied, especially for their ability to respond to various environmental conditions present in the human body. Therefore, pH− and temperature−sensitive hydrogels can deliver insulin with high−specific efficiency and controlled release. However, the slow adaptation and fragility of hydrogels may compromise insulin delivery [203]. The combination of nanotechnology with environment−sensitive

hydrogels can be advantageous for producing effective systems that protect insulin from the GI conditions and allows a target and controlled delivery [204].

1.3.3.3 Polymeric micelles

In the recent years, polymeric micelles have received increased attention as useful functional nanomaterials for oral delivery of insulin. Micelles have been developed as delivery carriers for peptides and proteins, which can be entrapped inside the core of nanomicelles and be orally delivered [3,120,121].

The efficacy of these micellar formulations was evaluated *in vivo* using diabetic Wistar rats as a model of T1D. A specific formulation was selected for further studies in normal New Zealand rabbits. The efficacy of insulin encapsulated in micelles in oily formulations revealed to be dose dependent with similar efficacy if formulated as insulin emulsion. If EDTA was predelivered 40 min before the delivery of insulin oily solution, the antihyperglycemic effect was highly enhanced, with the area under the curve (percentage of reduced glycemia) value increasing from 28.5 to 167.1. The improvement of the insulin oral absorption induced by the previous delivery of EDTA was probably due to enzymatic inhibition, reduction of gut mobility and opening of paracellular junctions [177].

Recently, a novel glucose−responsive complex polymeric micelle was developed through the self−assembly of two types of diblock copolymers, PEG−b−poly(aspartic acid−co−aspartamidophenylboronic acid) (Asp−co−AspPBA) and PNIPAM−b−P(Aspco−AspPBA) [178]. With the unique core–shell–corona structure containing a continuous PNIPAM membrane shell around the glucose−responsive core, these micelles were proven to exhibit remarkably reversible swelling in response to glucose. This response led to the on–off regulation of insulin release due to the reversible expansion of the PEG channels embedded in the PNIPAM membrane. Furthermore, the continuous PNIPAM membrane of the micelle could provide effective insulin protection against protease degradation, making this system an outstanding candidate for oral insulin delivery.

Another intelligent system capable of releasing insulin in response to the glucose levels was reported by Zhang *et al.* [179]. They developed glucose−responsive polymeric micelles prepared via the self−assembly of the amphiphilic polymers

PEG−blockpoly([2−phenyl boronic esters−1,3−dioxane−5−ethyl] methylacrylate−co−[2−pyrenyl boronic esters−1,3−dioxane−5−ethyl] methylacrylate) (b−P[PBDEMAco−PyBDEMA], having different PBDEMA and PyBDEMA contents. The random distribution of PyBDEMA and PBDEMA in the hydrophobic core provided three advantages to this delivery system of insulin. The strongly hydrophobic PyBDEMA with inert glucose−responsiveness at pH 7.4 effectively dispersed glucose−responsive PPBDEMA segment, resulting in polymeric micelles with notable glucose−responsiveness under physiological pH 7.4. In second, the introduction of PyBDEMA in the hydrophobic core significantly enhanced the LC and EE of insulin that could reach 73 and 20%, respectively. Finally, due to the presence of strongly hydrophobic PyBDEMA, the morphology of polymeric micelles was maintained in response to glucose. This type of polymeric micelles constructed by such strategy of dispersing glucose−responsive groups has both lower apparent pKa and better sensitivity to glucose.

Some limitations associated with the use of polymeric micelles include the relatively high levels of polymer that are needed to avoid dissolution in the GI tract. Another disadvantage is the immature technology for drug incorporation in a physical manner. Yokoyama *et al.* reported that physical incorporation efficiencies depended on various factors in drug incorporation processes [205]. Presently, there seem to be no universal incorporation methods applicable to any polymer [121]. Furthermore, in some methods, although drug incorporation is easy and efficient on a small laboratory scale, it may be difficult on a large industrial scale.

1.3.3.4 Liposomes

Liposomes can encapsulate peptides and proteins and thereby increase their stability *in vivo* [181,206]. Although liposome systems have potential in oral drug delivery, their stability under the physiologic conditions of the GI tract is a concern [207]. For example, Zhang *et al.* modified liposomes with various lectins, resulting in insulin−loaded liposomes with a size range from 166.2 to 194.1 nm and EE from 30.3 to 82.5% [26]. After oral administration of lectin−modified insulin−loaded liposomes to diabetic mice or rats, the blood glucose levels clearly decreased. These results suggested that lectin−modified

liposomes could enhance the intestinal absorption of insulin. Lectin is a specific ligand that shows affinity for a receptor located in the GI cavity and can be grafted on the surface of drug carriers to mediate an adhesive interaction between the carrier and the biological surface [26,168].

Oral insulin can also be formulated in the form of niosomes, nonactive surfactant−containing liposomes [180], which prevent the degradation of insulin by encapsulation in addition to the surfactant in its hydrophilic matrix [208]. Niosomes prepared with a mixture of cholesterol and nonionic surfactants protected insulin against *in vitro* proteolytic degradation, and only 26.3% of insulin was released during 24 h in simulated intestinal fluid (SIF) [181]. Another group designed insulin−containing archaeosomes, liposomes that are made of archaeobacterial membrane lipids containing diether and/or tetraether lipids, using polar lipid fraction E from *Sulfolobus acidocaldarius* [209]. The authors found that the archaeosomes had better stability in simulated GI fluids without enzymes, compared with a conventional liposome prepared by egg phosphatidylcholine and cholesterol. As carriers of oral insulin, archaeosomes were superior in reducing the blood glucose levels in diabetic mice compared with conventional liposomes.

1.3.3.5 SLN

SLN are spherical particles made of lipids or lipid blends (solid at body temperature) with a mean diameter between 50 and 1000 nm. SLN show good tolerability, biodegradation and the possibility of industrial−scale production [210,211]. It has been reported that the nanoencapsulation of insulin in lipid NP has improved its BA, prolonged its blood residence time and/or modified its biodistribution [171,206].

The preparation of insulin−loaded cetyl palmitate SLN demonstrated potential for the oral delivery of insulin [171]. The insulin LC in SLN was improved by increasing insulin liposolubility. The solubilization of insulin into mixed reverse micelles was performed by using bile salts and phospholipids, and its transformation into SLN occurred through reverse micelle−double emulsion method. Stearic and palmitic acids were used as a biocompatible lipid matrix [182]. The NP' surface was modified by CS to improve their penetration in the GI tract. Moreover, CS provided stealth properties to SLN, preventing their uptake by

phagocytosis. The PA values were within 5.1–8.3 and 7.7% for SLN and CS−coated SLN, respectively [75]. WGA binds specifically to the cell membranes and is taken up into the cells by receptor−mediated endocytosis [212]. Zhang *et al.* utilized the advantages of WGA and formulated SLN modified with WGA to enhance the oral delivery of insulin [102]. Insulin−loaded SLN or WGA modified SLN were administered orally to rats, and the relative PA values were 4.46 and 6.08%, whereas the relative BA values were 4.99 and 7.11%, respectively.

1.3.4 Oral insulin & low BA: Interest for the market?

It is well established that an extensive presystemic metabolism, inactivation in acidic pH of the upper GI tract and poor penetration through the intestine membrane are factors responsible for the reduced BA of orally delivered insulin, as well as simpler factors such as dietary habits. Therefore, it may appear counterintuitive to focus on the development of an oral formulation of insulin because it implies a predictable pharmacokinetic response. However, various methods and formulations have been explored to improve the oral BA of insulin, particularly in the last decade [73,75,132].

The highest oral insulin BA reported was remarkably lower than the values commonly found for s.c. delivery [166]. Nevertheless, other particularities were found for oral delivery systems of insulin, such as the duration of action that is sustained for a longer period of time and/or its biodistribution is modified [166]. In preclinical studies, nanoencapsulated insulin revealed higher BA values compared with oral−free insulin, demonstrating the fundamental role of polymers that protect insulin from the harsh environment of the GI tract and improve its absorption, leading it to be partially or entirely activated at the final sites of action. It was also observed that escalating doses of oral insulin formulations does not always induce a further improved pharmacological response. Instead, higher doses were found to increase the insulin BA and decrease the PA [166]. Two hypotheses can be considered: with the lowest dose, a full suppression of the hepatic glucose production is established; and/or only a particular amount of insulin is absorbed despite an increase in dose.

Furthermore, Elsayed *et al.* demonstrated that the absorption of oral insulin was

affected by food ingestion, decreasing its PA [134]. Therefore, if all preclinical studies of oral insulin delivery are influenced in a similar manner, the results obtained so far are overestimated because few studies have evaluated the effect of food intake, as explained above. The low biopotency of oral insulin is reflected in the need for higher amounts of insulin compared with s.c. insulin. Until recently, this was an impractical scenario for oral insulin due to commercial considerations. However, the supply of insulin and its price can support such a strategy [213].

Low BA also means that most oral insulin is not absorbed and may remain in the GI tract, which is likely to be degraded by peptidases and proteases. A concern that needs to be addressed in safety studies is whether insulin, a known mitogen associated with an increased risk of several cancers, including colon cancer, will increase the incidence of cancer if administered orally [165,214].

The relatively high doses of oral insulin needed to achieve a significant metabolic effect raises the theoretical possibility of an insulin overdose if insulin absorption is acutely increased by biological or environmental factors (e.g., unique foods, stress or activity). Additionally, the impact of food intake on the BA and pharmacodynamic properties of oral insulin formulations, as well as their variability, would most certainly become less important in the context of a basal oral insulin formulation [162]. Based on the current treatment practices, this formulation may be a true alternative for use of long−acting insulin analogues in addition to other oral antidiabetic drugs in the treatment of patients with T2D.

1.3.5 Clinical trials with oral insulin – how far are we?

An electronic literature search was performed to identify the number of publications related to the oral administration of insulin in the last two decades. The search engine Web of Science™ was utilized for this purpose on 5 August 2016, and the following search terms were applied: (“oral insulin“ or [“oral delivery“ near/2 insulin] or [“oral administration“ near/2 insulin]) and (scale*up or “micro“ or *nano* or monolayer* or “*in vivo*“), no limitation on reports type were applied; (“oral insulin“ or [“oral delivery“ near/2 insulin] or [“oral administration“ near/2 insulin]), only patents or clinical trials were considered.

The literature search identified approximately 1000 publications concerning oral

insulin (Figure 1.8), as searched by the topics described above. Oral insulin has been exhaustively studied as a strategy for the effective treatment of diabetes, as insulin formulations have already shown to protect insulin from the harsh conditions of the GI tract and to contribute to insulin intestinal absorption. Accordingly, the goal to achieve a successful oral insulin formulation seems closer, although almost oral insulin formulations continue failing to reach clinical trials.

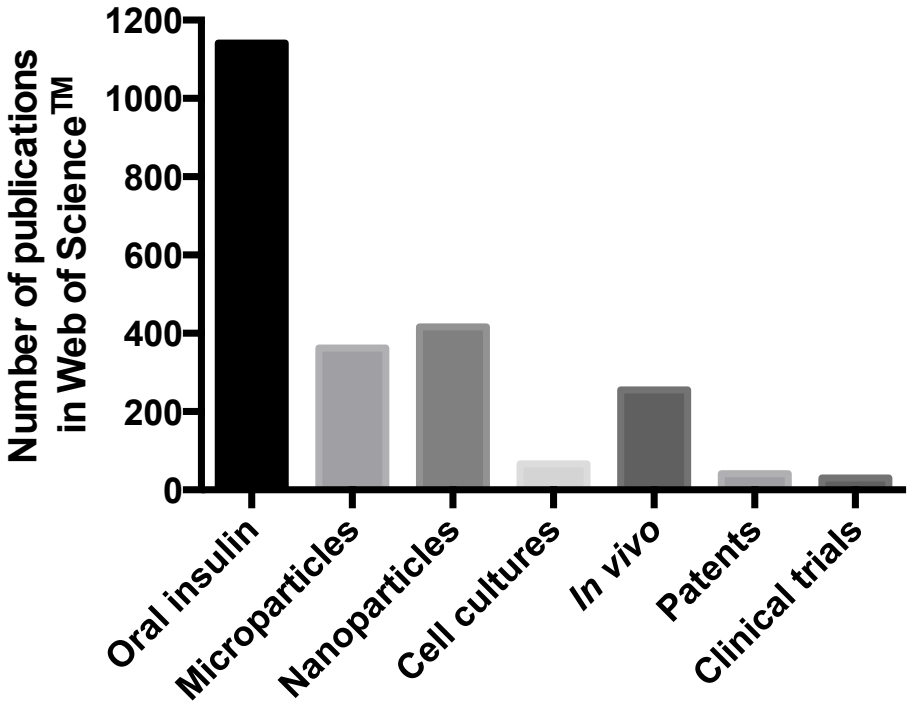

Figure 1.8. Distribution of the number of publications related to oral administration of insulin, refining the research subject, over the last two decades.

Micro– and nanosystems of insulin compose ca. 68% of the total publications found, which is justified by the advantages they offer to overcome various obstacles, including those mentioned before. The number of publications addressing early pharmacological developments – with *in vitro* or *in vivo* studies – is impressive at first glance; however, a

small amount entered clinical development. An even more remarkable finding was the reduced number of *in vitro* studies – with cell culture models – compared with *in vivo* studies. Only one−quarter of the research that reaches *in vivo* studies is previously submitted to the cell culture models. In an early development stage, *in vitro* studies are preferred as a screening tool, as they allow rapid assessment of the potential permeability and metabolism, elucidate the transport mechanism and pathway and are an opportunity to minimize time consuming and expensive animal studies. The design of an efficient oral insulin formulation will not be achieved unless the absorption mechanisms and behavior at the cellular level are well known, which constitute a major obstacle for oral insulin. The increasing usefulness of cell culture models is only justified if it accurately mimics the human intestinal epithelial barrier. However, a triple co−culture *in vitro* cell model was established recently [37], based on Caco−2, HT29−MTX and Raji B lymphocytes. Until then, *in vitro* cell models were based on two types of cells only, discarding the role of some cells in the absorption of insulin formulations. The hypothesis that suggests that three types of cell lines together may better reproduce the intestinal epithelium leads to a better correlation with *in vivo* data, which can be a useful tool to realize the potential failures of oral insulin formulations in *in vivo* studies. The lack of information at the cellular level is, from the author's perspective, responsible, at least in part, for the low number of studies reaching clinical trials.

The incredibly high number of publications related to oral insulin is also reflected in the number of registered patents, which search for simpler and economically viable systems. However, there is no guarantee on how many of these patents have been licensed. In fact, the number of clinical trials is approximately equivalent to two thirds of the number of patents, meaning that the other third is probably still not processed. Reviews regarding patents that provide novel approaches for oral insulin deliver were recently published [215,216].

Scientists have accepted the challenge of translating laboratory discoveries to a commercial production of insulin. Although worldwide research of oral insulin formulations is at various stages of drug development, most of the companies that have claimed to be developing an oral insulin formulation have failed in Phase II clinical studies, showing insufficient metabolic control in patients with diabetes [138]. The challenges in oral insulin development regarding clinical trials and the failure and success of various companies have

been described in multiple reviews [33,99,105]. Table 1.7 summarizes the oral insulin formulations currently in clinical trials conducted by various pharmaceutical companies.

Table 1.7. Oral insulin delivery technologies undergoing clinical trials.

Company	Product	System	Clinical trial status	Ref.
Oramed	ORMD−0801	Enteric coating and absorption enhancers	Completed Phase IIa in T1D; Completed Phase IIb in T2D; Approved by FDA for Phase IIb in T2D.	[217]
Biocon	IN−105	Chemical modification of insulin with a small PEG and penetration enhancers	Phase III in T2D failed to clear the primary endpoint; Completed Phase I in collaboration with Bristol Myers Squibb.	[218]
NovoNordisk − Merrion	NN1953 NN1954 NN1956	Absorption enhancers that activate micelle formation	Completed Phase I; Initiated Phase IIa with NN1953.	[219]
NovoNordisk − Emisphere	Eligen	Penetration enhancers−Salcaproza te sodium	Completed Phase IIIa in T2D.	[220]
Diabetology	Capsulin	Enteric−coating, absorption enhancers and a solubiliser	Phase II in T1D and T2D; Phase IIb planned for T2D.	[221]
Oshadi drug administrati on	Oshadi oral insulin	Enteric capsules with insulin blended with silica NP and a polysaccharide suspended in oil	Completed Phase II in T1D.	[222]
Diasome	HDV−I	Liposomes with hepatic targeting	Completed Phase II in T1D and T2D; Approved by FDA for Phase III.	[142]

The small number of clinical trials in comparison with published preclinical studies indicates that oral insulin is still battling to move on from clinical testing [162]. Moreover, some recently published clinical data represent results from trials that were conducted more than 10 years ago and/or from developments that have been discontinued [162].

It must be emphasized that these proof−of−concept trials confirm, without exception, that oral insulin delivery is feasible and that the results are promising for further development [162].

The characteristic features of diabetes and pathological events during the disease in animal models, such as rats or mice, are quite similar to that of humans. Therefore, the preclinical phase study is always performed before going to a clinical phase study. Rodent based animal models have been widely used for studying diabetes. Each has specific traits of diabetes, and insufficient characterization of some models can raise doubts over conclusions, especially in extrapolating the results obtained from these animal models to humans. The use of the pig, particularly minipigs, has been suggested as more appropriate for the oral insulin BA studies due to the higher similarity between the pig and human digestive tract. The use of more than one animal model, especially if one is mammalian, may substantially increase the cost of preclinical studies and be prohibitive for many researchers, but it will contribute to increased reliability of the oral insulin BA studies during the preclinical phase and will consequently increase industry's attraction. Regardless of the animal model chosen, experimental factors affecting the variability of the human response, such as the study of fasting and prandial regimens and whether the animal's glycemic control impacts the oral insulin BA, should be considered. Additionally, reporting and discriminating changes in the animal health states, including the number of deaths and the reason for those deaths, is important.

Future research will define if more insulin formulations will become available and affordable to the thousands who are awaiting relief from the stress and distress of daily insulin injections. As Peter Kurtzhals once said, "The simplicity and convenience of oral insulin would be amazing. While it takes time to learn how to inject insulin with a pen, everyone knows how to swallow a pill. This in turn could support greater compliance and lead to much better treatment outcomes to the benefit of patients, healthcare providers and society".

1.4 LONG−TERM THERAPEUTIC CONCERN

Although human clinical studies for long−term applications are still required, the investigation field has experienced difficulty in the development of an oral insulin delivery system. There are concerns about unwanted absorption of antigens or toxic substances from the gut lumen during oral delivery of nanoencapsulated insulin. In the case of CS insulin−loaded NP, the absorption enhancement was specific for the loaded insulin only and did not promote the intestinal absorption of the endotoxin lipopolysaccharide. On the basis of these results, it was concluded that CS−based NP can be used as a safe carrier for the oral delivery of insulin [223].

Other therapeutic concerns are related to sustained immune responses to oral insulin by the production of neutralizing antibodies that can compromise its efficacy or safety [224]. This is of special consideration since the role of the M cells in the NP transport was elucidated, because these specialized epithelial cells are responsible for antigen sampling at the interface of the mucosal surfaces.

Once insulin has a relatively narrow therapeutic window, factors such as age, genomic factors, pathophysiological conditions and other individual variations must be thoroughly evaluated, since they could affect the GI transport.

Moreover, since insulin is a mitogen implicated in the increased risk of colorectal cancer [214,225], the risk of its oral administration also needs to be considered, although there are already studies showing that in fact insulin does not contribute to this disease process [226].

The diabetic condition is one example where pathophysiological−induced changes occur in the absorptive capacity of the GI mucosa for particulates [227]. Thus, insulin−loaded NP absorption studies should take this fact into account since it can influence the results, namely the absorption of NP through the GI tract and their transit to secondary organs.

1.5 AIM AND OUTLINE OF THESIS

The aim of the work presented in this thesis was to disclose the behavior of dual CS/ALB−coated ADS−based NP after oral delivery, during the passage through the intestinal

epithelium until its final destination, in order to improve the oral response of insulin for the treatment of diabetes. The specific objectives of this thesis were:

1. To improve the physical properties of the CS/ALB−coated insulin−loaded ADS−based NP, by investigating the influence of some parameters of the emulsification/internal gelation and polyelectrolyte complexation techniques on the final performance of the nanosystem, and, to probe insulin bioactivity after each step of the process.
2. To study the impact of the passage through the GI environment on the aggregation of the NP and how this impact further influences the insulin release and permeability across the intestinal Caco−2, Caco−2/HT29−MTX and Caco−2/HT29−MTX/Raji B monolayers.
3. To assess the role of each type of cell of the intestinal Caco−2/HT29−MTX/Raji B monolayers, that represent enterocytes, goblet and M cells, respectively, on the permeability of insulin.
4. To evaluate the biodistribution of the NP after oral delivery and compare the oral PA of insulin between type 1 and type 2 diabetic animal models.
5. To characterize the independent effects of CS and ALB coatings on the insulin release profiles and at the cellular level, and, to study the insulin uptake and the molecular mechanisms used across the intestinal Caco−2/HT29−MTX/Raji B monolayers.

1.6 REFERENCES

[1] Yaturu, S. Insulin therapies: Current and future trends at dawn. World Journal of Diabetes 2013;4:1−7.

[2] Adams, G. G.; Harding, S. E. Drug delivery systems for the treatment of diabetes mellitus: State of the art. Current Pharmaceutical Design 2013;19:7244−63.

[3] Plapied, L.; Duhem, N.; des Rieux, A.; Préat, V. Fate of polymeric nanocarriers for oral drug delivery. Current Opinion in Colloid & Interface Science 2011;16:228−37.

[4] Gerich, J. E. Novel insulins: expanding options in diabetes management. American Journal of Medicine 2002;113:308−16.

[5] Quellhorst, E. Insulin therapy during peritoneal dialysis: pros and cons of various forms of administration. Journal of the American Society of Nephrology 2002;13:S92−S6.

[6] Shantha, T. R.; Shantha, J. G. Inhalation insulin and oral and nasal insulin sprays for diabetics: panacea or evolving future health disaster part II. Townsend Letter 2009;106−10.

[7] Rekha, M. R.; Sharma, C. P. Glutamine−chitosan microparticles as oral insulin delivery matrix: *In vitro* characterization. Journal of Applied Polymer Science 2011;122:2374−82.

[8] Brange, J.; Langkjaer, L. Insulin formulation and delivery. Pharmaceutical Biotechnology 1997;10:343−409.

[9] Antosova, Z.; Mackova, M.; Kral, V.; Macek, T. Therapeutic application of peptides and proteins: parenteral forever? Trends in Biotechnology 2009;27:628−35.

[10] Makhlof, A.; Werle, M.; Tozuka, Y.; Takeuchi, H. A mucoadhesive nanoparticulate system for the simultaneous delivery of macromolecules and permeation enhancers to the intestinal mucosa. Journal of Controlled Release 2011;149:81−8.

[11] Reis, C. P.; Veiga, F. J.; Ribeiro, A. J.; Neufeld, R. J.; Damgé, C. Nanoparticulate biopolymers deliver insulin orally eliciting pharmacological response. Journal of Pharmaceutical Sciences 2008;97:5290−305.

[12] Sonaje, K.; Chuang, E. Y.; Lin, K. J.; Yen, T. C.; Su, F. Y.; Tseng, M. T.; Sung, H. W. Opening of epithelial tight junctions and enhancement of paracellular permeation by chitosan: microscopic, ultrastructural, and computed−tomographic observations. Molecular Pharmaceutics 2012;9:1271−9.

[13] Bernkop−Schnurch, A.; Krauland, A. H.; Leitner, V. M.; Palmberger, T. Thiomers: potential excipients for non−invasive peptide delivery systems. European Journal of Pharmaceutics and Biopharmaceutics 2004;58:253−63.

[14] Dave, N.; Hazra, P.; Khedkar, A.; Manjunath, H. S.; Iyer, H.; Suryanarayanan, S. Process and purification for manufacture of a modified insulin intended for oral delivery. Journal of Chromatography A 2008;1177:282−6.

[15] Su, F.−Y.; Lin, K.−J.; Sonaje, K.; Wey, S.−P.; Yen, T.−C.; Ho, Y.−C.; Panda, N.; Chuang, E.−Y.; Maiti, B.; Sung, H.−W. Protease inhibition and absorption enhancement by functional nanoparticles for effective oral insulin delivery. Biomaterials 2012;33:2801−11.

[16] Zhang, L.; Song, L.; Zhang, C.; Ren, Y. Improving intestinal insulin absorption efficiency through coadministration of cell−penetrating peptide and hydroxypropyl−β−cyclodextrin. Carbohydrate Polymers 2012;87:1822−7.

[17] Asada H, D. T., Waki M, Adachi S, Fujita T, Yamamoto A, Muranishi S. Absorption characteristics of chemically modified−insulin derivatives with various fatty acids in the small and large intestine. Journal of Pharmaceutical Ssciences 1995;84:682−7.

[18] Bernkop−Schnurch, A.; Schmitz, T. Presystemic metabolism of orally administered peptide drugs and strategies to overcome it. Current Drug Metabolism 2007;8:509−17.

[19] Morishita, M.; Kamei, N.; Ehara, J.; Isowa, K.; Takayama, K. A novel approach using functional peptides for efficient intestinal absorption of insulin. Journal of Controlled Release 2007;118:177−84.

[20] Chalasani, K. B.; Russell−Jones, G. J.; Yandrapu, S. K.; Diwan, P. V.; Jain, S. K. A novel vitamin B12−nanosphere conjugate carrier system for peroral delivery of insulin. Journal of Controlled Release 2007;117:421−9.

[21] Petrus, A. K.; Vortherms, A. R.; Fairchild, T. J.; Doyle, R. P. Vitamin B(12) as a carrier for the oral delivery of insulin. Chemmedchem 2007;2:1717−21.

[22] Sajeesh, S.; Sharma, C. Cyclodextrin−insulin complex encapsulated polymethacrylic acid based nanoparticles for oral insulin delivery. Interational Journal of Pharmaceutics 2006;325:147−54.

[23] Gong, R. M.; Li, C. C.; Zhu, S. X.; Zhang, Y. Y.; Du, Y.; Jiang, J. H. A novel pH−sensitive hydrogel based on dual crosslinked alginate/N−alpha−glutaric acid chitosan for oral delivery of protein. Carbohydrate Polymers 2011;85:869−74.

[24] Morishita, M.; Goto, T.; Nakamura, K.; Lowman, A. M.; Takayama, K.; Peppas, N. A. Novel oral insulin delivery systems based on complexation polymer hydrogels: Single and multiple administration studies in type 1 and 2 diabetic rats. Journal of Controlled Release 2006;110:587−94.

[25] Lin, Y.; Chen, C.; Liang, H.; Kulkarni, A.; Lee, P.; Chen, C.; Sung, H. Novel nanoparticles for oral insulin delivery via the paracellular pathway. Nanotechnology 2007;18:1 − 11.

[26] Zhang, N.; Ping, Q. N.; Huang, G. H.; Xu, W. F. Investigation of lectin−modified insulin liposomes as carriers for oral administration. International Journal of Pharmaceutics 2005;294:247−59.

[27] Katsuma, M.; Watanabe, S.; Kawai, H.; Takemura, S.; Sako, K. Effects of absorption promoters on insulin absorption through colon−targeted delivery. International Journal of Pharmaceutics 2006;307:156−62.

[28] Maroni, A.; Zema, L.; Del Curto, M. D.; Foppoli, A.; Gazzaniga, A. Oral colon delivery of insulin with the aid of functional adjuvants. Advanced Drug Delivery Reviews 2012;64:540−56.

[29] Aboubakar, M.; Couvreur, P.; Pinto−Alphandary, H.; Gouritin, B.; Lacour, B.; Farinotti, R.; Puisieux, F.; Vauthier, C. Insulin−loaded nanocapsules for oral administration: *In vitro* and *in vivo* investigation. Drug Development Research 2000;49:109−17.

[30] Shaji, J.; Patole, V. Protein and peptide drug delivery: Oral approaches. Indian Journal of Pharmaceutical Sciences 2008;70:269−77.

[31] Woitiski, C. B.; Sarmento, B.; Carvalho, R. A.; Neufeld, R. J.; Veiga, F. Facilitated nanoscale delivery of insulin across intestinal membrane models. International Journal of Pharmaceutics 2011;412:123−31.

[32] Ensign, L. M.; Cone, R.; Hanes, J. Oral drug delivery with polymeric nanoparticles: The gastrointestinal mucus barriers. Advanced Drug Delivery Reviews 2012;64:557−70.

[33] Ribeiro, A.; Seiça, R.; Veiga, F. Nanoparticles for oral delivery of insulin. In: Coelho J, editor. Drug delivery systems: advanced technologies potentially applicable in personalised treatment. Advances in Predictive, Preventive and Personalised Medicine. 4: Springer Netherlands; 2013. p. 109−25.

[34] Sarmento, B.; Martins, S.; Ferreira, D.; Souto, E. B. Oral insulin delivery by means of solid lipid nanoparticles. International Journal of Nanomedicine 2007;2:743−9.

[35] Hussain, N.; Florence, A. T. Utilizing bacterial mechanisms of epithelial cell entry: invasin−induced oral uptake of latex nanoparticles. Pharmaceutical Research 1998;15:153−6.

[36] Jani, P.; Halbert, G. W.; Langridge, J.; Florence, A. T. Nanoparticle uptake by the rat gastrointestinal mucosa: quantitation and particle size dependency. Journal of Pharmacy and Pharmacology 1990;42:821−6.

[37] Antunes, F.; Andrade, F.; Araujo, F.; Ferreira, D.; Sarmento, B. Establishment of a triple co−culture *in vitro* cell models to study intestinal absorption of peptide drugs. European Journal of Pharmaceutics and Biopharmaceutics 2013;83:427−35.

[38] Damge, C.; Maincent, P.; Ubrich, N. Oral delivery of insulin associated to polymeric nanoparticles in diabetic rats. Journal of Controlled Release 2007;117:163−70.

[39] Hussain, N.; Jani, P. U.; Florence, A. T. Enhanced oral uptake of tomato lectin−conjugated nanoparticles in the rat. Pharmaceutical Research 1997;14:613−8.

[40] Chen, M.−C.; Sonaje, K.; Chen, K.−J.; Sung, H.−W. A review of the prospects for polymeric nanoparticle platforms in oral insulin delivery. Biomaterials 2011;32:9826−38.

[41] Balimane, P. V.; Chong, S. Cell culture−based models for intestinal permeability: A critique. Drug Discovery Today 2005;10:335−43.

[42] Gullberg, E.; Leonard, M.; Karlsson, J.; Hopkins, A. M.; Brayden, D.; Baird, A. W.; Artursson, P. Expression of specific markers and particle transport in a new human intestinal M−cell model. Biochemical and Biophysical Research Communications 2000;279:808−13.

[43] Peppas, N. A.; Carr, D. A. Impact of absorption and transport on intelligent therapeutics and nanoscale delivery of protein therapeutic agents. Chemical Engineering Science 2009;64:4553−65.

[44] Carr, D. A.; Peppas, N. A. Assessment of poly(methacrylic acid−co−N−vinyl pyrrolidone) as a carrier for the oral delivery of therapeutic proteins using Caco−2 and HT29−MTX cell lines. Journal of Biomedical Materials Research Part A 2010;92A:504−12.

[45] Fonte, P.; Nogueira, T.; Gehm, C.; Ferreira, D.; Sarmento, B. Chitosan−coated solid lipid nanoparticles enhance the oral absorption of insulin. Drug Delivery and Translational Research 2011;1:299−308.

[46] des Rieux, A.; Ragnarsson, E. G. E.; Gullberg, E.; Preat, V.; Schneider, Y. J.; Artursson, P. Transport of nanoparticles across an *in vitro* model of the human intestinal follicle associated epithelium. European Journal of Pharmaceutical Sciences 2005;25:455−65.

[47] Kadiyala, I.; Loo, Y. H.; Roy, K.; Rice, J.; Leong, K. W. Transport of chitosan−DNA nanoparticles in human intestinal M−cell model versus normal intestinal enterocytes. European Journal of Pharmaceutical Sciences 2010;39:103−9.

[48] Khullar, O. V.; Griset, A. P.; Gibbs−Strauss, S. L.; Chirieac, L. R.; Zubris, K. A. V.; Frangioni, J. V.; Grinstaff, M. W.; Colson, Y. L. Nanoparticle migration and delivery of paclitaxel to regional lymph nodes in a large animal model. Journal of the American College of Surgeons 2012;214:328−37.

[49] Reddy, S. T.; van der Vlies, A. J.; Simeoni, E.; Angeli, V.; Randolph, G. J.; O'Neill, C. P.; Lee, L. K.; Swartz, M. A.; Hubbell, J. A. Exploiting lymphatic transport and complement activation in nanoparticle vaccines. Nature Biotechnology 2007;25:1159−64.

[50] Reis, C. P.; Damge, C. Nanotechnology as a promising strategy for alternative routes of insulin delivery. Nanomedicine: Cancer, Diabetes, and Cardiovascular, Central Nervous System, Pulmonary and Inflammatory Diseases 2012;508:271−94.

[51] Pabst, O.; Mowat, A. M. Oral tolerance to food protein. Mucosal Immunology 2012;5:232−9.

[52] Rao, D. A.; Forrest, M. L.; Alani, A. W. G.; Kwon, G. S.; Robinson, J. R. Biodegradable PLGA based nanoparticles for sustained regional lymphatic drug delivery. Journal of Pharmaceutical Sciences 2010;99:2018−31.

[53] Maher, S.; Ryan, K. B.; Ahmad, T.; O'Driscoll, C. M.; Brayden, D. J. Nanostructured biomaterials for overcoming biological barriers. In: Alonso MJ, Csaba NS, editors. Nanostructured biomaterials for overcoming biological barriers: The Royal Society of Chemistry; 2012. p. 39−62.

[54] Kim, D.; El−Shall, H.; Dennis, D.; Morey, T. Interaction of PLGA nanoparticles with human blood constituents. Colloids and Surfaces B−Biointerfaces 2005;40:83−91.

[55] Morachis, J. M.; Mahmoud, E. A.; Almutairi, A. Physical and chemical strategies for therapeutic delivery by using polymeric nanoparticles. Pharmacological Reviews 2012;64:505−19.

[56] Allémann, E.; Leroux, J.−C.; Gurny, R. Polymeric nano− and microparticles for the oral delivery of peptides and peptidomimetics. Advanced Drug Delivery Reviews 1998;34:171−89.

[57] des Rieux, A.; Fievez, V.; Garinot, M.; Schneider, Y.−J.; Préat, V. Nanoparticles as potential oral delivery systems of proteins and vaccines: A mechanistic approach. Journal of Controlled Release 2006;116:1−27.

[58] Werle, M.; Takeuchi, H.; Bernkop−Schnuerch, A. Modified chitosans for oral drug delivery. Journal of Pharmaceutical Sciences 2009;98:1643−56.

[59] Hillaireau, H.; Couvreur, P. Nanocarriers' entry into the cell: relevance to drug delivery. Cellular and Molecular Life Sciences 2009;66:2873−96.

[60] Bareford, L. A.; Swaan, P. W. Endocytic mechanisms for targeted drug delivery. Advanced Drug Delivery Reviews 2007;59:748−58.

[61] Conner, S. D.; Schmid, S. L. Regulated portals of entry into the cell. Nature 2003;422:37−44.

[62] Norbury, C. C. Drinking a lot is good for dendritic cells. Immunology 2006;117:443−51.

[63] Hamman, J. H.; Enslin, G. M.; Kotze, A. F. Oral delivery of peptide drugs − Barriers and developments. BioDrugs 2005;19:165−77.

[64] Norris, D. A.; Puri, N.; Sinko, P. J. The effect of physical barriers and properties on the oral absorption of particulates. Advanced Drug Delivery Reviews 1998;34:135−54.

[65] Sinko, P. J.; Ming, H.; Amidon, G. L. Carrier mediated transport of amino acids, small peptides, and their drug analogs. Journal of Controlled Release 1987;6:115−21.

[66] Korjamo, T.; Heikkinen, A. T.; Monkkonen, J. Analysis of unstirred water layer in *in vitro* permeability experiments. Journal of Pharmaceutical Sciences 2009;98:4469−79.

[67] Porter, C. J. H.; Trevaskis, N. L.; Charman, W. N. Lipids and lipid−based formulations: optimizing the oral delivery of lipophilic drugs. Nature Reviews Drug Discovery 2007;6:231−48.

[68] Woodley, J. Bioadhesion − New possibilities for drug administration? Clinical Pharmacokinetics 2001;40:77−84.

[69] Sarmento, B.; Ribeiro, A.; Veiga, F.; Sampaio, P.; Neufeld, R.; Ferreira, D. Alginate/chitosan nanoparticles are effective for oral insulin delivery. Pharmaceutical Research 2007;24:2198−206.

[70] Yin, L. C.; Ding, J. Y.; He, C. B.; Cui, L. M.; Tang, C.; Yin, C. H. Drug permeability and mucoadhesion properties of thiolated trimethyl chitosan nanoparticles in oral insulin delivery. Biomaterials 2009;30:5691−700.

[71] Jintapattanakit, A.; Junyaprasert, V. B.; Kissel, T. The role of mucoadhesion of trimethyl chitosan and PEGylated trimethyl chitosan nanocomplexes in insulin uptake. Journal of Pharmaceutical Sciences 2009;98:4818−30.

[72] Rekha, M. R.; Sharma, C. P. Synthesis and evaluation of lauryl succinyl chitosan particles towards oral insulin delivery and absorption. Journal of Controlled Release 2009;135:144−51.

[73] Zhang, X.; Sun, M.; Zheng, A.; Cao, D.; Bi, Y.; Sun, J. Preparation and characterization of insulin−loaded bioadhesive PLGA nanoparticles for oral administration. European Journal of Pharmaceutical Sciences 2012;45:632−8.

[74] Wang, X.; Zheng, C.; Wu, Z. M.; Teng, D. G.; Zhang, X.; Wang, Z.; Li, C. X. Chitosan−NAC nanoparticles as a vehicle for nasal absorption enhancement of insulin. Journal of Biomedical Materials Research Part B−Applied Biomaterials 2009;88B:150−61.

[75] Fonte, P.; Andrade, F.; Araujo, F.; Andrade, C.; das Neves, J.; Sarmento, B. Chitosan−coated solid lipid nanoparticles for insulin delivery. Nanomedicine: Cancer, Diabetes, and Cardiovascular, Central Nervous System, Pulmonary and Inflammatory Diseases 2012;508:295−314.

[76] Jin, Y.; Song, Y.; Zhu, X.; Zhou, D.; Chen, C.; Zhang, Z.; Huang, Y. Goblet cell−targeting nanoparticles for oral insulin delivery and the influence of mucus on insulin transport. Biomaterials 2012;33:1573−82.

[77] Yuan, H.; Chen, C.−Y.; Chai, G.−h.; Du, Y.−Z.; Hu, F.−Q. Improved transport and absorption through gastrointestinal tract by pegylated solid lipid nanoparticles. Molecular Pharmaceutics 2013;10:1865−73.

[78] Tang, B. C.; Dawson, M.; Lai, S. K.; Wang, Y.−Y.; Suk, J. S.; Yang, M.; Zeitlin, P.; Boyle, M. P.; Fu, J.; Hanes, J. Biodegradable polymer nanoparticles that rapidly penetrate the human mucus barrier. Proceedings of the National Academy of Sciences of the United States of America 2009;106:19268−73.

[79] Lai, S. K.; Wang, Y.−Y.; Hanes, J. Mucus−penetrating nanoparticles for drug and gene delivery to mucosal tissues. Advanced Drug Delivery Reviews 2009;61:158−71.

[80] Yun, Y.; Cho, Y. W.; Park, K. Nanoparticles for oral delivery: Targeted nanoparticles with peptidic ligands for oral protein delivery. Advanced Drug Delivery Reviews 2013;65:822−32.

[81] Nellans, H. N. Mechanisms od peptide and protein−absorption. 1.Paracellular intestinal transport−modulation of absorption. Advanced Drug Delivery Reviews 1991;7:339−64.

[82] Pappenheimer, J. R.; Reiss, K. Z. Contribution of solvent drag through intercellular−junctions to absorption of nutrients by the small−intestine of the rat. Journal of Membrane Biology 1987;100:123−36.

[83] Sonaje, K.; Chen, Y. J.; Chen, H. L.; Wey, S. P.; Juang, J. H.; Nguyen, H. N.; Hsu, C. W.; Lin, K. J.; Sung, H. W. Enteric−coated capsules filled with freeze−dried chitosan/poly(gamma−glutamic acid) nanoparticles for oral insulin delivery. Biomaterials 2010;31:3384−94.

[84] Orci, L.; Malaisselagae, F.; Ravazzola, M.; Rouiller, D.; Renold, A. E.; Perrelet, A.; Unger, R. Morphological basis for intercellular communication between alpha−cells and beta−cells in endocrine pancreas. Journal of Clinical Investigation 1975;56:1066−70.

[85] Salamat−Miller, N.; Johnston, T. P. Current strategies used to enhance the paracellular transport of therapeutic polypeptides across the intestinal epithelium. International Journal of Pharmaceutics 2005;294:201−16.

[86] Sung, H.−W.; Sonaje, K.; Liao, Z.−X.; Hsu, L.−W.; Chuang, E.−Y. pH−responsive nanoparticles shelled with chitosan for oral delivery of insulin: from mechanism to therapeutic applications. Accounts of Chemical Research 2012;45:619−29.

[87] Lin, Y.−H.; Sonaje, K.; Lin, K. M.; Juang, J.−H.; Mi, F.−L.; Yang, H.−W.; Sung, H.−W. Multi−ion−crosslinked nanoparticles with pH−responsive characteristics for oral delivery of protein drugs. Journal of Controlled Release 2008;132:141−9.

[88] Sadeghi, A. M. M.; Dorkoosh, F. A.; Avadi, M. R.; Weinhold, M.; Bayat, A.; Delie, F.; Gurny, R.; Larijani, B.; Rafiee−Tehrani, M.; Junginger, H. E. Permeation enhancer effect of chitosan and chitosan derivatives: Comparison of formulations as soluble polymers and nanoparticulate systems on insulin absorption in Caco−2 cells. European Journal of Pharmaceutics and Biopharmaceutics 2008;70:270−8.

[89] Sonaje, K.; Lin, K.−J.; Wey, S.−P.; Lin, C.−K.; Yeh, T.−H.; Nguyen, H.−N.; HsuA, C.−W.; Yen, T.−C.; Juang, J.−H.; Sung, H.−W. Biodistribution, pharmacodynamics and pharmacokinetics of insulin analogues in a rat model: Oral delivery using pH−responsive nanoparticles vs. subcutaneous injection. Biomaterials 2010;31:6849−58.

[90] Sonaje, K.; Lin, Y. H.; Juang, J. H.; Wey, S. P.; Chen, C. T.; Sung, H. W. *In vivo* evaluation of safety and efficacy of self−assembled nanoparticles for oral insulin delivery. Biomaterials 2009;30:2329−39.

[91] Nguyen, H. N.; Wey, S. P.; Juang, J. H.; Sonaje, K.; Ho, Y. C.; Chuang, E. Y.; Hsu, C. W.; Yen, T. C.; Lin, K. J.; Sung, H. W. The glucose−lowering potential of exendin−4 orally delivered via a pH−sensitive nanoparticle vehicle and effects on subsequent insulin secretion *in vivo*. Biomaterials 2011;32:2673−82.

[92] Daugherty, A. L.; Mrsny, R. J. Transcellular uptake mechanisms of the intestinal epithelial barrier − Part one. Pharmaceutical Science & Technology Today 1999;2:144−51.

[93] Fasano, A. Innovative strategies for the oral delivery of drugs and peptides. Trends in Biotechnology 1998;16:152−7.

[94] Blanchette, J.; Kavimandan, N.; Peppas, N. A. Principles of transmucosal delivery of therapeutic agents. Biomedicine & Pharmacotherapy 2004;58:142−51.

[95] Iversen, T. G.; Skotland, T.; Sandvig, K. Endocytosis and intracellular transport of nanoparticles: Present knowledge and need for future studies. Nano Today 2011;6:176−85.

[96] Reix, N.; Parat, A.; Seyfritz, E.; Van Der Werf, R.; Epure, V.; Ebel, N.; Danicher, L.; Marchioni, E.; Jeandidier, N.; Pinget, M.; Frère, Y.; Sigrist, S. *In vitro* uptake evaluation in Caco−2 cells and *in vivo* results in diabetic rats of insulin−loaded PLGA nanoparticles. International Journal of Pharmaceutics 2012;437:213−20.

[97] Bendayan, M.; Ziv, E.; Ben−Sasson, R.; Bar−On, H.; Kidron, M. Morpho−cytochemical and biochemical evidence for insulin absorption by the rat ileal epithelium. Diabetologia 1990;33:197 − 204.

[98] Bendayan, M.; Ziv, E.; Gingras, D.; Ben−Sasson, R.; Bar−On, H.; Kidron, M. Biochemical and morpho−cytochemical evidence for the intestinal absorption of insulin in control and diabetic rats. Comparison between the effectiveness of duodenal and colon mucosa. Diabetologia 1994;37:119 − 26.

[99] Shah, D.; Shen, W. C. Transcellular delivery of an insulin−transferrin conjugate in enterocyte−like Caco−2 cells. Journal of Pharmaceutical Sciences 1996;85:1306−11.

[100] Han, L.; Zhao, Y.; Yin, L.; Li, R.; Liang, Y.; Huang, H.; Pan, S.; Wu, C.; Feng, M. Insulin−loaded ph−sensitive hyaluronic acid nanoparticles enhance transcellular delivery. AAPS PharmSciTech 2012;13:836−45.

[101] Thompson, C.; Cheng, W.; Gadad, P.; Skene, K.; Smith, M.; Smith, G.; McKinnon, A.; Knott, R. Uptake and transport of novel amphiphilic polyelectrolyte−insulin nanocomplexes by Caco−2 cells−towards oral insulin. Pharmaceutical Research 2011;28:886−96.

[102] Zhang, N.; Ping, Q.; Huang, G.; Xu, W.; Cheng, Y.; Han, X. Lectin−modified solid lipid nanoparticles as carriers for oral administration of insulin. International Journal of Pharmaceutics 2006;327:153−9.

[103] Russell−Jones, G. J. Use of targeting agents to increase uptake and localization of drugs to the intestinal epithelium. Journal of Drug Targeting 2004;12:113−23.

[104] Kilpatrick, D. C.; Pusztai, A.; Grant, G.; Graham, C.; Ewen, S. W. B. Tomato lectin resists digestion in the mammalian alimentary canal and binds to intestinal villi without deleterious effects. FEBS Letters 1985;185:299−305.

[105] Florence, A. T.; Hillery, A. M.; Hussain, N.; Jani, P. U. Nanoparticles as carriers for oral peptide absorption−studies on particles uptake and fate. Journal of Controlled Release 1995;36:39−46.

[106] Weissenboeck, A.; Bogner, E.; Wirth, M.; Gabor, F. Binding and uptake of wheat germ agglutinin−grafted PLGA−nanospheres by Caco−2 monolayers. Pharmaceutical Research 2004;21:1917−23.

[107] Lochner, N.; Pittner, F.; Wirth, M.; Gabor, F. Wheat germ agglutinin binds to the epidermal growth factor receptor of artificial Caco−2 membranes as detected by silver nanoparticle enhanced fluorescence. Pharmaceutical Research 2003;20:833−9.

[108] Chalasani, K.; Russell−Jones, G.; Jain, A.; Diwan, P.; Jain, S. Effective oral delivery of insulin in animal models using vitamin B12−coated dextran nanoparticles. Journal of Controlled Release 2007;122:141−50.

[109] Jang, M. H.; Kweon, M. N.; Iwatani, K.; Yamamoto, M.; Terahara, K.; Sasakawa, C.; Suzuki, T.; Nochi, T.; Yokota, Y.; Rennert, P. D.; Hiroi, T.; Tamagawa, H.; Iijima, H.; Kunisawa, J.; Yuki, Y.; Kiyono, H. Intestinal villous M cells: an antigen entry site in the mucosal epithelium. Proceedings of the National Academy of Sciences of the United States of America 2004;101:6110−5.

[110] Fievez, V.; Plapied, L.; des Rieux, A.; Pourcelle, V.; Freichels, H.; Wascotte, V.; Vanderhaeghen, M.−L.; Jerome, C.; Vanderplasschen, A.; Marchand−Brynaert, J.; Schneider, Y.−J.; Preat, V. Targeting nanoparticles to M cells with non−peptidic ligands for oral vaccination. European Journal of Pharmaceutics and Biopharmaceutics 2009;73:16−24.

[111] Cui, F.; Shi, K.; Zhang, L.; Tao, A.; Kawashima, Y. Biodegradable nanoparticles loaded with insulin−phospholipid complex for oral delivery: Preparation, characterization and *in vivo* evaluation. Journal of Controlled Release 2006;114:242−50.

[112] Damge, C.; Aprahamian, M.; Humbert, W.; Pinget, M. Ileal uptake of polyalkylcyanoacrylate nanocapsules in the rat. Journal of Pharmacy and Pharmacology 2000;52:1049−56.

[113] Azizi, A.; Kumar, A.; Diaz−Mitoma, F.; Mestecky, J. Enhancing oral vaccine potency by targeting intestinal M cells. Plos Pathogens 2010;6:e1001147.

[114] Frey, A.; Giannasca, K. T.; Weltzin, R.; Giannasca, P. J.; Reggio, H.; Lencer, W. I.; Neutra, M. R. Role of the glycocalyx in regulating access of microparticles to apical plasma membranes of intestinal epithelial cells: Implications for microbial attachment and oral vaccine targeting. Journal of Experimental Medicine 1996;184:1045−59.

[115] Neutra, M. R.; Phillips, T. L.; Mayer, E. L.; Fishkind, D. J. Transport of membrane−bound macromolecules by M−cells in follicle−associated epithelium of rabbit peyer patch. Cell and Tissue Research 1987;247:537−46.

[116] Owen, R. L. Sequential uptake of horseradish−peroxidase by lymphoid follicle epithelium of peyers patches in normal unobstructed mouse intestine−ultrastructure study. Gastroenterology 1977;72:440−51.

[117] Jepson, M. A.; Simmons, N. L.; Savidge, T. C.; James, P. S.; Hirst, B. H. Selective binding and transcytosis of latex microspheres by rabbit intestinal M−cells. Cell and Tissue Research 1993;271:399−405.

[118] Clark, M. A.; Jepson, M. A.; Hirst, B. H. Exploiting M cells for drug and vaccine delivery. Advanced Drug Delivery Reviews 2001;50:81−106.

[119] Aprahamian, M.; Michel, C.; Humbert, W.; Devissaguet, J. P.; Damge, C. Transmucosal passage of polyalkylcyanoacrylate nanocapsules as a new drug carrier in the small intestine. Biology of the Cell / Uunder the Auspices of the European Cell Biology Organization 1987;61:69−76.

[120] Lu, Y.; Park, K. Polymeric micelles and alternative nanonized delivery vehicles for poorly soluble drugs. International Journal of Pharmaceutics 2013;453:198−214.

[121] Simões, S.; Figueiras, A.; Veiga, F.; Concheiro, A.; Alvarez−Lorenzo, C. Polymeric micelles for oral drug administration enabling locoregional and systemic treatments. Expert Opinion on Drug Delivery 2015;12:297−318.

[122] Yin, L.; Ding, J.; Fei, L.; He, M.; Cui, F.; Tang, C.; Yin, C. Beneficial properties for insulin absorption using superporous hydrogel containing interpenetrating polymer network as oral delivery vehicles. International Journal of Pharmaceutics 2008;350:220−9.

[123] Woitiski, C.; Neufeld, R.; Veiga, F.; Carvalho, R.; Figueiredo, I. Pharmacological effect of orally delivered insulin facilitated by multilayered stable nanoparticles. European Jounal of Pharmaceutical Sciences 2010;41:556 − 63.

[124] Ali Khan A, M. J., Mohtar N, Darwis Y. Advanced drug delivery to the lymphatic system: lipid−based nanoformulations. International Journal of Nanomedicine 2013;8:2733−44.

[125] Zhang, N.; Ping, Q.; Huang, G.; Han, X.; Cheng, Y.; Xu, W. Transport characteristics of wheat germ agglutinin−modified insulin−liposomes and solid lipid nanoparticles in a perfused rat intestinal model. Journal of Nanoscience and Nanotechnology 2006;6:2959−66.

[126] Niu, M. M.; Lu, Y.; Hovgaard, L.; Guan, P. P.; Tan, Y. A.; Lian, R. Y.; Qi, J. P.; Wu, W. Hypoglycemic activity and oral bioavailability of insulin−loaded liposomes containing bile salts in rats: The effect of cholate type, particle size and administered dose. European Journal of Pharmaceutics and Biopharmaceutics 2012;81:265−72.

[127] Carino, G. P.; Jacob, J. S.; Mathiowitz, E. Nanosphere based oral insulin delivery. Journal of Controlled Release 2000;65:261−9.

[128] Sarmento, B.; Ferreira, D. C.; Jorgensen, L.; van de Weert, M. Probing insulin's secondary structure after entrapment into alginate/chitosan nanoparticles. European Journal of Pharmaceutics and Biopharmaceutics 2007;65:10−7.

[129] Wu, Z. M.; Zhou, L.; Guo, X. D.; Jiang, W.; Ling, L.; Qian, Y.; Luo, K. Q.; Zhang, L. J. HP55−coated capsule containing PLGA/RS nanoparticles for oral delivery of insulin. International Journal of Pharmaceutics 2012;425:1−8.

[130] Xiaoyang, L.; Jianping, Q.; Yunchang, X.; Xi, Z.; Shunwen, H.; Ying, X.; Yi, L.; Wei, W. Nanoemulsions coated with alginate/chitosan as oral insulin delivery systems: Preparation, characterization, and hypoglycemic effect in rats. International Journal of Nanomedicine 2012;8:

[131] Sarmento, B.; Ribeiro, A.; Veiga, F.; Ferreira, D.; Neufeld, R. Oral bioavailability of insulin contained in polysaccharide nanoparticles. Biomacromolecules 2007;8:3054−60.

[132] Prusty, A. k.; Sahu, S. K. Development and evaluation of insulin incorporated nanoparticles for oral administration. ISRN Nanotechnology 2013;2013:6.

[133] Ma, E.−l.; Ma, H.; Liu, Z.; Zheng, C.−x.; Duan, M.−x. *In vitro* and *in vivo* evaluation of a novel oral insulin formulation. Acta Pharmacologica Sinica 2006;27:1382–8.

[134] Elsayed, A.; Remawi, M. A.; Qinna, N.; Farouk, A.; Badwan, A. Formulation and characterization of an oily−based system for oral delivery of insulin. European Journal of Pharmaceutics and Biopharmaceutics 2009;73:269−79.

[135] Alexander T, F. Nanoparticle uptake by the oral route: Fulfilling its potential? Drug Discovery Today: Technologies 2005;2:75−81.

[136] Jia, X.; Chen, X.; Xu, Y.; Han, X.; Xu, Z. Tracing transport of chitosan nanoparticles and molecules in Caco−2 cells by fluorescent labeling. Carbohydrate Polymers 2009;78:323−9.

[137] Takeuchi, H.; Yamamoto, H.; Kawashima, Y. Mucoadhesive nanoparticulate systems for peptide drug delivery. Advanced Drug Delivery Reviews 2001;47:39−54.

[138] Heinemann, L.; Jacques, Y. Oral insulin and buccal insulin: a critical reappraisal. Journal of Diabetes Science and Technology 2009;3:568−84.

[139] Mutalik, M. Long−waited dream of oral insulin: Where did we rich? Asian Journal of Pharmaceutical and Clinical Research 2011;4:15−20

[140] Thatcher, H. S. The oral administration of insulin to rabbits. Experimental Biology and Medicine 1924;21:368−70.

[141] Kawada, J. U. N.; Tanaka, N.; Nozaki, Y. No reduction of blood glucose in diabetic rats after oral administration of insulin liposomes prepared under acidic conditions. Endocrinologia Japonica 1981;28:235−8.

[142] Diasome Pharmaceuticals [July 13, 2016]. Available from: http://diasomepharmaceuticals.com/.

[143] Opie, E. L. On the relation of chronic interstitial pancreatitis to the islands of langerhans and to diabetes melittus. The Journal of Experimental Medicine 1901;5:397−428.

[144] Nobel Prize [July 13, 2016]. Available from: http://www.nobelprize.org/educational/medicine/insulin.

[145] Berger, M. Oral insulin 1922−1992: The history of continuous ambition and failure. In: Berger M, Grier F, editors. Georg Thieme Verlag. Germany: Frontiers In Insulin Pharmacology; 1993. p. 144−8.

[146] Ryle, A.; Sanger, F.; Smith, L.; Kitai, R. The disulphide bonds of insulin. Biochemical Journal 1955;60:541−56.

[147] Ferguson, J. E. A. Oral blood sugar lowering compositions. Google Patents; 1965.

[148] Meienhofer, J.; Schnabel, E.; Bremer, H.; Brinkhoff, O; Zabel, R.; Sroka, W.; Klostermeyer, H.; Brandenburg, D.; Okuda, T.; Zahn, Z. Synthese der insulinketten und ihre kombination zu insulinaktiven praparaten. Zeitschrift für Naturforschung B. A Journal of Chemical Sciences 1963;18b:1120.

[149] Genentech [July 13, 2016]. Available from: http://www.gene.com.

[150] Pozzilli, P.; Pitocco, D.; Visalli, N.; Cavallo, M. G.; Buzzetti, R.; Crino, A.; Spera, S.; Suraci, C.; Multari, G.; Cervoni, M.; Bitti, M. L. M.; Matteoli, M. C.; Marietti, G.; Ferrazzoli, F.; Faldetta, M. R. C.; Giordano, C.; Sbriglia, M.; Sarugeri, E.; Ghirlanda, G.; Grp, I. No effect of oral insulin on residual beta−cell function in resent−onset Type I diabetes (the IMDIAB VII). Diabetologia 2000;43:1000−4.

[151] Generex biotechnology [July 13, 2016]. Available from: http://www.generex.com.

[152] Lopez, J. E.; Peppas, N. A. Cellular evaluation of insulin transmucosal delivery. Journal of Biomaterials Science−Polymer Edition 2004;15:385−96.

[153] Davis, M. E.; Chen, Z.; Shin, D. M. Nanoparticle therapeutics: An emerging treatment modality for cancer. Nature Reviews Drug Discovery 2008;7:771−82.

[154] Vauthier, C.; Bouchemal, K. Processing and scale−up of polymeric nanoparticles. In: Prokop A, editor. Intracellular Delivery. Fundamental Biomedical Technologies. 5: Springer Netherlands; 2011. p. 433−56.

[155] Raghava Srivalli, K. M.; Mishra, B. Drug nanocrystals: A way toward scale−up. Saudi Pharmaceutical Journal 2014;

[156] Galindo−Rodríguez, S. A.; Puel, F.; Briançon, S.; Allémann, E.; Doelker, E.; Fessi, H. Comparative scale−up of three methods for producing ibuprofen−loaded nanoparticles. European Journal of Pharmaceutical Sciences 2005;25:357−67.

[157] Ranjan, A.; Mukerjee, A.; Helson, L.; Vishwanatha, J. Scale up, optimization and stability analysis of Curcumin C3 complex−loaded nanoparticles for cancer therapy. Journal of Nanobiotechnology 2012;10:38.

[158] Xiliang, Q.; Yang, C.; Tiesong, L.; Peng, H.; Jun, W.; Ping, L.; Xiaolong, G. Large−scale synthesis of silver nanoparticles by aqueous reduction for low−temperature sintering bonding. Journal of Nanomaterials 2014;2014:1−8.

[159] Levin, M. Pharmaceutical process scale−up. New York: Marcel Dekker; 2002.

[160] Song, L.; Zhi, Z.−l.; Pickup, J. C. Nanolayer encapsulation of insulin−chitosan complexes improves efficiency of oral insulin delivery. International Journal of Nanomedicine 2014;9:2127−36.

[161] Fonte, P.; Araújo, F.; Reis, S.; Sarmento, B. Oral insulin delivery: How far are we? Journal of Diabetes Science and Technology 2013;7:520−31.

[162] Zijlstra, E.; Heinemann, L.; Plum−Mörschel, L. Oral insulin reloaded: A structured approach. Journal of Diabetes Science and Technology 2014;8:458−65.

[163] Leader, B.; Baca, Q. J.; Golan, D. E. Protein therapeutics: A summary and pharmacological classification. Nature Reviews Drug Discovery 2008;7:21−39.

[164] Wong, T. Design of oral insulin delivery systems. Journal of Drug Targeting 2010;18:79−92.

[165] Lopes, M. A.; Abrahim, B. A.; Cabral, L. M.; Rodrigues, C. R.; Seiça, R. M. F.; de Baptista Veiga, F. J.; Ribeiro, A. J. Intestinal absorption of insulin nanoparticles: Contribution of M cells. Nanomedicine: Nanotechnology, Biology and Medicine 2014;10:1139−51.

[166] Lopes, M. A.; Abrahim, B. A.; Seica, R.; Veiga, F.; Rodrigues, C. R.; Ribeiro, A. J. Intestinal uptake of insulin nanoparticles: Facts or myths? Current Pharmaceutical Biotechnology 2014;15:629−38.

[167] Reis, C.; Neufeld, R.; Ribeiro, A.; Veiga, F. Nanoencapsulation II. Biomedical applications and current status of peptide and protein nanoparticulate delivery systems. Nanomedicine: Nanotechnology, Biology and Medicine 2006;2:53−65.

[168] Zhang, X.; Qi, J.; Lu, Y.; He, W.; Li, X.; W, W. Biotinylated liposomes as potential carriers for the oral delivery of insulin. Nanomedicine: Nanotechnology, Biology and Medicine 2014;10:167−76.

[169] Almeida, A.; Souto, E. Solid lipid nanoparticles as a drug delivery system for peptides and proteins. Advanced Drug Delivery Reviews 2007;59:478−90.

[170] Pan, Y.; Li, Y.−J.; Zhao, H.−Y. e. a. Bioadhesive polysaccharide in protein delivery system: chitosan nanoparticles improve the intestinal absorption of insulin *in vivo*. Internation Journal of Pharmaceutics 2002;249:139−47.

[171] Sarmento, B.; Martins, S.; Ferreira, D.; Souto, E. Oral insulin delivery by means of solid lipid nanoparticles. International Journal of Nanomedicine 2007;2:743−9.

[172] Yun, Y.; Cho, Y.; Park, K. Nanoparticles for oral delivery: Targeted nanoparticles with peptidic ligands for oral protein delivery. Advanced Drug Delivery Reviews 2013;65:882−32.

[173] Peppas, N. A. Devices based on intelligent biopolymers for oral protein delivery. International Journal of Pharmaceutics 2004;277:11−7.

[174] Teply, B. A.; Tong, R.; Jeong, S. Y.; Luther, G.; Sherifi, I.; Yim, C. H.; Khademhosseini, A.; Farokhzad, O. C.; Langer, R. S.; Cheng, J. The use of charge−coupled polymeric microparticles and micromagnets for modulating the bioavailability of orally delivered macromolecules. Biomaterials 2008;29:1216−23.

[175] Jafari, B.; Rafie, F.; Davaran, S. Preparation and characterization of a novel smart polymeric hydrogel for drug delivery of insulin. BioImpacts 2011;1:135−43.

[176] Morishita, M.; Goto, T.; Takayama, K.; Peppas, N. Oral insulin delivery systems based on complexation polymer hydrogels. Journal of Drug Delivery Science and Technology 2006;16:19−24.

[177] Li, C.−L.; Deng, Y.−J. Oil−based formulations for oral delivery of insulin. Journal of Pharmacy and Pharmacology 2004;56:1101−7.

[178] Liu, G.; Ma, R.; Ren, J.; Li, Z.; Zhang, H.; Zhang, Z.; An, Y.; Shi, L. A glucose−responsive complex polymeric micelle enabling repeated on−off release and insulin protection. Soft Matter 2013;9:1636−44.

[179] Zhang, G.; Zhang, X.; Shen, H.; Yang, J.; Yang, J. Smarter glucose−sensitivity of polymeric micelles formed from phenylborate ester−co−pyrenylboronic ester for insulin delivery at physiological pH. RSC Advances 2014;4:49964−73.

[180] Mahale, N. B.; Thakkar, P. D.; Mali, R. G.; Walunj, D. R.; Chaudhari, S. R. Niosomes: Novel sustained release nonionic stable vesicular systems — An overview. Advances in Colloid and Interface Science 2012;183–184:46−54.

[181] Pardakhty, A.; Varshosaz, J.; Rouholamini, A. *In vitro* study of polyoxyethylene alkyl ether niosomes for delivery of insulin. International Journal of Pharmaceutics 2007;328:130−41.

[182] Liu, J.; Gong, T.; Wang, C.; Zhong, Z.; Zhang, Z. Solid lipid nanoparticles loaded with insulin by sodium cholate−phosphatidylcholine−based mixed micelles: Preparation and characterization. International Journal of Pharmaceutics 2007;340:153−62.

[183] Morishita, M.; Goto, T.; Peppas, N. A.; Joseph, J. I.; Torjman, M. C.; Munsick, C.; Nakamura, K.; Yamagata, T.; Takayama, K.; Lowman, A. M. Mucosal insulin delivery systems based on complexation polymer hydrogels: Effect of particle size on insulin enteral absorption. Journal of Controlled Release 2004;97:115−24.

[184] Damgé, C.; Reis, C.; Maincent, P. Nanoparticle strategies for the oral delivery of insulin. Expert Opinion on Drug Delivery 2008;5:45−68.

[185] Kumari, A.; Yadav, S. K.; Yadav, S. C. Biodegradable polymeric nanoparticles based drug delivery systems. Colloids and Surfaces B: Biointerfaces 2010;75:1−18.

[186] Ponchel, G.; Irache, J.−M. Specific and non−specific bioadhesive particulate systems for oral delivery to the gastrointestinal tract. Advanced Drug Delivery Reviews 1998;34:191−219.

[187] Ma, Z.; Lim, T. M.; Lim, L.−Y. Pharmacological activity of peroral chitosan−insulin nanoparticles in diabetic rats. International Journal of Pharmaceutics 2005;293:271−80.

[188] Foss, A. C.; Goto, T.; Morishita, M.; Peppas, N. A. Development of acrylic−based copolymers for oral insulin delivery. European Journal of Pharmaceutics and Biopharmaceutics 2004;57:163−9.

[189] Radwan, M.; Aboul−Enein, H. The effect of oral absorption enhancers on the *in vivo* performance of insulin loaded poly(ethylcyanoacrylate) nanospheres in diabetic rat. Journal of Microencapsulation 2002;19:225−35.

[190] Radwan, M. Enhancement of absorption of insulin−loaded polyisobutylcyanoacrylate nanospheres by sodium cholate after oral and subcutaneous administration in diabetic rats. Drug Development and Industrial Pharmacy 2001;27:981−9.

[191] Ubaidulla, U.; Sultana, Y.; Ahmed, F.; Khar, R.; Panda, A. Chitosan phthalate microspheres for oral delivery of insulin: Preparation, characterization, and *in vitro* evaluation. Drug Delivery 2007;14:19−23.

[192] Hua, Q. Insulin: A small protein with a long journey. Protein & Cell 2010;1:537−51.

[193] Bajpai, A. K.; Shukla, S. K.; Bhanu, S.; Kankane, S. Responsive polymers in controlled drug delivery. Progress in Polymer Science 2008;33:1088−118.

[194] Rajeswari, T. Non invasive insulins: advanced insulin
therapy over this decade. Journal of Animal and Plant Sciences 2011;1:12−20.

[195] Chaturvedi, K.; Ganguly, K.; Nadagouda, M. N.; Aminabhavi, T. M. Polymeric hydrogels for oral insulin delivery. Journal of Controlled Release 2013;165:129−38.

[196] Peppas, N.; Wood, K.; Blanchette, J. Hydrogels for oral delivery of therapeutic proteins. Expert Opinion on Biological Therapy 2004;4:881−7.

[197] Wood, K. M.; Stone, G. M.; Peppas, N. A. The effect of complexation hydrogels on insulin transport in intestinal epithelial cell models. Acta Biomaterialia 2010;6:48−56.

[198] Sajeesh, S.; Bouchemal, K.; Marsaud, V.; Vauthier, C.; Sharma, C. P. Cyclodextrin complexed insulin encapsulated hydrogel microparticles: An oral delivery system for insulin. Journal of Controlled Release 2010;147:377−84.

[199] Lakkakula, J. R.; Maçedo Krause, R. W. A vision for cyclodextrin nanoparticles in drug delivery systems and pharmaceutical applications. Nanomedicine: Nanotechnology, Biology and Medicine 2014;9:877−94.

[200] Simões, S.; Veiga, F.; Torres−Labandeira, J.; Ribeiro, A.; Concheiro, A.; Alvarez−Lorenzo, C. Syringeable self−assembled cyclodextrin gels for drug delivery. Current Topics in Medicinal Chemistry 2014;14:494−509.

[201] Simoes, S. M. N.; Rey−Rico, A.; Concheiro, A.; Alvarez−Lorenzo, C. Supramolecular cyclodextrin−based drug nanocarriers. Chemical Communications 2015;51:6275−89.

[202] Zhang, L.; Zhu, W.; Song, L.; Wang, Y.; Jiang, H.; Xian, S.; Ren, Y. Effects of hydroxylpropyl−β−cyclodextrin on *in vitro* insulin stability. International Journal of Molecular Sciences 2009;10:2031−40.

[203] Qiu, Y.; Park, K. Environment−sensitive hydrogels for drug delivery. Advanced Drug Delivery Reviews 2001;53:321−39.

[204] Laroui, H.; Sitaraman, S. V.; Merlin, D. Chapter six − Gastrointestinal delivery of anti−inflammatory nanoparticles. In: Nejat D, editor. Methods in Enzymology. Volume 509: Academic Press; 2012. p. 101−25.

[205] Yokoyama, M.; Opanasopit, P.; Okano, T.; Kawano, K.; Maitani, Y. Polymer design and incorporation methods for polymeric micelle carrier system containing water−insoluble anticancer agent camptothecin. Journal of Drug Targeting 2004;12:373−84.

[206] Li, P.; Nielsen, H.; Müllertz, A. Oral delivery of peptides and proteins using lipid−based drug delivery system. Expert Opinion on Drug Delivery 2012;9:1289−304.

[207] Fricker, G.; Kromp, T.; Wendel, A.; Blume, A.; Zirkel, J.; Rebmann, H.; Setzer, C.; Quinkert, R.−O.; Martin, F.; Müller−Goymann, C. Phospholipids and lipid−based formulations in oral drug delivery. Pharmaceutical Research 2010;27:1469−86.

[208] Pardakhty, A.; Moazeni, E.; Varshosaz, J.; Hajhashemi, V.; Rouholamini Najafabadi, A. Pharmacokinetic study of niosome−loaded insulin in diabetic rats. DARU Journal of Pharmaceutical Sciences 2011;19:404−11.

[209] Li, Z.; Chen, J.; Sun, W.; Xu, Y. Investigation of archaeosomes as carriers for oral delivery of peptides. Biochemical and Biophysical Research Communications 2010;394:412−7.

[210] Müller, R. H.; Mäder, K.; Gohla, S. Solid lipid nanoparticles (SLN) for controlled drug delivery − a review of the state of the art. European Journal of Pharmaceutics and Biopharmaceutics 2000;50:161−77.

[211] Müller, R.; Lippacher, A.; S., G. Solid lipid nanoparticles (SLN) as carrier system for the controlled release of drugs. In: DL W, editor. Handbook of Pharmaceutical Controlled Release Technology. NY, USA: Marcel Dekker; 2000. p. 377–91

[212] Wirth, M.; Hamilton, G.; Gabora, F. Lectin−mediated drug targeting: Quantification of binding and internalization of wheat germ agglutinin and solatium tuberosum lectin using Caco−2 and HT−29 cells. Journal of Drug Targeting 1998;6:95−104.

[213] Arbit, E.; Kidron, M. Oral insulin: The rationale for this approach and current developments. Journal of Diabetes Science and Technology 2009;3:562−7.

[214] Giovannucci, E. Insulin and colon−cancer. Cancer Causes & Control 1995;6:164−79.

[215] Kanzarkar, M.; Pathak, P. P.; Vaidya, M.; Brumlik, C.; Choudhury, A. Oral insulin−delivery system for diabetes mellitus. Pharmaceutical Patent Analyst 2015;4:29−36.

[216] Navgire, S. D.; Satpute, A. S.; Pandey, S.; Patil, A. T. Recent patents on oral insulin delivery. Recent Patents on Drug Delivery and Formulation 2014;8:202−5.

[217] Oramed Pharmaceuticals [July 13, 2016]. Available from: http://www.oramed.com/.

[218] Biocon [Ju3ly 1, 2016]. Available from: http://www.biocon.com/.

[219] Merrion Pharmaceuticals [July 13, 2016]. Available from: http://www.merrionpharma.com.

[220] Emisphere [July 13, 2016]. Available from: http://www.emisphere.com.

[221] Diabetology [July 13, 2016]. Available from: http://diabetology.co.uk/.

[222] Oshadi drug administration [July 13, 2016]. Available from: https://clinicaltrials.gov/ct2/show/NCT01973920.

[223] Sonaje, K.; Lin, K. J.; Tseng, M. T.; Wey, S. P.; Su, F. Y.; Chuang, E. Y.; Hsu, C. W.; Chen, C. T.; Sung, H. W. Effects of chitosan−nanoparticle−mediated tight junction opening on the oral absorption of endotoxins. Biomaterials 2011;32:8712−21.

[224] Barbosa, M. D. F. S.; Celis, E. Immunogenicity of protein therapeutics and the interplay between tolerance and antibody responses. Drug Discovery Today 2007;12:674−81.

[225] Argiles, J. M.; Lopez−Soriano, F. J. Insulin and cancer (Review). International Journal of Oncology 2001;18:683−7.

[226] Bao, Y.; Nimptsch, K.; Meyerhardt, J. A.; Chan, A. T.; Ng, K.; Michaud, D. S.; Brand−Miller, J. C.; Willett, W. C.; Giovannucci, E.; Fuchs, C. S. Dietary insulin load, dietary insulin index, and colorectal cancer. Cancer Epidemiology Biomarkers & Prevention 2010;19:3020−6.

[227] McMinn, L. H.; Hodges, G. M.; Carr, K. E. Gastrointestinal uptake and translocation of microparticles in the streptozotocin−diabetic rat. Journal of Anatomy 1996;189:553−9.

CHAPTER 2

PROBING INSULIN BIOACTIVITY IN ORAL NANOPARTICLES PRODUCED BY ULTRASONICATION–ASSISTED EMULSIFICATION/INTERNAL GELATION

2.1 ABSTRACT

ADS−based particles obtained by emulsification/internal gelation technology can be considered suitable carriers for oral insulin delivery. A rational study focused on the emulsification and particle recovery steps was developed in order to reduce particles to the nanosize range while keeping insulin bioactivity. There was a decrease in the size when ultrasonication was used during emulsification, which was more pronounced when a cosurfactant was added. Ultrasonication add−on after particle recovery decreased the aggregation and led to a narrower nanoscale particle−size distribution. The insulin EE was 99.3 ± 0.5%, attributed to the strong pH−stabilizing electrostatic effect between insulin and the NP' matrix polymers. Interactions between these polymers and insulin were predicted using molecular modeling studies through quantum mechanics calculations that allowed for the prediction of the interaction model. *In vitro* release studies indicated well−preserved integrity of the NP in SGF. CD spectroscopy proved conformational stability of insulin and FTIR spectroscopy technique showed rearrangements of insulin structure during processing. Moreover, *in vivo* biological activity in diabetic rats revealed no statistical difference when compared to nonencapsulated insulin, demonstrating the retention of insulin activity. Our results demonstrated that the ADS−based NP efficiently stabilized the loaded protein structure, presenting good physical properties for oral delivery of insulin.

2.2 INTRODUCTION

The challenge of orally administered insulin has been addressed in order to help relieve the pain and stress caused during insulin injections by millions of diabetics. Insulin is a peptide drug and therefore it is a challenge for oral delivery, due to enzymatic degradation in the GI tract and, particularly, to the difficulty to permeate the intestinal epithelium.

Much research has been focused on an oral insulin delivery system that mimics the physiologic pattern of insulin secretion [1−4]. To ensure enteric protection, recent advances in nanoencapsulation resulted in an increasing growth of innovative formulations such as micro− [5,6] and NP [7,8]. In drug delivery, NP have demonstrated numerous advantages over conventional formulations [9,10]. Particle size plays a crucial role in biomedical applications, namely on biorecognition [11], biodistribution [12], bioadhesion [13], biocompatibility [14], and biodegradation [15]. However, most techniques for producing submicron particles require organic solvents, high temperature, or vigorous agitation, which are potentially harmful parameters to the structure of insulin and consequently lead to loss of activity. Submicron particles have been produced under particularly mild processing conditions by using emulsification/internal gelation technology, which has previously been applied to the production of larger−sized microparticles [16−19] and micron− and nanometer−sized particles [20]. This technology involves experimental conditions such as nonextreme values of temperature and pH and refraining from using harsh chemicals. All of those conditions are potentially threats to the stability of peptides and proteins. Indeed, this technology makes use of naturally occurring polymers such as alginate and dextran sulfate, which are a suitable choice due to their excellent biocompatibility, drug carrying ability, adjustable controlled−release property, lower cost, abundance in nature, and easier application [21]. Previous studies revealed that the presence of a copolymer, such as dextran sulfate, enhances the loading of hydrophilic drugs and that the type of polymer has a considerable effect on the LC [22].

However, one of the limitations of the emulsification/internal gelation technology consists of the difficulty to obtain monodispersed populations of particles. As drug−delivery systems, the size control and size uniformity of carriers are of great interest to generate *in vitro* and *in vivo* reproducible as well as repeatable profiles and behaviors, which will further result in benefits in clinical use [23]. ADS−particles show polydispersed populations,

characterized by a wide size distribution which derives from micro− and NP and also aggregates coexistence [24], characteristic of the emulsification methods using biodegradable polymers [25]. Over the past years, emulsification−based technologies have been optimized to produce polysaccharide−based particles with a lower size and monodispersed populations [20,26−28]. Ultrasonication is particularly effective in breaking up the aggregates of particles, thereby reducing their size and polydispersity [29]. However, ultrasonication has also been related to the formation of protein aggregates with structural changes [30].

As delivery systems for insulin, the most important characteristics of particles include size distribution, EE, and the release profile of insulin from particles while maintaining the biological activity of insulin during and after processing. From an industrial and economic perspective, the EE is crucial especially in the case of proteins, which are expensive products [31].

Stability is a major challenge especially when insulin is encapsulated in polymeric particles using an emulsion−based technique. The emulsification step is identified as critical for protein inactivation and aggregation. The hydrophobic interface created between the water and oily solvent, and the hydrophobic interactions between the protein and polymer, may lead to adsorption of insulin at the interface, which results in insulin unfolding and/or aggregation [32−34]. In addition, the shear used for the emulsification can also contribute to insulin denaturation [35]. Hence, maintaining the native conformation of insulin during the encapsulation process is highly important, which otherwise may lead to protein aggregation and immunogenicity.

The purpose of this work was to develop a formulation of insulin−loaded biopolymer−based NP produced by emulsification/internal gelation technique with good physical properties for oral delivery and assess how emulsion droplet size may affect the resultant particles, while probing the activity of insulin after each step of the process. The emulsification step was performed with and without ultrasonication assistance and in the presence of one or two surfactants. The recovery strategy of particles was also investigated to increase the recovery yield and ensure the removal of residual oil from the surface of particles. For better insight about the formation of ADS−particles, molecular modeling studies were performed. Here, quantum mechanics calculations were employed to understand the electronic properties of the multicomponent system of ADS.

Particles were characterized according to size distribution, surface charge, morphology, EE, and *in vitro* insulin release behavior. The activity of insulin during and after each stage of processing was assessed either *in vitro* or *in vivo*.

2.3 MATERIALS AND METHODS

2.3.1 Materials

Low−viscosity sodium alginate (viscosity of 1% solution at 25 °C, 4–12 cP), dextran sulfate, sorbitan monooleate (Span® 80), phosphotungstic acid, trifluoroacetic acid (TFA) 99%, acetonitrile (ACN) (LiChrosolv) HPLC grade, sodium citrate dehydrate and Nile red were all obtained from Sigma−Aldrich (USA). Calcium carbonate was obtained from Setacarb (France), paraffin oil from Scharlau (Spain), insulin 100 IU/mL (Actrapid®) from Novo Nordisk A/S (Denmark) and poloxamer 188 (Lutrol® F68) from BASF (Germany).

2.3.2 ADS−based particles preparation

The insulin−loaded particles were prepared through a modified emulsification/internal gelation technique [20,24]. Briefly, the water in oil (W/O) emulsion was formed by mixing the ADS−matrix with the oil phase. An aqueous solution of sodium alginate (2.0%, w/v) and dextran sulfate (0.75%, w/v) was prepared by stirring (100 rpm) overnight. Insulin was added and dissolved (100 IU/mL, 10 mL). Then, an aqueous suspension of ultrafine calcium carbonate (5%, w/v) was ultrasonicated for 30 min to break up crystal aggregates, and was dispersed at calcium–alginate mass ratio of 1.0:0.3. The resultant dispersion was emulsified within paraffin oil (aqueous phase/oil phase 50/50, v/v) facilitated by sorbitan monooleate (2%, v/v) by impeller−stirring homogenization (1600 rpm). The effects of cosurfactant addition, poloxamer 188, keeping the hydrophilic–lipophilic balance (HLB) required for a W/O emulsion (HLB = 4–6) [36] and ultrasonication add−on during the emulsification step at different times (10, 15, 20, 25, and 30 min) as well as at different ultrasonic amplitudes (30, 45 and 60%) were tested.

After emulsification, gelation was induced by addition of paraffin oil containing glacial acetic acid (molar ratio of acid–calcium, 3.5) to solubilize the calcium dispersed in the ADS−droplets for 15 min. Unloaded particles were prepared as controls.

2.3.4 Particle recovery

The oil−dispersed alginate particles were recovered through an extraction medium [20] (protocol A) consisting of acetate buffer solution (pH 4.5) (USP 34) with dehydrating solvents (acetone, isopropanol, and hexane) added under continual stirring (600 rpm) followed by centrifugation (12500*g* at 4 °C for 10 min). Different extraction protocols (B–F) were developed, which can be seen in Table 2.1.

Table 2.1. Composition of the protocols media to recover the emulsion−dispersed particles. The solvents included in the protocol A were added simultaneously and particles were separated by centrifugation (12500*g* at 4 °C for 10 min); the other protocols began with dissolution in hexane (protocols B−E) or hexane/acetate buffer pH 4.5 (protocol F) for 1 h before the addition of the other solvents and the particles were separated by decantation.

	Emulsion/solvent volume ratio					
Protocol	**Hexane**	**Acetate buffer pH 4.5**	**Methanol**	**Isopropanol**	**Acetone**	**Ethanol**
A	1.00:0.04	1:0.56	–	1:0.12	1:0.16	–
B	1.00:1.50	–	1:3	1:2.00	–	–
C	1.00:1.50	–	1:3	–	1:2.00	–
D	1.00:1.50	–	1:5	–	–	–
E	1.00:0.50	–	–	1:0.70	–	1:1.0
F	1.00:0.15	1:1.25	–	1:0.20	–	1:0.3

The other protocols included a first step where the oil−dispersed particles were submitted to extraction with hexane (protocols B–E) or a hexane/acetate buffer mixture (protocol F) for 1 h in an orbital shaker. Particle recovery occurred after the addition of the other solvents by decantation. Different volume ratios of the dehydrating solvents with acetate buffer were studied. The recovery yield was determined by measuring insulin content in the aqueous phase after particle recovery (Equation 1):

$$\text{Recovery yield } (\%) = \frac{\text{Insulin in the aqueous phase}}{\text{Total amount of insulin}} \times 100 \quad (1)$$

Before emulsification, the oil phase was stained with Nile red to better assess the efficiency of the oil elimination from the particles.

Added solvents to recover the particles were removed by using a rotoevaporator system (BUCHI, V−700, Vacuum controller V−870/B−491/R−210) under reduced pressure at controlled temperature.

2.3.5 Ultrasonication exposure

The ultrasonication was applied to the aqueous suspension of particles with an ultrasonicator (Sonics®, VCX130; Sonics & Materials, CT, USA) with an amplitude of 60% for 5 and 10 min in order to break up agglomerates. The temperature was kept below 25 °C by using an ice bath.

2.3.6 Determination of insulin content

Insulin was extracted from particles through dissolution in sodium citrate (55 mM) prepared in phosphate buffer solution (PBS) at pH 7.4 (USP 34) for 1 h in an orbital shaker. After particle dissolution, the medium was centrifuged (12500*g* at 4 °C for 10 min) and the insulin content in the supernatant was assessed by HPLC.

2.3.7 Emulsion and particle size analysis

The emulsion droplet size measurements were performed by dynamic light scattering (DLS) (DelsaNano C, Beckman Coulter Delsa™, Germany). The measurements were carried out at 25 °C with a detection angle of 60°. The size distribution was represented by normalized intensity distribution. The instrument was routinely checked and calibrated using a standard latex particle kit (Beckman Coulter, Inc., Germany).

The particle−size distribution analysis was performed by laser diffraction (LD) using a particle size analyzer (Beckman Coulter® LS 13 320; Beckman Coulter, Inc., FL, USA) with polarization intensity differential scattering (PIDS). The real and the imaginary refractive index were set to 1.36 and 0.01, respectively. Three measurements of 90 s were used and the size distribution was represented by volume, given as diameter values corresponding to percentiles of 10, 50, and 90% together with the relative span value. The particle size before and after each cycle of ultrasonication was additionally investigated by DLS.

2.3.8 ζ−potential analysis

The surface charge was determined by electrophoretic light scattering using a ζ−potential analyzer (DelsaNano C, Beckman Coulter Delsa™, Germany) at pH 4.5 and 25 °C. The equipment was routinely checked and calibrated using mobility standard (Beckman Coulter, Inc.).

2.3.9 Insulin EE

The insulin EE was calculated by the difference between the total amount of insulin used to prepare the particles and the amount of free insulin per total amount of insulin. The insulin−loaded particles were separated from the aqueous supernatant containing free insulin by centrifugation (12500*g* at 4 °C for 10 min), and the amount of free insulin was determined by HPLC.

2.3.10 Morphological analysis

The morphology of the single surfactant−assisted particles was monitored by scanning electron microscopy (SEM). The suspension was diluted in deionized water (Milli−Q) (1:10, v/v) and dried in a desiccator for 24 h. The particle morphology was observed using a scanning electron microscope (Phenom G2 Pure). The shape, surface, and mass spectroscopy of the cosurfactant and ultrasonication−assisted particles were analyzed by field environmental (FE)−cryo−SEM scanning microscope (EDS−JEOL JSM 6301 F, Oxford INCA Energy 350, Gatan Alto 2500). Phosphotungstic acid−stained particles were frozen using liquid nitrogen slush (− 210 °C) under vacuum to allow their fracture in order to obtain a fresh and clean surface for examination. Then, the samples were sublimated at −90 °C for 4 min to remove top layers of water molecules. Finally, thr samples were sputter coated with gold/palladium for 40 s, followed by image capturing.

2.3.11 Insulin retention/release studies

For determination of the insulin retention/release profile in enzyme−free simulated digestive fluids, 5 mL of the aqueous suspension of particles were incubated in 10 mL of SGF without pepsin (USP 34) at 37 °C for 2 h with shaking of 100 strokes/min using a shaking water bath (SS40−D; GRANT, UK), followed by the incubation of the particles in 10 mL of SIF without pancreatin (USP 34) for 6 h. Sample aliquots were collected and replaced by the same volume of fresh incubation medium at predetermined times. For the determination of the insulin released from the particles, withdrawn samples were centrifuged at 12500*g* at 4 °C for 10 min before HPLC injection. The difference between the initial amount of insulin and the insulin in the supernatant corresponds to the amount of insulin retained within the particles.

2.3.12 Insulin quantification

Insulin was analyzed by HPLC (LC−2010 HT; Shimadzu Co., Japan) equipped with a quaternary pump, a column 5 µm, 4.6 × 250 mm (X−Terra RP 18; Waters Co., MA, USA), and precolumn 5 µm, 4 × 4 mm (Purospher STAR RP−18; Merck KGaA, Germany). The mobile phase consisted of ACN and 0.1% TFA aqueous solution initially set in the ratio of 30:70 (v/v), which was linearly changed to 40:60 (v/v) over 5 min. From 5 to 10 min, the ratio of 40:60 (v/v) was kept constant. Eluent was pumped at a flow rate of 1 mL/min, the injection volume was 20 µL, and the detection wavelength was 214 nm. The chromatograms were recorded and the peak area responses were measured using an automatic integrator [37].

2.3.13 Quantum mechanical studies

The three−dimensional structures of sodium alginate and dextran sulfate were constructed using a software program (Spartan'10 v1.1.0; Wavefunction, Inc., CA, USA). Each structure was submitted to energy minimization to obtain the most energetically stable conformation. Then, the geometry optimization by the PM6 semiempirical method was conducted and the stereoelectronic properties were obtained, such as the frontier molecular orbitals, highest occupied molecular orbital (HOMO) and lowest unoccupied molecular orbital (LUMO), distribution coefficient, and energy, dipole moment vector, and volume. The quantum chemical calculations for the other polymers were also performed, such as cellulose sulfate [38], sodium polyphosphate [39], and sodium carboxymethylcellulose [40], previously described as reinforcement polymers.

2.3.14 Conformational stability of insulin

2.3.14.1 CD spectroscopy

To evaluate the conformational stability of the insulin released from the particles, CD spectroscopy was performed with a spectropolarimeter (Olis DSM 20 CD; On−line

Instrument Systems, GA, USA) equipped with a temperature controller, continuously purged with nitrogen, and controlled by GLOBALWORKS software. Spectra were collected at 37 °C using a 0.1 cm cell over the wavelength range of 200–260 nm. A scanning speed (7 nm/min) with a 6−second response time was employed. Each spectrum represents an average of three consecutive scans, and blank buffer subtraction and data analysis were performed. The molar ellipticity of insulin was calculated as (Equation 2):

$$\text{CD signal} \times \frac{\text{Mean residual weight of each insulin redidue}}{\text{Insulin concentration}} \quad (2)$$

, where insulin concentration is mg/mL × cell pathlength (0.1 cm). The concentration of insulin was determined by UV absorption at 276 nm, using a molar extinction coefficient of 6,070 $M^{-1}{\cdot}cm^{-1}$. The samples for CD analysis were prepared by dissolution in PBS pH 7.4. The spectra of the insulin released from the NP collected before and after rotoevaporation and ultrasonication were compared with that of the nonencapsulated insulin solution made in PBS pH 7.4 at a similar concentration. The secondary structure components (α−helix, β−sheet, turn, and random coil) of the insulin samples were estimated through the CDSSTR algorithm with reference set 7 from the DICHROWEB website (http://dichroweb.cryst.bbk.ac.uk/html/home.shtml) [41].

2.3.14.2 FTIR spectroscopy

The nonencapsulated insulin in solution before and after ultrasonication and the insulin entrapped into the ADS−particles before and after ultrasonication were analyzed through the FTIR technique. All the spectra were collected with 256 scans and a 4 cm^{-1} resolution in the region of 4,000−6,00 cm^{-1}. The insulin spectra were obtained following a double subtraction procedure [42], followed by a 15−point Savitsky–Golay second derivative, and a baseline correction using a 3− to 4−point adjustment at the amide I region (1,710−1,590 cm^{-1}). Finally, all the spectra were area−normalized for further comparison. All of the described spectral treatment was performed using the HorizonMB FTIR software (ABB, Switzerland) [43].

2.3.15 Insulin biological activity

Animals were maintained and tested in accordance with the Federation of European Laboratory Animal Science Association (FELASA) and the European Union Council Directive 86/609/EEC. Animals' procedures and manipulations were conducted according to the ethical principles and guidelines for housing and experiments on animals of the Direcção Geral de Alimentação e Veterinária (DGAV). Male Wistar rats weighing 250–350 g were housed under controlled temperature and humidity, and a 12–12−h light–dark cycle. Diabetes was induced with single intraperitoneal injection of 60 mg/kg streptozotocin (STZ) freshly prepared in citrate buffer pH 4.5 to damage the pancreatic cells. During the 24 h after STZ injection, rats were given 5% glucose physiologic solution to prevent hypoglycemia due to pancreatic damage. After 3 days, rats with frequent urination, loss of weight, and fasting plasma glucose levels higher than 250 mg/dL were randomized into three groups (n = 6 per group) for *in vivo* studies. The animals were fasted for 12 h before the experiments with free access to water. To minimize the diurnal blood glucose fluctuations, the experiments were performed during the 12−h light cycle.

The insulin bioactivity was analyzed in diabetic rats after s.c. administration at 2 IU/kg. The animals were tested in two different studies, in which the same groups were used. In the first study, insulin was extracted from the NP through dissolution in sodium citrate (55 mM) prepared in PBS at pH 7.4. The unloaded particles were submitted to the same treatment and were used as negative control. The nonencapsulated insulin was used as positive control. Two days after the first administration, the second study was carried out with the formulations dispersed in water. Then, the insulin entrapped in the NP was tested, and the unloaded NP and nonencapsulated insulin were used as negative and positive controls, respectively.

Blood samples were collected from the tip of the tail vein during an 8−hour span and the blood glucose levels were measured using the ACCU−CHEK Aviva device.

2.3.16 Statistical analysis

All the experiments were performed in triplicate and are represented as mean ± s.d.. The statistical evaluation was performed with a one−way analysis of variance (ANOVA) followed by Bonferroni post hoc−test (SPSS 20.0, USA). A $p < 0.05$ was taken as the criterion of significance. The level of significance was set at probabilities of $^{*}p < 0.05$, $^{**}p < 0.01$, and $^{***}p < 0.001$.

2.4 RESULTS AND DISCUSSION

Several factors could affect the size of the ADS−particles obtained by emulsification, namely the stirring speed, the emulsification time, the viscosity of both internal and external phases, the concentration and type of surfactant, and the recovery protocol [44,45]. For the design and development of the insulin−loaded ADS−particles, additional components and steps were integrated into the previously described particles obtained by emulsification, and their influence on the physicochemical and biological parameters, such as the size distribution and the insulin EE, were evaluated.

The protein stability during formulation and product−development costs remain major challenges in the pilot scale−up of micro− and NP which need to be addressed at all levels of research and development so a novel technology can be successfully achieved. Thus, probing insulin secondary structure during the the nanoencapsulation process was of major concern, and was assessed whenever possible.

2.4.1 Emulsion size analysis

Submicron size carriers have previously been shown to enable the insulin absorption through the intestinal membranes [46,47]. The influence of the NP' size is obvious, giving rise to the possibility that larger−sized particles may remain in the PP, which are rich in M−cells, and lead to slower action. Smaller NP, if appropriately charged, can pass through the lymphatic pathway and later enter the systemic circulation [3]. Therefore, it is admitted

that the optimal size for NP to be taken up by the M−cells would be below 1 μm [48], and more precisely, below 200 nm [49,50].

Accordingly, the first approach in this study was to reduce the W/O emulsion droplet size to the nanoscale. An insufficient dispersion of the phases during emulsification results in large particles with wide size distribution [51]. The final size of NP depends on the globule size throughout the emulsification process [52], which is mainly determined by the energy input, as well as by the nature of the emulsifying agent/agents [53]. To verify the influence of these factors on the emulsion size distribution, ultrasonication add−on for 15 and 30 min and different ultrasonic amplitudes were tested. It was noticed that an increase in the ultrasonication time until 15 min led to a displacement of the emulsion size−distribution curve toward lower size (Figure 2.1), with median diameters decreasing from 1,119 to 442 nm. On the other hand, increasing the time of ultrasonication until 30 min led to bigger emulsion droplets. According to these results, there was an optimal ultrasonication time of 15 min, and beyond it coalescence may become predominant due to the cavitation phenomena. Therefore, the ultimate size would occur when a balance between droplet breakup and re−coalescence is assured [54]. In this work, the optimal condition was an ultrasonication amplitude of 60% for 15 min. Different ultrasonic amplitudes were tested at 15 min of emulsification (data not shown) and the smallest emulsion median diameter was obtained with 60%.

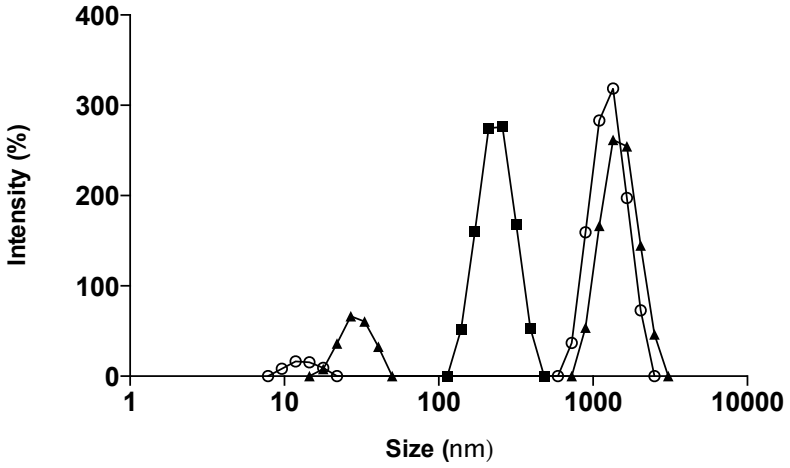

Figure 2.1. Influence of the ultrasonication time on the emulsion size distribution. Notes: Empty circles: without sonication. After 15 min (full squares) and 30 min (full triangles) of ultrasonication exposure.

The influence of the addition of the cosurfactant poloxamer 188 on the emulsion size distribution at different time points ranging from 10 to 30 min of emulsification was also evaluated (Figure 2.2). Maintaining the initial percentage of the surfactant used, the lowest ratio of sorbitan monooleate/poloxamer 188 required to achieve the necessary HLB to obtain a W/O emulsion (1.84% [v/v] of sorbitan monooleate and 0.16% [w/v] of poloxamer 188) was employed. There was a decrease in the emulsion size when the cosurfactant was added.

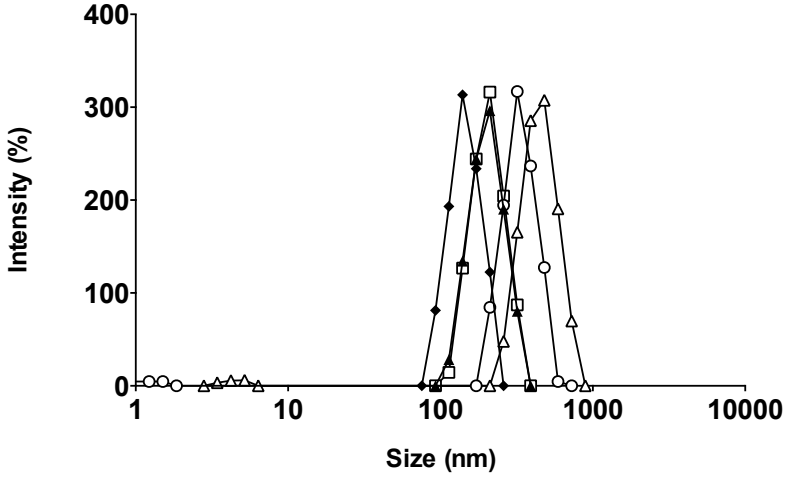

Figure 2.2. Influence of the cosurfactant addition on the emulsion size distribution. Notes: After 10 min (empty squares), 15 min (full diamonds), 20 min (full triangles), 25 min (empty circles), and 30 min (empty triangles) of ultrasonication exposure.

The effect of the ultrasonication time in the presence of the cosurfactant led to similar results, since periods higher than 15 min increased the diameter of the emulsion droplets, but with only 10 min of exposure, the decrease was less efficient (Figure 2.2). The use of sorbitan monooleate/poloxamer 188 decreased the median diameters of the emulsion droplets from 442 to 317 nm after 15 min of ultrasonication exposure. This phenomenon can be expected, since a blend of surfactants with high and low HLB are known to produce more stable emulsions than do single surfactants, since they provide better coverage at the interface [55]. Nanoemulsions are all characterized by a great stability in suspension due to their very small size, essentially due to significant steric stabilization between droplets [56].

2.4.2 Particle recovery

The recovery yield of the six protocols studied was evaluated both by its capacity to eliminate residual oil and oil droplets, and by insulin content in the recovered particles. In the standard protocol [20], oil−dispersed particles were recovered by a washing step (protocol A, Table 2.1) associated with centrifugation, which resulted in 29.4 ± 7.2% (Figure 2.3) of the insulin content. Insulin losses could have been due to particle stress during either their preparation or recovery. Firstly, during washing used to remove the residual oil from the surface of the particles, insulin may have been drawn out, in which smaller particles were probably more affected. Secondly, the centrifugal force may have also contributed to insulin losses, due to the porous nature of the alginate particles. Thus, the balance between the insulin retention inside the ADS−particles, the protocol extraction, and/or the centrifugal force was considered. The other protocols (B–F) were designed by varying the solvent proportions, and the centrifugal force was replaced by gravity separation. Generally, the higher the shear put into creating the emulsion, the finer the droplets produced, and the more stable the emulsion. However, very stable emulsions are more difficult to break [57]. Therefore, the difficulty to recover oil−dispersed particles to the aqueous suspension takes on special importance when lower−sized particles are considered.

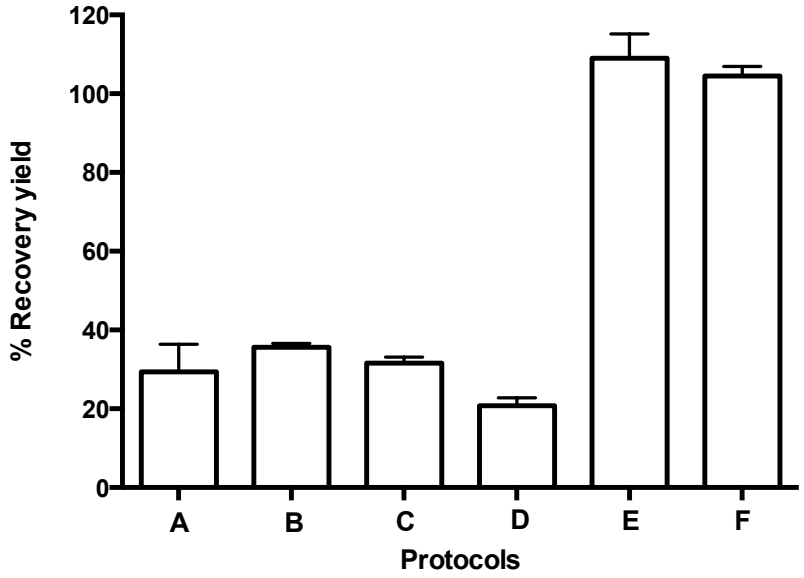

Figure 2.3. Influence of the protocol extractions (A–F) on the insulin−based particles recovery yield from the oil phase. Note: Each value represents mean ± s.d., n = 3.

All the protocols began with the emulsion dissolution in hexane for 1 h, which was considered as the minimum time for complete dissolution. Hexane is often used as a solvent for oil extraction due to its lower boiling point for easy removal after extraction, its nonpolar nature, and its low toxicity when compared to other solvents [58]. The protocols B–D were also ineffective as recovery media (Figure 2.3). On the other hand, the insulin content after the application of the protocol E was 103.4 ± 1.2%, demonstrating its efficacy. The protocol E was composed of hexane, ethanol, and isopropanol. Ethanol and isopropanol are suitable solvents and have also been used on other NP formulations [59]. Bilati *et al.* have shown that the mean particle size was dependent on polarity decrease [60], and therefore mixtures of ethanol and isopropanol (less polar−solvent than ethanol) with different proportions were evaluated. In order to minimize the use of these organic solvents, acetate buffer pH 4.5 was included in the washing protocol and the protocol F was chosen, enabling the overall quantification of insulin (Figure 2.3). The attainment of recovery yields higher than 100%, as happened with the particles recovered using the protocols E and F, can be explained by

some variations of the volumes used during all steps included in the particle production and recovery, which may change the theoretical insulin content to values higher or lower than expected. The Nile red–stained oil phase allowed for the confirmation of effective oil removal from the aqueous phase, since all the fluorescence was present in the upper phase (oil phase) during decantation.

2.4.3 Removal of organic solvents

The organic solvents were removed from the extracted particles by rotoevaporation. The best conditions capable of removing all the organic solvents, keeping the particles (with the maximum amount of insulin content) in the aqueous phase, were 40 °C, 70 mbar, for 15 min. It is well established that all proteins unfold above their melting temperature [61]. The melting point described for insulin was 63 ± 1 °C, a point where both the size and the intensity start to increase significantly [62]. Below this temperature, the insulin tertiary structure is believed to be stable [37,62]; therefore, the chosen rotoevaporation temperature would not affect the insulin tertiary structure. Furthermore, insulin is unaffected by pressures of 48,000 bar in the solid state at room temperature, which may be due to its relative rigidity combined with its small size [63].

2.4.4 Particle size analysis

The presence of aggregates was macroscopically observed after the single surfactant–assisted particle recovery. Insulin and the biopolymers (both alginate and dextran sulfate) have opposite charges, allowing electrostatic interactions to occur, which may contribute to the particle aggregation [64].

The size distribution of particles is shown in Figure 2.4 in terms of volume. The diameters of particles corresponding to the percentiles of 10, 50, and 90% as well as the span values are depicted in Table 2.2. Concerning the single surfactant–assisted particles, two different populations can be observed: a small one consisting of NP and low–sized particles (< 6 μm); and the main range consisting of higher–sized microparticles (D90 = 326 ±

128 μm). These particles possess, therefore, a wide size distribution, with the predominant percentage being of microparticles, probably due to the presence of aggregates, and a lower percentage of low−sized particles.

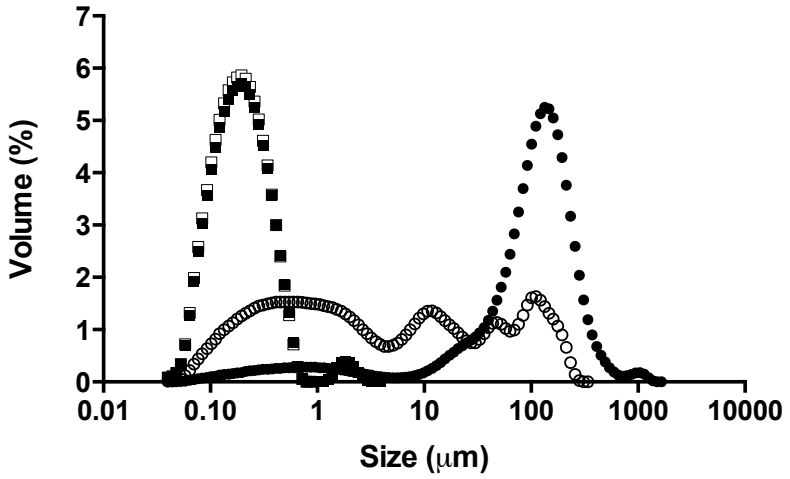

Figure 2.4. Size distribution of the particles under the following processing steps. Notes: Full circles: single surfactant−assisted particles. Empty circles: cosurfactant and ultrasonication−assisted particles. Full squares: after 5 min of ultrasonication exposure. Empty squares: after 10 min of ultrasonication exposure.

Table 2.2. Granulometric distribution of the particles. Notes: The particles were prepared with: A) single surfactant; and B) cosurfactant and ultrasonication−assistance. Diameter values (mean ± s.d., n = 3) corresponding to percentiles of 10, 50, and 90%, and span values after each processing.

	LD				DLS	
Formulation	**D10 (µm)**	**D50 (µm)**	**D90 (µm)**	**Span value**	**Mean (nm)**	**PdI**
A	14 ± 11	125 ± 24	326 ± 128	2.49	–	–
B	0.134 ± 0.039	0.659 ± 0.054	11 ± 3	16.09	556 ± 12	0.24
B 5−min ultrasonication	0.092 ± 0.056	0.199 ± 0.439	0.437 ± 0.320	1.73	293 ± 4	0.30
B 10−min ultrasonication	0.091 ± 0.032	0.194 ± 0.064	0.407 ± 0.061	1.63	248 ± 2	0.27

Abbreviations: PdI, polydispersity index; D, diameter.

The emulsion optimization and recovery−medium development resulted in particles with a median size of 659 nm, with a higher population of particles in the nanometer range, while the higher−sized microparticles, which constituted the main population before, sharply decreased (D90 = 11 ± 3 µm). The strategies implied in the emulsion optimization (blend of cosurfactants and ultrasonication add−on) were essential to the size reduction observed, since the emulsion droplets produced during the emulsification step originate the final particles. In order to achieve a unique population of NP, the ultrasonication add−on after the particle recovery was chosen as a strategy to eliminate or decrease aggregation and therefore to allow a narrower particle−size distribution. Maintaining the same amplitude applied in the emulsion optimization (60%), the effect of ultrasonication on the particle size distribution was evaluated and compared for 5 and 10 min. After 5 min of the exposure to ultrasonication, the particles showed a deviation to the left of the distribution

curve (Figure 2.4), predominantly to the nanoscale, with a slight and isolated population of approximately 2 μm. Consequently, the percentile values suffered a huge decrease, as can be seen in Table 2.2. After 10 min of ultrasonication, on the other hand, a single population of NP was observed. These particles were also analyzed by DLS. The results are depicted in Table 2.2, being consistent with the results obtained by LD and confirming the nanoscale size range of particles.

2.4.5 ζ−potential analysis

The results summarized in Table 2.3 exhibit that the ADS−NP are strongly negatively charged with ζ−potentials ranging from −53.4 to −60.4 mV. The negative ζ−potential values are essentially due to the surface charges of alginate and dextran sulfate chains at pH 4.5, which confer negative charges to the NP. The charge behavior of the NP was also studied at different pHs, namely at alginate pKa and at pH 1.5. At alginate pKa, the alginate chains are almost neutral and the ζ−potential of the particles increased from −59.6 to −25.0 mV. The particle charge was due to the sulfate dextran chains that remained permanently charged since they have a negative first pKa value and a second pKa value near 2.65. At pH 1.5, the blocks of dextran sulfate chains become positive and the ζ−potential increased to −9.2 mV. Thus, the NP' charge is essentially due to the matrix of alginate and dextran sulfate, which was proven by the charge behavior of the NP at different pHs. No effect of the roto-evaporation and ultrasonication was detected on the NP' ζ−potential, highlighting the absence of any physical stability changes. The unloaded NP presented similar results compared to the insulin−loaded NP, demonstrating no effect of insulin regarding particle charge. The ζ−potential of the insulin−loaded NP was expected to be less negative compared to the unloaded NP, given the positive charge of insulin at pH below its isoelectric point (pI): 5.3. The adsorption of insulin on the surface of the NP may be assumed as negligible and insulin was mainly incorporated inside the NP' matrix. The ζ−potential of both the insulin−loaded and the unloaded NP at pH 6.8 decreased approximately by 10 mV (data not shown), since the matrix of biopolymers became more ionized. The magnitude of the ζ−potential may indicate the potential electrostatic stability of the NP, with values greater than 30 mV or less than −30 mV related to the NP with higher stability in suspension and

lower aggregation tendency. The particles are strongly charged at pH 4.5, which leads to the prevention of aggregation by repulsive forces upon random impact of th eadjacent particles, as previously reported [65].

Table 2.3. ζ−potential (mean ± s.d., n = 3) of the NP after each processing step at different pHs.

Formulation	pH 4.5 (mV)	pH = alginate pk_a (mV)	pH 1.5 (mV)
Insulin−loaded NP	−59.6 ± 11.5	−25.0 ± 2.8	−9.2 ± 2.0
− After rotoevaporation	−53.4 ± 6.4	−34.9 ± 1.5	−11.0 ± 3.6
− After ultrasonication	−60.4 ± 3.3	−27.6 ± 0.8	−9.3 ± 0.7
Unloaded NP	−50.9 ± 4.6	−29.8 ± 1.5	−8.0 ± 0.2

2.4.6 Insulin EE

The insulin EE value was 99.3 ± 0.5%, higher than that previously reported by our group [24,66]. This high level can be attributed to the pH effect of the NP' components. Insulin has an PI at approximately pH 5.368 and alginate has pKa values of 3.38 and 3.65 for mannuronic and guluronic residues, respectively [67]. Therefore, strong electrostatic attractions at the final pH of 4.5 may occur providing high EE of the oppositely charged protein [24]. Furthermore, calcium ions interact with the guluronic residues and can establish ionic bridges with the negatively charged carboxylic residues of insulin, strengthening the association between insulin and alginate [68]. The addition of poloxamer 188 can also contribute to the insulin EE due to the steric stabilization by the molecules of poloxamer [65].

2.4.7 Morphological analysis

The structure of the single surfactant−assisted particles was examined by SEM (Figure 2.5A). The presence of agglomerates with individual particles of approximately 5 μm can be seen. The structure of the the cosurfactant and ultrasonication−assisted NP was verified by cryo−SEM, which demonstrated good sphericity and smooth surfaces (Figure 2.5B). The size of the NP determined by the morphological analysis is in accordance with the previously measured size (by LS and DLS), lying in the nanoscale range. The smooth and dense particle surface could be due to residual surfactants, as observed previously [69]. Although both the particles demonstrated spherical shape, Figure 2.5B showed smaller particles with smoother surfaces. These particles were obtained from a more stable emulsion produced with cosurfactant and ultrasonication addition, which originated nanodroplets during emulsification. Small particles are known to dramatically enhance the Brownian motion, which further prevents particle aggregation, offers increased stability [70], and justifies the lower tendency of the cosurfactant and ultrasonication−assisted particles to aggregate compared to the single surfactant−assisted particles. The particles of Figure 2.5A had a more porous texture, contrary to the particles of Figure 2.5B, probably because during the recovery step they lost a significant amount of water during centrifugation, leading to a change of the polymeric structure [20]. Furthermore, the cosurfactant addition has been shown to make particles smoother and slightly porous in previous studies [71].

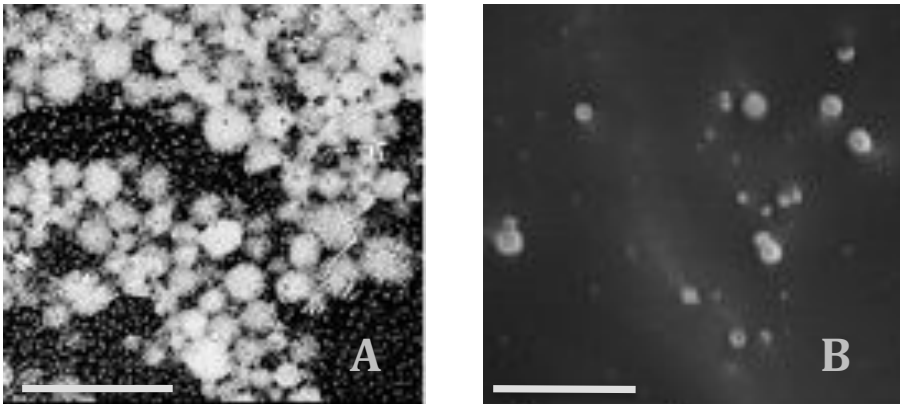

Figure 2.5. (A) Scale bar = 20 µm; SEM microphotograph of the single surfactant−assisted particles. (B) Scale bar = 1 µm; cryo−SEM microphotograph of the cosurfactant and ultrasonication−assisted particles.

2.4.8 Insulin retention/release studies

The insulin release from the NP was studied as a function of time in enzyme−free simulated digestive fluids as illustrated in Figure 2.6. The insulin−loaded NP showed the protective effect of the biopolymers at the beginning in SGF during the first 2 h. This retention capacity can be attributed to the gel strength of the NP in the dissolution media, preventing the release of insulin from the formulation [72]. Then, a burst release of insulin was noticed under basic conditions (pH 6.8) simulating the intestinal environment. In this pH, the polymers swell due to deprotonation [73], allowing the insulin release from the NP. The total insulin release was achieved during the following 3 h. The release profile of insulin showed a pH−dependent behavior, indicating that these NP are an effective controlled−delivery system for insulin. Previous studies with biopolymer particles also prepared with emulsification/internal gelation showed a burst release during the first 4 h but a sustained release profile up to 10 h, achieving only approximately 75% of the cumulative−released insulin [27]. Although a sustained release of insulin is desired, the insulin release should not take that long, unless the particles are sufficiently mucoadhesive

to stay in the intestinal epithelium, maintaining the insulin structure for such a prolonged period of time.

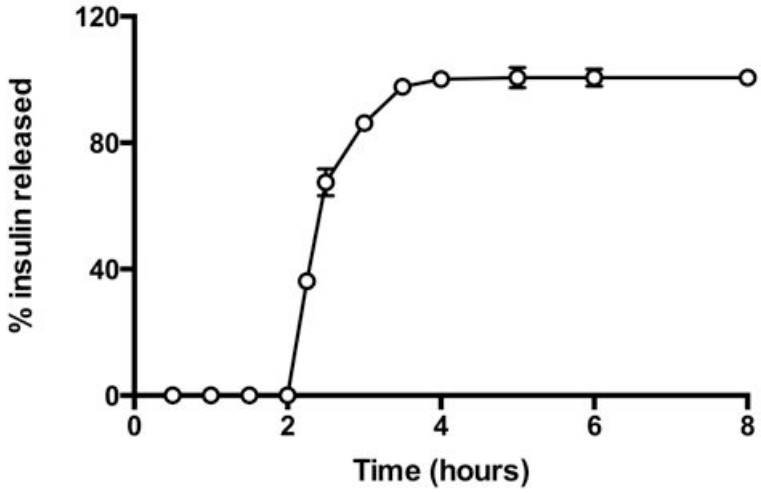

Figure 2.6. Insulin release profile simulated in pH 1.2 SGF for 2 h followed by 4 h in pH 6.8 SIF at 37 °C. Note: Each value represents mean ± s.d., n = 3.

2.4.9 Quantum mechanical studies

The theoretical parameter analysis showed a relationship between the HOMO and LUMO, the dipole moment vector, and the EE values (Table 2.4). The GAP value is the difference between the energies of the frontier orbitals (HOMO−LUMO) and plays a critical role in the chemical reactivity, which is related to the intermolecular interactions [74]. Previous experimental results [75] revealed that the reinforcement of alginate matrix with dextran sulfate presented the highest insulin EE and one of the lowest particle sizes, compared to the other anionic polymers. Considering the theoretical results for the reinforcement polymers, the HOMO−LUMO gap (Figure 2.7A) and the dipole moment values of dextran sulfate were the closest to the alginate values (Table 2.4). These findings can be directly related to important electrostatic interactions in the nanosystem formation and explain the high insulin EE found in our study.

Table 2.4. Theoretical studies of the HOMO−LUMO gap and dipole moment of the anionic polymers.

Anionic polymers	**HOMO−LUMO gap**	**Dipole moment (Debye)**
Sodium alginate	−9.34	16.55
Dextran sulfate	−9.50	11.85
Cellulose sulfate	−10.00	7.82
Sodium polyphosphate	−11.45	5.80
Sodium carboxymethylcellulose	−8.33	41.54

Besides, based on the HOMO and LUMO distribution coefficients and dipole moment vector orientation, it was possible to predict the interactions between alginate and dextran sulfate (Figure 2.7B). Based on these results, it could be seen that the negatively charged groups of alginate remain free to establish electrostatic interactions with the positively charged groups of the insulin surface. So, based on the HOMO and LUMO distributions coefficients, it was possible to suggest the interaction between sodium alginate and dextran sulfate. Considering the high value of insulin EE (99.3 ± 0.5%) obtained with these NP, a correlation between the theoretical studies and insulin EE can be predicted.

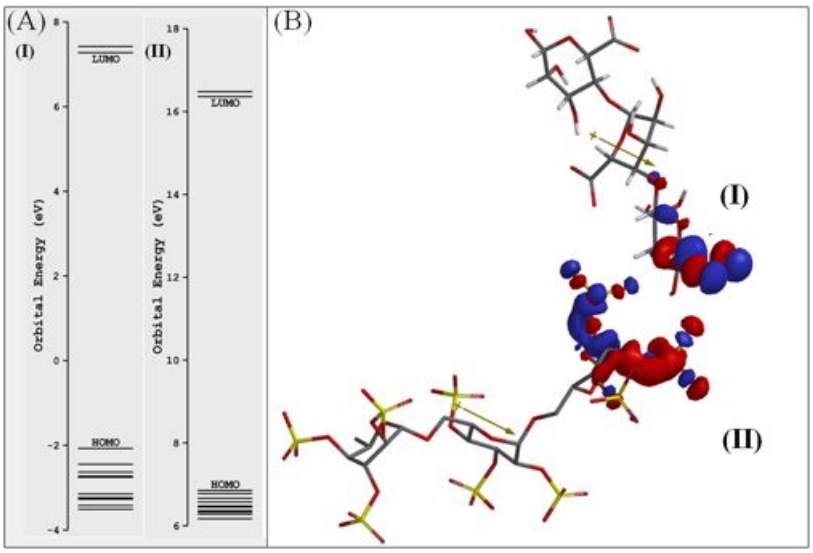

Figure 2.7. Predicted interaction between biopolymers based on the distribution of the frontier molecular orbitals (HOMO and LUMO). Notes: (A) HOMO−LUMO gap and (B) interaction between alginate (I) and dextran sulfate (II) based on their distribution coefficients of the HOMO and LUMO, respectively. The positive and negative regions are represented by blue and red colors, respectively.

2.4.10 Conformational stability of insulin

CD and FTIR are techniques that can provide structural information about proteins. The spectroscopic characterization of protein secondary structure is often partially unreliable when the samples are not extremely pure and abundant. This problem may be overcome by the combination of CD and FTIR [76]. The stability of the insulin encapsulated and released from NP was evaluated using these two techniques at different time points. Conformational changes in the secondary structure of insulin during each processing of encapsulation were monitored by CD and FTIR analysis.

2.4.10.1 CD spectroscopy

The conformation of proteins or peptides is important for the exertion of an optimal therapeutic effect and it can be easily damaged under conditions such as high temperature, mechanical manipulation, and exposure to organic solvents. Generally, the secondary structure (α−helix and β−sheet) can illustrate the efficacy of insulin. CD is regarded as one of the most effective methods to evaluate the secondary structures of proteins and peptides [77].

Figure 2.8 represents the CD spectra of the insulin secondary structures. The nonencapsulated insulin showed two minima at 210 and 220 nm, which is typical of predominant α−helix structure proteins. These results were in agreement with the results presented by other studies [68,78]. The CD spectra of the insulin released from the NP after the recovery, rotoevaporation, or exposure to ultrasonication revealed no substantial alterations in the two α−helix minima when compared to the nonencapsulated insulin. To better assess the structural transition, the CD spectra of insulin were de−convoluted through the software from the DICHROWEB website [41] and the results are displayed in Table 2.5. Practically no difference in the relative proportions of the secondary structure elements was detected along the preparation of the NP, suggesting no insulin fibrillation/aggregation among the conditions tested.

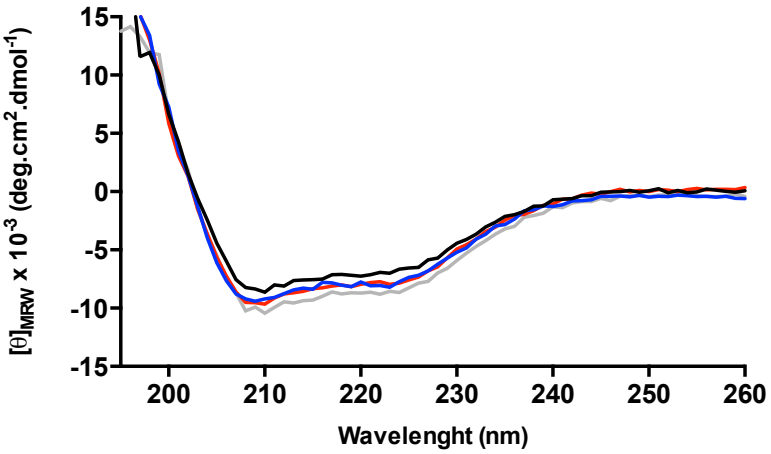

Figure 2.8. CD spectra of insulin in PBS at pH 7.4 and 25 °C. Notes: Solid black line: nonencapsulated insulin. Solid blue line: insulin released from the NP after recovery. Solid red line: insulin released from the NP after rotoevaporation. Solid grey line: insulin released from the NP after ultrasonication exposure.

Abbreviation: $[\theta]_{MRW}$, mean residue molar ellipticity.

Table 2.5. Estimation results of the secondary structural content of insulin extracted from the NP before and after the recovery, rotoevaporation, and ultrasonication as obtained from the CD spectral analyses.

Secondary structure content	**Nonencapsulated insulin (%)**	**Insulin released from NP after**		
		Recovery (%)	**Rotoevaporatoration (%)**	**Sonication (%)**
α	39	42	42	39
β	31	34	31	31
Turn	8	8	7	8
Unordered	22	21	21	22

2.4.10.2 FTIR spectroscopy

The second−derivative FTIR spectra of insulin are represented in Figure 2.9. The The characteristic bands found in the infrared spectra of proteins and polypeptides include the amide I and amide II. Amide I absorption arises from the amide bonds that link the amino acids and is directly related to the backbone conformation, with a major contribution from the C=O stretching vibration and minor contribution from the C–N stretching vibration. The major component of the amide I spectrum is the α−helix band, whereas the β−sheet and β−turn bands contribute less to the secondary structure [79]. The modifications of the α−helix are the most characteristic of protein denaturation and consequent loss of activity. The nonencapsulated insulin in solution is dominated by the α−helix content (1,655 cm^{-1}), but also the high− and low−frequency β−sheet content (1,682 and 1,614 cm^{-1}).

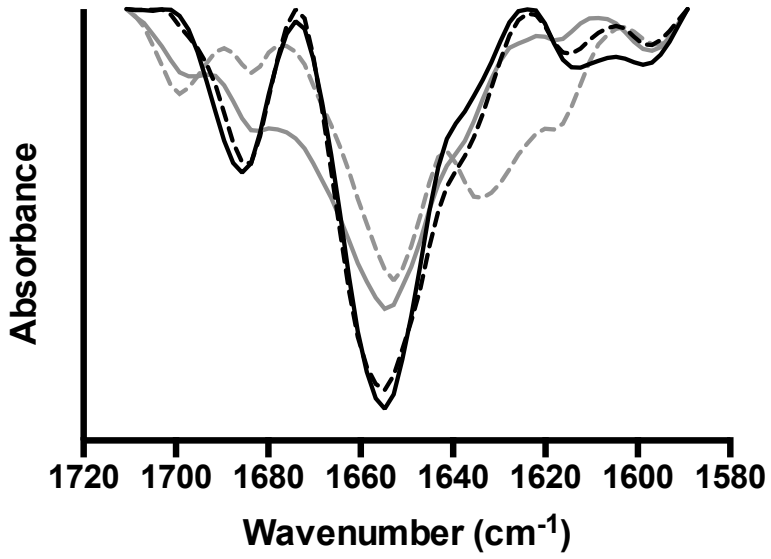

Figure 2.9. FTIR spectra of insulin. Notes: FTIR spectra of the nonencapsulated reference insulin in solution (solid black line), nonencapsulated insulin in solution after 10 min of ultrasonication exposure (dashed black line), insulin entrapped into the NP (solid grey line), and insulin entrapped into the NP after 10 min of ultrasonication exposure (dashed grey line).

In Figure 2.9 the spectrum of the nonencapsulated insulin in solution submitted to ultrasonication presented an area overlap of 0.92 compared to the nonencapsulated insulin without processing, indicating that ultrasonication slightly affects the insulin secondary structure. This structural modification motivated by ultrasonication was characterized just by a slight decrease on the α−helix band. The spectrum of the insulin−loaded NP submitted to ultrasonication presented an area−overlap of 0.75 compared to the nonencapsulated insulin in solution, which was similar to the formulation without ultrasonication (0.76), indicating that the native conformation of the insulin changed with either ultrasonication or formulation procedure and those changes were quantitatively similar. Besides similar area−overlap values, it was noticed that after the entrapment into the NP, the insulin structure changed, originating a decrease of the α−helix and β−sheet content. Furthermore, after ultrasonication of the insulin−loaded NP, the structure of insulin changed by decreasing its α−helix content at approximately 1,655 cm^{-1} and increasing the β−sheet at 1,635 cm^{-1}. These modifications are representative of insulin denaturation. The band at 1,700 cm^{-1} also indicated an unordered structural change. Besides the structural changes of insulin upon the entrapment into the NP and ultrasonication, the maintenance of the α−helix band on the second−derivative amide I FTIR spectra, despite some decrease, still is a good indicator of the insulin bioactivity. Additionally, the possible structural rearrangements of insulin upon entrapment into the NP may help to mitigate the decrease of the insulin bioactivity.

2.4.11 Insulin biological activity

The blood glucose profiles following the s.c. injection of insulin to diabetic rats at a dose level of 2 IU/kg are illustrated in Figures 2.10 and 2.11. The insulin released from the NP and the nonencapsulated insulin promoted a rapid and intense decrease of glycemia, hitting less than 20% of the initial values after 2 h (Figure 2.10). Then, the blood glucose levels increased, reaching approximately 70–90% of the basal values at 8 h. In the second study (Figure 2.11), the insulin entrapped into the NP showed a slight and less−pronounced decrease of glycemia (57% of the initial values) than the insulin released from the NP, whereas the nonencapsulated insulin provided a rapid and intense decrease of glycemia,

which was, however, also less pronounced than in the first study (35% of the initial values). Then, the blood glucose levels increased, reaching approximately 70% of the basal values at 8 h. The insulin entrapped into the NP allowed a more controlled and smooth antihyperglycemic effect over time than the insulin released from the NP, which was already in the free form (isolated from the polymeric matrix) when subcutaneously administered, enabling a faster and abrupt effect. There were no statistical differences between the groups treated with the same dose level of nonencapsulated insulin and insulin−loaded NP, confirming the retention of the insulin activity. The integrity of insulin after the nanoformulation and, consequently, its biological activity were insured.

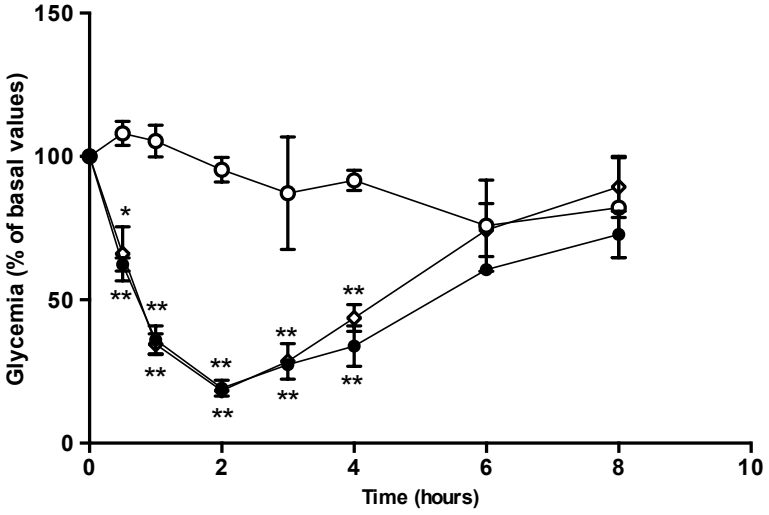

Figure 2.10. Blood glucose levels of diabetic Wistar rats after the s.c. administration of insulin. Notes: Full circles: nonencapsulated insulin. Empty diamonds: insulin released from the NP. Comparison is made to the extracted unloaded NP (empty circles). The formulations were administered in sodium citrate in PBS at pH 7.4. The results are expressed as mean ± s.d., n = 6 per group. Statistically different from the empty NP: $^{*}p < 0.05$; $^{**}p < 0.01$.

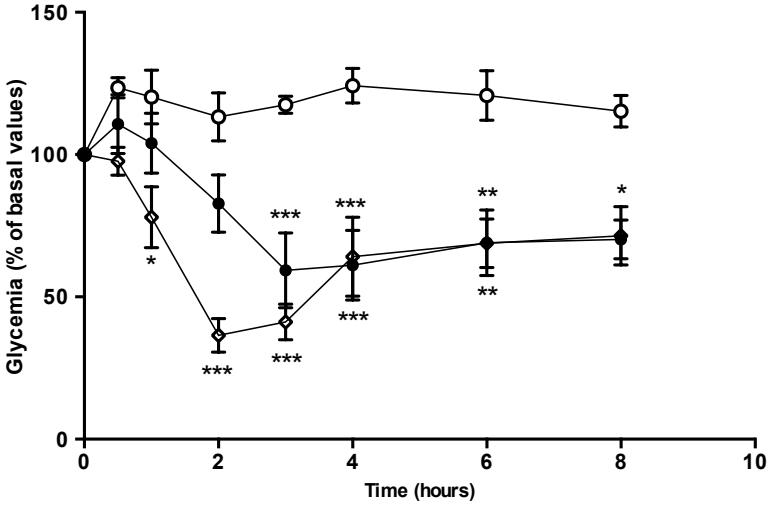

Figure 2.11. Blood glucose levels of diabetic Wistar rats after the s.c. administration of 2 IU/kg of insulin in water. Notes: Empty diamonds: nonencapsulated insulin. Full circles: insulin entrapped into the NP. Comparison is made to the unloaded NP (empty circles). The formulations were administered in water. The results are expressed as mean ± s.d., n = 6 per group. Statistically different from the empty NP: $^{*}p < 0.05$; $^{**}p < 0.01$; $^{***}p < 0.001$.

2.5 CONCLUSIONS

The emulsification/internal gelation technique was successfully optimized to overcome the drawbacks imposed by this technique, such as the wide size distribution in the microscale and the low recovery yield. These results demonstrated that the ultrasonication add−on was an efficient strategy that allowed the reduction of the size of the emulsion droplets and, therefore, the formation of particles in the nanoscale. This strategy was further improved using a blend of cosurfactants (sorbitan monooleate and poloxamer 188). The recovery of the oil−dispersed NP was also developed, achieving a maximum of insulin content in the aqueous phase. The further submission of these particles to ultrasonication led to a monodisperse population of particles in the nanoscale, observed by the deviation of the size−distribution profile from the micrometric to the nanometric range and the decrease of respective span values.

The molecular modeling studies brought an unprecedented evaluation of the quantum mechanics through studies of the biopolymers interactions. The results showed a relationship between the electronic properties and the insulin EE. Furthermore, they indicated electronic requirements to improve the EE, allowing for the prediction of the interaction model between sodium alginate and dextran sulfate.

Strongly negatively charged NP with high insulin EE and insulin retention within the NP in gastric simulation medium were obtained. The secondary structure of insulin tested by CD showed that insulin retained its biological activity during the process of encapsulation, while FTIR analysis showed rearrangements of the insulin structure. However, the biological activity of the released insulin from the NP after s.c. injection to diabetic Wistar rats demonstrated the retention of insulin activity. The insulin entrapped into the NP showed a slight and less−pronounced decrease than the insulin released from the NP, justified by the interaction of insulin with the biopolymers.

This optimized methodology with mild conditions for insulin during encapsulation and easily manipulated procedures allowed for the preparation of ADS−based insulin−loaded particles in the nanometric range with retention of insulin activity, which has important applications for the pharmaceutical field.

2.6 REFERENCES

[1] Carino, G. P.; Jacob, J. S.; Mathiowitz, E. Nanosphere based oral insulin delivery. Journal of Controlled Release 2000;65:261−9.

[2] Fonte, P.; Araújo, F.; Silva, C.; Pereira, C.; Reis, S.; Santos, H. A.; Sarmento, B. Polymer−based nanoparticles for oral insulin delivery: Revisited approaches. Biotechnology Advances 2015;

[3] Lopes, M. A.; Abrahim, B. A.; Cabral, L. M.; Rodrigues, C. R.; Seiça, R. M. F.; de Baptista Veiga, F. J.; Ribeiro, A. J. Intestinal absorption of insulin nanoparticles: Contribution of M cells. Nanomedicine: Nanotechnology, Biology and Medicine 2014;10:1139−51.

[4] Lopes, M. A.; Abrahim, B. A.; Seica, R.; Veiga, F.; Rodrigues, C. R.; Ribeiro, A. J. Intestinal uptake of insulin nanoparticles: Facts or myths? Current Pharmaceutical Biotechnology 2014;15:629−38.

[5] Déat−Lainé, E.; Hoffart, V.; Garrait, G.; Beyssac, E. Whey protein and alginate hydrogel microparticles for insulin intestinal absorption: Evaluation of permeability enhancement properties on Caco−2 cells. International Journal of Pharmaceutics 2013;453:336−42.

[6] Situ, W.; Chen, L.; Wang, X.; Li, X. Resistant starch film−coated microparticles for an oral colon−specific polypeptide delivery system and its release behaviors. Journal of Agricultural and Food Chemistry 2014;62:3599−609.

[7] Du, X.; Zhang, J.; Zhang, Y.; Li, S.; Lin, X.; Tang, X.; Zhang, Y.; Wang, Y. Decanoic acid grafted oligochitosan nanoparticles as a carrier for insulin transport in the gastrointestinal tract. Carbohydrate Polymers 2014;111:433−41.

[8] Samant M.; Banerjee S. S.; Taneja N.; Zope K.; Ghogale P.; J., K. J. Biophysical interactions of polyamidoamine dendrimer coordinated Fe_3O_4 nanoparticles with insulin. Journal of Biomedical Nanotechnology 2014;10:1286−93.

[9] Sakuma, S.; Hayashi, M.; Akashi, M. Design of nanoparticles composed of graft copolymers for oral peptide delivery. Advanced Drug Delivery Reviews 2001;47:21−37.

[10] Soppimath, K. S.; Aminabhavi, T. M.; Kulkarni, A. R.; Rudzinski, W. E. Biodegradable polymeric nanoparticles as drug delivery devices. Journal of Controlled Release 2001;70:1−20.

[11] Hwang, W. S.; Truong, P. L.; Sim, S. J. Size−dependent plasmonic responses of single gold nanoparticles for analysis of biorecognition. Analytical Biochemistry 2012;421:213−8.

[12] Hirn, S.; Semmler−Behnke, M.; Schleh, C.; Wenk, A.; Lipka, J.; Schäffler, M.; Takenaka, S.; Möller, W.; Schmid, G.; Simon, U.; Kreyling, W. Particle size−dependent and surface charge−dependent biodistribution of gold nanoparticles after intravenous administration. European Journal of Pharmaceutics and Biopharmaceutics 2011;77:407−16.

[13] Hassani, S.; Pellequer, Y.; Lamprecht, A. Selective adhesion of nanoparticles to inflamed tissue in gastric ulcers. Pharmaceutical Research 2009;26:1149−54.

[14] Akbar, N.; Mohamed, T.; Whitehead, D.; Azzawi, M. Biocompatibility of amorphous silica nanoparticles: Size and charge effect on vascular function, *in vitro*. Biotechnology and Applied Biochemistry 2011;58:353−62.

[15] Cui, X.; Hunter, W.; Yang, Y.; Chen, Y.; J, G. Biodegradation of pyrene in sand, silt and clay fractions of sediment. Biodegradation 2011;22:297−307.

[16] Alexakis, T.; Boadi, D. K.; Quong, D.; Groboillot, A.; O'Neill, I.; Poncelet D.; Neufeld, R. J. Microencapsulation of DNA within alginate microspheres and cross−linked chitosan

membranes for *in vivo* application. Applied Biochemistry and Biotechnology 1995;50:93–106.

[17] Poncelet, D.; Lencki, R.; Beaulieu, C.; Halle, J. P.; Neufeld, R. J.; Fournier, A. Production of alginate beads by emulsification/internal gelation. I. Methodology. Applied Microbiology and Biotechnology 1992;38:39−45.

[18] Quong, D.; Neufeld, R. J.; Skjåk−Bræk, G.; Poncelet, D. External versus internal source of calcium during the gelation of alginate beads for DNA encapsulation. Biotechnology and Bioengineering 1998;57:438−46.

[19] Ribeiro, A. J.; Neufeld, R. J.; Arnaud, P.; Chaumeil, J. C. Microencapsulation of lipophilic drugs in chitosan−coated alginate microspheres. International Journal of Pharmaceutics 1999;187:115−23.

[20] Reis, C.; Ribeiro, A.; Neufeld, R.; Veiga, F. Alginate microparticles as novel carrier for oral insulin delivery. Biotechnology and Bioengineering 2007;96:977−89.

[21] Stops, F.; Fell, J. T.; Collett, J. H.; Martini, L. G. Floating dosage forms to prolong gastro−retention — The characterisation of calcium alginate beads. International Journal of Pharmaceutics 2008;350:301−11.

[22] Abbaspour, M.; Makhmalzadeh, B.; Arastoo, Z.; Jahangiri, A.; Shiralipour, R. Effect of anionic polymers on drug loading and release from clindamycin phosphate solid lipid nanoparticles. Tropical Journal of Pharmaceutical Research 2013;12:477−82.

[23] Ma, T.; Wang, L.; Yang, T.; Ma, G.; Wang, S. Homogeneous PLGA−lipid nanoparticle as a promising oral vaccine delivery system for ovalbumin. Asian Journal of Pharmaceutical Sciences 2014;9:129−36.

[24] Reis, C.; Ribeiro, A.; Houng, S.; Veiga, F.; Neufeld, R. Nanoparticulate delivery system for insulin: Design, characterization and *in vitro*/*in vivo* bioactivity. European Journal of Pharmaceutical Sciences 2007;30:392 − 7.

[25] Gaumet, M.; Gurny, R.; Delie, F. Localization and quantification of biodegradable particles in an intestinal cell model: The influence of particle size. European Journal of Pharmaceutical Sciences 2009;36:465−73.

[26] Corzo−Martínez, M.; Soria, A. C.; Villamiel, M.; Olano, A.; Harte, F. M.; Moreno, F. J. Effect of glycation on sodium caseinate−stabilized emulsions obtained by ultrasound. Journal of Dairy Science 2011;94:51−8.

[27] Santos, A. C.; Cunha, J.; Veiga, F.; Cordeiro−da−Silva, A.; Ribeiro, A. J. Ultrasonication of insulin−loaded microgel particles produced by internal gelation: Impact on particle's size and insulin bioactivity. Carbohydrate Polymers 2013;98:1397−408.

[28] Zhang, J.; Peppard, T. L.; Reineccius, G. A. Double−layered emulsions as beverage clouding agents. Flavour and Fragrance Journal 2014;

[29] Kim, H.−Y.; Han, J.−A.; Kweon, D.−K.; Park, J.−D.; Lim, S.−T. Effect of ultrasonic treatments on nanoparticle preparation of acid−hydrolyzed waxy maize starch. Carbohydrate Polymers 2013;93:582−8.

[30] Stathopulos, P. B.; Scholz, G. A.; Hwang, Y.−M.; Rumfeldt, J. A. O.; Lepock, J. R.; Meiering, E. M. Sonication of proteins causes formation of aggregates that resemble amyloid. Protein Science 2004;13:3017−27.

[31] Fonte, P.; Soares, S.; Costa, A.; Andrade, J. C.; Seabra, V.; Reis, S.; Sarmento, B. Effect of cryoprotectants on the porosity and stability of insulin−loaded PLGA nanoparticles after freeze−drying. Biomatter 2012;2:329−39.

[32] Morlock, M.; Koll, H.; Winter, G.; Kissel, T. Microencapsulation of rh−erythropoietin, using biodegradable poly(d,l−lactide−co−glycolide): protein stability and the effects of stabilizing excipients. European Journal of Pharmaceutics and Biopharmaceutics 1997;43:29−36.

[33] Sah, H. Protein behavior at the water/methylene chloride interface. Journal of Pharmaceutical Sciences 1999;88:1320−5.

[34] Kang, F.; Singh, J. Conformational stability of a model protein (bovine serum albumin) during primary emulsification process of PLGA microspheres synthesis. International Journal of Pharmaceutics 2003;260:149−56.

[35] Andreas, K.; Zehbe, R.; Kazubek, M.; Grzeschik, K.; Sternberg, N.; Bäumler, H.; Schubert, H.; Sittinger, M.; Ringe, J. Biodegradable insulin−loaded PLGA microspheres fabricated by three different emulsification techniques: investigation for cartilage tissue engineering. Acta Biomaterialia 2001;7:1485−95.

[36] ICI Americas, i. The HLB system: A time−saving guide to emulsifier selection. Wilmington, Delaware ICI Americas Inc.; 1984.

[37] Sarmento B.; Martins S.; Ribeiro A.; Veiga F.; Neufeld R.; D., F. Development and comparison of different nanoparticulate polyelectrolyte complexes as insulin carriers. International Journal of Peptide Research and Therapeutics 2006;12:131–8.

[38] Canaple, L.; Rehor, A.; Hunkeler, D. Improving cell encapsulation through size control. Journal of Biomaterials Science, Polymer Edition 2002;13:783−96.

[39] Timmy, S.; Victor, S.; Sharma, C.; Kumari, J. Betacyclodextrin complexed insulin loaded alginate microspheres − Oral insulin delivery. Trends in Biomaterials and Artificial Organs 2002;15:48−53.

[40] Gursoy, A.; Karakus, D.; Okar, I. Polymers for sustained release formulations of dipyridamole−alginate microspheres and tabletted microspheres. Journal of Microencapsulation 1999;16:439−52.

[41] Whitmore, L.; Wallace, B. A. DICHROWEB, an online server for protein secondary structure analyses from circular dichroism spectroscopic data. Nucleic Acids Research 2004;32:W668−W73.

[42] Dong, A.; Huang, P.; Caughey, W. S. Protein secondary structures in water from second−derivative amide I infrared spectra. Biochemistry 1990;29:3303−8.

[43] Fonte, P.; Soares, S.; Sousa, F.; Costa, A.; Seabra, V.; Reis, S.; Sarmento, B. Stability study perspective of the effect of freeze−drying using cryoprotectants on the structure of insulin loaded into PLGA nanoparticles. Biomacromolecules 2014;15:3753−65.

[44] Chaouchi, S.; Hamdaoui, O. Acetaminophen extraction by emulsion liquid membrane using Aliquat 336 as extractant. Separation and Purification Technology 2014;129:32−40.

[45] Dâas, A.; Hamdaoui, O. Extraction of anionic dye from aqueous solutions by emulsion liquid membrane. Journal of Hazardous Materials 2010;178:973−81.

[46] Aboubakar, M.; Couvreur, P.; Pinto−Alphandary, H.; Gouritin, B.; Lacour, B.; Farinotti, R.; Puisieux, F.; Vauthier, C. Insulin−loaded nanocapsules for oral administration: *In vitro* and *in vivo* investigation. Drug Development Research 2000;49:109−17.

[47] Woitiski, C. B.; Sarmento, B.; Carvalho, R. A.; Neufeld, R. J.; Veiga, F. Facilitated nanoscale delivery of insulin across intestinal membrane models. International Journal of Pharmaceutics 2011;412:123−31.

[48] Gullberg, E.; Leonard, M.; Karlsson, J.; Hopkins, A. M.; Brayden, D.; Baird, A. W.; Artursson, P. Expression of specific markers and particle transport in a new human intestinal M−Cell model. Biochemical and Biophysical Research Communications 2000;279:808−13.

[49] des Rieux, A.; Fievez, V.; Garinot, M.; Schneider, Y.−J.; Préat, V. Nanoparticles as potential oral delivery systems of proteins and vaccines: A mechanistic approach. Journal of Controlled Release 2006;116:1−27.

[50] Florence, A. T. Nanoparticle uptake by the oral route: Fulfilling its potential? Drug Discovery Today: Technologies 2005;2:75−81.

[51] Silva, C.; Ribeiro, A.; Figueiredo, M.; Ferreira, D.; Veiga, F. Microencapsulation of hemoglobin in chitosan−coated alginate microspheres prepared by emulsification/internal gelation. The AAPS Journal 2005;7:E903−E13.

[52] Mainardes, R. M.; Evangelista, R. C. PLGA nanoparticles containing praziquantel: Effect of formulation variables on size distribution. International Journal of Pharmaceutics 2005;290:137−44.

[53] Dickinson, E. Interfacial interactions and the stability of oil−in−water emulsions. Pure and Applied Chemistry 1992;64:1721−4.

[54] Wu, Z. M.; Zhou, L.; Guo, X. D.; Jiang, W.; Ling, L.; Qian, Y.; Luo, K. Q.; Zhang, L. J. HP55−coated capsule containing PLGA/RS nanoparticles for oral delivery of insulin. International Journal of Pharmaceutics 2012;425:1−8.

[55] Attwood, D. F., A. FASTtrack: Physical pharmacy. Second ed. Pharmaceutical Press; 2008.

[56] Anton, N.; Benoit, J.−P.; Saulnier, P. Design and production of nanoparticles formulated from nano−emulsion templates — A review. Journal of Controlled Release 2008;128:185−99.

[57] Alvarado, V.; Wang, X.; Moradi, M. Stability proxies for water−in−oil emulsions and implications in aqueous−based enhanced oil recovery. Energies 2011;4:1058−86.

[58] Nwabanne, J. T. Kinetics and thermodynamics study of oil extraction from fluted pumpkin seed. International Journal of Multidisciplinary Sciences and Engineering 2012;3:11−5.

[59] Schubert, M. A.; Müller−Goymann, C. C. Solvent injection as a new approach for manufacturing lipid nanoparticles − Evaluation of the method and process parameters. European Journal of Pharmaceutics and Biopharmaceutics 2003;55:125−31.

[60] Bilati, U.; Allémann, E.; Doelker, E. Development of a nanoprecipitation method intended for the entrapment of hydrophilic drugs into nanoparticles. European Journal of Pharmaceutical Sciences 2005;24:67−75.

[61] Wang, W. Instability, stabilization, and formulation of liquid protein pharmaceuticals. International Journal of Pharmaceutics 1999;185:129−88.

[62] Elsayed, A.; Remawi, M. A.; Qinna, N.; Farouk, A.; Badwan, A. Formulation and characterization of an oily−based system for oral delivery of insulin. European Journal of Pharmaceutics and Biopharmaceutics 2009;73:269−79.

[63] Murphy, R. B. Anomalous stability of insulin at very high pressure. Experientia 1978;34:188−9.

[64] Nguyen, V. S.; Rouxel, D.; Hadji, R.; Vincent, B.; Fort, Y. Effect of ultrasonication and dispersion stability on the cluster size of alumina nanoscale particles in aqueous solutions. Ultrasonics Sonochemistry 2011;18:382−8.

[65] Woitiski, C. B.; Neufeld, R. J.; Ribeiro, A. J.; Veiga, F. Colloidal carrier integrating biomaterials for oral insulin delivery: Influence of component formulation on physicochemical and biological parameters. Acta Biomaterialia 2009;5:2475−84.

[66] Reis, C. P.; Neufeld, R. J.; Ribeiro, A. J.; Veiga, F. Nanoencapsulation I. Methods for preparation of drug−loaded polymeric nanoparticles. Nanomedicine: Nanotechnology, Biology and Medicine 2006;2:8 − 21.

[67] Draget, K. I.; Skjåk Bræk, G.; Smidsrød, O. Alginic acid gels: the effect of alginate chemical composition and molecular weight. Carbohydrate Polymers 1994;25:31−8.

[68] Sarmento, B.; Ferreira, D. C.; Jorgensen, L.; van de Weert, M. Probing insulin's secondary structure after entrapment into alginate/chitosan nanoparticles. European Journal of Pharmaceutics and Biopharmaceutics 2007;65:10−7.

[69] Magenheim, B.; Benita, S. Nanoparticle characterization: A comprehensive physicochemical approach. STP Pharma Sciences 1991;1:221−41.

[70] Sakulchaicharoen, N.; O'Carroll, D.; Herrera, J. Enhanced stability and dechlorination activity of pre−synthesis stabilized nanoscale FePd particles. Journal of Contaminant Hydrology 2010;118:117−27.

[71] Ahmed, M.; El−Rasoul, S.; Auda, S.; Ibrahim, M.; 61–69. Emulsification/internal gelation as a method for preparation of diclofenac sodium−sodium alginate microparticles. Saudi Pharmaceutical Journal 2013;21:61−9.

[72] Soni, M. L.; Kumar, M.; Namdeo, K. P. Sodium alginate microspheres for extending drug release: formulation and *in vitro* evaluation. International Journal of Drug Delivey 2 2010;64−8.

[73] George, M.; Abraham, T. E. Polyionic hydrocolloids for the intestinal delivery of protein drugs: Alginate and chitosan − a review. Journal of Controlled Release 2006;114:1−14.

[74] Murugavel, S.; Vijayakumar, S.; Nagarajan, S.; Ponnuswamy, A. Crystal Structure and DFT Studies of 4−(1−Benzyk−5−Methyl−1H−1,2,3−Triazol−4−YL)−6v(3−Methoxyphenyl)Pyrimidin−2−Amine. Journal of the Chilean Chemical Society 2014;59:2640−6.

[75] Silva, C. M.; Ribeiro, A. J.; Ferreira, D.; Veiga, F. Insulin encapsulation in reinforced alginate microspheres prepared by internal gelation. European Journal of Pharmaceutical Sciences 2006;29:148−59.

[76] Ascoli, G.; Pergami, P.; Luu, K.; Alkon, D.; Bramanti, E.; Bertucci, C.; Di Bari, L.; Salvadori, P. Use of CD and FT−IR to determine the secondary structure of purified proteins in the low−microgram range. Enantiomer 1998;3:371−81.

[77] Pocker, Y.; Biswas, S. B. Conformational dynamics of insulin in solution. Circular dichroic studies. Biochemistry 1980;19:5043−9.

[78] Li, X.; Qi, J.; Xie, Y.; Zhang, X.; Hu, S.; Xu, Y.; Lu, Y.; Wu, W. Nanoemulsions coated with alginate/chitosan as oral insulin delivery systems: Preparation, characterization, and hypoglycemic effect in rats. International Journal of Nanomedicine 2013;8:23−32.

[79] Nielsen, L.; Frokjaer, S.; Carpenter, J. F.; Brange, J. Studies of the structure of insulin fibrils by Fourier transform infrared (FTIR) spectroscopy and electron microscopy. Journal of Pharmaceutical Sciences 2001;90:29−37.

CHAPTER 3

ALGINATE–BASED MICRO– AND NANOPARTICLES COATED WITH CHITOSAN

3.1 ABSTRACT

Polymers and particularly biopolymers have an important effect on the surface charge and particle size of polymer−coated NP. Those NP' properties may have influence on their biological behavior, namely stability, membranes absorption, distribution and elimination. Polycationic biopolymers such as CS can be used to increase the stability of polyanionic alginate−based NP and to minimize the loss of the encapsulated insulin. Alginate and CS can crosslink together through electrostatic forces to form NP with protective properties as well as provide them the ability to improve the bioadhesion and permeability. A rational study was developed to optimize CS coating of insulin−loaded NP made of ADS. The physicochemical parameters of the NP, such as the surface charge and particle size, were investigated to provide the ideal CS concentration and NP/CS proportion, ensuring a more effective coating. Following the CS coating, an increase of the ζ−potential of the NP was observed. The NP coating with CS at 0.30% (w/v) and NP/CS proportion of 1.00:0.50 (v/v) presented the best value of ζ−potential (−22.4 ± 3.80 mV), as well as the lowest NP size. Therefore, this optimized formulation is a promising approach for the oral delivery of insulin.

3.2 INTRODUCTION

Nanotechnology has been emerging in the last decades and its advancement can stimulate the exploration of new drug delivery systems and lead to engineering revolutions [1]. Oral delivery of insulin is one of the most studied and challenging domains within the drug delivery systems. Strategies for the design and development of NP involve the use of multifunctional polymers, which possess biocompatible, biodegradable, hydrophilic and protective characteristics [2−4].

The effect of biopolymers in the NP size is an important parameter, since it determines the membranes absorption, distribution and fate of encapsulated drugs, such as insulin. In addition, the particle size also influences the stability, loading and release of insulin from the NP and, therefore, insulin uptake [5].

Polycationic polymers such as CS can be used to increase the stability of polyanionic alginate−based NP and to minimize the loss of encapsulated insulin [6]. CS (Figure 3.1) has been described as an absorption enhancer across mucosal epithelia, especially for proteins, by opening the epithelial TJ [7−9]. CS−coated NP could transiently and reversibly open the TJ between contiguous cells, while becoming unstable and disintegrated, due to their pH−sensitivity, and allow the transport of the released insulin via the paracellular pathway [10−12]. Alginate and CS can crosslink together through electrostatic force to form NP with protective properties with the ability to improve the permeability and bioadhesion [13−15]. A rational study was developed to optimize the CS coating. Physicochemical parameters, such as surface charge and particle size, were investigated to provide the ideal CS concentration, ensuring a more effective coating.

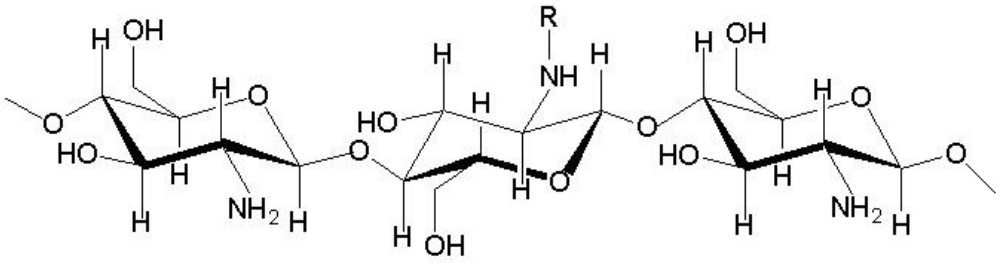

Figure 3.1. Chemical structure of CS (R = $COCH_3$).

3.3 MATERIALS AND METHODS

3.3.1 Materials

Low viscosity sodium alginate was purchased from Sigma (USA). CS (50 kDa) and ALB were purchased from Sigma–Aldrich Chimie (France). Calcium carbonate was obtained from Specialty Minerals Inc. (UK). Paraffin oil was supplied by Vaz Pereira (Portugal). Sorbitan monooleate (Span® 80), dextran sulfate (5 kDa) and PEG 4000 were purchased from Fluka, Chemie GmbH (Switzerland). Poloxamer 188 (Lutrol® F68) was supplied by BASF (Germany). Insulin was kindly donated by Hospitais da Universidade de Coimbra (Actrapid Insulin®, 100 IU/mL from Novo Nordisk, Denmark).

3.3.2 ADS–based NP preparation

A previously described technique [16] was slightly modified. The formation of the ADS–matrix through emulsion dispersion was followed by triggered instantaneous particle gelation. The aqueous phase was prepared as described in Chapter 2, with the addition of poloxamer 188 (0.16%, w/v). The resultant dispersion was emulsified within paraffin oil (aqueous phase/oil phase 50/50, v/v) facilitated by another non–ionic surfactant, sorbitane monooleate (1.84%, v/v), by impeller–stirring homogenization (1600 rpm) and tip–sonication at 60% (Sonics®, VCX130; Sonics & Materials, USA). After 15 min, gelation was

induced by the addition of paraffin oil containing glacial acetic acid (molar ratio acid−calcium, 3.5) to solubilize the calcium dispersed in the ADS−droplets during 15 min, with continued stirred and tip−sonication at 60%. NP were finally recovered from the external oily phase through the extraction procedure described in Chapter 2.

3.3.3 NP coating

The CS coating was simply applied through polyelectrolyte complexation. The CS−PEG solution at pH 4.5 was added dropwise to the uncoated ADS−based NP under magnetic stirring during 60 min. Finally, the CS−coated NP (CS−NP) were coated by dropwise addition of 1.00% (w/v) ALB solution at pH 5.1 under magnetic stirring during 30 min (ALB−NP).

3.3.4 ζ−potential analysis

The surface charge was determined as described in Chapter 2.

3.3.5 Size analysis

The particle size analysis was performed by LD, according to the methodology used in Chapter 2.

3.4 RESULTS AND DISCUSSION

Initially, the ADS−based NP presented a ζ−potential value of –31.2 ± 0.11 mV (n = 3). These NP were coated with a CS solution at 0.03% (w/v) [16], which revealed a ζ−potential value of –22.4 ± 0.89 mV (n = 3).

According to the literature, one of the main factors that influence the ζ−potential of CS−coated NP is the CS concentration [17]. Modifications of the CS concentration and NP/CS proportion were made to improve the effectiveness of the CS coating, resulting in the increase of the ζ−potentials values. Table 3.1 shows the effect of the CS concentration (0.30 and 1.00% [w/v]) and NP/CS proportion on the surface charge of the ADS−based NP. Following NP coating with CS at 0.30% (w/v), the NP surface charge changed when compared to the uncoated NP. The NP coated with CS at 0.30% (w/v) and in a proportion of 1.00:0.50 (NP/CS, v/v) led to the highest value of ζ−potential, which may be due to a better coating efficiency. The increase of the CS concentration to 1.00% (w/v) was not directly proportional to the ζ−potential values, i.e., the ζ−potential values did not increase when compared to the CS concentration of 0.30% (w/v). Probably, the excess of CS was not capable to encircle more alginate on the NP' surface. In this concentration, different proportions of the NP and CS solution were also tested, yet no variation of the ζ−potential value was observed.

Table 3.1. ζ−potential values (mean ± s.d., n = 3) of the CS−coated NP with CS solutions at 0.30 and 1.00% (w/v) and NP/CS proportion of 1.00:0.50, 1.00:0.52, 1.00:0.58 and 1.00:0.67 (v/v).

CS concentration (w/v) (%)	**NP/CS proportion (v/v)**	**ζ−potential (mV)**
0.30	1.00:0.50	−22.40 ± 3.80
	1.00:0.52	−24.09 ± 1.58
	1.00:0.58	−23.16 ± 0.27
	1.00:0.67	−22.79 ± 1.52
1.00	1.00:0.52	−30.44 ± 0.40
	1.00:0.58	−26.06 ± 0.53
	1.00:0.67	−24.38 ± 0.23

All the coated NP with 1.00:0.50 of NP/CS proportion (v/v) were submitted to ALB coating. In the case of the coated NP with CS at 0.30% (w/v), the ALB/CS−coated NP revealed

a ζ−potential value of –27.9 ± 0.38 mV. Changes in the NP ζ−potential indicated an effective CS coating, since the charge changed to higher positive values. The subsequent ALB coating, changed the NP ζ−potential to higher negative values, also ensuring that the ALB coating was successfully achieved.

The size analysis of the ALB/CS−coated NP showed better size values with CS concentrations at 0.03 and 0.30% (w/v) as well as lower polydispersity (Figure 3.2, Table 3.2). The best value of the NP ζ−potential (−22.40 ± 3.80 mV) as well as the lowest size (D50 = 2.56 ± 6.53 µm) were observed with CS at 0.30% (w/v), as can be seen in Tables 3.1 and 3.2, respectively. With CS at 1.00% (w/v), the size of the coated NP increased and a higher polydispersivity was observed, possible due to the aggregation of the excess of CS. The size analysis was performed before and after each coating process (Figure 3.3). After the ALB coating, it was observed a displacement of the size distribution curve to the left. This behavior may be due to the helical structure of ALB, resulting in a higher packaging membrane coating and polymeric matrix [18,19].

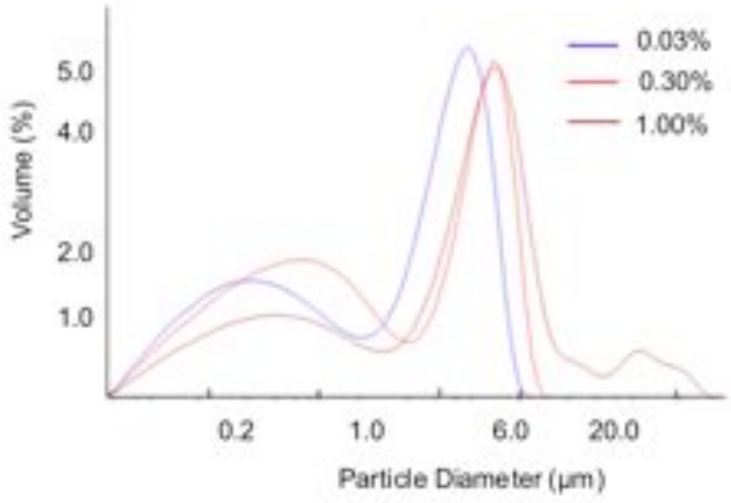

Figure 3.2. Influence of the CS concentration (0.03, 0.30 and 1.00% [w/v]) on the ALB/CS−coated NP size.

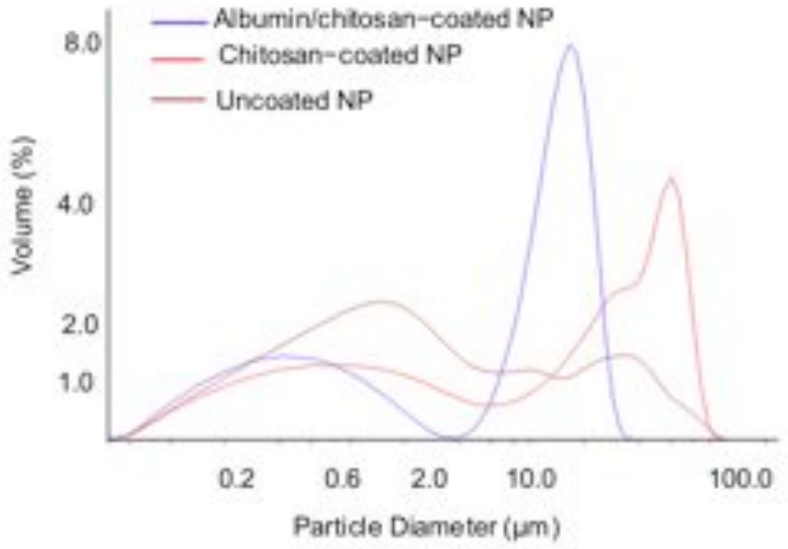

Figure 3.3. Influence of the CS− and ALB/CS−coatings on the NP size distribution.

Table 3.2. Effect of CS the concentration (0.03, 0.30 and 1.00% [w/v]) on the coated NP size (D50 ± s.d, n = 3).

CS concentration (w/v) (%)	Size (µm)
0.03	4.34 ± 4.80
0.30	2.56 ± 6.53
1.00	9.43 ± 35.01

3.5 CONCLUSIONS

A novel insulin ADS−based NP formulation was developed and characterized, concerning size and surface charge after the CS and ALB coatings. The CS concentration affected both properties and the best results were obtained with CS at 0.30% (w/v). The optimized formulation is a promising approach for the oral delivery of insulin.

3.6 REFERENCES

[1] Couvreur, P.; Dubernet, C.; Puisieux, F. Controlled drug delivery with nanoparticles: current possibilities and future trends. European Journal of Pharmaceutics and Biopharmaceutics 1995;41:2 − 13.

[2] Damge, C.; Maincent, P.; Ubrich, N. Oral delivery of insulin associated to polymeric nanoparticles in diabetic rats. Journal of Controlled Release 2007;117:163−70.

[3] Alonso, M. J. Nanomedicines for overcoming biological barriers. Biomedicine & Pharmacotherapy 2004;58:168−72.

[4] Cui, F.; Qian, F.; Yin, C. Preparation and characterization of mucoadhesive polymer−coated nanoparticles. International Journal of Pharmaceutics 2006;316:154−61.

[5] Mohanraj, V. J.; Chen, Y. Nanoparticles — A review. Tropical Journal of Pharmaceutical Research 2006;5:561−73.

[6] Huguet, M. L.; Groboillot, A.; Neufeld, R. J.; Poncelet, D.; Dellacherie, E. Hemoglobin encapsulation in chitosan/calcium alginate beads. Journal of Applied Polymer Science 1994;51:1427−32.

[7] Ilium, L. Chitosan and its use as a pharmaceutical excipient. Pharmaceutical Research 1998;15:1326−31.

[8] Kotzé, A. F.; Lueßen, H. L.; de Boer, A. G.; Verhoef, J. C.; Junginger, H. E. Chitosan for enhanced intestinal permeability: Prospects for derivatives soluble in neutral and basic environments. European Journal of Pharmaceutical Sciences 1999;7:145−51.

[9] Lueßen, H. L.; Rentel, C. O.; Kotzé, A. F.; Lehr, C. M.; de Boer, A. G.; Verhoef, J. C.; Junginger, H. E. Mucoadhesive polymers in peroral peptide drug delivery. IV. Polycarbophil and chitosan are potent enhancers of peptide transport across intestinal mucosae *in vitro*. Journal of Controlled Release 1997;45:15−23.

[10] Lin, Y.−H.; Mi, F.−L.; Chen, C.−T.; Chang, W.−C.; Peng, S.−F.; Liang, H.−F.; Sung, H.−W. Preparation and characterization of nanoparticles shelled with chitosan for oral insulin delivery. Biomacromolecules 2007;8:146−52.

[11] Sonaje, K.; Lin, K. J.; Wang, J. J.; Mi, F. L.; Chen, C. T.; Juang, J. H.; Sung, H. W. Self−assembled pH−sensitive nanoparticles: A platform for oral delivery of protein drugs. Advanced Functional Materials 2010;20:3695−700.

[12] Su, F.−Y.; Lin, K.−J.; Sonaje, K.; Wey, S.−P.; Yen, T.−C.; Ho, Y.−C.; Panda, N.; Chuang, E.−Y.; Maiti, B.; Sung, H.−W. Protease inhibition and absorption enhancement by functional nanoparticles for effective oral insulin delivery. Biomaterials 2012;33:2801−11.

[13] Sarmento, B.; Ferreira, D.; Veiga, F.; Ribeiro, A. Characterization of insulin−loaded alginate nanoparticles produced by ionotropic pre−gelation through DSC and FTIR studies. Carbohydrate Polymers 2006;66:1−7.

[14] Sarmento, B.; Ribeiro, A. J.; Veiga, F.; Ferreira, D.; J, N. R. Insulin−loaded nanoparticles are prepared by alginate ionotropic pre−gelation followed by chitosan polyelectrolyte complexation. Journal of Nanoscience and Nanotechnology 2007;7:2833−41.

[15] Yin, L. C.; Ding, J. Y.; He, C. B.; Cui, L. M.; Tang, C.; Yin, C. H. Drug permeability and mucoadhesion properties of thiolated trimethyl chitosan nanoparticles in oral insulin delivery. Biomaterials 2009;30:5691−700.

[16] Reis, C.; Ribeiro, A.; Veiga, F.; Neufeld, R.; Damgé, C. Polyelectrolyte biomaterial interactions provide nanoparticulate carrier for oral insulin delivery. Drug Delivery 2008;15:127−39.

[17] Li, X.; Qi, J.; Xie, Y.; Zhang, X.; Hu, S.; Xu, Y.; Lu, Y.; Wu, W. Nanoemulsions coated with alginate/chitosan as oral insulin delivery systems: Preparation, characterization, and hypoglycemic effect in rats. International Journal of Nanomedicine 2013;8:23−32.

[18] Akiyoshi, K.; Nishikawa, T.; Mitsui, Y.; Miyata, T.; Kodama, M.; Sunamoto, J. Self−assembly of polymer amphiphiles: thermodynamics of complexation between bovine serum albumin and self−aggregate of cholesterol−bearing pullulan. Colloids and Surfaces A: Physicochemical and Engineering Aspects 1996;112:91−5.

[19] Ferrer, M. L.; Duchowicz, R.; Carrasco, B.; de la Torre, J. G.; Acuña, A. U. The conformation of serum albumin in solution: a combined phosphorescence depolarization−hydrodynamic modeling study. Biophysical Journal 2001;80:2422−30.

CHAPTER 4

IMPACT OF *IN VITRO* GASTROINTESTINAL PASSAGE OF BIOPOLYMER–BASED NANOPARTICLES ON INSULIN ABSORPTION

4.1 ABSTRACT

Although the oral administration of insulin is recognized as the safest and most attractive, the insulin oral BA is usually reduced due to the susceptibility to acidic and enzymatic degradations in the GI tract and intrinsic low intestinal permeability. The nanoencapsulation of insulin is, thus, foreseen as promising approach to overcome most of these drawbacks. The effect of the GI environment on the aggregation of ADS−based nanometric−sized particles, uncoated or double−coated with CS and ALB, and its further influence on the insulin release and permeability at the cellular level was investigated *in vitro*. The swelling and aggregation behavior of the NP in gastric conditions was accompanied by the prevention of the insulin release. In intestinal conditions, the fast dissolution of the uncoated NP was responsible for a wide size distribution and for a burst release of insulin, while the size stability provided by the ALB/CS−coating led to a sustained release. The CS/ALB−coated NP were able to significantly increase the permeability of insulin across the cell−based engineered intestinal models, further enhanced by the presence of mucus layer and M−like cells. The influence of these models on the insulin permeability was compared to the curve that better adjusted to the mathematical kinetics of the insulin release from these biopolymeric−NP. Thus, a correlation between the size behavior of the NP upon passage in the GI tract and both the insulin release profile and permeation across the intestinal *in vitro* models was addressed. These results provide proof−of−concept evidence that the GI passage of the NP has a major influence on the oral absorption of macromolecules.

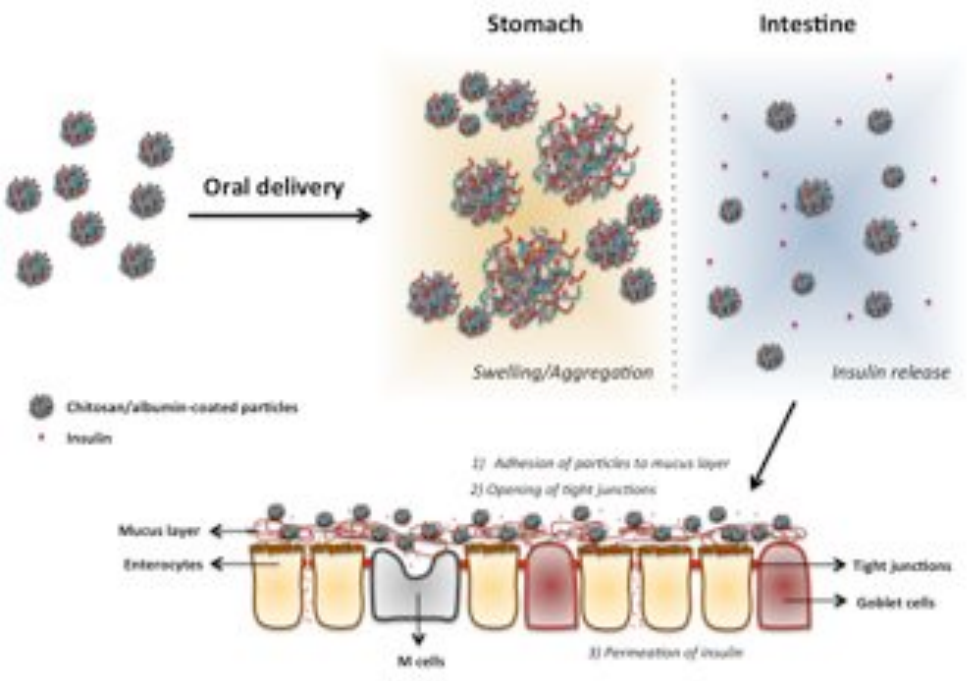

Graphical abstract: Behavior of the insulin–loaded biopolymer–based NP upon passage on the Gl tract. The intestinal pH triggered insulin release from the NP, allowing its permeability through the cell–based engineered intestinal models.

4.2 INTRODUCTION

Diabetes is a chronic disease with epidemic proportions throughout the world. The administration of insulin is required for the treatment of this condition, however, due to enzymatic degradation in the GI tract and poor permeability through the intestinal epithelium, the oral BA of insulin is very poor [1] compared to the most common route of insulin administration, the s.c. route. The oral administration is considered the safest and the most convenient alternative to deliver insulin, but it faces important challenges. In the last years, different formulation approaches have been explored to encapsulate insulin and deliver it orally. Nevertheless, these formulations only had a limited success and no oral insulin product has been commercially available yet.

The encapsulation of insulin into polymeric−NP is a powerful tool to improve the insulin oral BA. Among the most commonly polymers used to produce NP for oral delivery of insulin, natural biopolymers such as alginate, dextran sulfate and CS have demonstrated *in vivo* efficacy without toxicological effects when orally administered as NP [2−4]. Alginate and dextran sulfate are considered a suitable choice, due to their excellent biocompatibility, drug carrying ability, adjustable controlled−release property, lower cost, abundance in nature and easier application [5]. Previous studies revealed that the presence of a copolymer, such as dextran sulfate enhances the loading of hydrophilic drugs in alginate matrices [6]. The recent extensive research on several CS−based particulate systems also demonstrates a positive role of CS towards oral insulin delivery [7−9].

ADS−based NP coated with CS/PEG/ALB shell have shown efficiency as potential carriers for the oral delivery of insulin [3,4]. The alginate network forms an impermeable structure in acidic gastric conditions [10,11], preventing the premature insulin release in combination with dextran sulfate and increasing the insulin protection in combination with ALB, which is applied as a sacrificial target to GI proteases [12]. CS, as polycationic and mucoadhesive polymer is designed to significantly enhance the intestinal permeability of insulin by increasing the residence time at the site of absorption and transiently opening the TJ, allowing the paracellular transport of insulin across the intestinal epithelium [13,14]. This complexed structure acts as a synergistic effect, since at acidic pH, the high solubility of CS favored by the conversion of glucosamine units into the soluble form $R-NH_3^+$ [15] is inhibited by the alginate presence due to the swelling behavior of this polymer at low pH. On the

other hand, the rapid dissolution of alginate owing to the dissociation of the carboxylic groups at a higher pH is controlled by CS [16,17].

The use of NP in oral insulin delivery has been increased over the last decades mainly due their smaller size, which allows a higher surface area−to−volume ratio when compared to other delivery systems. Thus, it is important to understand the factors influencing their GI uptake, more precisely their size and aggregation phenomena. The impact of these factors on the GI absorption has been assessed mainly with polystyrene and latex particles but in most part of those studies neither the influence of the GI tract on the NP properties was the focus nor the *in vitro−in−vivo* correlation was a concern. The particle size is one of the most important properties of NP related to their biodistribution behavior and can be more or less easily modulated [18]. Actually, one of the main problems with the NP design remains in the fact that the intrinsic properties that may help to cross the GI tract may also significantly alter the further behavior in the blood [18]. Some studies have quantitatively assessed the oral absorption of NP, however a thorough understanding about the impact of the size and aggregation behavior within the GI tract is still missing due to incomplete particle characterization [19].

So far, very few reports about the NP properties *in situ* following oral administration and their relation with the percentage of the NP uptake are available. For instance, the particle size may suffer *in vivo* variations within the GI tract due to aggregation, particularly in the gastric pH and intestinal high ionic conditions. Taking into account that the effective particle size at the absorption surface of the GI tract increases with aggregation, a size−dependent absorption can be influenced [19]. Most of the studies associate their BA data with the characterization of the "as−dosed" material, but the *in vivo* aggregation state of NP has been often ignored as a factor affecting the particle uptake [19].

The aim of this work was to study the *in vitro* effect of the coating of CS and ALB on the ADS−NP size and aggregation behavior across the GI environment. Furthermore, the effect of these biopolymer−based NP on enhancing the insulin *in vitro* permeation through the intestinal membrane was also evaluated. The *in vitro* models of Caco−2, Caco−2/HT29−MTX and Caco−2/HT29−MTX/Raji B co−cultures were applied to understand the influence of each type of cell on the insulin intestinal permeability.

4.3 MATERIALS AND METHODS

4.3.1 Materials

Low viscosity sodium alginate (viscosity of 1% solution at 25 ºC, 4−12 cps), dextran sulfate, sorbitan monooleate (Span® 80), CS (50 kDa), bovine serum ALB, phosphotungstic acid, n−octanol, TFA 99% and ACN (LiChrosolv) HPLC grade were purchased from Sigma−Aldrich (Germany). Calcium carbonate was obtained from Setacarb (France), paraffin oil from Scharlau (Spain), insulin 100IU/mL Actrapid® from Novo Nordisk (Denmark) and poloxamer 188 (Lutrol® F68) from BASF (Germany).

Human colon carcinoma Caco−2, mucus producing HT29−MTX, and Human Burkitt's lymphoma Raji B cell lines were obtained from the American Type Culture Collection and used at passages 35–64, 8–29 and 1–13, respectively. Dulbecco's Modified Eagle Medium (DMEM), fetal bovine serum, L−glutamine, non−essential amino acids, 100 U/mL penicillin and 100 mg/mL streptomycin, trypsin–EDTA and Hank's balanced salt solution (HBSS) were purchased from Gibco (Invitrogen Corporation, Life Technologies, UK).

4.3.2 NP preparation and coating

NP were prepared by emulsification/internal gelation and coated with CS and ALB as described in Chapter 3.

4.3.3. NP characterization

The particle size analysis was performed by LD as described in Chapter 3.

The ζ−potential was measured by laser doppler electrophoresis using Zetasizer Nano ZS (Malvern Instruments Ltd., UK). The measurements were taken in a folded capillary electrophoresis cell at pH 4.5 and 25 °C with Milli−Q water. The equipment was routinely checked and calibrated using mobility standard (Beckman Coulter, Inc. Miami, FL, USA).

The morphological analysis was done by cryo−SEM, as explained in Chapter 2.

4.3.4. Determination of octanol/water partition coefficients

The partition coefficients for n−octanol/water of the ADS−, CS− and ALB−NP were determined by a shaking flask method [22]. After lyophilization, 80 mg of the NP were mixed with 9 mL n−octanol system (the organic and aqueous phases had been mutually saturated for 24 h) and allowed to equilibrate for 3 h. The final mixture was centrifuged for 2 min at 3500*g*. Insulin was used as the NP' probe and was extracted from the NP through dissolution in PBS at pH 7.4 (USP 34) for 3 h in an orbital shaker. After the ethanol addition (50/50, v/v) to precipitate alginate, the medium was centrifuged and the insulin content in tge supernatant was measured by HPLC, as previously described [23]. The water partition coefficients ($P_{o/w}$) were calculated as follows: $P_{o/w} = C_o/C_w$, where C_o and C_w refer to the concentration of insulin in the n−octanol phase and water phase, respectively. Nonencapsulated insulin was used as control.

4.3.5 Insulin EE and LC

The insulin EE was calculated by the difference between the total amount of insulin used to prepare the NP and the amount of insulin that remained loaded to the NP. The insulin−loaded NP were separated from the aqueous supernatant containing free insulin by centrifugation at 12000*g* for 10 min at 4 °C. Insulin was extracted from the NP through dissolution in PBS at pH 7.4, as described before. The insulin LC was calculated based on the dry mass of the NP obtained after lyophilization. The amount of the loaded insulin was determined by HPLC.

4.3.6 Differential scanning calorimetry (DSC) analysis

To assess the interactions between the polymers and confirm their presence in the NP' structure, thermograms were obtained using a Shimadzu DSC−50 system (Shimadzu, Japan). 2 mg of lyophilized samples were crimped in a standard aluminum pan and heated from 20 to 350 °C at a heating constant rate of 10 °C/min under constant purging of nitrogen

at 20 mL/min.

4.3.7 Size stability in simulated GI fluids

For the determination of the NP size and aggregation in the range of pH of simulated GI fluids, the incubation of the NP in SGF (USP 34) was firstly done in the range of pH 1.2−4.2, followed by the incubation in SIF (USP 34) at pH between 4.7 and 8.2. The pH in each medium was gradually increased, with a maximum duration of 2 h in each medium. Before and after each pH variation, the NP size was measured by LD. Results are expressed as the mean size (μm) and volume distribution (%) of the main population of the NP.

4.3.8 Insulin release profile in simulated GI fluids and protection against pepsin degradation

For the determination of the insulin retention/release profile in the simulated GI tract, enzyme−free simulated digestive fluids were used to determine the response of the insulin−loaded NP, minimizing enzymatic interferences. 5 mL of the NP suspension were incubated in 10 mL of SGF at 37 °C for 2 h with shaking of 100 strokes/min using a Shaking Water Bath (SS40−D, GRANT, UK), followed by incubation in 10 mL of SIF for 6 h. Sample aliquots were collected and replaced by the same volume of the fresh incubation medium at predetermined times. For the determination of the insulin released from the NP, the samples were centrifuged at 12000*g* for 10 min and the insulin content in the supernatant was analyzed by HPLC.

The release kinetics of the insulin from the ALB−NP was mathematically analyzed (Systat SigmaPlot version 12.1.) to better understand the impact of every coating material on the insulin release behavior.

To assess the insulin protective effect of the ALB−NP from pepsin degradation in the GI tract, 5 mL of the NP suspension were incubated in 10 mL of SGF containing pepsin. This effect was determined based on the usual dose of insulin−loaded NP orally administered (50 IU/kg) and the amount of proteases in the total fluid volume of the human stomach [24,25].

The insulin protection was determined in a ratio of 1:7 (insulin/pepsin) during 2 h at 37 °C with shaking of 100 strokes/min. After incubation, SIF was added to inactivate the pepsin and to release the insulin retained and protected in the NP' core. The insulin content was determined as described above. The effect of the NP in protecting insulin against pepsin was compared with the results obtained with the nonencapsulated insulin.

4.3.9 *In vitro* models

Caco−2 and HT29−MTX cells were grown separately in flasks in DMEM supplemented with 10% (v/v) fetal bovine serum, 1% (v/v) non−essential aminoacids, 1% (v/v) L−glutamine and 1% (v/v) of antibiotic/antimitotic mixture (final concentration of 100 U/mL penicillin and 100 U/mL of streptomycin), at 37 °C under a 5% CO_2 water saturated atmosphere. Upon confluence, the cells were harvested from flasks with trypsin–EDTA. Raji B cells were cultured in flasks with DMEM supplemented and with the same conditions as described above. To establish the co−culture *in vitro* models, the Caco−2 and HT29−MTX cells were mixed to a final density of 1 x 10^5 cells/cm^2 (90:10 proportion). The Caco−2 monolayer (1 x 10^5 cells/cm^2) was also seeded as control. Regarding the triple co−culture model, the Caco−2 and HT29−MTX cells were seeded as described before. After 14 days, the Raji B cells (1 x 10^6 cells/6−well) were added to the basolateral compartment of the Caco−2/HT29−MTX co−culture and maintained for 4–6 days. All the models were established on Transwell inserts (3 μm) and maintained for 21 days.

4.3.10 *In vitro* intestinal permeability studies

All the cell monolayers were used after 21 days in culture. For all the permeability studies, the culture medium was removed and the cell monolayers were washed with pre−warmed HBSS. The permeability experiments were run at 37 °C during 4 h from the apical to the basolateral chambers for both the nonencapsulated insulin and insulin−loaded NP, at a predetermined initial apical concentration. At different times, basolateral samples were collected and free−insulin amount was determined by HPLC. During the permeability studies, the cell monolayer integrity was monitored by TEER measurement using a volt−ohm

meter Millicell® ERS−2 (Millipore, USA).

The fraction of insulin released in SIF from the ALB−NP was plotted against the fraction of insulin that permeated across the three intestinal *in vitro* models along 4 h to better assess the potential and limitations of every cell culture model.

4.3.11 Statistical analysis

All the experiments were performed in triplicate and are represented as mean ± s.d.. The statistical evaluation was performed with one−way ANOVA followed by Bonferroni post hoc−test (SPSS 20.0, USA). A $p < 0.05$ was taken as the criterion of significance. The level of significance was set at probabilities of $^{*}p < 0.05$, $^{**}p < 0.01$, and $^{***}p < 0.001$.

4.4 RESULTS AND DISCUSSION

4.4.1 NP characterization

Particle properties such as the mean size, size distribution, charge and hydrophilicity are important parameters in the particle uptake or barrier crossing, since the first contact between the cell membrane and particle influences their interaction and possible uptake. Therefore, the particle size distribution, charge and hydrophilicity should be fully characterized [26]. In this study, multilayered NP encapsulating insulin were formed by alginate and dextran sulfate nucleating around calcium ions layered with CS/PEG/calcium chloride ($CaCl_2$), and subsequently coated with ALB. In order to evaluate the presence of micro− or nanoaggregates, the NP size was measured by LD. The ADS−NP had a mean diameter of 233.0 ± 0.3 nm and ζ−potential of −28.40 ± 0.89 mV. Further coating of the ADS−NP with CS considerably increased the NP size and a new population higher than 1 µm appeared probably due to the aggregation phenomena, which may be caused by the stickiness of the polymer [27,28]. The polycationic CS coating decreased the negative surface charge to −25.00 ± 0.82 mV, confirming the deposition of the positively charged polymer on the surface of the NP. Following ALB coating, it was observed a displacement of the size

distribution curve to the left with a mean diameter of 166.0 ± 0.8 nm and ζ−potential of −22.10 ± 0.76 mV. This behavior may be due to the composition of ALB, which is mainly composed by α−helical peptides, resulting in a higher packaging of the coating membrane and also of the polymeric matrix [21].

The CS layering is essential to stabilize the NP' core and interact with ALB that forms the sacrificial coating to protect insulin against proteases. NP with reduced size are known to establish improved contact with the intestinal cells than do bigger particles, facilitating the permeation via different mechanisms [29]. Furthermore, since the NP immobilized by the mucus can be cleared from the mucosal tissue, their size must be less than 500 nm [30] to avoid significant steric inhibition by the fiber mesh and adhesion to mucin fibers [31]. The decrease of the particle size after the ALB coating may be propitious for the NP escape from this effect. The insulin initially added to the formulation was almost completely encapsulated (EE = 98.74 ± 0.18%), and the LC was 2.43 ± 0.04%. These values seemed to be higher compared to previous formulations prepared by this technique [4,32], which could be justified by the use of a co−surfactant and ultrasonication assistance during emulsification, leading to a smaller and more stable nanoemulsion. Figure 4.1 shows the Cryo−SEM images of all the formulations. These results indicate that the particles are in the nanometer scale, according to what was obtained by the LD technique. The droplet shape of the the CS− and ALB−NP was quasi−circular and had a smooth profile, while the ADS−NP presented a more elongated shape. The population of ALB−NP represented in Figure 4.1C tend to have a spherical shape with sizes ranging between 300 and 650 nm. The cellular internalization of different types of NP has been described to be function of both size and shape curvature, wherein nanoscale cylindrical particles had a higher percentage of cellular internalization over time [33,34].

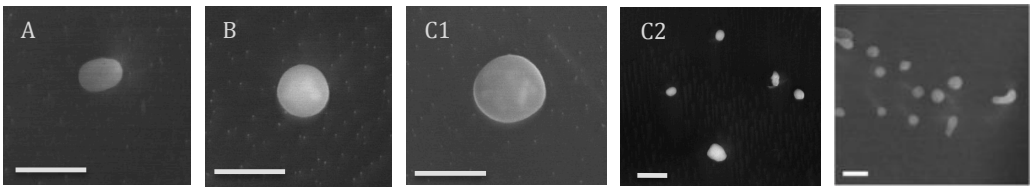

Figure 4.1. Cryo−SEM images of the (A) ADS−, (B) CS− and (C1, C2 and C3) ALB−NP; Scale bar = 1 μm.

The hydrophilicity has been described as an important parameter in determining the transport of NP across the mucus [35] and M cells [36]. This expectation was not investigated in this study, since according to the hydrophilic nature of the polymers, the NP were extremely hydrophilic before and after the coating and no insulin was detected in the octanol phase. Accordingly, all the content of nonencapsulated insulin was also detected in the aqueous phase. To date, only a few studies have correlated the cellular uptake with the hydrophilicity of the NP. Some authors have demonstrated that higher hydrophilicity is reflected in a decrease of the GI uptake [37−39]. However, the increase of hydrophilicity was also correlated with a change in the surface charge. Therefore, the results could not be conclusive, since the variation of the surface charge may also have an impact at the cellular level. More recently, Gaumet *et al.* studied the effect of the hydrophilicity independently of other parameters by using particles with the same size and charge, differing only in the surface hydrophilicity [26]. They demonstrated that the surface hydrophilicity is a determinant factor for the NP uptake and more specifically the negatively charged 100 or 300 nm CS−coated PLGA particles with high hydrophilicity appear to be the best candidates to target the intestinal cells. These findings highlight the potential interaction between our negatively charged and hydrophilic NP with the intestinal cells.

4.4.2 DSC analysis

The thermograms of alginate, dextran sulfate and CS, as we can see in Figure 4.2A, showed initial endothermic peaks at 84.3, 85.6 and 76.8 °C and higher exothermic peaks at

245.8, 204.5 and 308.2 °C, respectively. Endothermic peaks are correlated with the loss of water associated to the hydrophilic groups of the polymers while exothermic peaks resulted from the degradation of the polymers due to dehydration and depolymerization reactions most probably to the parcial decarboxilation of the protonated carboxylic groups and oxidation reactions of the polymers [40,41]. The thermogram of the alginate/dextran sulfate/CS physical mixture is also represented in Figure 4.2A and showed an endothermic peak at 90.2 °C, which was sifted to the right and an exothermic peak at 296.6 °C, which probably represents the coalescence of the endothermic polymer peaks. The peaks of the isolated polymers were different from those of the physical mixture probably because the complexation of the polymers resulted in new chemical bonds. The thermograms of the NP are represented in Figure 4.2B. The shifts on the endothermic and exothermic peaks of the NP represent the ionic interactions between the polymers, which led to the formation of new chemical entities with different thermal and absorption properties [41]. For instance, the exothermic peak of the ADS−NP was registered at 271.9 °C, broader and deviated to the left when compared with the isolated polymers (alginate and dextran sulfate). After the CS coating, the exothermic peak of the CS−NP shifted to 289.3 °C, a higher peak value than the ADS−NP' peak, which was interpreted as the CS interaction with alginate and dextran sulfate. Further ALB coating was responsible for broader peaks, although at similar temperatures.

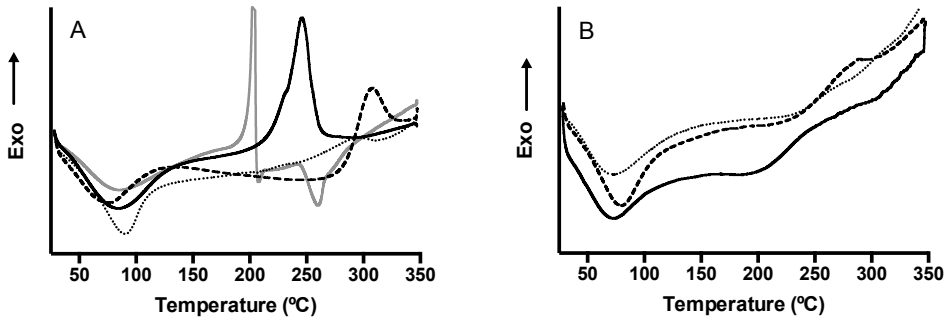

Figure 4.2. Thermograms of A) alginate (black solid line), dextran sulfate (grey solid line), CS (dashed line) and alginate/dextran sulfate/CS physical mixture (dotted line); B) ADS− (solid line), CS− (dashed line) and ALB−NP (dotted line).

4.4.3 Size stability in simulated GI fluids

Taking into account that this nanoparticulate drug delivery system is intended for oral administration, a critical study of these NP would be the evaluation of their size stability in the different media present in the GI tract. The particle size is considered as a critical parameter [42] but its impact on the uptake has not been carefully studied with biodegradable particles [26]. The interactions between the NP and the gastric and intestinal pH and ionic conditions should be evaluated to analyze their impact on the NP size, which consequently may influence the transport of the NP across the intestinal epithelium [26]. In this way, a study comprising a wide range of pH values was set in order to increase the *in vitro/in vivo* correlation. Therefore, the ADS−NP were compared with the coated NP (CS− and ALB−NP) with regard to their size, monitored during the passage of the NP in simulated GI fluids.

As shown in Figure 4.3, under simulated gastric pH there was a significant increase in the mean particle diameter for all the formulations but different trends were observed with an extensive aggregation of the ADS− and CS−NP, but only moderate aggregation of the ALB−NP.

When the ADS−NP were in SGF at pH 1.2, a big deviation of the size distribution to the micrometer range (ca. 87 μm) was observed (Figure 4.3A), demonstrating a strong influence of the acid pH on the particle size distribution. The destabilization of protein−based colloidal delivery systems under simulated gastric conditions may occur for a number of reasons, including loss of charge due to pH changes and electrostatic screening due to an increased ionic strength [43]. Alginate is usually in a crosslinked gel conformation with Ca^{2+} in the NP. However, with the pH decrease, the presence of monovalent cations (H^+ ions) can displace the bound between the Ca^{2+} and the G−blocks of alginate [44]. Therefore, the alginate chains that were previously very close and interlocked became free to take their minimum energy conformation. The COO^- still present in the alginic chains led to repulsive forces and the alginate chains took a more linear conformation. Furthermore, the dextran sulfate groups were predominantly only charged once (HSO_4^-) and the presumable interaction between this anionic polymer with the Ca^{2+} became weaker, leading to a decrease of the NP' network compaction. The charge of insulin at such low pH is highly positive and thus the electrostatic attractions with the polymers could have been replaced,

at least partially, by electrostatic repulsions, also contributing to the change of the NP' conformation. When the pH increased to 3.2, two similar populations were observed (ca. 1.3 and 50 μm), as can be noticed by the decrease of volume % of the main population. The reversibility of the alginate gel may have occurred, reorganizing the egg−box structure. However, there were other competitive cations in the medium, such as H^+ and Na^+, that could destabilize the calcium−alginate gel and therefore two populations were still present [44]. At pH 3.2, alginate gets closer to its pKa (pKa_1 ~ 3.38 and pKa_2 ~ 3.65) which led to a decrease of the alginate molecules in acidic conformation (COOH) towards 50% and the other 50% in basic conformation (COO^-), resulting in two different sized populations. With alginate simultaneously in two different conformations, it was expected that the distribution profile would also be splitted in two populations. The bigger population was probably the remaining of COOH groups of alginate that tend to change the conformation of the NP and led to particles aggregation, while the smaller population may be related to alginate in COO^- conformation ready to interact with cations in the medium. Above this pH, the % of the small population (ca 1.3 μm) started to increase while the bigger population (ca. 50 μm) disappeared.

In contrast to the alginate behavior, CS is soluble at low pH due to the protonation of the amino groups and insoluble at higher pH values [45]. The overall behavior of the CS−NP size in gastric pH (Figure 4.3B) was similar to the ADS−NP. At low pH, CS is strongly protonated (NH_3^+) and soluble, therefore some polymer could be free in the medium and the ADS−NP became exposed. Furthermore, alginate is less negatively charged and thus the electrostatic interactions with CS are weaker. As for the ADS−NP, a shift to the micrometer range was observed at pH 1.2, although less pronounced (ca. 25 μm). The authors explain this difference by the stabilization that CS offers to the NP. The interaction of CS with the negative groups of alginate prevented the interaction of those groups with H^+ and Na^+ of the medium, preventing the change of the NP structure into a linear conformation. Furthermore, some studies have demonstrated that the presence of PEG, a component of CS−NP, improves the stability of the NP, providing a hydrated steric barrier [46,47]. Therefore, the remained stability of PEG in the gastric conditions may protect the CS−NP, preventing the rapid dissolution of CS. At pH 4.2, the interaction between CS and alginate becomes stronger, since there is more alginate in the COO^- conformation to interact with

the NH_3^+ groups of CS. The particles started to shrink and the smaller population (ca. 1.3 µm) greatly increased.

With the last coating of ALB, the NP showed a much more stable behavior. One population around 20 µm between pH 1.2 and 3.2 (Figure 4.3C) was observed, which may be due to the particles swelling. At pH 4.2, an increase of the smaller population of ca. 1 µm was noticed (represented by the decrease of volume % of the main population), as the electrostatic interactions between ALB and CS became stronger.

From these data, it can be concluded that the acidic pH of the gastric medium is a key factor in the aggregation process of these NP, which are pH sensitive.

In order to provide a better insight of what happens in *in vivo* conditions in terms of NP size variation, the NP were further placed in SIF with pH increments over time.

In general, the NP size distribution was more stable in the intestinal pH. The size of the ADS−NP was mainly unaffected even if a bigger population (ca. 20 µm) was observed (data not shown). Above pH 5.7, both the anionic polymers and insulin are negatively charged and repulsive forces could occur. The dissolution of the alginate nucleus as a result of calcium loss started to occur as the pH increased and the destabilization of the NP' structure may be responsible for a wide size distribution.

The behavior of the ADS− and CS−NP in SIF was also very alike, except for the fact that the smaller population was more pronounced in the ADS− (Figure 4.3A) than in the CS−NP (Figure 4.3B), probably due to the effect of CS, preventing the burst dissolution of alginate.

Contrarily to the ADS− and CS−NP, the variations of the ALB−NP size in the intestinal pH were very slight (Figure 4.4C). The % of the population in the nanometer scale increased over time and the size distribution curve became narrower, which is probably due to the stronger interaction between CS and ALB. The helical structure of ALB might provide a higher packaging of the membrane coating and polymeric matrix of the ALB−NP, stabilizing their size [21].

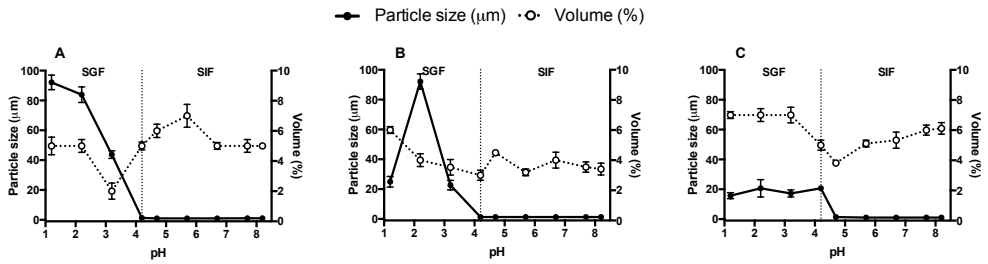

Figure 4.3. Size distribution of the A) ADS−, B) CS−, and C) ALB−NP during 2 h in contact with SGF at pH range 1.2−4.2 and with SIF at pH range 4.7−8.2. Error bars represent the mean ± s.d. (n = 3).

4.4.4 Insulin release profile in simulated GI fluids and protection against pepsin degradation

The *in vitro* insulin release tests intended to predict the release profiles of the hormone in conditions similar to the GI tract (stomach and small intestine). Firstly, the NP were added to SGF at pH 1.2, which mimics the gastric environment. Then, after 2 h, the release medium was changed to SIF at pH 6.8, which simulates the transit of the NP to the small intestine. The insulin release profile from the NP in gastric and intestinal conditions is shown in Figure 4.4. In SGF, the ADS− and CS−NP retained insulin during 2 h, while the ALB−NP released approximately 3% of insulin. As ALB interacts with CS that is on its turn complexed with the matrix, this protein network is somehow destabilized, which in turn can destabilize the NP' structure and allow the diffusion of insulin superficially−located in the exterior of the NP. In the acidic environment, the charge of insulin (pI = 5.3) [48] is highly positive, and thus, the interactions with alginate and dextran sulfate prevent the insulin release. Moreover, calcium forms ionic cross−links between the alginate polymer chains transforming the sol into a pre−gel state, which was responsible for the swelling behavior of the NP previously observed in the gastric pH. These interactions are likely to form a stable barrier to retain insulin and limit its release from the NP [45]. When in contact with SIF, different release profiles of insulin from the uncoated and coated NP were observed. In comparison with the dissolution profile of the coated NP, a very rapid release behavior of

insulin was observed from the ADS−NP. More than 50% of the insulin was released in the first 5 min and approximately 100% was released after 1 h. The electrostatic repulsions at intestinal pH between the negatively charged ADS−NP and insulin promoted the insulin release. This fast release of insulin from the ADS−NP is in accordance with the rapid dissolution of the ADS−NP previously observed, that led to the destabilization of the NP' structure and therefore to a wide size distribution. Compared to the ADS−NP, the release rate of insulin from the coated NP was slower, with approximately 35 and 45% of insulin released after 1 h for the CS− and ALB−NP, respectively. In the case of the CS−NP, a 3−hour sustained release in SIF was observed. The sustained release found in the coated NP may be efficient in protecting insulin in the intestinal environment minimizing the insulin loss due to enzymatic attack, thereby increasing its available amount to be uptaken by the epithelial cells and promoting successful systemic delivery of insulin *in vivo*. The impact of the NP coating on the insulin release in SIF can be explained by the synergistic effect between alginate and CS. The high solubility of CS in acidic pH is inhibited by the alginate presence, since alginate is insoluble at low pH [49]. On the other hand, the rapid dissolution of alginate in a higher pH is controlled by CS, given its stability at high pH [16,17]. The prevention of the burst dissolution of alginate by CS had an impact on the size distribution of the NP (Figure 4.3B) and was also reflected in the sustained release profile of insulin from the CS−NP (Figure 4.4). These results are in agreement with other reports in which CS has been described to be able to decrease the burst release effect of the encapsulated drugs [50,51].

The ALB−NP had a different behavior, as after 15 min in contact with SIF a burst release of insulin was followed by a slow release up to 3 h, reaching 100% of total release. The insulin release mechanism from the NP depends on the solubility of insulin and also on the swelling and erosion characteristics of the NP' matrix polymers [52,53]. Initially, the release is due to the part of insulin that is located at or near the interface of the NP. The small particle size may have contributed to the faster drug release as well.

Generally, in many experimental conditions, the mechanism of drug release from swellable polymeric−based NP follows a non−Fickian behavior [54]. The drug release mechanism from erodible hydrophilic polymeric matrices is a complex process, because several physical factors are involved, such as the penetration of the dissolution medium into the NP' matrix with consequent swelling and erosion of the NP and dissolution of the drug [55]. In such type of release mechanism, the Peppas model is usually fitted. Therefore, in the

present study, to determine the actual mechanism of the insulin release in SIF from the ALB−NP, the parameter 'n' of the Peppas equation was calculated. The correlation coefficient value was found to be 0.35 (R = 0.94); this indicates diffusion controlled rather than non−Fickian diffusion mechanism [56] from the ALB−NP.

The NP at low pH collapsed forming an impermeable network structure by the presence of alginate [10], retaining and potentially protecting insulin against the acidic and proteolytic degradation (Figure 4.5). The presence of ALB, which acts as a sacrificial target, provided full protection to the insulin−loaded ALB−NP in SGF with pepsin, in contrast with the fast degradation of the unprotected nonencapsulated insulin that occurred almost after 10 min. The structure of the ALB−NP was able to prevent the enzymatic degradation of insulin during 2 h.

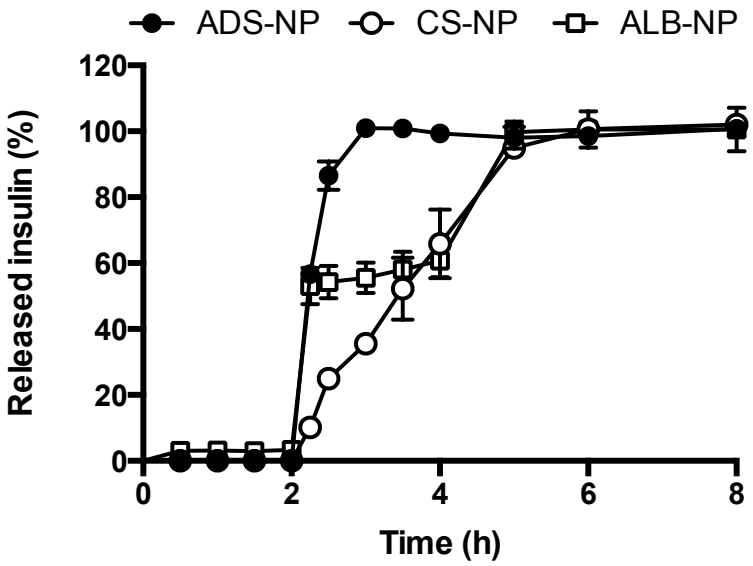

Figure 4.4. Insulin release profile in SGF (pH 1.2) for 2 h followed by 6 h in SIF (pH 6.8) at 37 °C of the ADS−, CS− and ALB−NP. Error bars represent mean ± s.d. (n = 3).

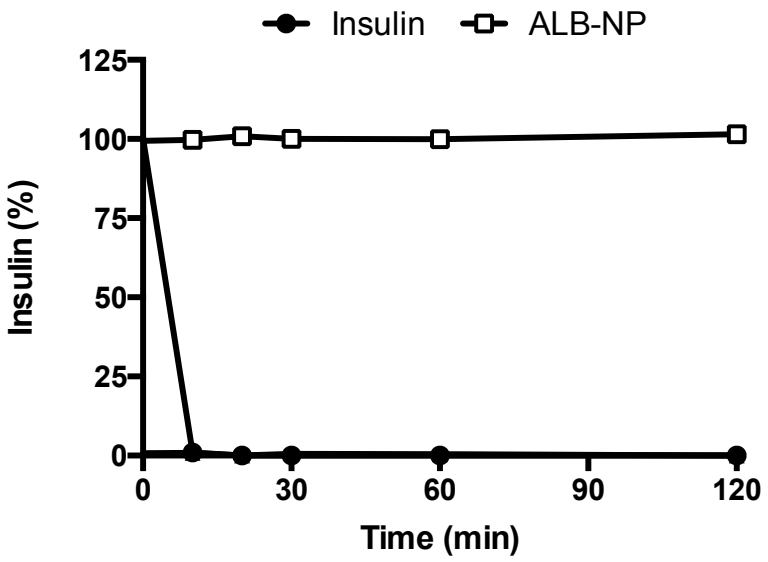

Figure 4.5. Remaining ratio of insulin after the incubation of the free insulin and the insulin−loaded ALB−NP in SGF (pH 1.2) with pepsin at 37 °C. Error bars represent mean ± s.d. (n = 3).

4.4.5 Permeability studies

To study the effect of the goblet and M cells in the permeability of insulin encapsulated into the NP, Caco−2, Caco2/HT29−MTX and Caco−2/HT29−MTX/Raji B models were used. This last model mimics the most important features of the small intestine, namely the presence of enterocytes (Caco−2 cells), the mucus−producing goblet cells (HT29−MTX) in physiological proportions (90:10) and the induction of M−like cells, as described elsewhere [57]. M cells have an important role in the intestinal absorption of drugs since they are specialized for antigen and microorganisms uptake, providing a possible gateway for the absorption of proteins, as well as for NP [39]. Together with Caco−2 and HT29−MTX cells, they form a monolayer where the cells are joined to each other by TJ, mimicking the intestinal epithelium [58].

The permeation profiles of insulin through the intestinal *in vitro* models are presented as cumulative transport over time in Figure 4.6. In all the monolayers, Caco−2,

Caco−2/HT29−MTX and Caco−2/HT29−MTX/Raji B, the insulin permeation when loaded to the ALB−NP was significantly higher than the nonencapsulated insulin. According to the release profile of insulin from the ALB−NP, a higher increment of the insulin permeation was observed in the first 15 min. In the following 3 h in SIF, insulin was totally released from the ALB−NP in a sustained pattern, which was reflected in the permeability of insulin across the monolayers. Contrarily to the results obtained for the ALB−NP, the nonencapsulated insulin permeability pattern was more constant over time, almost reaching a plateau after 30 min, even if the protein was totally available to permeate the monolayers since the beginning of the experiment. The most prominent effect of the ALB−NP in the insulin permeation was observed with the Caco−2/HT29−MTX and triple models. The higher permeation of insulin through the the Caco−2/HT29−MTX model was previously demonstrated [27,59]. The major limitations for the intestinal absorption of macromolecules, such as insulin, are the TJ and the protective mucus layer [60,61]. The incorporation of insulin into the NP showed an enhancement in the permeability across the cell monolayers, which is probably due to the CS properties. CS is a nontoxic cationic polysaccharide exhibiting mucoadhesive properties along with transient opening of the TJ, thereby enhancing the permeation across the intestinal epithelium [62−64]. Furthermore, the mucus layer that may act as an enzymatic barrier to the insulin absorption was overcome the by ALB coating [12]. An intimate contact of the nanoencapsulated insulin to the intestinal mucosa can be described by the diffusion theory of mucoadhesion as defined by Peppas et al. [65], related to interpenetration and entanglement of polymer chains within the mucus layer. Thus, the addition of the mucus−producing cells to the monolayer provided a better simulation of the natural conditions, which facilitate the insulin permeation [3].

The permeability across the triple co−culture was performed in order to understand the role of M−like cells in terms of insulin transport. Similar results were obtained with the Caco−2/HT29−MTX and triple co−culture models, as both significantly enhanced the insulin permeation, representing 1.3 and 1.4−fold enhancement of the insulin permeation coefficient, respectively, in comparison to the Caco−2 monolayer. These results suggested that both the HT29−MTX cells, and probably the mucus produced by these cells, and M−like cells were involved in the increase of the insulin permeability. The positive role of the goblet cells was previously demonstrated for poorly absorbed hydrophilic drugs [59,66], designating higher paracellular permeability in the co−culture system.

The permeability of the insulin−loaded ALB−NP across the established *in vitro* models showed to be associated with the *in vitro* insulin release mechanism of the nanosystem (Figure 4.7). The most common models (zero−order, first−order, Higuchi and Weibul) were fitted to our experimental results. The regression analysis verified that the Higuchi kinetic model was the most appropriate for describing the kinetic of the insulin release as confirmed by the correlation coefficient value (0.93). It revealed that the release of insulin from the NP occurred in a controlled manner. This *in vitro* correlation between the amount of insulin that is released from the NP and its permeability through the models that simulate the intestinal epithelium contributes to a better understanding of the influence of the GI passage in the intestinal permeation of macromolecules and NP. These studies are difficult to implement *in vivo* and according to the best of our knowledge this is the first approach of the influence of the GI passage at the level of the intestinal absorption of insulin-loaded NP with antihyperglycemic properties. The results showed that the transfer speed of insulin from the NP is not limiting for the *in vitro* permeability of insulin, free or encapsulated. The higher permeability rates of insulin across the co−culture models during the first 2−h test, when compared to the Caco−2 model, seemed to have a higher correlation with the curve that better adjusted to the mathematical kinetics of the insulin release from the ALB−NP. After 3 h, almost all insulin was available to permeate across the monolayers, but no statistical differences were observed between the *in vitro* models. Therefore, during the first 2 h of contact with the intestinal environment, a closer relation was found between the fraction of insulin released from the NP and the fraction that permeated the monolayers, especially when the HT29−MTX and M−like cells were included.

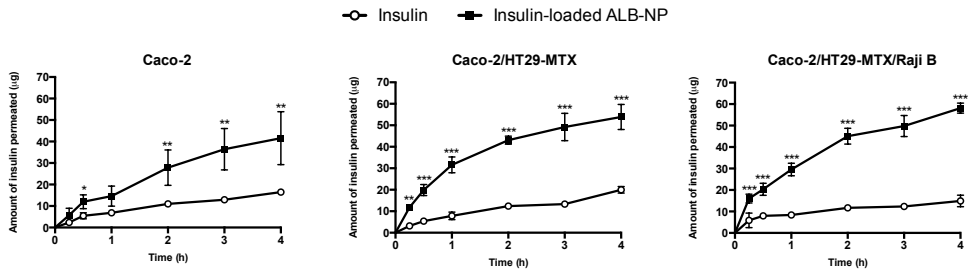

Figure 4.6. *In vitro* cumulative permeability profiles of insulin across the *in vitro* models. The level of significance was set at probabilities of $^{*}p < 0.05$, $^{**}p < 0.01$, and $^{***}p < 0.001$. Error bars represent mean ± s.d. ($n = 3$).

The gap time that exists between the moment when insulin is released from NP and the moment it permeates through the intestinal epithelium should be the lowest possible, since the longer insulin resides in contact with the mucus layer and intestinal enzymes, the more it could degrade, lose bioactivity and escape without being absorbed. Therefore, a fast release of insulin from NP might be desirable to ensure that a sufficient amount reaches the target site and provides therapeutic effects [67]. The values of TEER measured before and after the experiments were stable during 4 h (results not shown), demonstrating the integrity of the monolayers.

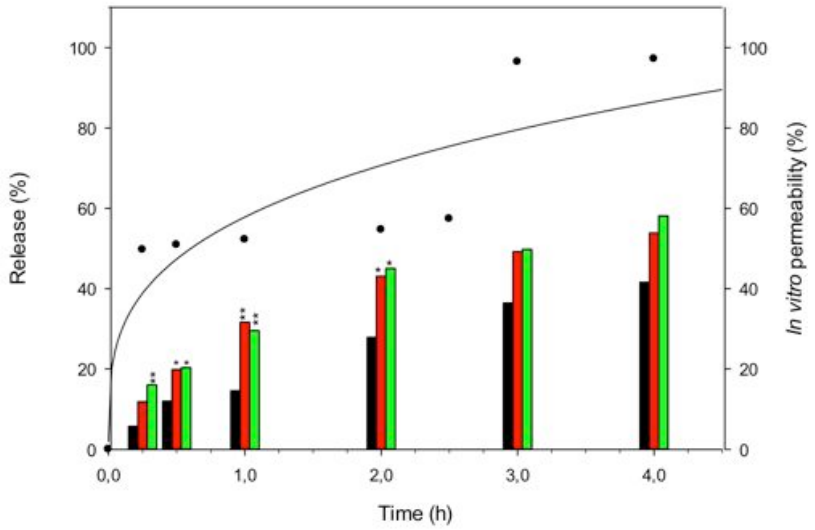

Figure 4.7. Comparison between the fraction of the released vs permeated insulin for 4 h−testing for the ALB−NP. The data from the *in vitro* release of insulin in SIF (black circles) was linearized (black line) according to the mathematical model designed to fit the release profile and plotted against the permeability through the Caco−2 (black bars), Caco−2/HT29−MTX (red bars) and Caco−2/HT29−MTX/Raji B (green bars) models. All the data sets were compared to the permeation of insulin across the Caco−2 monolayer. The level of significance was set at probabilities of $^{*}p < 0.05$, $^{**}p < 0.01$, and $^{***}p < 0.001$.

4.5 CONCLUSIONS

In the present study, a biopolymer−based nanosystem was developed to enhance the oral absorption of insulin. The system is composed of an ADS−core with spherical shape, negative ζ−potential values and high EE. The double coating with CS and ALB was successfully achieved, taking advantage of their protective, mucoadhesive and absorption−enhancing properties. The monitoring of the impact of the GI environment in the NP size and aggregation suggested the pH sensitivity of these biopolymers. The ALB−NP showed to provide better size stability in the GI conditions with less aggregation and more

uniformity of the size distribution, preventing the release of the majority of insulin in the gastric pH and sustaining the release in the intestinal pH to allow insulin to be released in the sites of absorption. Such results indicated that when given orally, minimal insulin would be released from the NP in the stomach while the remaining majority could achieve a sustained and complete release in the intestine following 3 h of administration. In the cellular experiments, the ALB−NP were found to significantly increase the permeability of insulin across the *in vitro* models, a pattern that was in accordance with the insulin release profile. The permeability of insulin across the intestinal epithelium was more prominent in the presence of the mucus layer and M−like cells, revealing their positive role on the insulin absorption. Overall, our results suggest that these biopolymer−based multilayered NP are a promising carrier towards the oral delivery of insulin.

4.6 REFERENCES

[1] Carino, G. P.; Mathiowitz, E. Oral insulin delivery. Advanced Drug Delivery Reviews 1999;35:249−57.

[2] Woitiski, C.; Neufeld, R.; Veiga, F.; Carvalho, R.; Figueiredo, I. Pharmacological effect of orally delivered insulin facilitated by multilayered stable nanoparticles. European Journal of Pharmaceutical Sciences 2010;41:556 − 63.

[3] Woitiski, C. B.; Sarmento, B.; Carvalho, R. A.; Neufeld, R. J.; Veiga, F. Facilitated nanoscale delivery of insulin across intestinal membrane models. International Journal of Pharmaceutics 2011;412:123−31.

[4] Reis, C. P.; Veiga, F. J.; Ribeiro, A. J.; Neufeld, R. J.; Damgé, C. Nanoparticulate biopolymers deliver insulin orally eliciting pharmacological response. Journal of Pharmaceutical Sciences 2008;97:5290−305.

[5] Stops, F.; Fell, J. T.; Collett, J. H.; Martini, L. G. Floating dosage forms to prolong gastro−retention — The characterisation of calcium alginate beads. International Journal of Pharmaceutics 2008;350:301−11.

[6] Abbaspour, M.; Makhmalzadeh, B.; Arastoo, Z.; Jahangiri, A.; Shiralipour, R. Effect of anionic polymers on drug loading and release from clindamycin phosphate solid lipid nanoparticles. Tropical Journal of Pharmaceutical Research 2013;12:477−82.

[7] Cui, F.; Qian, F.; Zhao, Z.; Yin, L.; Tang, C.; Yin, C. Preparation, characterization, and oral delivery of insulin loaded carboxylated chitosan grafted poly(methyl methacrylate) nanoparticles. Biomacromolecules 2009;10:1253−8.

[8] Li, X.; Guo, S.; Zhu, C.; Zhu, Q.; Gan, Y.; Rantanen, J.; Rahbek, U. L.; Hovgaard, L.; Yang, M. Intestinal mucosa permeability following oral insulin delivery using core shell corona nanolipoparticles. Biomaterials 2013;34:9678−87.

[9] Shrestha, N.; Shahbazi, M.−A.; Araújo, F.; Zhang, H.; Mäkilä, E. M.; Kauppila, J.; Sarmento, B.; Salonen, J. J.; Hirvonen, J. T.; Santos, H. A. Chitosan−modified porous silicon microparticles for enhanced permeability of insulin across intestinal cell monolayers. Biomaterials 2014;35:7172−9.

[10] George, M.; Abraham, T. E. Polyionic hydrocolloids for the intestinal delivery of protein drugs: Alginate and chitosan — A review. Journal of Controlled Release 2006;114:1−14.

[11] Kamiya, N.; Klibanov, A. M. Controling the rate of protein release from polyelectrolyte complexes. Biotechnology and Bioengineering 2003;82:590−4.

[12] Reis, C.; Ribeiro, A.; Houng, S.; Veiga, F.; Neufeld, R. Nanoparticulate delivery system for insulin: Design, characterization and *in vitro*/*in vivo* bioactivity. European Journal of Pharmaceutical Sciences 2007;30:392 − 7.

[13] Sonaje, K.; Lin, K.−J.; Tseng, M. T.; Wey, S.−P.; Su, F.−Y.; Chuang, E.−Y.; Hsu, C.−W.; Chen, C.−T.; Sung, H.−W. Effects of chitosan−nanoparticle−mediated tight junction opening on the oral absorption of endotoxins. Biomaterials 2011;32:8712−21.

[14] Fonte, P.; Andrade, F.; Araújo, F.; Andrade, C.; Neves, J. d.; Sarmento, B. Chapter fifteen − Chitosan−coated solid lipid nanoparticles for insulin delivery. In: Nejat D, editor. Methods in Enzymology. Volume 508: Academic Press; 2012. p. 295−314.

[15] Qin, C.; Li, H.; Xiao, Q.; Liu, Y.; Zhu, J.; Du, Y. Water−solubility of chitosan and its antimicrobial activity. Carbohydrate Polymers 2006;63:367−74.

[16] Fan, M.; Hu, Q.; Shen, K. Preparation and structure of chitosan soluble in wide pH range. Carbohydrate Polymers 2009;78:66−71.

[17] Borchard, W.; Kenning, A.; Kapp, A.; Mayer, C. Phase diagram of the system sodium alginate/water: A model for biofilms. International Journal of Biological Macromolecules 2005;35:247−56.

[18] Roger, E.; Lagarce, F.; Garcion, E.; Benoit, J.–P. Biopharmaceutical parameters to consider in order to alter the fate of nanocarriers after oral delivery. Nanomedicine 2010;5:287–306.

[19] Hinkley, G.; Carpinone, P.; Munson, J.; Powers, K.; Roberts, S. Oral absorption of PEG–coated versus uncoated gold nanospheres: Does agglomeration matter? Particle and Fibre Toxicology 2015;12:1–13.

[20] Lopes, M. A.; Abrahim–Vieira, B.; Oliveira, C.; Fonte, P.; Souza, A. M. T.; Lira, T.; Sequeira, J. A. D.; Rodrigues, C. R.; Cabral, L. M.; Sarmento, B.; Seiça, R.; Veiga, F.; Ribeiro, A. J. Probing insulin bioactivity in oral nanoparticles produced by ultrasonication–assisted emulsification/internal gelation. International Journal of Nanomedicine 2015;10:5865–80.

[21] Lopes, M.; Abrahim, B. A.; Rodrigues, C. R.; Veiga, F.; Cabral, L.; Ribeiro, A. J. Alginate–based micro and nanoparticles coated with chitosan. Journal of Chitin and Chitosan Science 2013;1:173–6.

[22] Vázquez, J. L.; Merino, S.; Doměnech, Ò.; Berlanga, M.; Viñas, M.; Montero, M. T.; Hernández–Borrell, J. Determination of the partition coefficients of a homologous series of ciprofloxacin: influence of the N–4 piperazinyl alkylation on the antimicrobial activity. International Journal of Pharmaceutics 2001;220:53–62.

[23] Sarmento, B.; Ribeiro, A.; Veiga, F.; Ferreira, D. Development and validation of a rapid reversed–phase HPLC method for the determination of insulin from nanoparticulate systems. Biomedical Chromatography 2006;20:898–903.

[24] McConnell, E. L.; Fadda, H. M.; Basit, A. W. Gut instincts: Explorations in intestinal physiology and drug delivery. International Journal of Pharmaceutics 2008;364:213–26.

[25] Vertzoni, M.; Dressman, J.; Butler, J.; Hempenstall, J.; Reppas, C. Simulation of fasting gastric conditions and its importance for the *in vivo* dissolution of lipophilic compounds. European Journal of Pharmaceutics and Biopharmaceutics 2005;60:413–7.

[26] Gaumet, M.; Gurny, R.; Delie, F. Localization and quantification of biodegradable particles in an intestinal cell model: The influence of particle size. European Journal of Pharmaceutical Sciences 2009;36:465–73.

[27] Fonte, P.; Nogueira, T.; Gehm, C.; Ferreira, D.; Sarmento, B. Chitosan–coated solid lipid nanoparticles enhance the oral absorption of insulin. Drug Delivery and Translational Research 2011;1:299–308.

[28] Sarmento, B.; Mazzaglia, D.; Bonferoni, M. C.; Neto, A. P.; do Céu Monteiro, M.; Seabra, V. Effect of chitosan coating in overcoming the phagocytosis of insulin loaded solid lipid nanoparticles by mononuclear phagocyte system. Carbohydrate Polymers 2011;84:919−25.

[29] Florence, A. T. Nanoparticle uptake by the oral route: Fulfilling its potential? Drug Discovery Today: Technologies 2005;2:75−81.

[30] Norris, D. A.; Puri, N.; Sinko, P. J. The effect of physical barriers and properties on the oral absorption of particulates. Advanced Drug Delivery Reviews 1998;34:135−54.

[31] Lai, S. K.; Wang, Y.−Y.; Hanes, J. Mucus−penetrating nanoparticles for drug and gene delivery to mucosal tissues. Advanced Drug Delivery Reviews 2009;61:158−71.

[32] Santos, A. C.; Cunha, J.; Veiga, F.; Cordeiro−da−Silva, A.; Ribeiro, A. J. Ultrasonication of insulin−loaded microgel particles produced by internal gelation: Impact on particle's size and insulin bioactivity. Carbohydrate Polymers 2013;98:1397−408.

[33] Gratton, S. E. A.; Ropp, P. A.; Pohlhaus, P. D.; Luft, J. C.; Madden, V. J.; Napier, M. E.; DeSimone, J. M. The effect of particle design on cellular internalization pathways. Proceedings of the National Academy of Sciences 2008;105:11613−8.

[34] Caldorera−Moore, M.; Guimard, N.; Shi, L.; Roy, K. Designer nanoparticles: Incorporating size, shape and triggered release into nanoscale drug carriers. Expert Opinion on Drug Delivery 2010;7:479−95.

[35] Verma, M.; Liu, S.; Chen, Y.; Meerasa, A.; Gu, F. Size−tunable nanoparticles composed of dextran−b−poly(D,L−lactide) for drug delivery applications. Nano Research 2012;5:49−61.

[36] Gaumet, M.; Gurny, R.; Delie, F. Interaction of biodegradable nanoparticles with intestinal cells: The effect of surface hydrophilicity. International Journal of Pharmaceutics 2010;390:45−52.

[37] Hillery, A. M.; Florence, A. T. The effect of adsorbed poloxamer 188 and 407 surfactants on the intestinal uptake of 60−nm polystyrene particles after oral administration in the rat. International Journal of Pharmaceutics 1996;132:123−30.

[38] Win, K. Y.; Feng, S.−S. Effects of particle size and surface coating on cellular uptake of polymeric nanoparticles for oral delivery of anticancer drugs. Biomaterials 2005;26:2713−22.

[39] des Rieux, A.; Ragnarsson, E. G. E.; Gullberg, E.; Preat, V.; Schneider, Y. J.; Artursson, P. Transport of nanoparticles across an *in vitro* model of the human intestinal follicle associated epithelium. European Journal of Pharmaceutical Sciences 2005;25:455−65.

[40] Mimmo, T.; Marzadori, C.; Montecchio, D.; Gessa, C. Characterisation of Ca– and Al–pectate gels by thermal analysis and FT−IR spectroscopy. Carbohydrate Research 2005;340:2510−9.

[41] Sarmento, B.; Ferreira, D.; Veiga, F.; Ribeiro, A. Characterization of insulin−loaded alginate nanoparticles produced by ionotropic pre−gelation through DSC and FTIR studies. Carbohydrate Polymers 2006;66:1−7.

[42] Florence, A. T. The oral absorption of micro− and nanoparticulates: Neither exceptional nor unusual. Pharmaceutical Research 1997;14:259−66.

[43] Lesmes, U.; McClements, D. J. Controlling lipid digestibility: Response of lipid droplets coated by β−lactoglobulin−dextran Maillard conjugates to simulated gastrointestinal conditions. Food Hydrocolloids 2012;26:221−30.

[44] Wang, X.; Garth Spencer, H. Calcium alginate gels: formation and stability in the presence of an inert electrolyte. Polymer 1998;39:2759−64.

[45] Woitiski, C. B.; Neufeld, R. J.; Ribeiro, A. J.; Veiga, F. Colloidal carrier integrating biomaterials for oral insulin delivery: Influence of component formulation on physicochemical and biological parameters. Acta Biomaterialia 2009;5:2475−84.

[46] des Rieux, A.; Fievez, V.; Momtaz, M.; Detrembleur, C.; Alonso−Sande, M.; Van Gelder, J.; Cauvin, A.; Schneider, Y. J.; Preat, V. Helodermin−loaded nanoparticles: Characterization and transport across an *in vitro* model of the follicle−associated epithelium. Journal of Controlled Release 2007;118:294−302.

[47] García−Fuentes, M.; Torres, D.; Alonso, M. J. Design of lipid nanoparticles for the oral design of lipid nanoparticles for the oral delivery of hydrophilic macromolecules. Colloids and Surfaces B: Biointerfaces 2003;27:159−68.

[48] Chien, Y. W. Human insulin: Basic sciences to therapeutic uses. Drug Development and Industrial Pharmacy 1996;22:753−89.

[49] Chaudhury, A.; Das, S. Recent advancement of chitosan−based nanoparticles for oral controlled delivery of insulin and other therapeutic agents. American Association of Pharmaceutical Scientists 2011;12:10−20.

[50] Araújo, F.; Shrestha, N.; Shahbazi, M.−A.; Fonte, P.; Mäkilä, E. M.; Salonen, J. J.; Hirvonen, J. T.; Granja, P. L.; Santos, H. A.; Sarmento, B. The impact of nanoparticles on the mucosal translocation and transport of GLP−1 across the intestinal epithelium. Biomaterials 2014;35:9199−207.

[51] Gupta, S.; Jain, A.; Chakraborty, M.; Sahni, J. K.; Ali, J.; Dang, S. Oral delivery of therapeutic proteins and peptides: A review on recent developments. Drug Delivery 2013;20:237−46.

[52] Zhang, X. G.; Teng, D. Y.; Wu, Z. M.; Wang, X.; Wang, Z.; Yu, D. M.; Li, C. X. PEG−grafted chitosan nanoparticles as an injectable carrier for sustained protein release. Journal of Materials Science: Materials in Medicine 2008;19:3525−33.

[53] Liu, J.; Zhang, S. M.; Chen, P. P.; Cheng, L.; Zhou, W.; Tang, W. X.; Chen, Z. W.; Ke, C. M. Controlled release of insulin from PLGA nanoparticles embedded within PVA hydrogels. Journal of Materials Science: Materials in Medicine 2007;18:2205−10.

[54] Li, P.; Dai, Y.−N.; Zhang, J.−P.; Wang, A.−Q.; Wei, Q. Chitosan−alginate nanoparticles as a novel drug delivery system for nifedipine. International Journal of Biomedical Science 2008;4:221−8.

[55] Nagarwal, R. C.; Ridhurkar, D. N.; Pandit, J. K. *In vitro* release kinetics and bioavailability of gastroretentive cinnarizinhydrochloride tablet. American Association of Pharmaceutical Scientists 2010;11:294−303.

[56] Ritger, P. L.; Peppas, N. A. A simple equation for description of solute release I. Fickman and non−Fickian release from non−swellable devices in the form of slabs, spheres, cylinders or discs. Journal of Controlled Release 1987;5:23−36.

[57] Araújo, F.; Sarmento, B. Towards the characterization of an *in vitro* triple co−culture intestine cell model for permeability studies. International Journal of Pharmaceutics 2013;458:128−34.

[58] Sarmento, B.; Andrade, F.; Silva, S. B. d.; Rodrigues, F.; das Neves, J.; Ferreira, D. Cell−based *in vitro* models for predicting drug permeability. Expert Opinion on Drug Metabolism & Toxicology 2012;8:607−21.

[59] Antunes, F.; Andrade, F.; Araújo, F.; Ferreira, D.; Sarmento, B. Establishment of a triple co−culture *in vitro* cell models to study intestinal absorption of peptide drugs. European Journal of Pharmaceutics and Biopharmaceutics 2013;83:427−35.

[60] Chen, M.−C.; Sonaje, K.; Chen, K.−J.; Sung, H.−W. A review of the prospects for polymeric nanoparticle platforms in oral insulin delivery. Biomaterials 2011;32:9826−38.

[61] Pillai, O.; Panchagnula, R. Insulin therapies – past, present and future. Drug Discovery Today 2001;6:1056−61.

[62] Chen, M.−C.; Mi, F.−L.; Liao, Z.−X.; Hsiao, C.−W.; Sonaje, K.; Chung, M.−F.; Hsu, L.−W.; Sung, H.−W. Recent advances in chitosan−based nanoparticles for oral delivery of macromolecules. Advanced Drug Delivery Reviews 2013;65:865−79.

[63] Hsu, L.−W.; Lee, P.−L.; Chen, C.−T.; Mi, F.−L.; Juang, J.−H.; Hwang, S.−M.; Ho, Y.−C.; Sung, H.−W. Elucidating the signaling mechanism of an epithelial tight−junction opening induced by chitosan. Biomaterials 2012;33:6254−63.

[64] Sonaje, K.; Chuang, E. Y.; Lin, K. J.; Yen, T. C.; Su, F. Y.; Tseng, M. T.; Sung, H. W. Opening of epithelial tight junctions and enhancement of paracellular permeation by chitosan: Microscopic, ultrastructural, and computed−tomographic observations. Molecular Pharmaceutics 2012;9:1271−9.

[65] Peppas, N. A.; Carr, D. A. Impact of absorption and transport on intelligent therapeutics and nanoscale delivery of protein therapeutic agents. Chemical Engineering Science 2009;64:4553−65.

[66] Walter, E.; Janich, S.; Roessler, B. J.; Hilfinger, J. M.; Amidon, G. L. HT29−MTX/Caco−2 cocultures as an *in vitro* model for the intestinal epithelium: *In vitro–in vivo* correlation with permeability data from rats and humans. Journal of Pharmaceutical Sciences 1996;85:1070–6.

[67] Dinarvand, M.; Kiani, M.; Mirzazadeh, F.; Esmaeili, A.; Mirzaie, Z.; Soleimani, M.; Dinarvand, R.; Atyabi, F. Oral delivery of nanoparticles containing anticancer SN38 and hSET1 antisense for dual therapy of colon cancer. International Journal of Biological Macromolecules 2015;78:112−21.

CHAPTER 5

IN VIVO BIODISTRIBUTION OF ORAL BIOPOLYMER–BASED NANOPARTICLES FOR THE TREATMENT OF TYPE 1 AND TYPE 2 DIABETES

5.1 ABSTRACT

This study aimed to assess the oral antihyperglycemic activity of insulin−loaded ADS−based NP dual coated with CS and ALB followed by *in vivo* oral biodistribution of the NP in which the ALB was labeled with technetium−99m (^{99m}Tc).

The oral administration of the 50 IU/kg insulin−loaded NP to T1D rats showed prolonged antihyperglycemic effects up to 12 h and relative PA of 5.04% comparing to the s.c. administration. The oral antihyperglycemic effect was further compared between T1D and T2D models by the intraperitoneal glucose tolerance test (IGTT), revealing that the effect lasted longer in the T1D model. The ^{99m}Tc−ALB revealed to be an efficient NP' tracer since there was no systemic absorption and the ^{99m}Tc−ALB−NP were capable of increasing their residence time in the intestinal epithelium of balb−c mice when compared with the ^{99m}Tc−ALB alone. Thus, this biopolymeric−based delivery nanosystem is a promising tool for the therapy of T1D and T2D.

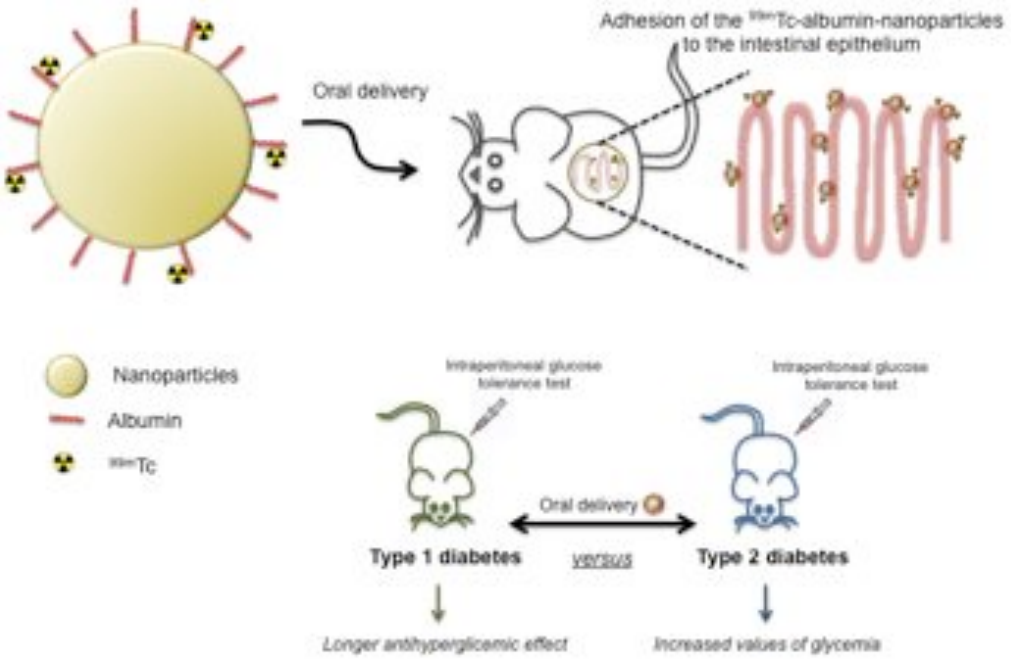

Graphical abstract: Biodistribution of the insulin–loaded ADS–based NP dual coated with CS and ^{99m}Tc–ALB after oral administration. The comparison of the oral antihyperglycemic effect between the T1D and T2D models after the IGTT revealed that the effect lasted longer in the T1D model and that the glycemia increased to a greater extend in the T2D model.

5.2 INTRODUCTION

Diabetes is a metabolic disorder that has reached epidemic dimensions around the world and requires chronic treatment. The primary mode of treatment of the T1D consists of an intensive insulin therapy, corresponding up to 4 injections per day [1,2]. The T2D is a more complex and incident form of diabetes (~ 90% of all the diabetic cases), caused by a blend of insulin resistance and inappropriate functional pancreatic β−cells [3,4]. Given the convenience, good patient compliance and more importantly, the mimicked pattern of physiological mechanism of insulin secretion after oral administration, the oral delivery of insulin has become the most desired route of administration [5]. However, as a result of the challenging barriers found in the GI tract [6] (e.g, acidic pH in the stomach, enzymatic degradation, mucus layer and TJ that bound the intestinal epithelial cells), oral insulin delivery is characterized by very low BA [6,7]. Aiming to overcome the drawbacks of this delivery route, several attempts to deliver insulin orally have been made in order to protect the protein following oral administration. The ideal oral insulin delivery system should fulfill at least three important fundamentals: i) resist against the GI enzymes and pH gradients, ii) prolong the insulin intestinal residence time to increase its permeability, iii) carry the bioactive insulin to the systemic circulation [8]. The success of an orally delivery system lies on the understanding and control of its biodistribution, which gives important information about the GI transit times and global tissue accumulation patterns. The biodistribution characteristics are important for the design and test of NP, in order to determine the particle size, coating materials, or other features to achieve an effective level of the NP in the final target [9]. In Chapter 4, a pH−responsive nanosystem dual coated with CS and ALB intended for the oral delivery of insulin was reported [10]. CS has been described for its ability to transiently open the TJ between contiguous cells [11,12] and to adhere to the anionic sialic acid residues present in the intestinal mucosa [13], whilst ALB had disclosed positive effects when used as an outermost coat to CS−based NP, such as the protective effect of insulin by acting as a sacrificial target to proteases, and by stabilizing the NP in the acidic [14,15] and intestinal environment [16]. The results previously obtained revealed that the ALB/CS−coated ADS insulin−loaded NP provided stability in the GI conditions, preventing the premature release of insulin in SGF [10]. Additionally, this nanosystem effectively adhered to the intestinal cells monolayers, increasing insulin permeability, thereby making an optimal

candidate to increase the insulin oral BA [10]. Based on the inherent characteristics of these NP, the assessment of their biodistribution takes special consideration and the study of these NP coated with ^{99m}Tc−ALB can contribute to better understand the ALB role and the NP' interactions throughout the gut as well as their degradation.

One can find in the literature reports of oral insulin formulations demonstrating antihyperglycemic effects in T1D [17−20] or T2D [21] animal models. However, to the best of our knowledge, a comparative study between the pharmacological effects of oral delivered insulin−loaded NP in both diabetic type models has never been done. Although the T2D patients are not dependent on exogenous insulin, the threatening that insulin administration will be needed later in their lifetime is real. Both T1D [22−24] and T2D [25,26] have been associated with modifications in the composition of the intestinal microbiota. Moreover, the T1D is characterized by an alteration of the energy balance due to the massive emission of urine and consequent huge intake of water to maintain the hydric balance. Therefore, there is a limited storage of triacylglycerols, due to the limited energy availability and lack of insulin to promote the synthesis of energy. In contrast, the T2D shows a completely different metabolic panorama, since the main problem is the insulin resistance and not the insulin availability. The insulin−resistance increases the glycemia since the threshold for the uptake of glucose is raised, leading to the synthesis of triacylglycerols and storage of lipids [27]. Therefore, the understanding of the different behavior of the T1D and T2D animal models after oral administration of insulin would be of great interest.

The main goal of our study was to evaluate the biodistribution of the ALB/CS−coated ADS insulin−loaded NP. Firstly, the ability of this nanosystem, prepared by emulsification/internal gelation, to improve the oral PA of insulin was assessed in both T1D and T2D animal models. In the second part, the biodistribution of the ^{99m}Tc−ALB−NP following its oral administration was also evaluated by camera−gamma imaging.

5.3 MATERIALS AND METHODS

5.3.1 Materials

Low viscosity sodium alginate (viscosity of 1% solution at 25 °C, 4−12 cps), dextran sulfate (5 KDa), sorbitan monooleate (Span® 80), CS (50 kDa), bovine serum ALB, PEG 4000,

phosphotungstic acid and STZ were purchased from Sigma−Aldrich (Germany). Calcium carbonate was obtained from Setacarb (France), paraffin oil from Scharlau (Spain), insulin 100IU/mL Actrapid® from Novo Nordisk (Denmark), poloxamer 188 (Lutrol®F68) from BASF (Germany) and $CaCl_2$ from Riedel−de−Haën (Germany). Wistar male rats weighing 250–300 g and balb−c mice weighing 22–26 g were purchased from Charles River (Spain) and GK rats were obtained from our local breeding colonies (Faculty of Medicine, University of Coimbra, Coimbra, Portugal).

Stannous chloride dehydrate, succinic dihydrazide and EDTA were obtained from Sigma−Aldrich (Italy). In all the procedures, ethanol, water and saline suitable for injection were employed.

Before use, Sep−Pak cartridges (Waters) were washed with 5.0 mL of sterile water and then steam sterilized. The ^{99m}Tc−pertechnetate was obtained from a generator ^{99}Mo/^{99m}Tc (GE Healthcare's Drytec™, UK).

5.3.2 NP preparation

The NP were prepared by the emulsification/internal gelation technique and polyelectrolyte complexation as described In Chapter 3.

5.3.3 NP characterization

The particle size distribution and morphology were analyzed as described in Chapter 2.

The methodology of the ζ−potential study was performed according to the description in Chapter 4.

5.3.4 Animals

The animals were kept and studied in accordance with the FELASA and the European Union Council Directive 86/609/EEC. The procedures and manipulations were performed

under the ethical principles and guidelines relative to housing and experiments on animals of the DGAV. The animals were accommodated under controlled temperature, humidity, and a 12–12h light–dark cycle. They were given standard laboratory feed and had free access to tap water.

According to the guiding ethical principles for the use of animals in testing, the 3Rs policy was followed. The animals were firstly used to determine the biological activity of insulin, important to guarantee that the insulin structure was well preserved and able to induce the desired therapeutic effect. After, the animals were used to test the oral effect of the NP.

5.3.5 Insulin biological activity

The insulin–loaded NP or insulin released from the NP in pH 7.4 PBS were subcutaneously injected to GK rats at 2 IU/kg. To analyze the biological activity of the insulin after nanoencapsulation, the IGTT was accomplished by previous intraperitoneal administration of 1.75 g/kg glucose solution. Three groups of animals were randomly obtained (n = 12 per group) corresponding to i) nonencapsulated insulin, ii) insulin released from the NP and iii) insulin–loaded NP. The blood samples were obtained from the tail vein at predetermined times during 3 h after the glucose administration, and compared to the basal levels.

5.3.6 Induction of T1D

For the diabetes induction, male Wistar rats weighing 250–350 g were injected intraperitoneally with 60 mg/kg STZ freshly prepared in citrate buffer pH 4.5, in order to destroy the pancreatic cells. During the next 24 h after the STZ administration, a physiologic solution of glucose (5%, w/v) was given to the rats to prevent hypoglycemia. After 7–10 days, rats presenting frequent urination, weight loss and fasting plasma glucose levels higher than 14 mM were randomized for *in vivo* studies.

5.3.7 Oral antihyperglycemic effect of the NP

The PA was determined by the plasma glucose levels obtained in diabetic Wistar rats. The antihyperglycemic effect was assessed by the reduction of the plasma glucose levels in comparison to the basal values in rats divided into four groups (n = 10 per group) corresponding to i) 50 IU/kg insulin−loaded NP, ii) 100 IU/kg insulin−loaded NP or iii) nonencapsulated insulin, all orally delivered by gavage, and iv) s.c. nonencapsulated insulin. The determined the pharmacodynamic parameters comprise the antihyperglycemic effect calculated by the area above the curve ($AAC_{0-24\ h}$) by linear trapezoidal method, the PA calculated as the cumulative antihyperglycemic effect relative to 100% PA of the s.c. nonencapsulated insulin, the time of minimum glycemia (T_{min}) and the minimum glucose concentration (C_{min}) in the blood [28].

5.3.8 IGTT in T1D, T2D models

The PA of the insulin−loaded NP determined by the IGTT was carried out in three groups of GK rats (n = 12 per group) orally administered by gavage with i) 50 IU/kg insulin−loaded NP, ii) empty NP, and iii) without administration, compared with the control Wistar rats (n = 10). In parallel, two groups of diabetic Wistar rats (n = 8 per group), corresponding to i) 50 IU/kg insulin−loaded NP and ii) empty NP, were also submitted to the IGTT. The NP were oral administered 10 h prior to the intraperitoneal administration of 1.75 g/kg glucose solution in both studies. The animals were fasted from 12 h before and 13 h after the oral administration. The plasma glucose levels were measured using the same experimental setup as previously described.

5.3.9 Preparation of the ^{99m}Tc−ALB and ^{99m}Tc−ALB−NP

ALB, the external layer of the NP, was selected to be labeled so it could be the NP' tracer during the biodistribution studies. ALB was labeled with a mixture of sodium thiosulfate (10 mg/mL), HCL (1N) and 1110 to 2220 MBq of $Na^{99m}TcO_4^-$ (1.0/1.0/0.5, v/v/v) heated at 100 °C for 3.5 min within a dry bath. The vial was cooled to room temperature and

2.5 mL of ALB were added. Then, the mixture was stirred by vortex and 2 mL of PBS at pH 7.4 were added. The NP were coated with ^{99m}Tc−ALB using the same experimental setup as previously described. After the coating, the suspension was washed by centrifugation and redispersion in Milli−Q water. The radiolabeling efficiency of ^{99m}Tc was assessed by instant thin−layer chromatography (ITLC) with silica−gel strips with two systems: i) sodium chloride 0.9% (w/v) to quantify the presence of $^{99m}TcO_4^-$ in the sample; and ii) acid citrate−dextrose to allow the isolation of the ^{99m}Tc−ALB/^{99m}Tc−ALB−NP with a R_f value equals to zero against to R_f of one for $^{99m}TcO_4^-$ and reduzed/hidrolized ^{99m}Tc. The radiolabeling efficiency was determined for 24 h after radiolabeling by camera−gamma method.

5.3.10 Biodistribution of the ^{99m}Tc−ALB−NP

The biodistribution of the insulin−loaded ^{99m}Tc−ALB−NP in mice balb−c was studied by camera−gamma after oral gavage administration. The radiotracer was administered to mice with an activity of 15.5 ± 2.6 MBq. The animals were sacrificed by cervical dislocation at 0, 30, 60, 90, 120, 180, 360 and 1440 min after administration (n = 4 per time, per radiotracer). The GI wall was separated from the GI content, carefully rinsed in running water and accurately weighted. All the images were acquired by camera−gamma (GE 400 AC) with a low energy high resolution collimator, 256 x 256 matrix, 2 min acquisition time and a zoom of 2. The percentage of the activity administered per mass unit (g) was calculated.

5.3.11 Statistical analysis

The statistical analysis was made by one−way ANOVA with Bonferroni post hoc−test (SPSS 20.0, USA). All the data sets were compared to the controls. The level of significance was set at probabilities of $^{*}p < 0.05$, $^{**}p < 0.01$, and $^{***}p < 0.001$. All the experiments are shown as mean ± s.d..

5.4 RESULTS AND DISCUSSION

5.4.1 NP characterization

NP nanoencapsulating insulin were produced by alginate and dextran sulfate linked with calcium ions and interacting with poloxamer 188, coated with CS and PEG, and subsequently layered with ALB. The interaction of the NP' components were previously confirmed by DSC, where the shifts on the endothermic and exothermic peaks of the NP were interpreted as the ionic interactions between alginate, dextran sulfate, CS and ALB, which afforded the formation of new chemical entities with changed absorption and thermal properties [10]. As can be seen in Figure 5.1, the NP presented a polydisperse distribution and spherical shape. The mean size of approximately 160−170 nm previously obtained [10] is in accordance with the size observed microscopically. Submicron size carriers have previously shown to promote the contact with the intestinal cells and enable the insulin absorption through different mechanisms [29,30].

These hydrophilic NP had a negative surface charge of −22.1 ± 0.76 mV. 100 or 300 nm CS−coated PLGA particles with negative charge and high hydrophilicity seem to be the best option to target the intestinal cells [31], supporting the possible interaction between our NP with the intestinal cells.

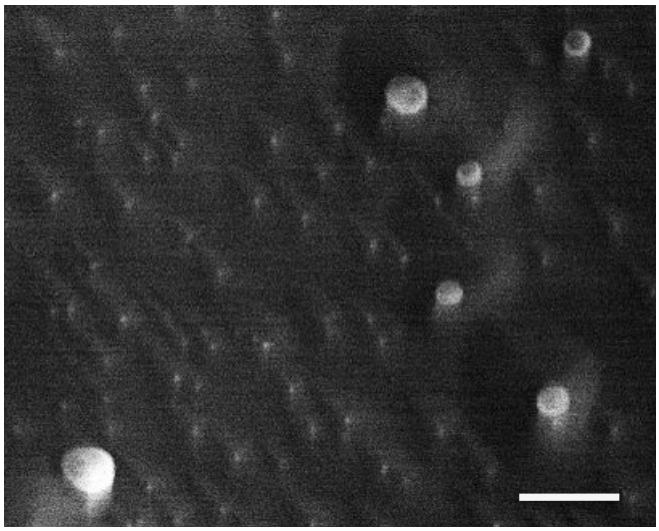

Figure 5.1. Cryo−SEM image of the NP; Scale bar = 500 nm.

5.4.2 Insulin biological activity

The results from the s.c. administration of insulin at a dose level of 2 IU/kg to the GK rats immediately before the glucose challenge are displayed in Figure 5.2. The behavior of these groups corresponding to subcutaneously administered i) nonencapsulated insulin, ii) insulin released from the NP and iii) insulin−loaded NP, in response to a glucose challenge, was very similar and no statistical differences were noticed between them, confirming the retention of the insulin bioactivity after nanoencapsulation. After 60 min, the glycemic values were normalized, except for the group receiving the insulin−loaded ALB−NP that only decreased the glycemia to the basal values after 90 min. Therefore, although not statistically different, the insulin entrapped into the NP had a slower effect on decreasing the glycemic values than the insulin released from the NP, which was already detached from the polymeric matrix when subcutaneously administered, and therefore able to act instantaneously as free−form insulin. The integrity of insulin after nanoencapsulation was ensured and as well as its biological activity.

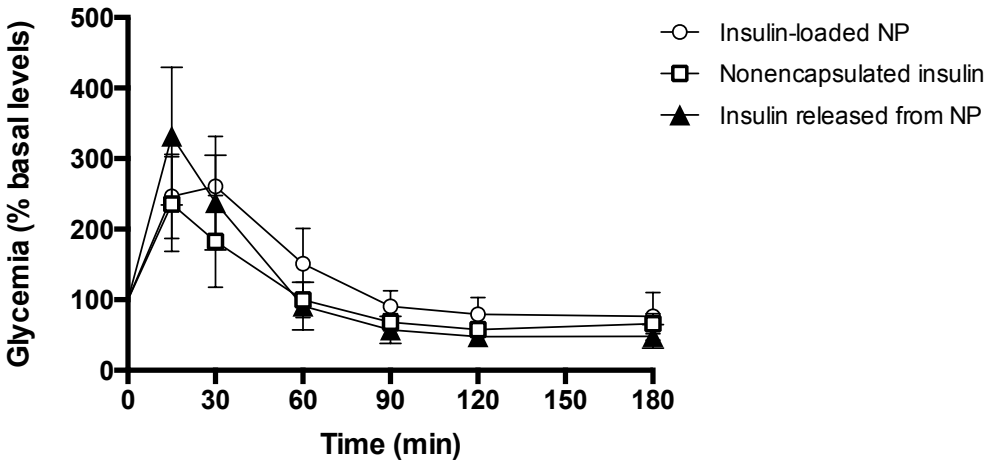

Figure 5.2. Glycemia of GK rats following the oral glucose challenge after s.c. administration of 2 IU/kg nonencapsulated insulin, insulin released from the NP or insulin−loaded NP. Error bars represent mean ± s.d. (n = 12 per group).

5.4.3 Oral antihyperglycemic effect of the NP in T1D model

The PA of the orally administered nanoencapsulated insulin was assessed at 50 IU/kg and 100 IU/kg insulin doses in 12 h fasted diabetic Wistar rats. The high initial blood glucose levels (> 14 mM) of the fasted T1D Wistar rats allows the clear assessment of the antihyperglycemic effect of the NP. The plasma glucose levels were compared to the s.c. injected nonencapsulated insulin at 2 IU/kg. Figure 5.3 illustrates the glucose level versus time profiles and the pharmacodynamic parameters are summarized in Table 1. A significant antihyperglycemic effect was observed between 8 to 12 h after the administration of the insulin−loaded NP, when compared to the nonencapsulated insulin.

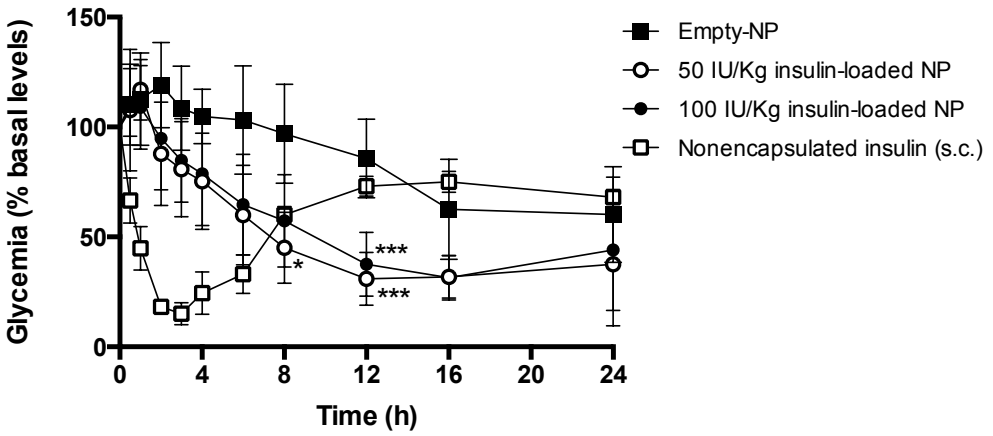

Figure 5.3. Plasma glucose levels of Wistar diabetic rats receiving 50 and 100 IU/kg insulin−loaded NP or empty NP all orally delivered and 2 IU/kg nonencapsulated insulin subcutaneously injected. The level of significance was set at probabilities of $^{*}p < 0.05$ and $^{***}p < 0.001$. Error bars represent mean ± s.d. (n = 10 per group).

Table 5.1. Pharmacodynamic parameters after oral delivery of the insulin−loaded NP at 50 and 100 IU/kg insulin doses, empty NP and after s.c. injection of 2 IU/kg nonencapsulated insulin. Data represent mean ± s.d., n = 10 per group.

Formulation	Insulin dose (IU/kg)	$AAC_{0-24\ h}$	PA (%)	T_{min} (h)	C_{min} (% basal glucose)
Insulin−loaded NP (oral)	50	1232	5.0	12	30.9 ± 12.1
Insulin−loaded NP (oral)	100	1124	2.3	16	31.4 ± 10.2
Empty NP (oral)	–	395	1.6	24	62.6 ± 21.8
Nonencapsulated insulin (s.c.)	2	978	100.0	3	15.0 ± 5.1

The plasma glucose levels were comparable for both doses of 50 and 100 IU/kg of

the insulin−loaded NP. The values of the cumulative hypoglycemic effect and their minimum relative blood glucose around 30% of the basal glucose level (15.8 ± 3.6 mM) were similar as shown in Table 5.1. No dose−response effect was observed for the concentrations tested, which may be understood as a saturation of the sites of absorption of insulin beyond 50 IU/kg. The glycemia decreasing effect of the oral delivered insulin−loaded NP became clear 2 h following their administration, and after 8 h a significantly reduced glycemia by 45% of the basal values was found ($p < 0.05$). The glycemic reductions attained after 10 h were –69% ($p < 0.05$) and –63% ($p < 0.05$) with the 50 and 100 IU/kg insulin−loaded NP, respectively. Compared with the s.c. insulin, the oral nanoencapsulated insulin revealed more sustained and long−term results, which is in very good accordance with previous studies [19,32]. At 24 h postdose, the glycemia was still reduced by ca. 40% of the basal values. The nanoscale size observed for these particles may be one accountable factor for the significant antihyperglycemic effect obtained, which increases the probability of uptake by the intestinal cells [33]. They demonstrated to have stable size behavior during the GI passage and to protect insulin in acidic conditions as well [10]. Moreover, the inherent mucoadhesive properties and capacity of transiently opening the TJ of CS may prolong the NP retention in the intestinal cells, promote the penetration into the mucus layer and increase the insulin paracellular transport [34,35].

The glucose level corresponding to all groups did not reach the initial values due to the prolonged fasted state of the animals [21]. The relative PA of the 50 IU/kg and 100 IU/kg insulin−loaded NP was 5.04 and 2.30%, respectively, acquired from the dose−corrected $AAC_{0–24\ h}$ relative to the s.c. insulin. The increased PA of the nanoencapsulated insulin compared to the empty NP indicated that the NP protected insulin from degradation and facilitated the intestinal absorption by increasing the residence time of insulin at the intestinal epithelium and internalization by the enterocytes [36].

5.4.4 IGTT in T1D, T2D models

The IGTT mimics the plasma glucose levels in a postprandial state and gives information on the antihyperglycemic effect as a result of the insulin performance on the glucose homeostasis [19]. The previous study revealed that the maximum antihyperglycemic

effect of the 50 IU/kg oral delivered insulin−loaded NP was achieved after 12 h. Therefore, the IGTT was done after 10 h of the oral administration of the formulations to detect the effect of the NP during the 3 h−test and compared between the T1D, T2D and control models. After the intraperitoneal glucose administration (1.75 g/kg) to Wistar diabetic rats (T1D), the plasma glucose levels of the rats increased to 326% after 30 min (Figure 5.4A). When the insulin−loaded NP were administered 10 h before the glucose challenge, the glucose levels also raised but to a lesser extent, reaching 282% of the initial values. The glucose levels decreased significantly faster after 90 min ($p < 0.05$) in the rats receiving the insulin−loaded NP than in those receiving the empty NP. The glycemia was decreased to 96% after 180 min in the group receiving the insulin−loaded NP, compared to the reduction to 183% in the control group ($p < 0.05$). Consequently, the insulin−loaded NP significantly enhanced the response to a glucose challenge in the T1D rats.

GK rats are characterized by impaired glucose−induced insulin secretion, decreased pancreatic β−cell mass and insulin sensitivity in the liver, and insulin resistance either in the muscles or in the adipose tissue [37]. The glycemic response in the control Wistar and GK rats after the intraperitoneal administration of glucose is shown in Figure 5.4B. The typical glucose intolerance of the GK rats was compared to the control Wistar rats, which demonstrated a rapid capacity to normalize the glycemic values. The blood glucose levels increased to 400% in the GK rats receiving the empty NP and to 470% in the GK rats without administration (both negative controls), after 30 min. As happened with the diabetic Wistar rats, when the insulin−loaded NP were administered 10 h before the glucose challenge, the glycemia also increased but to a lesser extent, attaining 320% of the initial values (from the basal mean value of 4.5 ± 0.5 mM). The increased values (%) in the GK rats compared to the diabetic Wistar rats are essentially due to their lower absolute basal glycemic values. After 90 min of the glucose challenge, a significantly faster reduction of the glycemia was observed in the rats receiving the insulin−loaded NP ($p < 0.05$), which was in accordance to the results obtained for the Wistar diabetic rats. After 180 min, the control groups decreased the glycemic values to 189 and 213% and the group receiving the insulin−loaded NP showed a greater decrease reaching 151%. At this time, no statistical differences were obtained between these groups, in contrast to the results from the Wistar diabetic rats. Although the pancreatic islets of the GK rats are faulty, this genetically modified animal model of T2D could still produce little amounts of insulin and glucagon [38]. Therefore, the

exogenous insulin can cover−up the outcome of the insulin−loaded NP. The comparison of the response between the control Wistar and GK rats indicated that the metabolic decomposition rate of glucose is slower in the second model [39]. All the GK groups had significant hyperglycemic values and a markedly decreased glucose tolerance compared with the Wistar rats. The insulin−loaded NP were capable of significantly improve the response to a glucose challenge, either in the T1D and T2D animal models.

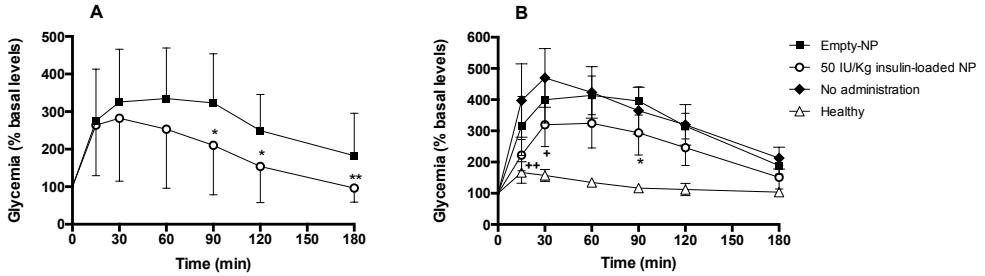

Figure 5.4. Glycemia following oral glucose challenge 10 h after the A) oral delivery of the 50 IU/kg insulin−loaded NP and empty NP to diabetic Wistar rats (n = 8 per group) and after B) oral delivery of the 50 IU/kg insulin−loaded NP, empty NP or without administration to GK rats, compared with control Wistar rats. The level of significance was set at probabilities of $^{*}p < 0.05$ (statistically different from empty NP) or $^{+}p<0.05$; $^{++}p<0.01$ (statistically different from no administration). Error bars represent mean ± s.d. (n ≥ 10 per group).

5.4.5 Biodistribution of the ^{99m}Tc−ALB−NP

The biodistrobution of the NP was analyzed in balb−c mice for further comparison with future biodistribuition studies, once this model, unlike rats model, possesses gallbladder. The ^{99m}Tc−ALB radiolabeling efficiency of approximately 96% achieved after 5 min was kept higher than 90% until 720 min. The ^{99m}Tc−ALB was then used to prepare the ^{99m}Tc−ALB−NP for the imaging study in order to monitor and evaluate their biodistribution in comparison to the ^{99m}Tc−ALB. The final ^{99m}Tc−ALB−NP showed a radiolabeling efficiency higher than 95% until 360 min after radiolabeling. The ^{99m}Tc−ALB−NP had a median diameter

of approximately 200 nm, demonstrating that the radiolabelling increased the NP size in approximately 30 nm.

Upon oral delivery, the progression of the ^{99m}Tc−ALB and ^{99m}Tc−ALB−NP throughout the GI tract was monitored for 1440 min (Figure 5.5) to ensure that the radiotracer was tracked during its full elimination from the GI tract. In the course of the time, the radiolabelled ALB and ALB−NP propagated from the stomach, small intestine and later to the large intestine. A clear difference can be observed between them from 30 to 120 min after oral administration. At 360 min post ingestion, the majority of the radioactivity was detected in the large intestine and at the end of the study no radioactivity was detected.

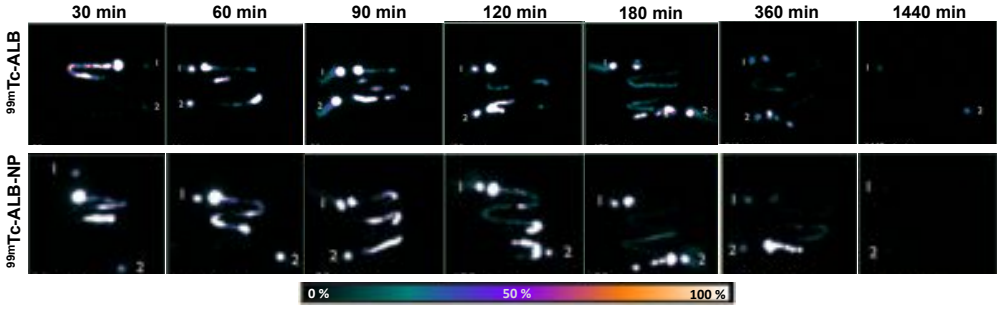

Figure 5.5. Progress over time of the ^{99m}Tc−ALB and ^{99m}Tc−ALB−NP observed after oral administration to a mice model. The number 1 and 2 in each image are anatomical marks, which indicate the stomach and cecum, respectively.

The ^{99m}Tc−ALB had a quick retention in the stomach wall (Figure 5.6) after oral administration, which remained for the following 90 min, while the ^{99m}Tc−ALB−NP only increased the radioactivity values 60 min after the administration, indicating that the multilayered NP triggered a delayed interaction of the radiotracer in this region. The presence of radioactivity in the stomach content decreased deeply over time, with less than 50% of the initial activity after 90 min for both radiotracers.

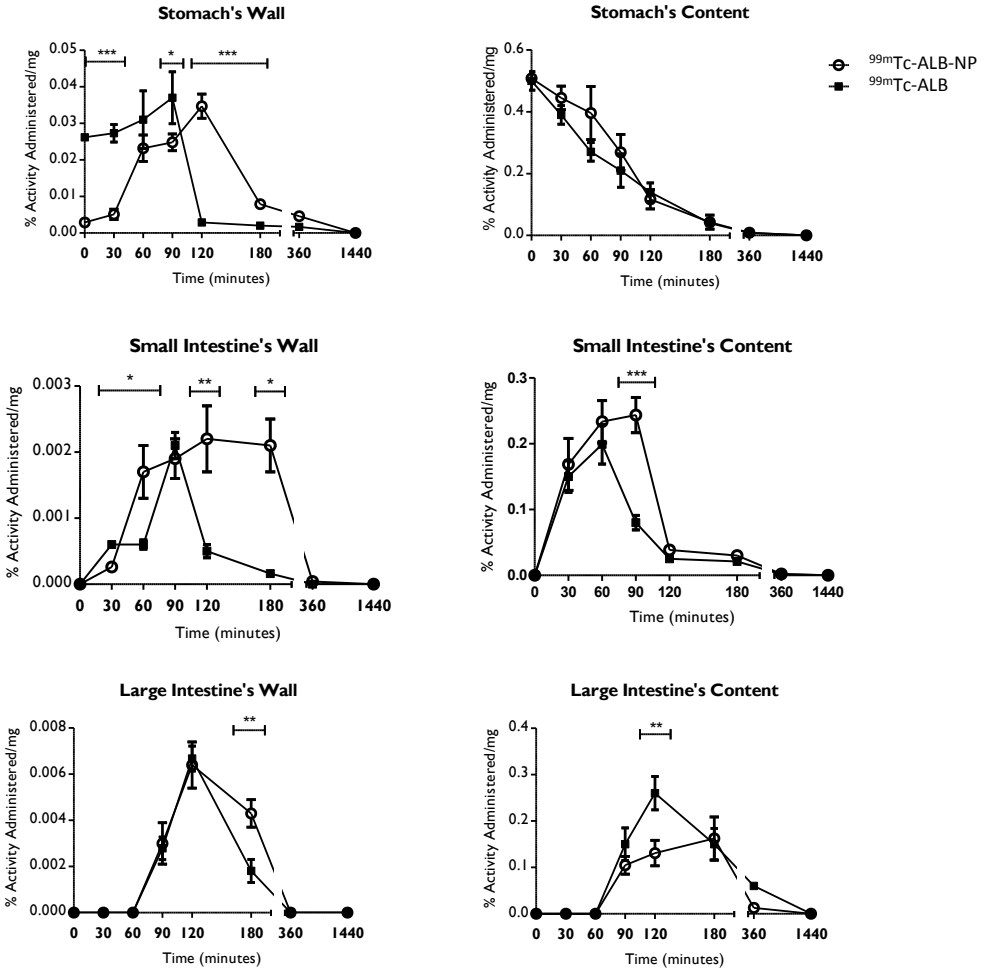

Figure 5.6. Percentage of the administered activity of the ^{99m}Tc−ALB and ^{99m}Tc−ALB−NP per mg of stomach, small and large intestine's walls and contents. The level of significance was set at probabilities of $^{*}p < 0.05$, $^{**}p < 0.01$, and $^{***}p < 0.001$. Error bars represent mean ± s.d. (n ≥ 3).

Due to the large surface area of the small intestine, it constitutes the main region for the drug absorption [40]. The radioactivity of the ^{99m}Tc−ALB−NP observed in the small intestine's wall between 120 and 180 min was significantly higher than the ^{99m}Tc−ALB radioactivity ($p < 0.05$). Furthermore, at 120 min, the radioactivity observed in the small

intestine's content deeply decreased, indicating that the strong interaction of the ALB–NP with the epithelial cells was responsible for the radioactivity detected in the epithelium. These results also indicate that the interaction between ALB and CS was successfully maintained throughout the small intestine passage. The inheritance of positive charge from CS allows the electrostatic interaction with ALB, which is negatively charged at the small intestinal pH [41]. Therefore, the mucoadhesive properties of CS could explain the augmented radioactivity observed for the ^{99m}Tc–ALB–NP in the small intestinal walls when compared to the ^{99m}Tc–ALB, which is in accordance with our previous report (Chapter 4) where insulin showed a higher permeation across the cell monolayers when encapsulated into the the NP [10]. The presence of radioactivity in the large intestine's content achieved higher values for the ^{99m}Tc–ALB than for the ^{99m}Tc–ALB–NP at 120 min, although similar values were obtained in the large intestine's wall at the same time. Therefore, no interaction of the ALB–NP with intestinal wall in this region was noticed, except at 180 min ($p < 0.01$). This result is probably due to the interaction between ALB and CS that gets weaker over time, possibly related with the increase of the pH along the intestine. Although the large intestine is considered to be a favorable site for peptide absorption due to the lack of peptidases in the luminal content, the penetration of the cellular membrane is more challenging than in the small intestine and the epithelial surface decreases from the pylorus towards the anus, suggesting less favorable characteristics for the drug absorption [42]. The absence of activity in the liver and thyroid (data not shown) revealed the high stability of the ^{99m}Tc–ALB after oral administration, since the free ^{99m}Tc presents high uptake by these organs.

ALB was included in this multilayer nanosystem to act as a sacrificial target to protect insulin against the harsh environment founded in the stomach after oral delivery. The ^{99m}Tc–ALB and ^{99m}TC–ALB–NP revealed a different pattern of intestinal interaction along the GI tract, suggesting that ALB was not totally degraded in the stomach and was still integrated in the NP' structure, which allows it to protect insulin and stabilize the NP in the intestinal environment as well. Furthermore, the increased contact of the NP with the intestinal epithelium demonstrated in the biodistribution studies, probably due to the mucoadhesive characteristics of the NP, support the antihyperglycemic effect obtained.

5.5 CONCLUSIONS

The reported work illustrated the antihyperglycemic effect of the 160−170 nm biopolymer−based NP dual coated with CS and ALB. A comparative study after the oral delivery of the insulin−loaded NP to the T1D and T2D models was for the first time carried out. The designed formulation provided a stabilized nanosystem within the GI environment, which resulted in significant antihyperglycemic effect after oral administration for both models, although the antihyperglycemic effect lasted longer in the model of T1D. The biodistribution studies revealed high stability of the radiotracer ^{99m}Tc−ALB after oral administration. Additionally, the ^{99m}Tc−ALB−NP could significantly enhance the interactions with the small intestinal walls, which could be associated with the mucoadhesive properties of CS. This behavior also indicated that ALB was not totally degraded in the stomach, which allowed the protection of insulin and stabilization of the NP in the intestinal environment as well. These results suggest that this nanosystem is a potential tool to accomplish high oral BA of insulin, which may also be useful for the oral delivery of other peptide or protein drugs. Clinically, it might be very promising for the therapy of T1D and T2D.

5.6 REFERENCES

[1] The Diabetes Control and Complications Trial Research Group. The effect of intensive treatment of diabetes on the development and progression of long−term complications in insulin−dependent diabetes mellitus. New England Journal of Medicine 1993;329:977−86.

[2] Berthe, E.; Lireux, B.; Coffin, C.; Goulet−Salmon, B.; Houlbert, D.; Boutreux, S.; Fradin, S.; Reznik, Y. Effectiveness of intensive insulin therapy by multiple daily injections and continuous subcutaneous infusion: A comparison study in type 2 diabetes with conventional insulin regimen failure. Hormone and Metabolic Research Journal 2007;39:224−9.

[3] Anuradha, R.; Saraswati, M.; Kumar, K. G.; Rani, S. H. Apoptosis of beta cells in diabetes mellitus. DNA and Cell Biology 2014;33:743−8.

[4] Dornadula, S.; Elango, B.; Balashanmugam, P.; Palanisamy, R.; Kunka Mohanram, R. Pathophysiological insights of methylglyoxal induced type−2 diabetes. Chemical Research in Toxicology 2015;28:1666−74.

[5] Arbit, E. The physiological rationale for oral insulin administration. Diabetes technology & therapeutics 2004 6:510−7.

[6] Carino, G. P.; Mathiowitz, E. Oral insulin delivery 1. Advanced Drug Delivery Reviews 1999;35:249−57.

[7] Goldberg, M.; Gomez−Orellana, I. Challenges for the oral delivery of macromolecules. Nature Reviews Drug Discovery 2003;2:289−95.

[8] Sonia, T. A.; Sharma, C. P. An overview of natural polymers for oral insulin delivery. Drug Discovery Today 2012;17:784−92.

[9] Lee, M. J.−E.; Veiseh, O.; Bhattarai, N.; Sun, C.; Hansen, S. J.; Ditzler, S.; Knoblaugh, S.; Lee, D.; Ellenbogen, R.; Zhang, M.; Olson, J. M. Rapid pharmacokinetic and biodistribution studies using cholorotoxin−conjugated iron oxide nanoparticles: A novel non−radioactive method. PLoS ONE 2010;5:e9536.

[10] Lopes, M. A.; Derenne, A.; Pereira, C.; Veiga, F. J. B.; Seica, R.; Sarmento, B.; Ribeiro, A. J. Impact of *in vitro* gastrointestinal passage of biopolymer−based nanoparticles on insulin absorption. RSC Advances 2016;6:20155−65.

[11] Artursson, P.; Lindmark, T.; Davis, S.; Illum, L. Effect of chitosan on the permeability of monolayers of intestinal epithelial cells (Caco−2). Pharmaceutical Research 1994 11:1358−61.

[12] Sonaje, K.; Lin, K.−J.; Tseng, M. T.; Wey, S.−P.; Su, F.−Y.; Chuang, E.−Y.; Hsu, C.−W.; Chen, C.−T.; Sung, H.−W. Effects of chitosan−nanoparticle−mediated tight junction opening on the oral absorption of endotoxins. Biomaterials 2011;32:8712−21.

[13] Lehr, C.−M.; Bouwstra, J. A.; Schacht, E. H.; Junginger, H. E. *In vitro* evaluation of mucoadhesive properties of chitosan and some other natural polymers. International Journal of Pharmaceutics 1992;78:43−8.

[14] Hurteaux, R.; Edwards−Lévy, F.; Laurent−Maquin, D.; Lévy, M.−C. Coating alginate microspheres with a serum albumin−alginate membrane: Application to the encapsulation of a peptide. European Journal of Pharmaceutical Sciences 2005;24:187−97.

[15] Woitiski, C. B.; Neufeld, R. J.; Ribeiro, A. J.; Veiga, F. Colloidal carrier integrating biomaterials for oral insulin delivery: Influence of component formulation on physicochemical and biological parameters. Acta Biomaterialia 2009;5:2475−84.

[16] Woitiski, C. B.; Sarmento, B.; Carvalho, R. A.; Neufeld, R. J.; Veiga, F. Facilitated nanoscale delivery of insulin across intestinal membrane models. International Journal of Pharmaceutics 2011;412:123−31.

[17] Reis, C. P.; Veiga, F. J.; Ribeiro, A. J.; Neufeld, R. J.; Damgé, C. Nanoparticulate biopolymers deliver insulin orally eliciting pharmacological response. Journal of Pharmaceutical Sciences 2008;97:5290−305.

[18] Sarmento, B.; Ribeiro, A.; Veiga, F.; Ferreira, D.; Neufeld, R. Oral bioavailability of insulin contained in polysaccharide nanoparticles. Biomacromolecules 2007;8:3054−60.

[19] Woitiski, C.; Neufeld, R.; Veiga, F.; Carvalho, R.; Figueiredo, I. Pharmacological effect of orally delivered insulin facilitated by multilayered stable nanoparticles. European Journal of Pharmaceutical Sciences 2010;41:556 − 63.

[20] Zhang, X.; Sun, M.; Zheng, A.; Cao, D.; Bi, Y.; Sun, J. Preparation and characterization of insulin−loaded bioadhesive PLGA nanoparticles for oral administration. European Journal of Pharmaceutical Sciences 2012;45:632−8.

[21] Li, X.; Qi, J.; Xie, Y.; Zhang, X.; Hu, S.; Xu, Y.; Lu, Y.; Wu, W. Nanoemulsions coated with alginate/chitosan as oral insulin delivery systems: Preparation, characterization, and hypoglycemic effect in rats. International Journal of Nanomedicine 2013;8:23−32.

[22] Gülden, E.; Wong, F. S.; Wen, L. The gut microbiota and type 1 diabetes. Clinical Immunology 2015;159:143−53.

[23] Hu, C.; Wong, F. S.; Wen, L. Type 1 diabetes and gut microbiota: Friend or foe? Pharmacological Research 2015;98:9−15.

[24] Wirth, R.; Bódi, N.; Maróti, G.; Bagyánszki, M.; Talapka, P.; Fekete, É.; Bagi, Z.; Kovács, K. L. Regionally distinct alterations in the composition of the gut microbiota in rats with streptozotocin−induced diabetes. PLoS ONE 2014;9:e110440.

[25] Larsen, N.; Vogensen, F. K.; van den Berg, F. W. J.; Nielsen, D. S.; Andreasen, A. S.; Pedersen, B. K.; Al−Soud, W. A.; Sørensen, S. J.; Hansen, L. H.; Jakobsen, M. Gut microbiota in human adults with type 2 diabetes differs from non−diabetic adults. PLoS ONE 2010;5:e9085.

[26] Zhang, Y.; Zhang, H. Microbiota associated with type 2 diabetes and its related complications. Food Science and Human Wellness 2013;2:167−72.

[27] Díaz−Silva, M.; Grasa, M. M.; López−Martí, J.; Fernández−López, J. A.; Remesar, X.; Alemany, M. Effect of oral oleoyl−estrone on the energy balance of diabetic rats. Hormone and Metabolic Research 2003;35:471−8.

[28] McMinn, L. H.; Hodges, G. M.; Carr, K. E. Gastrointestinal uptake and translocation of microparticles in the streptozotocin−diabetic rat. Journal of Anatomy 1996;189:553−9.

[29] Florence, A. T. Nanoparticle uptake by the oral route: Fulfilling its potential? Drug Discovery Today: Technologies 2005;2:75−81.

[30] Lopes, M. A.; Abrahim, B. A.; Cabral, L. M.; Rodrigues, C. R.; Seiça, R. M. F.; de Baptista Veiga, F. J.; Ribeiro, A. J. Intestinal absorption of insulin nanoparticles: Contribution of M cells. Nanomedicine: Nanotechnology, Biology and Medicine 2014;10:1139−51.

[31] Gaumet, M.; Gurny, R.; Delie, F. Localization and quantification of biodegradable particles in an intestinal cell model: The influence of particle size. European Journal of Pharmaceutical Sciences 2009;36:465−73.

[32] Liu, M.; Zhang, J.; Zhu, X.; Shan, W.; Li, L.; Zhong, J.; Zhang, Z.; Huang, Y. Efficient mucus permeation and tight junction opening by dissociable "mucus−inert" agent coated trimethyl chitosan nanoparticles for oral insulin delivery. Journal of Controlled Release 2016;222:67–77.

[33] Zauner, W.; Farrow, N. A.; Haines, A. M. R. *In vitro* uptake of polystyrene microspheres: Effect of particle size, cell line and cell density. Journal of Controlled Release 2001;71:39−51.

[34] Damge, C.; Reis, C. P.; Maincent, P. Nanoparticle strategies for the oral delivery of insulin. Expert Opinion on Drug Delivery 2008;5:45−68.

[35] Ma, Z. S.; Lim, T. M.; Lim, L. Y. Pharmacological activity of peroral chitosan−insulin nanoparticles in diabetic rats. International Journal of Pharmaceutics 2005;293:271−80.

[36] Florence, A. T. The oral absorption of micro− and nanoparticulates: Neither exceptional nor unusual. Pharmaceutical Research 1997;14:259−66.

[37] Movassat, J.; Bailbé, D.; Lubrano−Berthelier, C.; Picarel−Blanchot, F.; Bertin, E.; Mourot, J.; Portha, B. Follow−up of GK rats during prediabetes highlights increased insulin action and fat deposition despite low insulin secretion. American Journal of Physiology − Endocrinology and Metabolism 2008;294:E168−E75.

[38] Portha, B.; Lacraz, G.; Chavey, A.; Figeac, F.; Fradet, M.; Tourrel−Cuzin, C.; Homo−Delarche, F.; Giroix, M.−H.; Bailbé, D.; Gangnerau, M.−N.; Movassat, J. Islet structure

and function in the GK rat. In: Islam MS, editor. Islets of Langerhans, 2 ed: Springer Netherlands; 2014. p. 1−22.

[39] Buschard, K.; Thon, R. Diabetic animal models. In: Hau J, Hoosier GLV, editors. Handbook of Laboratory Animal Science. II. Second ed. USA: CRC Press; 2003. p. 172.

[40] Pang, K. S. Modeling of intestinal drug absorption: Roles of transporters and metabolic enzymes (for the gillette review series) Drug Metabolism and Disposition 2003;31:1507−19.

[41] Lopes, M.; Shrestha, N.; Correia, A.; Shahbazi, M.−A.; Sarmento, B.; Hirvonen, J.; Veiga, F.; Seiça, R.; Ribeiro, A.; Santos, H. A. Dual chitosan/albumin−coated alginate/dextran sulfate nanoparticles for enhanced oral delivery of insulin. Journal of Controlled Release 2016;232:29−41.

[42] Kimura, T.; Sudo, K.; Kanzaki, Y.; Miki, K.; Takeichi, Y.; Kurosaki, Y.; Nakayama, T. Drug absorption from large intestine: Physicochemical factors governing drug absorption. Biological and Pharmaceutical Bulletin 1994 17:327−33.

CHAPTER 6

DUAL CHITOSAN/ALBUMIN–COATED ALGINATE/DEXTRAN SULFATE NANOPARTICLES FOR ENHANCED ORAL DELIVERY OF INSULIN

6.1 ABSTRACT

The potential of NP to overcome the barriers for oral delivery of protein drugs have led to the development of platforms capable of improving their BA. However, despite the progresses in drug delivery technologies, the success of oral delivery of insulin remains elusive and the disclosure of insulin mechanisms of absorption remains to be clarified. To overcome multiple barriers faced by oral insulin and to enhance the insulin permeability across the intestinal epithelium, here insulin−loaded ADS−NP were formulated and dual−coated with CS and ALB. The nanosystem was characterized by its pH−sensitivity and mucoadhesivity, which enabled to prevent 70% of *in vitro* insulin release in simulated gastric conditions and allowed a sustained insulin release following the passage to simulated intestinal conditions. The pH and time−dependent morphology of the NP was correlated to the release and permeation profile of insulin. The dual CS/ALB coating of the ADS−NP demonstrated augmented intestinal interactions with the intestinal cells in comparision to the uncoated NP, resulting in a higher permeability of insulin across Caco−2/HT29−MTX/Raji B cell monolayers. The permeability of the insulin−loaded ALB−NP was reduced after the temperature was decreased and after co−incubation with chlorpromazine, suggesting an active insulin transport by CME. Moreover, the permeability inhibition with the pre−treatment with sodium chlorate suggested that the interaction between the glycocalix and the NP was critical for the insulin permeation. Overall, the developed nanosystem has clinical potential for the oral delivery of insulin and therapy of T1D.

6.2 INTRODUCTION

Diabetes is a group of metabolic and chronic disorders that results from the partial or absolute loss of insulin production and/or insulin resistance in target cells. The primary mode of treatment of T1D consists of exogenous insulin therapy, which is also required at a later stage in patients with T2D. To overcome the limitations of the current s.c. administration of insulin, oral delivery has emerged as the most desirable alternative route of administration because of its convenience and good patient compliance [1,2]. More importantly, the oral route is considered the most physiological, since it closely mimics the endogenous insulin pathway and provides better glucose homeostasis [3]. However, despite the efforts of researchers and the desire of the diabetic patients, there is still no product on the market for oral delivery of insulin. The oral BA of insulin is very poor, which is essentially due to enzymatic digestion of insulin in the GI tract and the low permeability through the epithelial cell layer in the intestine [4,5].

To date, different strategies have been used to improve the oral insulin absorption [6−10] and, among these strategies, NP may represent a closer approach to reach a successful oral insulin delivery nanosystem [10−12]. More precisely, biopolymer−based NP have been explored and gained a lot of consideration, given their established biocompatibility and biodegradability [13,14]. For example, alginate−based NP have been shown to successfully incorporate enzymes, drugs and proteins by entrapping or attaching them to the particles' matrix [15]. Previous studies revealed that the incorporation of an anionic copolymer, such as dextran sulfate, enhanced the loading of hydrophilic drugs in alginate matrices [16,17]. The vast exploration of CS−based NP over the last years has also demonstrated that this biopolymer plays an important role in the insulin oral BA [10]. CS, a mucoadhesive cationic biopolymer, is able to promote the mucus and cellular adhesion, increasing the residence time of the delivery systems at the site of absorption, thereby increasing the oral BA [10,18−20]. Moreover, CS is also known to increase the permeability of the drugs by transiently opening the cellular TJ present between the intestinal epithelial cells [21]. The application of ALB as an outermost coat to CS−based NP has revealed to act as a sacrificial target to avoid insulin degradation by preventing proteases from accessing insulin within the NP, and by stabilizing the NP either in the acidic [22−24] or intestinal environment [25]. ALB is a versatile protein carrier for drug delivery, characterized by its

non−immunogenic, nontoxic, biodegradable and biocompatible properties [26,27]. ALB−NP have gained considerable attention due to their high binding capacity to various drugs [26].

However, the behavior of biopolymers−based NP when in contact with the intestinal barrier and specific cellular and molecular interactions with the principal cells comprising this barrier (*e.g.*, enterocytes, the mucus−producing goblet and M cells) remains to be clarified. Different pathways have been hypothesized to be involved in the transport of either free and/or NP−associated insulin. These pathways include: (i) paracellular transport; (ii) transcytosis through enterocytes; (iii) receptor−mediated transcytosis; and the transcellular pathway used by the M cells in the PP [28]. Due to their high transcytotic capacity and ability to transport NP [29], the M cells offer a putative way for the oral delivery of nanoencapsulated peptides [30]. In the case of the transcellular pathway, the transport begins by an uptake that depends on the type of endocytosis involved: macropinocytosis, CME, caveolae−mediated endocytosis or caveolae− and clathrin− independent endocytosis [31]. Whether insulin uptake occurs through one or more pathway is still unknown, since the studies elucidating the absorption mechanisms of insulin do not make use of cell−based intestinal models that reproduce the enterocytes, and goblet and M cells simultaneously [28].

Therefore, the aim of this work was to evaluate the effectiveness of insulin−loaded biopolymeric−NP on the insulin permeability across intestinal epithelial cells. The independent effects of the CS and ALB coatings were evaluated through an extensive characterization of the NP with impact both on insulin release profiles in biological fluids and at the cellular level. Finally, a systematic evaluation of the cellular and molecular mechanisms used by the NP to transport insulin across the intestine was also performed.

6.3 MATERIALS AND METHODS

6.3.1 Materials and cell culturing

Human recombinant insulin (MW 5800 Da), low viscosity sodium alginate (viscosity of 1% solution at 25 ºC, 4–12 cps), dextran sulfate, sorbitan monooleate (Span® 80), low molecular weight CS, bovine serum ALB, paraffin oil, FITC, dimethylsulfoxide (DMSO), sodium azide, filipin complex from *Streptomyces filipinensis*,

2−(*N*−morpholino)−ethanesulfonic acid (MES), 1−ethyl−3−(3−(dimethylamino)−propyl)−carbodiimide (EDC), *N*−hydroxysuccinimide (NHS), 4−(2−hydroxyethyl)−1−piperazineethanesulfonic acid (HEPES) and glutaraldehyde were purchased from Sigma−Aldrich (USA). Calcium carbonate was obtained from Setacarb and poloxamer 188 (Lutrol® F68) from BASF (Germany). Sodium chlorate was purchased from Acros Organics (Spain). Protamine sulfate and chlorpromazine hydrochloride were obtained from Tokyo Chemical Industry (Japan). HBSS, PBS, Alexa−Fluor 488®, Versene and heat inactivated fetal bovine serum (FBS) were purchased from Life Technologies. Dulbecco's Modified Eagle's medium (DMEM), L−glutamine, non−essential amino acids (NEAA), penicillin (100 IU/mL) and streptomycin (100 mg/mL), EDTA and trypsin were purchased from HyClone.

Human colon adenocarcinoma Caco−2, lymphocytes Raji B and human gastric adenocarcinoma AGS cells were obtained from American Type Culture Collection. Goblet−like HT29−MTX cells were kindly provided by Dr. T. Lesuffleur (INSERM U178, Villejuif, France).

6.3.2 NP preparation

The ADS−NP were prepared by emulsification/internal gelation followed by polyelectrolyte complexation [32]. A schematic representation of the technique is shown in Figure 6.1. Briefly, the formation of the ADS matrix through emulsion dispersion was followed by triggered instantaneous particle gelation. The nonionic triblock copolymer poloxamer 188 (0.16%, w/v) was added to an aqueous solution of sodium alginate (0.02%, w/v) and dextran sulfate (0.0075%, w/v). After that, an aqueous suspension of ultrafine calcium carbonate (0.05%, w/v) was sonicated for 30 min at 50% to break−down crystal aggregates and dispersed at calcium/alginate mass ration of 1.0:0.3. The resultant dispersion was emulsified within paraffin oil (aqueous phase/oil phase 50/50, v/v) facilitated by another non−ionic surfactant, sorbitane monooleate (1.84%, v/v), by impeller−stirring homogenization (1600 rpm) and tip−sonication at 50%. After 15 min, gelation was induced by addition of paraffin oil containing glacial acetic acid (molar ratio acid−calcium, 3.5) to solubilize calcium dispersed in the the ADS droplets during 15 min, with continued stirring

and tip−sonication. The drug loading was performed by simultaneously dispersing an insulin solution (7 mg/mL in 0.01 M HCl) during the gelation process. The ADS−NP were recovered through an extraction procedure as described in Chapter 2 [32]. The ADS−NP were further washed by centrifugation at 6000 rpm for 10 min and dispersed in Milli−Q water by tip−sonication.

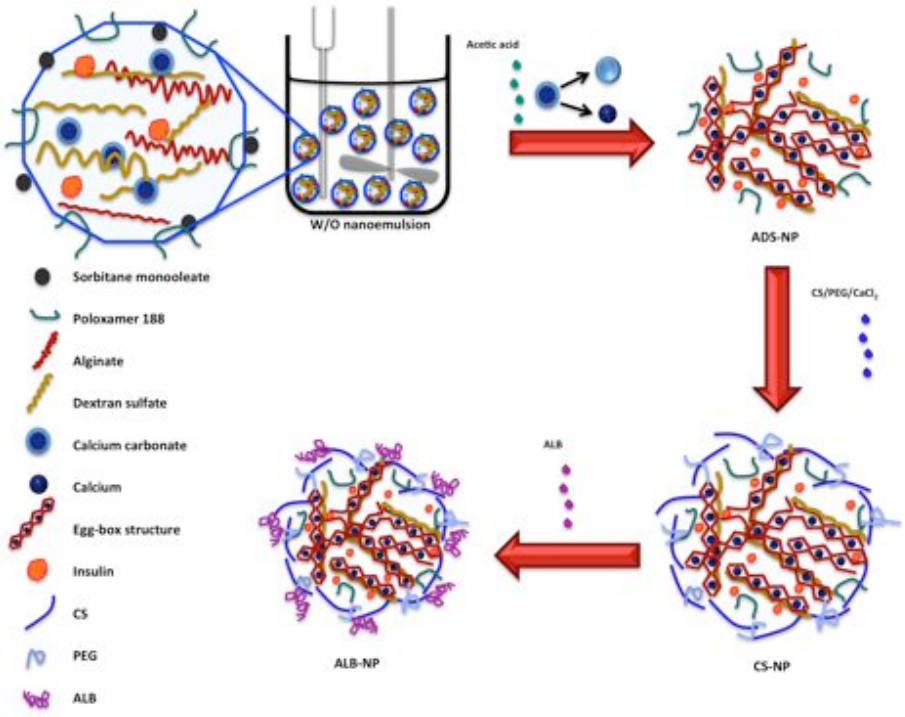

Figure 6.1. Schematic representation of the emulsification/internal gelation technique used to prepare the insulin−loaded ADS−NP. The formation of the egg−box structure (calcium/alginate gel) was induced by the pH decrease of the W/O nanoemulsion, which enabled the controlled release of calcium. The insulin entrapment in the NP' matrix was reinforced by the presence of dextran sulfate. The dual coating was applied by polyelectrolyte complexation by dropwise addition of CS and ALB, sequentially.

6.3.3 NP coating

CS solution (0.3%, w/v) was prepared by dissolving CS in Milli−Q water containing 0.5% (v/v) acetic acid overnight under magnetic stirring, followed by the addition of PEG (0.15%, w/v) and $CaCl_2$ (1.5%, w/v) with pH adjustments to 4.6, followed by filtration through a paper filter Millipore #4. The CS−NP were obtained after dropwise addition of CS/PEG/$CaCl_2$ solution to the ADS−NP diluted (1:4) with Milli−Q water (CS/alginate mass ration of 1:0.07) under magnetic stirring.

Finally, the CS−NP were coated by dropwise addition of 1.0% (w/v) ALB solution at pH 5.1 (ALB/CS mass ration of 1:0.2) under magnetic stirring. The supernatant containing unbound polymer was separated through the NP concentration to 4 mg/mL by centrifugation in filters with a membrane pore size of 100 kDa (Amicon Ultra; Merck Millipore Ltd.). Afterwards, the CS− and ALB−NP were homogenized by tip−sonication for 30 s.

6.3.4 NP characterization

After production, the NP were characterized for their average particle size (*Z*−average), PdI, and average ζ−potential, using a Malvern Zetasizer Nano ZS instrument (Malvern Instruments Ltd, UK). For these measurements, samples were diluted in Milli−Q water at a concentration of 0.4 mg/mL.

The morphology of the NP was studied by transmission electron microscopy (TEM) (Jeol JEM−1400, Jeol Ltd., Japan) using an acceleration voltage of 120 kV. For sample preparation, the NP were dispersed in Milli−Q water and dropped on a carbon coated copper TEM grid before air−drying at room temperature overnight. To assess the pH−dependent morphology of the NP over time, the NP were dispersed in HBSS−MES (pH 5.5) or HBSS−HEPES (pH 7.4) buffers and stirred at 100 rpm for 30 min and 3 h, before preparing the samples for TEM analysis.

6.3.5 EE and LC of insulin

To determine the EE and LC of the prepared NP, the amount of insulin associated to the NP was calculated. This calculation was made according to the follow Equations 1 and 2:

$$EE\ (\%) = \frac{Amount\ of\ insulin\ loaded\ in\ the\ NP}{Total\ amount\ of\ insulin} \times 100 \quad (1)$$

$$LD\ (\%) = \frac{Amount\ of\ insulin\ loaded\ in\ the\ NP}{Total\ amount\ of\ NP} \times 100 \quad (2)$$

Insulin was extracted from the NP through dissolution in PBS at pH 7.4 during 3 h. After the NP dissolution, the medium was centrifuged and the mass of insulin in the supernatant was measured, corresponding to the EE. The LC was calculated based on the dried mass of the NP obtained after lyophilization (HETO LyoPro 3000, Heto/Holten A&S, Denmark).

6.3.6 HPLC quantification

Insulin was quantified by HPLC (Agilent 1260, Agilent Technologies, USA) with a C18 column (4.6 × 150 mm, 5 µm, Supelco Discovery®, USA). The mobile phase consisted of ACN and 0.1% TFA. The flow was initially set at the ratio of 30:70 (ACN: 0.1% TFA, v/v), and linearly changed to 40:60 (v/v) gradient over 5 min. The flow rate was 1.0 mL/min and the injected volume of the sample was 75 µL. The column temperature and detection wavelength were set at room temperature and 214 nm, respectively. The total area under the peak was used to quantify insulin.

6.3.7 *In vitro* release tests

The *in vitro* release studies of insulin were conducted from 10 mg of the NP in dialysis diffusion bags (Spectra/Por®, Biotech CE, MWCO 100,000, Spectrum Laboratories Inc., USA). The release of insulin was measured by immersing the dialysis diffusion bag in 50

mL of SGF (USP 34) at pH 1.2. After 2 h, the medium was replaced by SIF (USP 34) at different pH−values (pH 5.5 and pH 7.4). Aliquots of 100 µL were collected at specific time points during the dissolution experiments and the withdrawn volume was replaced with fresh pre−heated buffer, keeping the volume constant. The collected aliquots were analyzed by HPLC in order to quantify the insulin released from the NP over time. The nonencapsulated insulin release profile was used as control. All the tests were performed at 37 °C and 100 rpm under sink conditions.

6.3.8 Fluorescent labeling of the NP

The covalent labeling of Alexa Fluor® 488 (Life Technologies, USA) to alginate was performed in MES buffer (pH 5.2) using the EDC/NHS coupling chemistry. Briefly, 1 mg of the ADS−NP were dispersed in 1 mL of 10 mM MES buffer solution containing EDC and NHS (final concentrations 30 mM) and mixed for 2 h at room temperature in the dark to activate the carboxylic groups on the alginate. After sonication for 30 s, Alexa Fluor® 488 was added at a ratio of 200:1 of the NP to dye, and allowed to stir overnight at 200 rpm. Afterwards, the Alexa Fluor® 488−labelled NP were washed twice with Milli−Q water.

A solution of FITC (0.2%, w/v) dissolved in DMSO was added dropwise to 70 mg of insulin dissolved in 35 mL of 0.1 M Na_2CO_3 and mixed for 8 h at 4 °C in the dark. After that, NH_4Cl was added to a final concentration of 50 mM and incubated for another 2 h at 4 °C to stop the coupling reaction. The FITC−insulin was then dialyzed by using a membrane with 8−10 kDa for 72 h at 4 °C in the dark. Afterwards, the FITC−insulin was lyophilized for 24 h.

6.3.9 Cell culturing

Human gastric adenocarcinoma AGS (passages #10–15), human colon adenocarcinoma Caco−2 (passages #31–39), goblet−like HT29−MTX (passages #30–39) and lymphocytes Raji B cells (passages #26–35) were grown separately in culture flasks in a complete medium consisting of DMEM supplemented with 10% (v/v) FBS, 1% (v/v) L−glutamine, 1% (v/v) NEAA, and 1% (v/v) antibioticeantimitotic mixture (final concentration

of 100 IU/mL penicillin and 100 IU/mL streptomycin). The cell cultures were kept in a standard incubator (16 BB gas, Heraeus Instruments GmbH, Germany) at 37 °C in an atmosphere of 5% CO_2 and 95% relative humidity.

6.3.10 Cell viability studies

The cell viability experiments were performed on AGS, Caco−2 and HT29−MTX cells. The cells were seeded separately at concentrations of 1×10^5 cells/mL into 96−well plates (Corning Inc., USA). The cells were allowed to attach to the wells for 24 h. The medium was then removed and the cells were washed twice using fresh HBSS−HEPES buffer (pH 7.4). Afterwards, 100 µL of the NP were added to the cells at different concentrations (1, 0.5, 0.25 and 0.1 mg/mL) and incubated for a period of 3 h for the AGS cells, and for 6 h for the Caco−2 and HT29−MTX at 37 °C. After incubation, the cells were washed twice with fresh HBSS−HEPES buffer. Next, 50 µL of fresh HBSS−HEPES and 50 µL of CellTiter−Glo® reagent assay (Promega Corporation, USA) were added to the wells as described elsewhere [33]. A positive (1% Triton X−100) and negative control (HBSS−HEPES buffer solution) were also prepared and treated similarly to the sample wells. The luminescence was measured using a Varioskan Flash Multimode Reader (Thermo Fisher Scientific, USA).

6.3.11 Cell−NP interactions

To verify the interactions between the cells and the NP, Caco−2:HT29−MTX co−cultures in the proportion of 90:10 were seeded in Lab−Tek 8−chamber slides (Thermo Fisher Scientific Inc., USA) and allowed to attach for 24 h. Afterwards, the cells were washed twice with fresh pre−heated HBSS−MES buffer (pH 5.5). Then, 200 µL of the Alexa Fluor® 488−loaded NP (0.5 mg/mL) were added to the cells and incubated at 37 °C for 3 h. After incubation, the cells were washed twice with fresh pre−heated HBSS−MES buffer. Then, the plasma membrane was stained by adding 200 µL of CellMask™ DeepRed (Invitrogen, USA) and incubated for 3 min at 37 °C. The excess of staining solution was washed twice with fresh HBSS−MES buffer and the cells were fixed using 2.5% glutaraldehyde for 20 min at

room temperature. The intercellular localization of the Alexa 488®–loaded NP was then observed using a Leica SP5 confocal microscope (Leica Microsystems, Germany).

6.3.12 Cellular association analyses by flow cytometry

Caco–2:HT29–MTX co–cultures were seeded in 6–well plates at a density of 7×10^5 cells/mL in a ratio of 90:10 and allowed to attach for 48 h at 37 °C. The cells were then washed with HBSS–MES (pH 5.5) and incubated with the Alexa Fluor®–labeled NP (0.5 mg/mL) for 3 h. Afterwards, the cells were washed three times with HBSS–MES buffer to remove the NP not associated with the cells and detached by incubating with 0.5 mL of Versene for 15 min. Then, the cells were centrifuged and the supernatant removed and re–suspended in 700 µL of basic sorting buffer that consists in 1 × PBS (Ca/Mg^{2+} free) with 5 mM of EDTA and 25 mM of MES, to avoid the cells aggregation and analyzed right after using a Beckman Coulter Galios™ Flow Cytometer with a laser excitation wavelength of 488 nm. The results were analysed using the software Kaluza Analysis Version 1.3. About 10,000 events were obtained for each sample. Data were analyzed and plotted using Weasel software.

6.3.13 Preparation of the triple co–culture cell monolayers

To prepare the triple co–culture intestinal cellular monolayer, 1.5×10^5 cells/mL of Caco–2 and HT29–MTX cells in a ratio of 90:10 were seeded in 12–Transwell® cell culture inserts and were allowed to grow and differentiate for 14 days with medium replacement every other day. Then, 1.0×10^5 Raji B cells were added to the basolateral chamber for 7 days more, in order to induce the phenotype change of the Caco–2 cells into M cells and to obtain a triple co–culture model [34].

6.3.14 Intestinal permeability experiments

The permeability experiments across the cell monolayers were performed from the apical (0.5 mL) to basolateral direction (1.5 mL) in HBSS–HEPES (pH 7.4) or HBSS–MES (pH 5.5) at 37 °C using an orbital shaker (100 rpm). After removing the cell culture medium, 0.5 mL of the nonencapsulated insulin or insulin–loaded NP at the concentration of 0.5 mg/mL were pipetted into the apical side of the inserts. At different time points (15, 30, 60, 120 and 180 min), 100 µL samples were taken from the basolateral side of the inserts and the same volume of fresh HBSS–HEPES (pH 7.4) or HBSS–MES (pH 5.5) buffer was added to retain a constant volume of the medium. The amounts of insulin permeated across the cell monolayers were determined by a Human Insulin Elisa Kit (Mercodia, Sweden), according to the manufacturer's instructions. The cumulative amounts of insulin transported across the monolayers were calculated from the concentrations measured in the basolateral compartment. The P_{app} was calculated as described elsewhere [25].

6.3.15 Morphological characterization of the co–culture monolayers

After the permeability studies in HBSS–HEPES at pH 7.4, the NP suspension was carefully removed and the cells were fixed with 2.5% glutaraldehyde for 20 min at room temperature. The wells were then washed twice with sodium cacodylate buffer (NaCac) for 3 min. Afterwards, the cells were post–fixed with 1% osmium tetroxide in 0.1 M NaCac buffer (pH 7.4) and then dehydrated and embedded in epoxy resin. Ultrathin sections (60 nm) were cut perpendicular to the insert, post–stained with uranyl acetate and examined with TEM using an acceleration voltage of 120 kV.

6.3.16 Cellular uptake studies

The cellular uptake studies were performed using the same experimental setup as for the intestinal permeability studies. However, the NP were loaded with FITC–insulin. The FITC–insulin–loaded NP were added in the exact same conditions as for the permeability

studies with incubation at 37 °C for 3 h with shaking at 100 rpm. The cells were lysed using a cell lysing buffer after incubation. The lysate was then centrifuged at 4000*g* for 5 min to remove the supernatant. Finally, the supernatant was analyzed for fluorescence ($\lambda_{excitation}$ = 490 nm and $\lambda_{emission}$ = 520 nm) using a Varioskan Flash multimode Reader (Thermo Fisher Scientific, USA) to measure the amount of insulin present bound or within the mucus layer or cell monolayers.

6.3.17 Assessment of transport pathways

To identify the possible transport mechanism of the insulin−loaded NP by the intestinal cells, the monolayers were prepared using the same experimental setup as for the intestinal permeability studies. The permeability of insulin across the cell monolayers was performed by incubating cells in different conditions or treating them with specific agents [11]: (i) to study the effect of temperature on the insulin permeability, the cells were incubated with NP at 4 °C for 3 h; (ii) to test the effect of sodium azide, an active transport inhibitor, 100 mM sodium azide was dissolved in the NP suspension and incubated with cells for 3 h at 37 °C; (iii) to study the effect of protamine treatment, an adsorptive−mediated endocytosis inhibitor, 1 mM protamine sulfate was dissolved in the NP suspension and incubated with cells for 3 h at 37 °C; (iv) to investigate the effect of desulfurization, the cells were pre−incubated with 35 mM sodium chlorate in the cell culture medium for 48 h, rinsed twice with HBSS−HEPES (pH 7.4) buffer and incubated with the NP suspension for 3 h at 37 °C [35]; and (v, vi) to examine the effects of chlorpromazine and filipin, which are clathrin and caveolae endocytosis inhibitors, respectively, the cells were incubated with 10 mg/mL of chlorpromazine or 1 mg/mL of filipin dissolved in the NP suspension and treated for 3 h at 37 °C [36]. In addition, the control samples were conducted at 37 °C for 3 h without any treatment and the cumulative amounts of insulin transported across the monolayers were calculated from the concentrations measured in the basolateral compartment.

6.3.18 Statistical analysis

Measured values are represented as mean ± s.d. of at least three independent

experiments. One−way ANOVA with Bonferroni post hoc−test (SPSS 20.0, USA) was used to analyze the data. The level of significance was set at probabilities of $^{*}p < 0.05$, $^{**}p < 0.01$, and $^{***}p < 0.001$.

6.4 RESULTS AND DISCUSSION

6.4.1 NP characterization

The characteristics of the designed NP based on the mean size, PdI, ζ−potential, EE and LC are represented in Table 6.1. All the types of NP presented average sizes of ca. 300 nm, with PdI values ≤ 0.30. NP with reduced size are known to establish improved contact with the intestinal cells than do bigger particles, facilitating the permeation via different mechanisms [37]. Furthermore, since the NP immobilized by the mucus can be cleared from the mucosal tissue, their size must be less than 500 nm [38] to avoid significant steric inhibition by the fiber mesh and adhesion to mucin fibers [39]. The decrease of the NP size was also correlated with an increase of the cohesive energy of the NP and, therefore, their stability [40]. Further TEM visualization of the NP provided more detailed information on the size distribution and also on the morphological surface properties of the NP. The TEM images shown in Figure 6.2 support the results in terms of mean size. Our ADS−NP presented irregular shapes and no apparent structural changes were detected after their coating with CS.

On one hand, the coverage of CS onto the ADS−NP (CS−NP) surface is derived from the electrostatic interactions between the negatively carboxylic groups (COO^{-}) of alginate and the sulfate groups (SO_4^{2-}) of dextran sulfate with the protonated amine groups (NH_3^{+}) of CS, leading to the formation of a less delineated shape of the NP (Figure 6.2B) and an increase in the mean size ($p < 0.05$). On the other hand, the helical structure of ALB has been described to be responsible for the increase packing of the NP' membrane and polymeric matrix [24]. Our results are in accordance with those reports, which can be seen by the decrease in the NP size after the ALB coating (ALB−NP) ($p < 0.05$), as well as by the more compacted structure observed in Figure 6.2C. The effect of ALB on the NP size may be related to changes in the electrical state, in which the increase or decrease of the electrical repulsions lead the particles to swell or shrink, respectively [22,41]. Their size presented the

smaller PdI value (0.17) suggesting the stability of the system in terms of size distribution, given its higher homogeneity. These results are in very good accordance with a previous study [22], where ALB provided electrostatic stabilization to the NP.

Table 6.1. Size, PdI, ζ−potential, EE and LC of insulin of the ADS−, CS− and ALB−NP. Results are presented as mean ± s.d. ($n \geq 3$). The values of the CS− and ALB−NP were compared to the ADS−NP ($^{*}p < 0.05$, $^{**}p < 0.01$, and $^{***}p < 0.001$).

NP	Size (nm)	PdI	ζ−potential (mv)	EE (%)	LC (%)
ADS	313.2 ± 2.8	0.30	−30.6 ± 0.8	72.4 ± 3.3	10.1 ± 2.8
CS	338.8 ± 5.8*	0.25	+53.9 ± 1.2***	21.9 ± 2.8*	4.8 ± 0.4*
ALB	300.8 ± 3.8*	0.17	+28.9 ± 0.9***	30.7 ± 3.4*	6.2 ± 1.4

Regarding the surface charge, the ADS−NP were negatively charged (−30.6 ± 0.8 mV) as expected by the nature of the polymers used. The negatively charged mucus layer on the intestinal epithelium would lead to electrostatic repulsion of the NP that are also negatively charged preventing them to get closer and to interact with intestinal cells [42]. Therefore, CS was used as a strategy to improve the interaction of these NP with the intestinal epithelium. CS is a positively charged mucoadhesive polymer, known to increase the contact time of the NP with the intestinal layer, which may lead to a wide absorptive surface and subsequently enhanced drug absorption [28]. Moreover, CS is an efficient intestinal absorption enhancer, able to transiently open the TJ between the epithelial cells [43]. Further CS coating of the NP was successfully confirmed by the drastic increment of the ζ−potential from −30.6 to +53.9 mV ($p < 0.001$), and also by a slight increase of the NP size by ca. 25 nm ($p < 0.05$). The ALB−NP had a ζ−potential value lower than the CS−NP (−28.9 mV; $p < 0.001$), given the negative charge of ALB at pH 5.1.

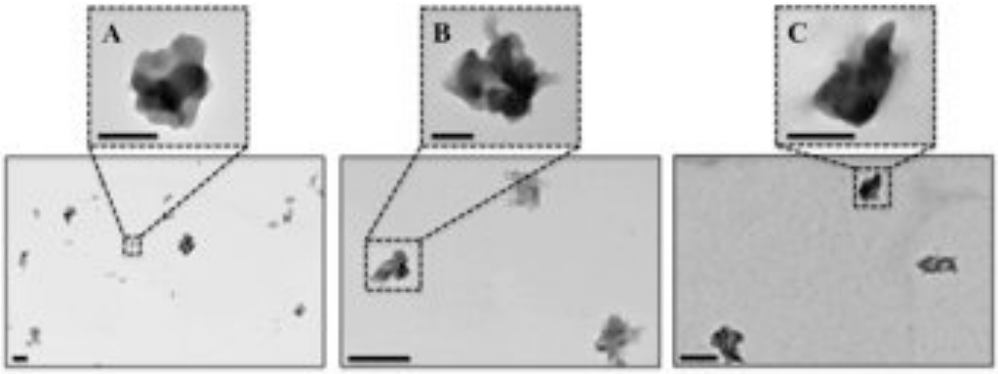

Figure 6.2. TEM images of the (A) ADS−, (B) CS−, and (C) ALB−NP. Scale bars = 500 nm. Scale bars in inset = 200 nm.

6.4.2 EE and LC of insulin

The ADS−NP showed the highest EE with 72.4 ± 3.3% of the initial protein encapsulated inside the NP (Table 6.1). The encapsulation of insulin inside the NP can be attributed to the electrostatic interactions among the NP' components at pH ~ 5. Insulin has an pI around 5.3 [44], alginate has pK_a values of 3.38 and 3.65 for mannuronic (M) and guluronic (G) residues [45], respectively, and dextran sulfate has a negative first pK_a value and a second pK_a value near 2 [46]. Therefore, strong electrostatic attractions between the positively charged protein and the negatively charged polymers may occur. Furthermore, calcium ions interact with the G residues and can establish ionic bridges with the negatively charged carboxylic residues of insulin, strengthening the association between insulin and alginate [47]. The addition of poloxamer 188 can also contribute to the insulin EE due to the steric stabilization by molecules of poloxamer [22].

After the coating, the CS− and ALB−NP had EE values of 21.9 ± 2.8 and 30.7 ± 3.4%, respectively. The reduction in the EE for both the CS− and ALB−NP may be due to an additional step of mixing of the NP with the CS, which could have led to some premature release of the drug [18]. Moreover, the protonated amine groups of both insulin and CS may compete together to the negatively charged groups of alginate and dextran sulfate, making the ADS network weaker and leading to some insulin loss. When ALB was added to the

nanosystem, ca. 10% more of insulin was retained inside the ALB−NP when compared to the CS−NP. We hypothesize that the difference in the electrostatic interactions that occurred between the ALB and CS may attenuate the competition between insulin and CS for the same groups of the ADS matrix. The ADS−NP also presented the highest LC of 10.1 ± 2.8%, compared to 4.8 ± 0.4 and 6.2 ± 1.4% for the CS− and ALB−NP, respectively. The LC results are in accordance with the EE values, since the CS coating decreased the amount of insulin encapsulated inside the NP, which was slightly improved after the ALB coating. Higher LC of insulin are preferable, because even for degradable particles, the use of unreasonably high quantities of the carrier can lead to toxicity problems of the carrier [48].

6.4.3 pH−dependent morphology of the NP

These multilayered biopolymer−based NP have the capacity to respond to pH variations in a remarkable way. The synergistic effect described between alginate and CS, together with the protective and stabilizing effect offered by ALB, are the reasons for the morphological differences observed in Figure 6.3. Alginate is a polymer characterized by its rapid dissolution at high pH, due to the dissociation of the carboxylic groups [49]. When in contact with the buffer at pH 5.5 during 30 min, the ADS−NP adopted a spherical−like shape, which may be related to an initial stabilizing effect of the ionic external medium. However, after 3 h of incubation, the morphology of the ADS−NP was similar to the ones observed with the NP in water (Figure 6.2A), showing that the ADS−NP were stable at pH 5.5. Furthermore, a rapid dissolution was observed when the ADS−NP were in contact with the buffer at pH 7.4. After 30 min of incubation, intact NP could still be observed simultaneously with the dissolved matrix, but after 3 h of incubation, the NP showed almost totally compromised structures.

The insoluble nature of CS at high pH−values is responsible for the different shapes observed for the CS−NP. After 3 h of incubation at pH 5.5, an obvious difference could be identified between the shapes of the ADS− and CS−NP. The CS−NP showed a tendency for aggregation with a combination of elongated and spherical−shaped NP. By increasing the pH to 7.4, the CS−NP adopted a round−shape and the fast dissolution of the ADS−NP was prevented by the presence of CS.

After 30 min of incubation, the ALB–NP reached an ionic equilibrium with the external medium and after 3 h of incubation their network changed, which can be explained by the dissolution of alginate and insolubilization of CS, partially disrupting the matrix of the NP. Moreover, the helical structure of ALB might have induced the packaging of the NP' polymeric matrix [24]. This tightly packed structure is explained by the strong interaction between the negatively charged ALB with the positively charged CS, which resulted in the major decrease in the NP size observed after 3 h of incubation. We hypothesize that the decrease of the ALB–NP size at pH 7.4 is also related to the complete dissolution of the alginate chains that were more exposed in the NP' structure leading to a readjustment of the NP' structure and generating smaller NP.

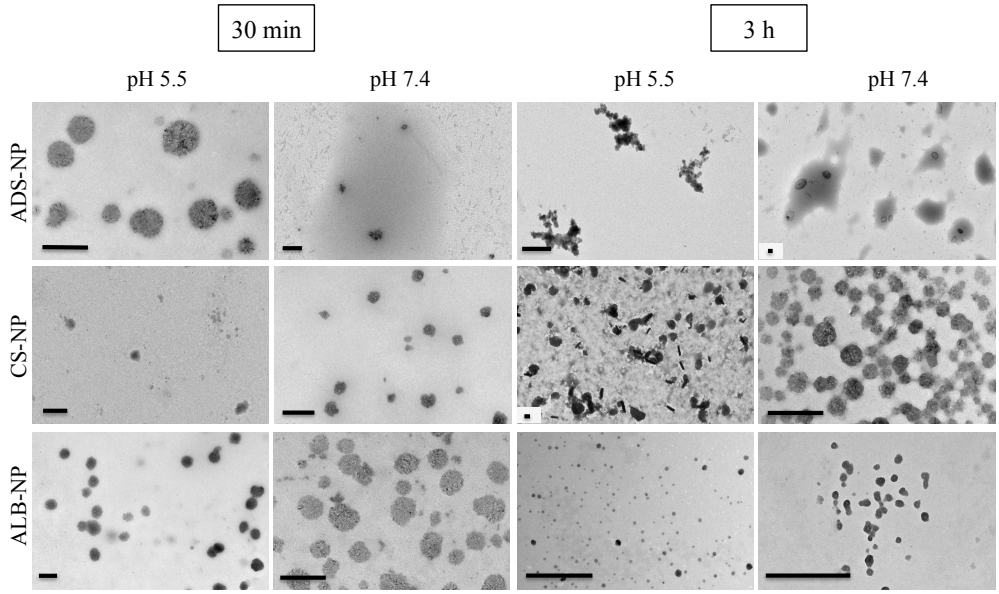

Figure 6.3. The pH–dependent morphology of the ADS–, CS– and ALB–NP after incubation in HBSS–MES (pH 5.5) and HBSS–HEPES (pH 7.4) for 30 min and 3 h. Scale bars = 200 nm.

6.4.4 *In vitro* release tests

Next, the capacity of the NP to control the insulin release in response to changes in the pH was evaluated. To predict the release profiles in conditions similar to the GI tract (stomach and intestine), the NP were firstly added to SGF at pH 1.2, which mimics the gastric environment. After 2 h, the release medium was changed to SIF, which simulates the transit to the intestinal environment. The pH of the GI tract increases gradually from gastric pH (1.2–2.5) to pH 5.0–6.0 in the small intestine [50,51] and to 6.8 and 7.2 in the proximal and distal colonic regions, respectively [52]. Therefore, different pH−values were used (pH 5.5 and 7.4) to increase the *in vitro*/*in vivo* correlation of the study. The release profiles of insulin from the NP are shown in Figure 6.4.

The NP released up to 35% of insulin at pH 1.2 for 2 h. At such low pH, the charge of insulin (pI = 5.3) is highly positive, and thus, the interactions with alginate and dextran sulfate prevented the insulin release. Acidic environments are responsible for the protonation of the carboxyl groups of alginate, and the chains tend to aggregate. Moreover, calcium forms ionic cross−links between the alginate polymer chains resulting in a sol−gel transition [53]. This might form a stable barrier to retain insulin and limit its release from the NP [22]. In comparison to the capacity of the NP to retain insulin in the gastric conditions, a much higher release rate (almost 80%) was observed for nonencapsulated insulin due to the high solubility of insulin at this low pH.

The increase in pH in the intestinal medium triggered the insulin release from the CS− and ALB−NP. The release of insulin from the ADS−NP was only noticed as the pH−value was increased from 5.5 to 7.4. The mechanism of the insulin release in these conditions is probably due to the dissolution of the alginate nucleus as a result of calcium loss, and also due to the electrostatic repulsion between alginate and insulin, which are both negatively charged at neutral pH [54,55]. Ionically cross−linked alginate gels are rapidly destabilized by the release of the calcium ions crosslinking the gel into the surrounding media due to exchange reactions with monovalent cations present in the medium such as sodium ions [56]. The increase in pH allows this reaction to occur when the ratio of sodium to calcium ions becomes 30 or above [57]. Therefore, considering that the main ion in the intestinal fluids is sodium, the dissolution of alginate would also occur in physiologic conditions [58]. Therefore, the amount of insulin retained within the NP at pH 5.5 may be tightly bound to

the alginate nucleus, which is corroborated by the preserved structure of the ADS−NP after 3 h at pH 5.5, as observed in the TEM images in Figure 6.3. Contrarily, at pH 7.4 these NP were almost completely dissolved, although a more extensive dissolution for a longer period may be required for additional release [22].

The insulin release from the CS− and ALB−NP at pH 7.4 was more sustained than at pH 5.5, where burst−type release profiles were observed. At pH 7.4, the solubility of CS becomes compromised (pKa = 6.5), and this insolubility may be responsible for the prevention of the NP' structure disruption, retaining insulin for a longer period of time. In contrast, a complete release of insulin from the CS−NP at pH 5.5 was achieved after 2 h. Insulin was probably released from the CS−NP by diffusion [59,60]. However, this fast release was also responsible for the consequent precipitation of insulin over the next 3 h. Nonencapsulated insulin also precipitated upon the passage from pH 1.2 to pH 5.5. Insulin contains several functional groups with different charges and with different acid or basic behaviors depending on the pH−conditions. At pH 5.5 (approximately the insulin pI), the net charge of the amino acids is balanced leading to a formally uncharged molecule, more non−polar and with remarkably decreased solubility [61]. Contrarily to all the types of formulations and also to the nonencapsulated insulin, the ALB−NP greatly improved the release of insulin up to ca. 100% at pH 5.5 after 2 h and prevented the insulin precipitation (ca. 80% was maintained in solution) during the following 3 h. The ALB coating effect was essential to release insulin and prevent its precipitation at pH 5.5, playing an important role on the insulin protection and particle stabilization [46]. As previously observed in Figure 6.3, the ALB−NP became smaller over the time when in contact with both buffers (pH 5.5 and 7.4), which may explain the higher release rate of insulin from these NP. These findings are in very good agreement with a previous report in the literature that showed that the increase in the surface area−to−volume ratio of the NP with decreasing size is responsible for the highest release rates of the encapsulated drug [62]. The study was conducted separately at pH 5.5 and 7.4 to have a clear understanding about the release profile in both pHs. If the particles subjected to pH 5.5 were placed sequentially in pH 7.4, only the ADS−NP would reveal additional information, since the CS− and ALB−NP released 100% of insulin after 2 h in pH 5.5 and no release would be observed when introduced to pH 7.4.

The release experiments confirmed the potential of the ALB−NP to significantly increase the dissolution rate of insulin at pH 5.5 and release the protein in a sustained

manner at pH 7.4, while protecting the drug inside the nanostructure at pH 1.2. Such results indicate that when given orally, minimal amounts of insulin would be released from the NP in the stomach, while the remaining portion could achieve a complete and sustained release in the intestine following 4 h of administration.

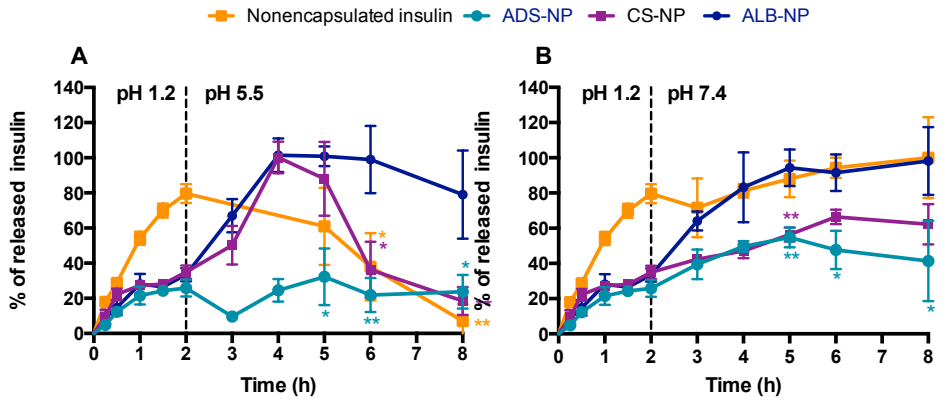

Figure 6.4. *In vitro* cumulative release profiles of insulin from the ADS−, CS− and ALB−NP at pH 1.2 for 2 h followed by (A) pH 5.5 and (B) pH 7.4 for 6 h. All the experiments were performed at 37 °C and 100 rpm. Data sets from 5 h onwards were compared to nonencapsulated insulin. The level of significance was set at probabilities of $^{*}p < 0.05$, $^{**}p < 0.01$, and $^{***}p < 0.001$. Error bars represent mean ± s.d. ($n = 3$).

6.4.5 Cell viability studies

As a result of the promising pH−triggered release of insulin in GI conditions, the *in vitro* safety and cytocompatibility of the NP were analyzed in AGS, Caco−2 and HT29−MTX cells. The cell lines were selected due to their importance as suitable models mimicking the different cell−types of the GI tract (*e.g.*, stomach, enterocytes and mucus secreting cells) and, therefore, relevant in the oral route of administration. Although the Raji B cells were included in the following studies, these cells are in suspension and are used to induce M−phenotype of the Caco−2 cells and are never in contact with the particles. Therefore, viability studies were not performed with this type of cells. The *in vitro* viability of the cells

was analyzed by exposing them to the NP at different concentrations (0.1, 0.25, 0.5, and 1 mg/mL) for different incubation times (3 h for the AGS cells, and 6 h for the Caco−2 and HT29−MTX cells), as shown in Figure 6.5. The rationale for using different concentrations of NP was to understand if there was any concentration dependent toxicity and to evaluate the lowest concentration of the NP that can be safely administrated for a future *in vivo* setup. Although the natural cellular and chemical complexity of co−cultures makes them more realistic models of human physiology, previous reports have demonstrated that the mucus layer acts as a mechanical barrier reducing the interaction of particles with the cellular co−cultures of Caco−2/HT29−MTX and subsequently leading to minor toxicity, when compared to Caco−2 cells alone [63]. Furthermore, while the Caco−2 cells viability was strongly affected by the presence of biorelevant media (fed state SIF), no toxic effect was detected for the co−culture of Caco−2/HT29−MTX in terms of viability and lactate dehydrogenase release [64]. Therefore, the viability was performed in individual cells to analyze the interaction between each cell type with the NP and understand the cause of possible toxic effects.

For the AGS cells, the non−related toxicity values with regards to the NP concentration can be observed in Figure 6.5A. Except for the highest concentration, the ADS−NP showed cell viabilities higher than 90%. The CS−NP showed elevated cytotoxicity with the two highest concentrations, which was reversed after the ALB coating. For the Caco−2 cells, it can be observed that all the NP at all concentrations, except the highest concentration of the CS−NP, showed cell viability values higher than 75% after 6 h of exposure. The more satisfactory results were obtained for the HT29−MTX cells, in which no toxicity effects were detected, independently of the type and concentration of NP tested. These results are in agreement with other reports in the literature showing that the presence of the mucus layer on top of the HT29−MTX cells prevents the strong interaction between the cells and the NP, thereby minimizing any cell damage [10,18]. In contrast, the absence of such mucus layer in the Caco−2 cells increases the probability of cytotoxicity. The absence of cytotoxicity of the ADS−NP in both intestinal cells and in the majority of the tested concentrations in the AGS cells is hypothetically attributed to the surface negative charge of the NP, which result in low cellular interaction and reduced cytotoxicity. Moreover, the biocompatibility properties of alginate and dextran sulfate are well described in the literature [22,65]. On the opposite side, the CS− and ALB−NP are extremely positively

charged and, therefore, are internalized/associated to a greater extent than the negatively charged ones, which may lead to increased toxicity levels [66,67]. The ALB−NP also demonstrated less toxicity effect than the CS−NP, corroborating the NP charge influence on the cellular viability, since the ALB−NP are less positively charged. The relatively low cytotoxicity of these NP could be ascribed to the presence of biocompatible (and biodegradable) polymers on their surface [65,68]. Furthermore, the hydrophilic nature of the NP is responsible for weak interactions with the cells' membranes, thus increasing the cytocompatibility of the NP [69,70].

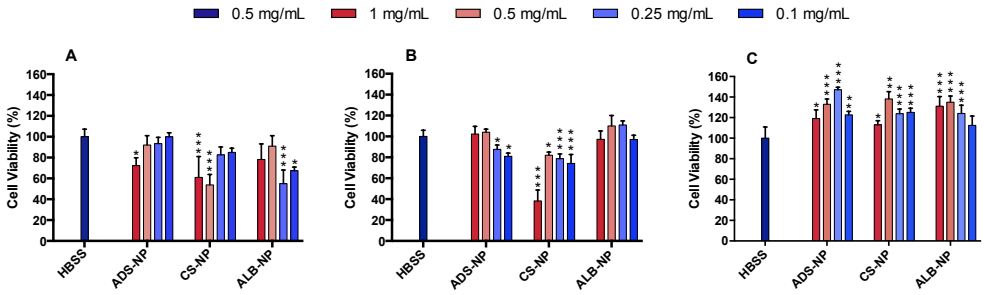

Figure 6.5. Cell viability of the intestinal cells exposed to the ADS−, CS− and ALB−NP, assessed by the CellTiter−Glo® luminescence assay. The ATP−content of AGS (A), Caco−2 (B) and HT29−MTX (C) cells after 3 (A) and 6 h (B and C) incubation with different NP concentrations at 37 °C was investigated. All data sets were compared to the negative control HBSS−HEPES buffer. The level of significance was set at probabilities of $^{*}p < 0.05$, $^{**}p < 0.01$, and $^{***}p < 0.001$. Error bars represent mean ± s.d. ($n \geq 3$).

6.4.6 Interaction of the NP with Caco−2:HT29−MTX co−culture cells

Caco−2 and HT29−MTX cells represent enterocytes and goblet cells, respectively, which comprise the two most abundant cells in the intestinal epithelia. Therefore, in order to demonstrate the potential of the prepared NP to interact with intestinal cells, Caco−2/HT29−MTX co−culture in a 90:10 proportion was used as a reliable model to predict the *in vivo* performance of the developed NP [34]. As can be seen in Figure 6.6, the confocal

fluorescence microscope images showed no interactions between the cells and the ADS−NP. Regarding the CS− and ALB−NP, it was observed that even after multiple washes, the NP were still present in contact with the cells. The yellow color that resulted from the overlap of the green and red labeling channels in the merged pictures revealed a very close contact with the NP co−localized with the cell membranes. The CS− and ALB−NP seemed also to be located inside the cells.

To quantify the cell–particle interactions, the flow cytometry experiments were also performed (Figure 6.7). The ADS−NP increased the interactions with the cells compared to the control ($p < 0.001$), but the fluorescence intensities of the cells incubated with the CS− and ALB−NP were considerably shifted to the right ($p < 0.001$) compared to the ADS−NP. This was a clear evidence of the high cellular association of the coated NP and the cells. This result is explained due to the presence of the mucoadhesive CS on the surface of the NP, which potentiates stronger electrostatic interactions when the mucus layer is present in the cellular co−culture. Moreover, the positive charge of the NP increases the affinity to the negatively charged cells' membrane [18,71]. The presence of an ALB layer also demonstrated to have a positive role towards insulin transport across the intestinal membrane by stabilizing insulin in the intestinal conditions [25]. Therefore, our results showed high accordance with these findings and demonstrated that the positive effect of the ALB layer in the NP still allowed the mucoadhesive properties of CS to be functional, acting as a synergistic multilayer nanosystem.

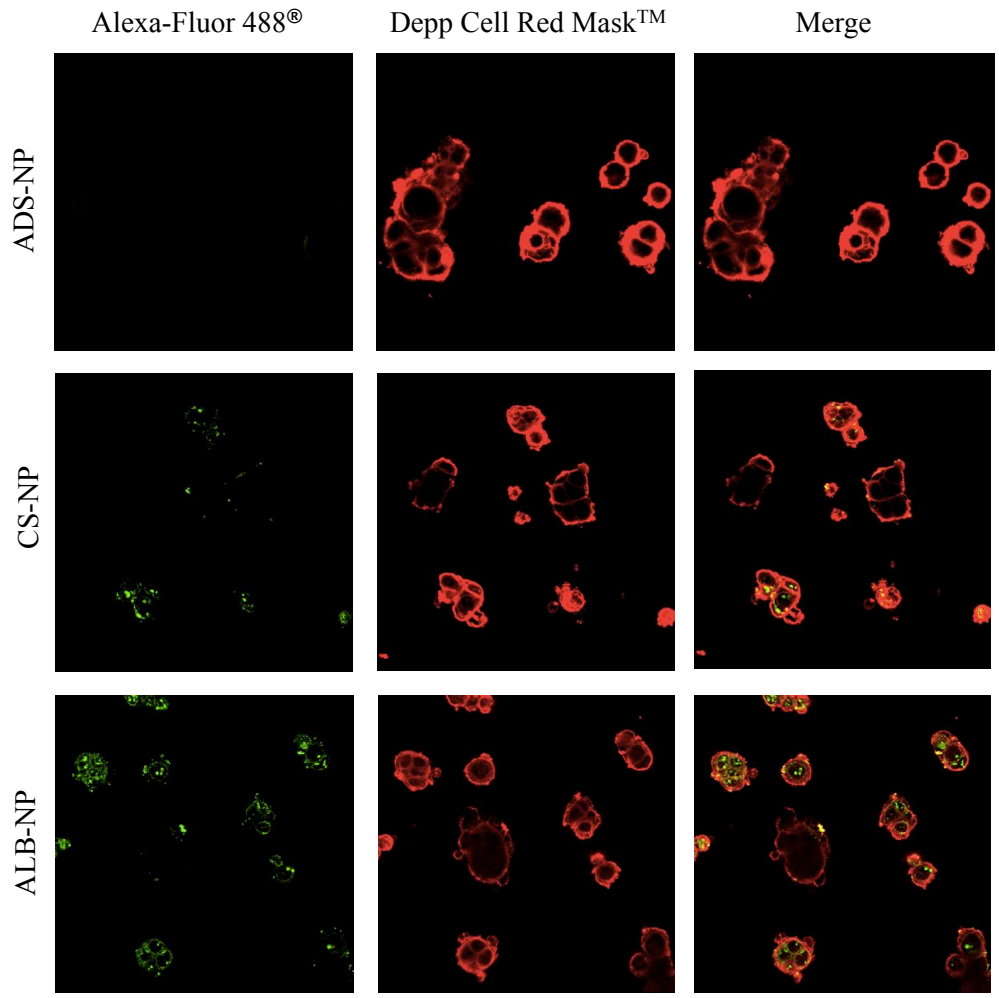

Figure 6.6. Qualitative cell–NP localization by confocal fluorescence microscopy after incubation of the NP with the cells for 3 h at 37 °C. The NP were labeled with Alexa Fluor® 488 and the cells' membrane were stained with CellMask™ DeepRed (Invitrogen, USA). Red: cell membranes stained with Cell–Mask™ Deep Red; green: Alexa Fluor® 488–labeled NP; yellow: co–localization of the NP and the cell membranes.

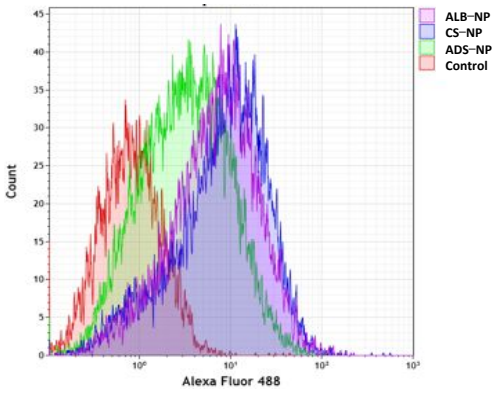

Sample	Positive events (%)
Control	2.97 ± 0.01
ADS-NP	8.83 ± 0.74
CS-NP	14.95 ± 0.24
ALB-NP	12.14 ± 0.35

Figure 6.7. Flow cytometry quantification of the interactions of the ADS−, CS− and ALB−NP with the Caco−2/HT29−MTX co−culture cells. The cells were incubated with the NP for 3 h at 37 °C. The table summarizes the percentage of positive events for each sample. Data is shown as mean ± s.d. ($n \geq 3$).

6.4.7 Permeability studies

To analyze the permeability of the insulin−loaded NP and assess the independent role of each polymer in the NP' structure, a triple co−culture of Caco−2/HT29−MTX/Raji B model was used [34]. This cellular intestinal monolayer model mimics in a more accurately way the *in vivo* conditions, as it includes the enterocytes, the mucus−producing goblet cells in physiological proportions (90:10), and the M cells in the PP [28]. After the addition of the Raji B cells to the monolayer in order to convert the enterocytes in cells with M−phenotype, the values of the TEER had an increment of ca. 14.2% (not statistically significant), which is in accordance with previous reports [34].

As can be observed in Figure 6.8, the permeation profiles at pH 5.5 (Figure 6.8A) in comparison to pH 7.4 (Figure 6.8B) presented different trends. The insolubility of the nonencapsulated insulin observed at pH 5.5 in the release studies (Figure 6.4A) is in accordance with these results, where a steady permeability profile and reduced amounts of insulin were obtained after 30 min reaching less than 0.25% of the initial amount after 180 min. The absorption of proteins and peptides across the intestinal epithelium is limited mainly by the presence of TJ and by the mucus layer [72]. However, the biopolymer−based

NP were able to significantly enhance the insulin permeation across the intestinal cells at pH 5.5, as compared to the nonencapsulated insulin. Furthermore, this permeability improvement was even higher (ca. 2.4% of the initial amount) when the CS−NP were used, as it can be seen by the differences in the P_{app}−values. Following the release of insulin from the CS−NP after 2 h at pH 5.5 (Figure 6.4A), the insulin that showed to rapidly precipitate in the medium was now able to permeate across the monolayer from the apical to the basolateral side, which may be related to the sustained permeation profile obtained, preventing the accumulation of insulin in the apical side and further precipitation. The differences obtained between the amounts of insulin across the cell monolayers by the ADS− and CS−NP may be due to the CS mucoadhesive properties and capacity to transiently opening the TJ, thereby increasing the insulin permeation across the intestinal epithelium [43,73,74]. The ADS−NP are negatively charged, which may lead to repulsions between the NP and the negatively charged mucin. This problem was overcome after CS coating, which provided positive charges to the NP' surface, enabling the closer contact and longer retention of the CS−NP in the cellular mucus layer. No significant statistical difference was observed between the P_{app} of insulin delivered from the CS− and ALB−NP.

When analyzing the permeability at pH 7.4 (Figure 6.8B), the amount of nonencapsulated insulin that crossed the monolayer after 3 h was higher (ca. 1.1% of the initial amount) than at pH 5.5, with ca. 5−fold increase of the P_{app} value. This can be explained by the higher amount of insulin available to permeate across the cell monolayers at pH 7.4, as observed in the release studies in Figure 6.4B. The insulin release from both the ADS− and CS−NP at pH 7.4 after 3 h was ca. 50% of the initial insulin, whereas the ALB−NP released almost 100% (Figure 6.4B). The higher insulin release explains why the permeability values of insulin from the ALB−NP were ca. 2.9− and 3.6−fold compared to the ADS− and CS−NP, respectively, resulting in the permeation of more than 4% of the initial amount of insulin. Moreover, previous reports have showed that the use of ALB as an outermost coating to the CS−NP improved the protection of insulin from the degradation by the GI proteases, acting as a sacrificial target instead for insulin [13], and that the ALB layer was crucial to improve insulin uptake across the intestinal monolayers [25]. ALB could stabilize insulin in the intestinal conditions, representing a 3.4−fold increase of the insulin permeability across the Caco−2/HT29 cell monolayers [25]. Concerning the ADS−NP, only a slight improvement of the insulin permeability was detected at pH 7.4 compared to the

nonencapsulated insulin. One possible explanation for this could be the rapid dissolution of the ADS−NP at pH 7.4, which did not allow the NP to interact with the cells long enough, which was observed by the absence of the NP in the TEM images of the Caco−2/HT20−MTX/Raji B cells monolayers (see Figure 6.9). Similar results for the insulin permeation at pH 7.4 were observed for the CS−NP. At lower pH (5.5), the free amine groups of the CS chains are present in a protonated form, allowing the CS−NP to exhibit their mucoadhesive properties. However, at pH 7.4, the amine groups become deprotonated and the CS molecules lose their charge and solubility [75], which may explain the lower permeability obtained for insulin at this pH compared to pH 5.5.

Nevertheless, the TEM images in Figure 6.9 showed that both the CS− and ALB−NP increased the interactions with the cell monolayers, highlighting the mucoadhesive properties of CS, which were in very good agreement with the confocal fluorescence microscope images shown in Figure 6.6. These results indicate that the permeation of insulin was enhanced by encapsulating it into the ADS−NP, which was further improved after the CS and ALB coatings on their surface when the permeation experiments were performed at pH 5.5 and 7.4, respectively.

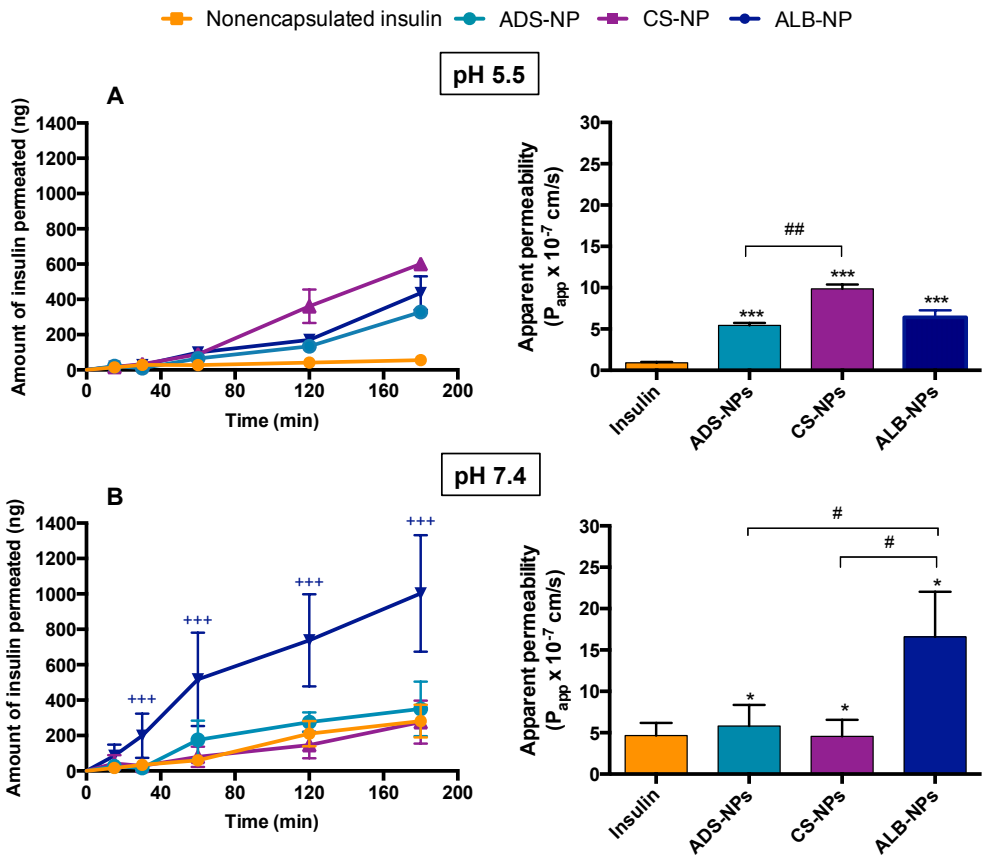

Figure 6.8. *In vitro* cumulative permeability profiles and P_{app} coefficient of insulin and insulin–loaded NP across the Caco–2/HT29–MTX/Raji B co–culture monolayers. All experiments were conducted from the apical–to–basolateral direction in (A) HBSS–MES (pH 5.5) and (B) HBSS–HEPES buffer (pH 7.4) at 37 °C. Data sets were compared to nonencapsulated insulin ($^{*}p < 0.05$, $^{**}p < 0.01$, and $^{***}p < 0.001$), between them ($^{\#}p < 0.05$, $^{\#\#}p < 0.01$, and $^{\#\#\#}p < 0.001$), and between the different pHs ($^{+}p < 0.05$, $^{++}p < 0.01$, and $^{+++}p < 0.001$). Error bars represent mean ± s.d. ($n \geq 3$).

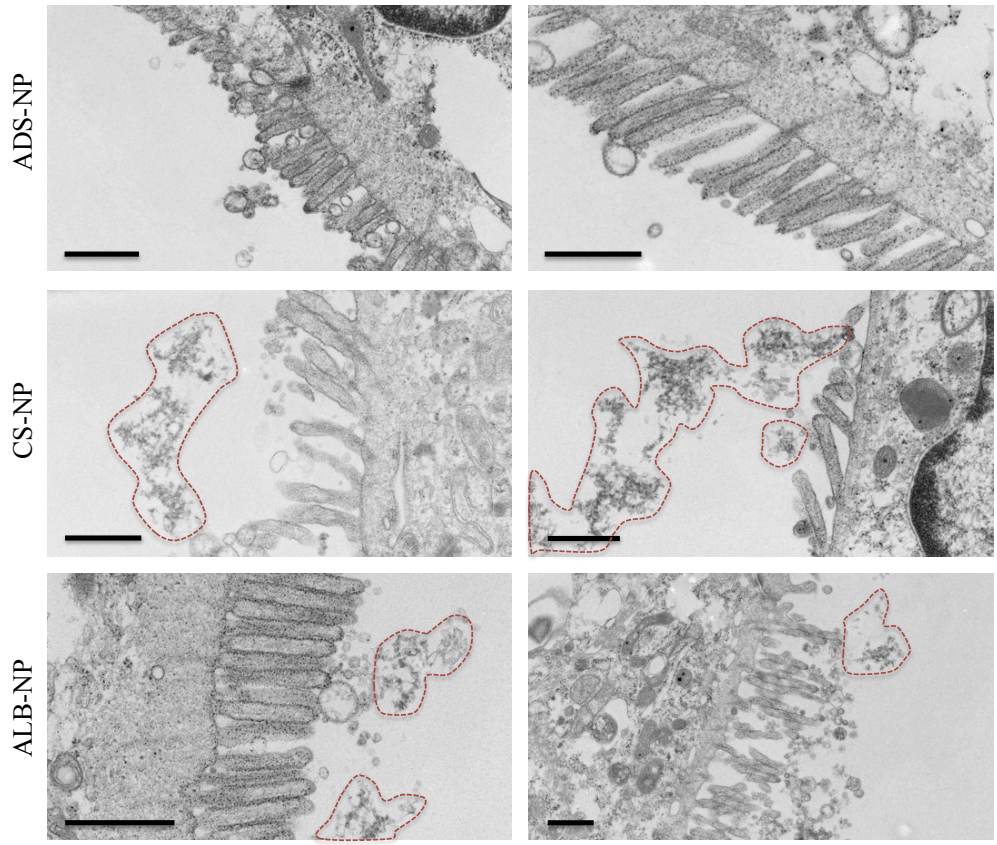

Figure 6.9. TEM images of flat embedded ultrathin sections showing the interaction of the NP (delimitated by red dotted lines) with the Caco−2/HT29−MTX/Raji B co−culture monolayers in HBSS−HEPES buffer (pH 7.4) at 37 °C. No ADS−NP were found in the monolayers; the CS− and ALB−NP were observed in the vicinity of the cell membranes. Scale bars = 500 nm.

6.4.8 FITC−insulin uptake study

The amount of FITC−insulin bound to or within the cells and mucus layer at pH 5.5 and 7.4 is displayed in Figure 6.10. At pH 5.5 (Figure 6.10A), the highest amount of FITC−insulin present inside or in the vicinity of cells was found for the nonencapsulated insulin ($p < 0.001$). These results were in very good accordance with the permeability studies at such pH−values, where the P_{app} of the nonencapsulated insulin was the lowest value

obtained, *i.e.*, insulin was retained in the cells and/or mucus layer and was not able to permeate across the monolayer. Concerning the insulin−loaded NP, the CS and ALB−NP showed increased P_{app} compared to the ADS−NP, which was also related with the lowest amount of FITC−insulin bound/within the cells. At pH 7.4 (Figure 6.10B), a significant increase of FITC−insulin associated to cells was obtained with the CS−NP compared either to the nonencapsulated insulin or to the ADS− and ALB−NP ($p < 0.001$). The insulin−loaded ALB−NP exhibited the highest P_{app}−values compared to the other tested formulations ($p < 0.05$), whereas the CS−NP had no positive effect on the insulin permeation across the monolayers. The mucoadhesive properties of CS were responsible for the increase of FITC−insulin in the vicinity or within the cells, but the presence of ALB was crucial to allow the permeation of insulin from the apical to the basolateral side of the intestinal monolayers. As can be observed in Figure 6.10, the amount of FITC−insulin in association with the intestinal cells was higher at pH 5.5 than at pH 7.4. At pH 5.5, insulin is almost uncharged (pI = 5.3), whereas at pH 7.4 the protein becomes negatively charged. The negative charge of insulin at pH 7.4 may lead to electrostatic repulsions with the negatively charged mucus layer on the intestinal epithelium, being responsible for the less amount of insulin retained by the intestinal cells.

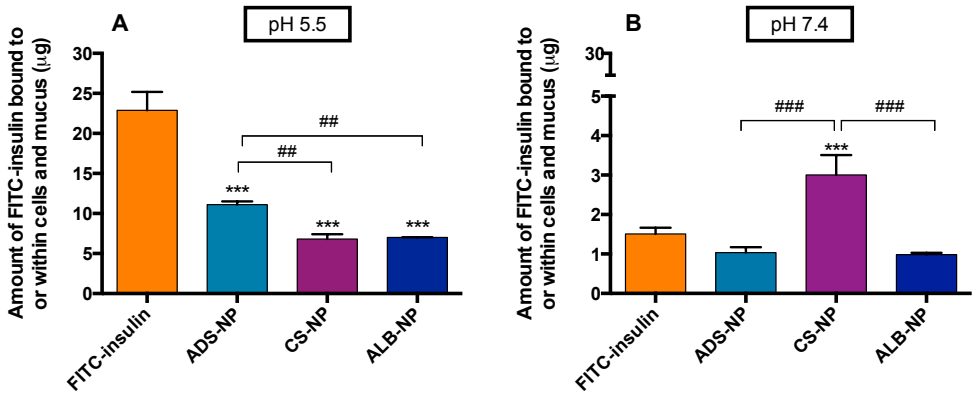

Figure 6.10. Amount of FITC–insulin attached or uptaken in the Caco–2/HT29–MTX/Raji B co–culture monolayers in (A) HBSS–MES (pH 5.5) and (B) HBSS–HEPES buffer (pH 7.4) at 37 °C. Data sets were compared to nonencapsulated insulin ($^{*}p < 0.05$, $^{**}p < 0.01$, and $^{***}p < 0.001$) and between them ($^{\#}p < 0.05$, $^{\#\#}p < 0.01$, and $^{\#\#\#}p < 0.001$). Error bars represent mean ± s.d. ($n \geq 3$).

6.4.9 Transport pathway of insulin

To identify the pathway by which insulin permeated the triple co–culture of Caco–2/HT29–MTX/Raji B, the ALB–NP were incubated under different conditions. Figure 6.11 displays the effect of each condition on the insulin permeability. The depletion of intracellular stores of ATP by sodium azide or low temperatures (4 °C) are two responsible factors for the inhibition of the membrane traffic. However, while the ATP depleted cells were described to have unchanged free quantity of clathrin, the decrease of temperature was related to a reduction of this quantity and also to an increase in the number of coated pits at the level of the plasma membrane [76]. The insulin permeability was significantly reduced at 4 °C ($p < 0.01$), but no differences were observed after incubation of the monolayers with sodium azide. An active transport for insulin has already been described several times in the literature [11,77,78]. At lower temperature, in opposite to the ATP depletion conditions, most of the clathrin of the cell is polymerized, and thus, this protein is not available for assembly into new coated pits [76], which suggests a clathrin–mediated

transport for insulin. These findings are in accordance with the inhibition of insulin permeability obtained after the addition of chlorpromazine ($p < 0.01$), which disrupts the assembly and disassembly of clathrin. Although a decrease of the insulin permeability was also obtained in the presence of filipin, the disruption of the caveolae's structure was not found to statistically influence the insulin transport. Previous reports demonstrated similar results with CS−based NP, where the cellular uptake was significantly inhibited by the presence of chlorpromazine, but was not affected by the presence of filipin across the Caco−2 monolayers [79].

The transport of insulin across the intestinal monolayers was also markedly decreased with the pretreatment of sodium chlorate ($p < 0.01$). This agent inhibits the glycosaminoglycan sulfation, which could disturb the electrostatic interactions between the ALB−NP and the glycocalyx on the apical membrane, which is oppositely charged, and therefore reduce the insulin permeation. These results are also consistent with the reported internalization of insulin−loaded trimethyl CS chloride NP by HT29−MTX cells [11].

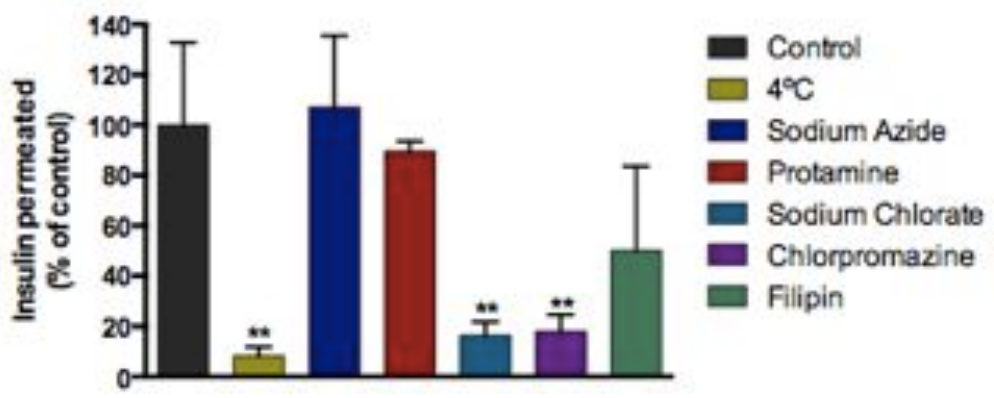

Figure 6.11. Insulin permeability of the ALB−NP across the Caco−2/HT29−MTX/Raji B co−culture monolayers at different conditions. Data sets were compared to the control ($^{*}p < 0.05$, $^{**}p < 0.01$, and $^{***}p < 0.001$). Error bars represent mean ± s.d. (n ≥ 3).

6.5 CONCLUSIONS

In the present study, the effect of biopolymer−based NP was evaluated on the insulin release in the GI tract and permeation across a triple co−culture of Caco−2/HT29−MTX/Raji B cell model. The nanosystem composed of ADS−matrix and dual coated with CS/ALB exhibited pH−sensitive and mucoadhesive properties. About 70% of insulin was successfully retained inside the NP in the gastric environment and slowly released following passage to intestinal conditions. The NP showed different behaviors in terms of morphology, release profile and interaction with the intestinal cells at different pH−values (5.5 and 7.4). The presence of ALB in the NP' coating provided electrostatic stabilization and significantly increased the dissolution rate of insulin from the NP. In both the environments, the presence of CS and ALB was essential to enhance the NP' interactions with the intestinal cells and further increase the insulin permeability, which was demonstrated to occur by an active transport mediated by clathrin endocytosis. The electrostatic interactions between the positively charged NP and the negatively charged glycocalix was also crucial for the insulin permeation to occur. These results suggest the potential of the developed nanosystem composed of biocompatible and biodegradable polymers to improve the permeability of insulin across the intestinal wall when orally delivered, and its clinical potential is envisaged for the therapy of T1D.

6.6 REFERENCES

[1] Wong, T. W. Design of oral insulin delivery systems. Journal of Drug Targeting 2009;18:79−92.

[2] Chen, M.−C.; Sonaje, K.; Chen, K.−J.; Sung, H.−W. A review of the prospects for polymeric nanoparticle platforms in oral insulin delivery. Biomaterials 2011;32:9826−38.

[3] Specian, R. D.; Oliver, M. G. Functional biology of intestinal goblet cells. American Journal of Physiology 1991;260:C183−C93.

[4] Carino, G. P.; Mathiowitz, E. Oral insulin delivery. Advanced Drug Delivery Reviews 1999;35:249−57.

[5] Lopes, M. A.; Abrahim, B. A.; Seica, R.; Veiga, F.; Rodrigues, C. R.; Ribeiro, A. J. Intestinal uptake of insulin nanoparticles: Facts or myths? Current Pharmaceutical Biotechnology 2014;15:629−38.

[6] Lee, E.; Lee, J.; Jon, S. A novel approach to oral delivery of insulin by conjugating with low molecular weight chitosan. Bioconjugate Chemistry 2010;21:1720−3.

[7] Déat−Lainé, E.; Hoffart, V.; Garrait, G.; Jarrige, J.−F.; Cardot, J.−M.; Subirade, M.; Beyssac, E. Efficacy of mucoadhesive hydrogel microparticles of whey protein and alginate for oral insulin delivery. Pharmaceutical Research 2013;30:721−34.

[8] Shan, W.; Zhu, X.; Liu, M.; Li, L.; Zhong, J.; Sun, W.; Zhang, Z.; Huang, Y. Overcoming the diffusion barrier of mucus and absorption barrier of epithelium by self−assembled nanoparticles for oral delivery of insulin. American Chemical Society nano 2015;9:2345−56.

[9] Sheng, J.; Han, L.; Qin, J.; Ru, G.; Li, R.; Wu, L.; Cui, D.; Yang, P.; He, Y.; Wang, J. N−trimethyl chitosan chloride−coated PLGA nanoparticles overcoming multiple barriers to oral insulin absorption. ACS Applied Materials & Interfaces 2015;7:15430−41.

[10] Shrestha, N.; Shahbazi, M.−A.; Araújo, F.; Zhang, H.; Mäkilä, E. M.; Kauppila, J.; Sarmento, B.; Salonen, J. J.; Hirvonen, J. T.; Santos, H. A. Chitosan−modified porous silicon microparticles for enhanced permeability of insulin across intestinal cell monolayers. Biomaterials 2014;35:7172−9.

[11] Jin, Y.; Song, Y.; Zhu, X.; Zhou, D.; Chen, C.; Zhang, Z.; Huang, Y. Goblet cell−targeting nanoparticles for oral insulin delivery and the influence of mucus on insulin transport. Biomaterials 2012;33:1573−82.

[12] Zhao, X.; Shan, C.; Zu, Y.; Zhang, Y.; Wang, W.; Wang, K.; Sui, X.; Li, R. Preparation, characterization, and evaluation *in vivo* of Ins−SiO_2−HP55 (insulin−loaded silica coating HP55) for oral delivery of insulin. International Journal of Pharmaceutics 2013;454:278−84.

[13] Reis, C. P.; Veiga, F. J.; Ribeiro, A. J.; Neufeld, R. J.; Damgé, C. Nanoparticulate biopolymers deliver insulin orally eliciting pharmacological response. Journal of Pharmaceutical Sciences 2008;97:5290−305.

[14] Lim, H.−P.; Tey, B.−T.; Chan, E.−S. Particle designs for the stabilization and controlled−delivery of protein drugs by biopolymers: A case study on insulin. Journal of Controlled Release 2014;186:11−21.

[15] Paques, J. P.; van der Linden, E.; van Rijn, C. J. M.; Sagis, L. M. C. Preparation methods of alginate nanoparticles. Advances in Colloid and Interface Science 2014;209:163−71.

[16] Reis, C.; Ribeiro, A.; Houng, S.; Veiga, F.; Neufeld, R. Nanoparticulate delivery system for insulin: Design, characterization and *in vitro*/*in vivo* bioactivity. European Journal of Pharmaceutical Sciences 2007;30:392 − 7.

[17] Abbaspour, M.; Makhmalzadeh, B.; Arastoo, Z.; Jahangiri, A.; Shiralipour, R. Effect of anionic polymers on drug loading and release from clindamycin phosphate solid lipid nanoparticles. Tropical Journal of Pharmaceutical Research 2013;12:447−82.

[18] Araújo, F.; Shrestha, N.; Shahbazi, M.−A.; Fonte, P.; Mäkilä, E. M.; Salonen, J. J.; Hirvonen, J. T.; Granja, P. L.; Santos, H. A.; Sarmento, B. The impact of nanoparticles on the mucosal translocation and transport of GLP−1 across the intestinal epithelium. Biomaterials 2014;35:9199−207.

[19] Araújo, F.; Shrestha, N.; Shahbazi, M.−A.; Liu, D.; Herranz−Blanco, B.; Mäkilä, E. M.; Salonen, J. J.; Hirvonen, J. T.; Granja, P. L.; Sarmento, B.; Santos, H. A. Microfluidic assembly of a multifunctional tailorable composite system designed for site specific combined oral delivery of peptide drugs. American Chemical Society nano 2015;9:

[20] Shrestha, N.; Shahbazi, M.−A.; Araújo, F.; Mäkilä, E.; Raula, J.; Kauppinen, E. I.; Salonen, J.; Sarmento, B.; Hirvonen, J.; Santos, H. A. Multistage pH−responsive mucoadhesive nanocarriers prepared by aerosol flow reactor technology: A controlled dual protein−drug delivery system. Biomaterials 2015;68:9−20.

[21] Sonaje, K.; Lin, K.−J.; Tseng, M. T.; Wey, S.−P.; Su, F.−Y.; Chuang, E.−Y.; Hsu, C.−W.; Chen, C.−T.; Sung, H.−W. Effects of Chitosan−nanoparticle−mediated tight junction opening on the oral absorption of endotoxins. Biomaterials 2011;32:8712−21.

[22] Woitiski, C. B.; Neufeld, R. J.; Ribeiro, A. J.; Veiga, F. Colloidal carrier integrating biomaterials for oral insulin delivery: Influence of component formulation on physicochemical and biological parameters. Acta Biomaterialia 2009;5:2475−84.

[23] Hurteaux, R.; Edwards−Lévy, F.; Laurent−Maquin, D.; Lévy, M.−C. Coating alginate microspheres with a serum albumin−alginate membrane: Application to the encapsulation of a peptide. European Journal of Pharmaceutical Sciences 2005;24:187−97.

[24] Lopes, M.; Abrahim, B. A.; Rodrigues, C. R.; Veiga, F.; Cabral, L.; Ribeiro, A. J. Alginate−based micro and nanoparticles coated with chitosan. Journal of Chitin and Chitosan Science 2013;1:173−6.

[25] Woitiski, C. B.; Sarmento, B.; Carvalho, R. A.; Neufeld, R. J.; Veiga, F. Facilitated nanoscale delivery of insulin across intestinal membrane models. International Journal of Pharmaceutics 2011;412:123−31.

[26] Elzoghby, A. O.; Samy, W. M.; Elgindy, N. A. Albumin−based nanoparticles as potential controlled release drug delivery systems. Journal of Controlled Release 2012;157:168−82.

[27] Kratz, F.; Fichtner, I.; Beyer, U.; Schumacher, P.; Roth, T.; Fiebig, H.; Unger, C. Antitumour activity of acid labile transferrin and albumin doxorubicin conjugates in *in vitro* and *in vivo* human tumour xenograft models. European Journal of Cancer 1997;33:175.

[28] Lopes, M. A.; Abrahim, B. A.; Cabral, L. M.; Rodrigues, C. R.; Seiça, R. M. F.; de Baptista Veiga, F. J.; Ribeiro, A. J. Intestinal absorption of insulin nanoparticles: Contribution of M cells. Nanomedicine: Nanotechnology, Biology and Medicine 2014;10:1139−51.

[29] Fievez, V.; Plapied, L.; des Rieux, A.; Pourcelle, V.; Freichels, H.; Wascotte, V.; Vanderhaeghen, M.−L.; Jerome, C.; Vanderplasschen, A.; Marchand−Brynaert, J.; Schneider, Y.−J.; Preat, V. Targeting nanoparticles to M cells with non−peptidic ligands for oral vaccination. European Journal of Pharmaceutics and Biopharmaceutics 2009;73:16−24.

[30] Cui, F.; Shi, K.; Zhang, L.; Tao, A.; Kawashima, Y. Biodegradable nanoparticles loaded with insulin−phospholipid complex for oral delivery: Preparation, *in vitro* characterization and *in vivo* evaluation. Journal of Controlled Release 2006;114:242−50.

[31] Conner, S. D.; Schmid, S. L. Regulated portals of entry into the cell. Nature 2003;422:37−44.

[32] Lopes, M. A.; Abrahim−Vieira, B.; Oliveira, C.; Fonte, P.; Souza, A. M. T.; Lira, T.; Sequeira, J. A. D.; Rodrigues, C. R.; Cabral, L. M.; Sarmento, B.; Seiça, R.; Veiga, F.; Ribeiro, A. J. Probing insulin bioactivity in oral nanoparticles produced by ultrasonication−assisted emulsification/internal gelation. International Journal of Nanomedicine 2015;10:5865−80.

[33] Shahbazi, M.−A.; Hamidi, M.; Mäkilä, E. M.; Zhang, H.; Almeida, P. V.; Kaasalainen, M.; Salonen, J. J.; Hirvonen, J. T.; Santos, H. A. The mechanisms of surface chemistry effects of mesoporous silicon nanoparticles on immunotoxicity and biocompatibility. Biomaterials 2013;34:7776−89.

[34] Araújo, F.; Sarmento, B. Towards the characterization of an *in vitro* triple co−culture intestine cell model for permeability studies. International Journal of Pharmaceutics 2013;458:128−34.

[35] Mislick, K. A.; Baldeschwieler, J. D. Evidence for the role of proteoglycans in cation−mediated gene yransfer. Proceedings of the National Academy of Sciences of the United States of America 1996;93:12349−54.

[36] Rejman, J.; Bragonzi, A.; Conese, M. Role of clathrin− and caveolae−mediated endocytosis in gene transfer mediated by lipo− and polyplexes. Molecular Therapy 2005;12:468−74.

[37] Florence, A. The oral absorption of micro− and nanoparticulates: Neither exceptional nor unusual. Pharmaceutical Research 1997;14:259−66.

[38] Norris, D. A.; Puri, N.; Sinko, P. J. The effect of physical barriers and properties on the oral absorption of particulates. Advanced Drug Delivery Reviews 1998;34:135−54.

[39] Lai, S. K.; Wang, Y.−Y.; Hanes, J. Mucus−penetrating nanoparticles for drug and gene delivery to mucosal tissues. Advanced Drug Delivery Reviews 2009;61:158−71.

[40] Heni, W.; Vonna, L.; Haidara, H. Experimental characterization of the nanoparticle size effect on the mechanical stability of nanoparticle−based coatings. Nano Letters 2015;15:442−9.

[41] Thu, B.; Bruheim, P.; Espevik, T.; Smidsrød, O.; Soon−Shiong, P.; Skjåk−Bræk, G. Alginate polycation microcapsules: I. Interaction between alginate andpolycation. Biomaterials 1996;17:1031−40.

[42] Zhang, X.; Sun, M.; Zheng, A.; Cao, D.; Bi, Y.; Sun, J. Preparation and characterization of insulin−loaded bioadhesive PLGA nanoparticles for oral administration. European Journal of Pharmaceutical Sciences 2012;45:632−8.

[43] Chen, M.−C.; Mi, F.−L.; Liao, Z.−X.; Hsiao, C.−W.; Sonaje, K.; Chung, M.−F.; Hsu, L.−W.; Sung, H.−W. Recent advances in chitosan−based nanoparticles for oral delivery of macromolecules. Advanced Drug Delivery Reviews 2013;65:865−79.

[44] Chien, Y. W. Human insulin: Basic sciences to therapeutic uses. Drug Development and Industrial Pharmacy 1996;22:753−89.

[45] Draget, K. I.; Skjåk Bræk, G.; Smidsrød, O. Alginic acid gels: The effect of alginate chemical composition and molecular weight. Carbohydrate Polymers 1994;25:31−8.

[46] Reis, C.; Ribeiro, A.; Veiga, F.; Neufeld, R.; Damgé, C. Polyelectrolyte biomaterial interactions provide nanoparticulate carrier for oral insulin delivery. Drug Delivery 2008;15:127−39.

[47] Sarmento, B.; Ferreira, D. C.; Jorgensen, L.; van de Weert, M. Probing insulin's secondary structure after entrapment into alginate/chitosan nanoparticles. European Journal of Pharmaceutics and Biopharmaceutics 2007;65:10−7.

[48] Morishita, M.; Peppas, N. A. Is the oral route possible for peptide and protein drug delivery? Drug Discovery Today 2006;11:905−10.

[49] Borchard, W.; Kenning, A.; Kapp, A.; Mayer, C. Phase diagram of the system sodium alginate/water: A model for biofilms. International Journal of Biological Macromolecules 2005;35:247−56.

[50] Dressman, J.; Berardi, R.; Dermentzoglou, L.; Russell, T.; Schmaltz, S.; Barnett, J.; Jarvenpaa, K. Upper gastrointestinal (GI) pH in young, healthy men and women. Pharmaceutical Research 1990;7:756−61.

[51] Balamuralidhara, V.; Pramodkumar, T. M.; Srujana, N.; Venkatesh, M. P.; Gupta, N. V.; Krishna, K. L.; Gangadharappa, H. V.; . pH sensitive drug delivery systems: A review. American Journal of Drug Discovery and Development 2011;1:24−48.

[52] McConnell, E. L.; Fadda, H. M.; Basit, A. W. Gut instincts: Explorations in intestinal physiology and drug delivery. International Journal of Pharmaceutics 2008;364:213−26.

[53] Zhao, Y.; Hu, F.; Evans, J. J.; Harris, M. T. Study of sol–gel transition in calcium alginate system by population balance model. Chemical Engineering Science 2011;66:848−58.

[54] Ferreira Almeida, P.; Almeida, A. J. Cross−linked alginate–gelatine beads: A new matrix for controlled release of pindolol. Journal of Controlled Release 2004;97:431−9.

[55] Kikuchi, A.; Kawabuchi, M.; Watanabe, A.; Sugihara, M.; Sakurai, Y.; Okano, T. Effect of Ca^{2+}−alginate gel dissolution on release of dextran with different molecular weights. Journal of Controlled Release 1999;58:21−8.

[56] Lee, K. Y.; Mooneya, D. J. Alginate: Properties and biomedical applications. Progress in Polymer Science 2012 37:106– 26.

[57] Iskakov, R. M.; Kikuchi, A.; Okano, T. Time−programmed pulsatile release of dextran from calcium−alginate gel beads coated with carboxy−N−propylacrylamide copolymers. Journal of Controlled Release 2002;80:57−68.

[58] de Beer, E. J.; Johnston, C. G.; Wilson, D. W. The composition of the intestinal secretions. The Journal of Biological Chemistry 1935;108:113−20.

[59] Avadi, M. R.; Sadeghi, A. M. M.; Mohamadpour Dounighi, N.; Dinarvand, R.; Atyabi, F.; Rafiee−Tehrani, M. *Ex vivo* evaluation of insulin nanoparticles using chitosan and arabic gum. ISRN Pharmaceutics 2011;2011:6.

[60] Prusty, A. k.; Sahu, S. K. Development and evaluation of insulin incorporated nanoparticles for oral administration. ISRN Nanotechnology 2013;2013:6.

[61] Klingler, C.; Müller, B. W.; Steckel, H. Insulin−micro− and nanoparticles for pulmonary delivery. International Journal of Pharmaceutics 2009;377:173−9.

[62] Eltayeb, M.; Stride, E.; Edirisinghe, M. Preparation, characterization and release kinetics of ethylcellulose nanoparticles encapsulating ethylvanillin as a model functional component. Journal of Functional Foods 2015;14:726−35.

[63] Antoine, D.; Pellequer, Y.; Tempesta, C.; Lorscheidt, S.; Kettel, B.; Tamaddon, L.; Jannin, V.; Demarne, F.; Lamprecht, A.; Béduneau, A. Biorelevant media resistant co−culture model mimicking permeability of human intestine. International Journal of Pharmaceutics 2015;481:27−36.

[64] Georgantzopoulou, A.; Serchi, T.; Cambier, S.; Leclercq, C. C.; Renaut, J.; Shao, J.; Kruszewski, M.; Lentzen, E.; Grysan, P.; Eswara, S.; Audinot, J.−N.; Contal, S.; Ziebel, J.; Guignard, C.; Hoffmann, L.; Murk, A. J.; Gutleb, A. C. Effects of silver nanoparticles and ions on a co−culture model for the gastrointestinal epithelium. Particle and Fibre Toxicology 2016;13:1−17.

[65] Lopes, M.; Abrahim, B.; Veiga, F.; Seiça, R.; Cabral, L.; Ribeiro, A. Alginate−based micro− and nanoparticles: Biocompatibility and biodegradability. In: Taylor & Francis Group. Encyclopedia of Biomedical Polymers and Polymeric Biomaterials: Taylor & Francis Group; 2014.

[66] Kumari, A.; Yadav, S. K. Cellular interactions of therapeutically delivered nanoparticles. Expert Opinion on Drug Delivery 2011;8:141−51.

[67] Verma, A.; Stellacci, F. Effect of surface properties on nanoparticle–cell interactions. Small 2010;6:12−21.

[68] Rampino, A.; Borgogna, M.; Blasi, P.; Bellich, B.; Cesàro, A. Chitosan nanoparticles: Preparation, size evolution and stability. International Journal of Pharmaceutics 2013;455:219−28.

[69] Kobayashi, K.; Wei, J.; Iida, R.; Ijiro, K.; Niikura, K. Surface engineering of nanoparticles for therapeutic applications. Polymer Journal 2014;46:460−8.

[70] Clark, M. A.; Jepson, M. A.; Hirst, B. H. Exploiting M cells for drug and vaccine delivery. Advanced Drug Delivery Reviews 2001;50:81−106.

[71] Sarmento, B.; Ribeiro, A.; Veiga, F.; Ferreira, D.; Neufeld, R. Oral bioavailability of insulin contained in polysaccharide nanoparticles. Biomacromolecules 2007;8:3054−60.

[72] Bakhru, S. H.; Furtado, S.; Morello, A. P.; Mathiowitz, E. Oral delivery of proteins by biodegradable nanoparticles. Advanced Drug Delivery Reviews 2013;65:811−21.

[73] Sonaje, K.; Chuang, E.−Y.; Lin, K.−J.; Yen, T.−C.; Su, F.−Y.; Tseng, M. T.; Sung, H.−W. Opening of epithelial tight junctions and enhancement of paracellular permeation by chitosan: Microscopic, ultrastructural, and computed−tomographic observations. Molecular Pharmaceutics 2012;9:1271−9.

[74] Hsu, L.−W.; Lee, P.−L.; Chen, C.−T.; Mi, F.−L.; Juang, J.−H.; Hwang, S.−M.; Ho, Y.−C.; Sung, H.−W. Elucidating the signaling mechanism of an epithelial tight−junction opening induced by chitosan. Biomaterials 2012;33:6254−63.

[75] Bansal, V.; Sharma, P. K.; Sharma, N.; Pal, O. P.; Malviya, R. Applications of chitosan and chitosan derivatives in drug delivery. Advances in Biological Research 2011;5:28−37.

[76] Courtoy, P. J. Endocytosis: From cell biology to health, disease and therapy. Berlin, Germany: Springer Science & Business Media; 1992.

[77] Mao, S.; Germershaus, O.; Fischer, D.; Linn, T.; Schnepf, R.; Kissel, T. Uptake and transport of PEG−Graft−trimethyl−chitosan copolymer−insulin nanocomplexes by epithelial cells. Pharmaceutical Research 2005;22:2058−68.

[78] Thompson, C.; Cheng, W.; Gadad, P.; Skene, K.; Smith, M.; Smith, G.; McKinnon, A.; Knott, R. Uptake and transport of novel amphiphilic polyelectrolyte−insulin nanocomplexes by Caco−2 cells — Towards oral insulin. Pharmaceutical Research 2011;28:886−96.

[79] Ma, Z. S.; Lim, L. Y. Uptake of chitosan and associated insulin in Caco−2 cell monolayers: A comparison between chitosan molecules and chitosan nanoparticles. Pharmaceutical Research 2003;20:1812−9.

CHAPTER 7

CONCLUSIONS AND FUTURE PERSPECTIVES

7.1 CONCLUSIONS

Dual CS/ALB−coated ADS−based NP were developed as an oral carrier nanosystem for insulin, and were evaluated based on their ability to enhance the permeability of the encapsulated insulin through the intestinal epithelium.

In the first study, the influence of the formulation and process parameters of the preparation method, emulsification/internal gelation, on the physical properties of the ADS−particles were carefully evaluated. The final particles were characterized by a monodisperse population in the nanoscale, strong negative charge, high EE, high insulin retention within the SGF, being the secondary structure of insulin ensured during and after the process of encapsulation. Further molecular modeling studies showed a relationship between the electronic properties and insulin EE, allowing for the prediction of the interaction model between sodium alginate and dextran sulfate.

In the next study, the coating of the prepared ADS−NP was applied by the polyelectrolyte complexation technique through the addition of CS and ALB. To ensure an effective coating of the NP, different concentrations of CS and ratios of CS:NP were studied based on the physicochemical parameters of the NP, such as surface charge and particle size. The CS concentration affected both properties and the best results, namely the lowest size and ζ−potential values, were obtained with chitosan at 0.3% (w/v).

Next, the effect of the GI environment on the aggregation of the ADS−based nanometric−sized particles, uncoated or double−coated with CS and ALB was investigated, and its further influence on the insulin release and permeability at the cellular level was also evaluated. The NP size and aggregation across the GI tract suggested the pH sensitivity of these biopolymers. The dual CS/ALB−coated ADS−based NP showed to provide the better size stability in GI conditions with less aggregation and more uniformity of size distribution, preventing the release of the majority of insulin in the gastric pH and sustaining the release in the intestinal pH up to 3 h. In the cellular experiments, this dual−coated nanosystem exhibited enhanced insulin permeability across the *in vitro* intestinal cell monolayers. The permeability of insulin across the intestinal epithelium was more prominent in the presence of the mucus layer and M−like cells, revealing their positive role on the insulin absorption. The influence of the intestinal cell monolayer models on the insulin permeability was compared to the curve that better adjusted to the mathematical kinetics of the insulin

release from the NP, which exhibited a pattern of insulin permeability in accordance with the insulin release profile.

The following study consisted of evaluating the biodistribution of the ALB/CS−coated ADS insulin−loaded NP after oral administration, as well as compare their antihyperglycemic effect after oral delivery to T1D and T2D animal models. The results revealed a significant reduction of the blood glucose levels for both models up to 12 h, although the effect lasted longer in the T1D model. The radiolabeling of the external NP' layer of ALB with technetium (^{99m}Tc−ALB) was a successful strategy toward NP' tracer since there was no systemic absorption of it, confirming the high stability of the radiotracer. Additionally, the ^{99m}Tc−ALB−NP significantly augmented the interactions with the small intestinal walls, which could be attributed to the mucoadhesive properties of CS. The NP biodistribution profile suggested that ALB was not totally degraded in the stomach, which allowed the protection of insulin and stabilization of the NP in the intestinal environment as well.

Finally, the NP performance was enhanced and insulin drug loading was increased by 2.6−fold, the size was kept with higher uniformity and the charge was reverted from negative to positive, in order to increase the contact with the negatively charged intestinal cells. The independent effects of the CS and ALB coatings were evaluated through an extensive characterization of the NP with impact both on the insulin release profiles in biological fluids and at the cellular level. The pH and time−dependent morphology of the NP were found to be correlated with the release profile and interaction with intestinal cells at different pH−values (5.5 and 7.4). The presence of ALB in the NP coating provided electrostatic stabilization and significantly increased the dissolution rate of insulin from the NP. In both the environments, the presence of CS and ALB was essential to enhance the NP' interactions with the intestinal cells and further increase the insulin permeability. Furthermore, a systematic evaluation of the cellular and molecular mechanisms used by the NP in the uptake and transport of insulin across the intestine revealed the involvement of several pathways. The permeability of insulin was reduced after the temperature was decreased and after co−incubation with chlorpromazine, suggesting an active insulin transport by CME. Moreover, the inhibition with the pre−treatment with sodium chlorate suggested that the interaction between the negatively charged glycocalix and the positively charged NP was critical for the insulin permeation.

Overall, the nanosystem developed in this thesis, ALB/CS−coated ADS insulin−loaded NP, composed of biocompatible and biodegradable polymers, showed great potential to increase the antihyperglycemic effect as well as improve the permeability of insulin across the intestinal wall when orally delivered, and its clinical potential is envisaged for the therapy of diabetes.

7.2 FUTURE PERSPECTIVES

In the future, a better understanding of the mechanisms involved in the intestinal absorption of insulin will certainly allow the improvement of insulin efficacy if delivered by the oral route. Some pharmaceutical companies have already reached clinical trials; however, most have abandoned their delivery systems at the first stage of development. It would be very important to disclose the possible causes of their failures.

With hopes of developing better oral insulin formulations, the future is also waiting for challenges of more effective and sustained insulin delivery, proof of optimum efficacy in human beings, safety and tolerability issues, patient affordability and long−term effects of oral insulin formulations. The authors anticipate that the appearance of an oral insulin formulation on the market in a ten−year perspective is a challenge, although further research will define if the oral insulin BA will become economically viable.

It is unquestionable that the oral delivery of insulin is the most effective and desired way to replace the invasive route. The several limitations associated to oral biomolecules have been responsible for the challenges faced by the researchers to reach a successful formulation. The constant growth of the biotechnology field has allowed the cost−effectiveness and pilot−scale production of proteins and peptides, including insulin, intended for oral administration, in which some are in clinical stage of development. The amount of insulin required for therapeutic effects together with the formulation development costs remain major challenges in pilot scale−up, which need to be addressed at all levels of research and development. However, the fact is that, since the discovery of insulin, for nearly a century, diabetes therapy remains to be the s.c. administration of insulin, with the inherent risks of life threatening hypoglycemia triggered by its narrow therapeutic window. The desire to minimize the chronic micro− and macrocardiovascular

disease associated with diabetes, have led to alternative therapies of insulin [1]. The enhancement of the therapeutic efficacy and safety of the s.c. insulin administration walk in the direction to intermediate measures of glucose, lipid and body weight management and even to the measurement of the disease mortality. Therefore, it would be a great advance in the diabetes control if the glycemia were controlled in a timely, closed−loop fashion, simulating pancreatic function [2].

T2D constitutes a more complex disease than T1D, given its association with multiple other abnormalities. Obesity is considered the main contributor for the deterioration of the diabetes condition; therefore, the development of a therapy that would allow patients to effectively control their weight is fundamental for diabetes care. Bariatric surgeries and anti−obesity drugs have gained considerable interest in this area [1].

The need for more effective therapies holds researchers and pharmaceutical industries' attention, but with the heterogeneity of the disease hardly one single delivery method will fulfill all the patients needs.

7.3 REFERENCES

[1] Zaykov, A.; Mayer, J.; DiMarchi, R. Pursuit of a perfect insulin. Nature Reviews Drug Discovery 2016;15:425−39.

[2] Mathieu, C.; Rodbard, H. W.; Cariou, B.; Handelsman, Y.; Philis−Tsimikas, A.; Ocampo Francisco, A. M.; Rana, A.; Zinman, B. A comparison of adding liraglutide versus a single daily dose of insulin aspart to insulin degludec in subjects with type 2 diabetes (BEGIN: VICTOZA ADD−ON). Diabetes, Obesity and Metabolism 2014;16:636–44.